American Petroleum Institute

Evaluating Hydrocarbon Removal from Source Zones and its Effect on Dissolved Plume Longevity and Magnitude

Regulatory Analysis and Scientific Affairs Department

PUBLICATION NUMBER 4715
SEPTEMBER 2002

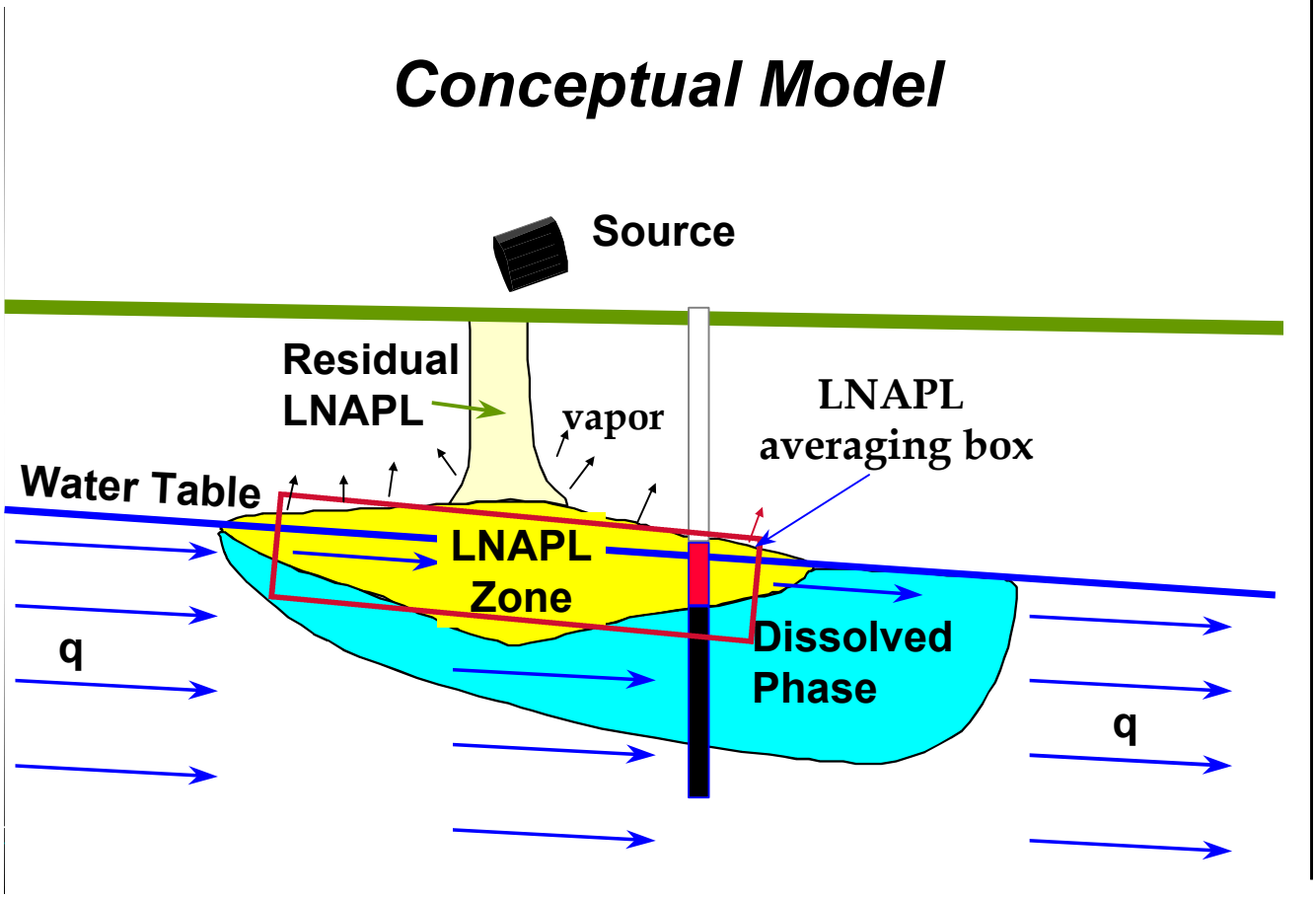

Evaluating Hydrocarbon Removal from Source Zones and its Effect on Dissolved Plume Longevity and Magnitude

Regulatory Analysis and Scientific Affairs Department

API PUBLICATION NUMBER 4715

PREPARED UNDER CONTRACT BY:

DAVID HUNTLEY, PH.D.
DEPARTMENT OF GEOLOGICAL SCIENCES
SAN DIEGO STATE UNIVERSITY

G.D. BECKETT, C.HG.
SAN DIEGO STATE UNIVERSITY AND
AQUI-VER,INC.
LA JOLLA, CA 92037

SEPTEMBER 2002

American Petroleum Institute

ACKNOWLEDGMENTS

API STAFF CONTACT

Harley Hopkins, Regulatory Analysis and Scientific Affairs Department

MEMBERS OF THE API SOIL AND GROUNDWATER TECHNICAL TASK FORCE

MEMBERS OF THE GW-63 PROJECT TEAM:

Ade Adenekan, ExxonMobil Corporation
Ed Brost, Shell Global Solutions
Tim Buscheck, ChevronTexaco Energy Research and Technology Co.
Chen Chiang, Shell Global Solutions
George DeVaull, Shell Global Solutions
Dan Irvin, Conoco, Inc.
Steve Jester, Conoco, Inc.
Kris Jimenez, ExxonMobil Corporation
Urmas Kelmser, ChevronTexaco Energy Research and Technology Co.
Ravi Kolhatkar, BP p.l.c
Vic Kremesec, BP p.l.c
Al Ligouri, ExxonMobil Corporation
Tom Maldonato, ExxonMobil Corporation
Ed Payne, (formerly) ExxonMobil Corporation
Tom Peargin, ChevronTexaco Energy Research and Technology Co.
Aldofo Silva, Canadian Petroleum Products Institute
Curt Stanley, Equilon Enterprises LLC
Terry Walden, BP p.l.c
Andrea Walter, Petro Canada
Lesley Hay Wilson, Sage Risk Solutions

TABLE OF CONTENTS

List of Appendices

LIST OF FIGURES

FOREWORD

API PUBLICATIONS NECESSARILY ADDRESS PROBLEMS OF A GENERAL NATURE. WITH RESPECT TO PARTICULAR CIRCUMSTANCES, LOCAL, STATE, AND FEDERAL LAWS AND REGULATIONS SHOULD BE REVIEWED.

API IS NOT UNDERTAKING TO MEET THE DUTIES OF EMPLOYERS, MANUFACTURERS, OR SUPPLIERS TO WARN AND PROPERLY TRAIN AND EQUIP THEIR EMPLOYEES, AND OTHERS EXPOSED, CONCERNING HEALTH AND SAFETY RISKS AND PRECAUTIONS, NOR UNDERTAKING THEIR OBLIGATIONS UNDER LOCAL, STATE, OR FEDERAL LAWS.

NOTHING CONTAINED IN ANY API PUBLICATION IS TO BE CONSTRUED AS GRANTING ANY RIGHT, BY IMPLICATION OR OTHERWISE, FOR THE MANUFACTURE, SALE, OR USE OF ANY METHOD, APPARATUS, OR PRODUCT COVERED BY LETTERS PATENT. NEITHER SHOULD ANYTHING CONTAINED IN THE PUBLICATION BE CONSTRUED AS INSURING ANYONE AGAINST LIABILITY FOR INFRINGEMENT OF LETTERS PATENT.

EXECUTIVE SUMMARY

For many decades, the oil production industry has recognized that significant limitations exist to complete extraction of oil from geologic formations. Attempts to recover fuels and crude oil (collectively known as light nonaqueous phase liquids or LNAPL) accidentally released to the subsurface encounter similar limitations. This report explains how multiphase fluid mechanics (mixed presence of LNAPL, water, vapor) relate to these recovery limitations. The report further explains how the endpoints to recovery relate to both the longevity of the LNAPL as a source of dissolved-phase and vapor-phase constituents and to the downgradient dissolved-phase concentrations. This work is focused on LNAPLs, but the general principles also apply to many aspects of dense nonaqueous phase liquid (DNAPL) recovery and risk.

Release of an LNAPL to the subsurface introduces the potential of several risk factors to nearby receptors: (1) Vapor phase migration of volatile constituents from LNAPL in the vadose zone to the surface. (2) Dissolution of constituents from LNAPL in the vadose zone through infiltration of recharging waters, and subsequent downgradient movement of those constituents once those waters encounter the water table. (3) Release of sufficient LNAPL that it exceeds the capacity of the vadose zone to absorb it, resulting in the accumulation of a mobile LNAPL lens above and below the original groundwater table. (4) Upward vapor phase migration of volatile constituents from the above LNAPL lens to the land surface, and (5) Downgradient migration of dissolved-phase constituents resulting from dissolution of the LNAPL lens.

This report was prepared to synthesize the physical and chemical behavior of LNAPL in contact with groundwater, and to link those aspects to cleanup expectations. It does not deal with the mechanisms related to risk factors (1) and (2) above, which are processes limited to the vadose zone. The report deals with the zone between the top of the LNAPL capillary fringe and the lowermost observation of LNAPL in the aquifer. The report outlines the following:

1. The fundamental theory, with supporting field and laboratory observations, that controls the distribution and mobility of LNAPL and water between the top of the LNAPL capillary fringe and the lowermost occurrence of LNAPL in the aquifer.

2. The effect of remediation on the distribution and mobility of both the LNAPL and water within the zone of interest.

3. The dissolution of compounds from the LNAPL into groundwater flowing both through and below the LNAPL-impacted interval.

4. Volatilization of that LNAPL.

5. The effects of all of the above on the concentrations of soluble LNAPL constituents both within the source area and downgradient of the source area.

When LNAPL distribution and cleanup are linked to chemistry, the hydraulic recovery limitations can be placed in a risk-benefit context. The linked physical and chemical calculations show why, under many conditions, hydraulic recovery of LNAPL may have little or no benefit in reducing the magnitude or longevity of the risk downgradient from the LNAPL source area. The technical evaluations also show that chemical alteration of the LNAPL source may achieve compound specific cleanup goals that cannot be reached through hydraulic methods. For any remediation strategy, the short and long term benefits can be evaluated against the cost, time, and probability of achieving cleanup targets.

The fundamental principles described in this report have been organized into a software utility, called LNAST (**LN**APL Dissolution **a**nd Transport **S**creening **T**ool). This software utility links the series of analytic solutions that predict LNAPL distribution, dissolution, volatilization, and downgradient dissolved-phase concentration through time, both with and without remediation through hydraulic means. Because the assessment described in this report has several linked aspects, or "tools", for assessing LNAPL impacts, cleanup, and chemical transport, we will refer the combination of the underlying principles, the resulting mathematical solutions, and the software as a "toolkit".

Because the solutions are analytic, they make many simplifying assumptions. Therefore, the linked suite of physical and chemical calculations will not provide a detailed representation of the site. The calculations described in this report, whether solved in a spreadsheet environment or using the software utility, are designed as screening tools only. The results of the calculations cannot be precisely calibrated to site conditions, just as the results of other screening models cannot. The toolkit described in this report is most properly considered as a quantitative conceptual model to be used for screening decision-making. There is a deliberate compromise between screening analytic methods versus numerical calculations that can consider a more complete range of complexities. While it is clear that conditions not considered by the software utility, such as complex vertical and lateral variations in soil properties, seasonally varying groundwater elevations, and laterally varying groundwater flow velocities near the LNAPL are important, the parameters necessary for such evaluations are not often available. Further, the effort involved in numerical multiphase, multidimensional modeling is significant. The approach presented here is therefore designed to use available information in the best manner possible, but it should be clear that uncertainty will exist in the results. The recommended use of the toolkit is expected to produce conservative results. If more accurate or detailed assessment is needed, numerical modeling and/or advanced data collection will be warranted, consistent with the higher-tiered levels of effort in many risk assessment guidelines (e.g., Risk-Based Corrective Action, ASTM 1995; Risk Assessment Guidance for Superfund, EPA, 1995). Therefore, while simple to use, this screening conceptual evaluation method requires good user judgment and awareness of the limitations.

The presence of multiple phases (water, LNAPL, vapor) in porous material influences the movement and transport of each phase under ambient or remediated conditions. Multiphase fluid mechanics and other principles are used to estimate the pore fluid fractions and their mobility under a variety of conditions. The distribution and composition of the LNAPL then determines the equilibrium chemical partitioning into groundwater and vapor. Ultimately, the application of these principles results in estimates of the time dependent concentration of soluble components partitioning out of the LNAPL and into groundwater, with a link to vapor flux under ambient flow and partitioning conditions. For instance, one could look at chemical partitioning from an LNAPL source that has had no remediation action, or one could consider the same source after some cleanup effort (but not during that effort). This toolkit does not directly consider institutional controls, such as plume containment, that are often an important component of risk management. However, one could use the toolkit to consider the time frame over which an institutional control might be appropriate.

Chemical concentration is the metric of this toolkit. All other things being equal, risk is proportional to the chemical concentration reaching receptors. Therefore, one can evaluate the risk/benefit of various LNAPL remediation strategies by looking at the concentration reduction associated with remediation. Specific site risk must be calculated separately by the user, as risk depends not only on the concentrations reaching the receptors, but also other factors in the exposure scenario, including the receptor characteristics, current and future land use, and other factors that are not part of this work.

In developing this multiphase approach, several observations and conclusions have been reached regarding the importance of LNAPL distribution, its chemical character, and source remediation. Several technical issues are isolated and summarized below.

The Effect of Soil Type

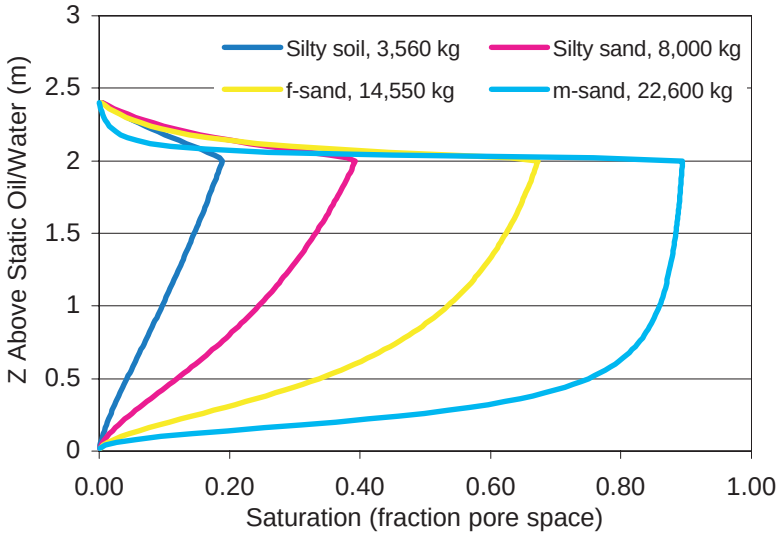

Figure E-1. Gasoline saturation curves for 2 m observed well thhickness in several soils at vertical equilibrium. The total mass is for a 10 x 5 m areal extent.

For a given observed well thickness, LNAPL saturation and mass decreases strongly in the zone between the LNAPL/air and LNAPL/water interfaces in the well as the pore size gets smaller (Figure E-1). This, in turn, has a strong impact on the relative source longevity, which is also, dependent on the groundwater flow conditions. If one assumes the same net regional groundwater flow through all soils, then depletion is fastest in the fine-grained materials, because of less mass and greater relative water flow (Figure E-2a). If the same gradient is

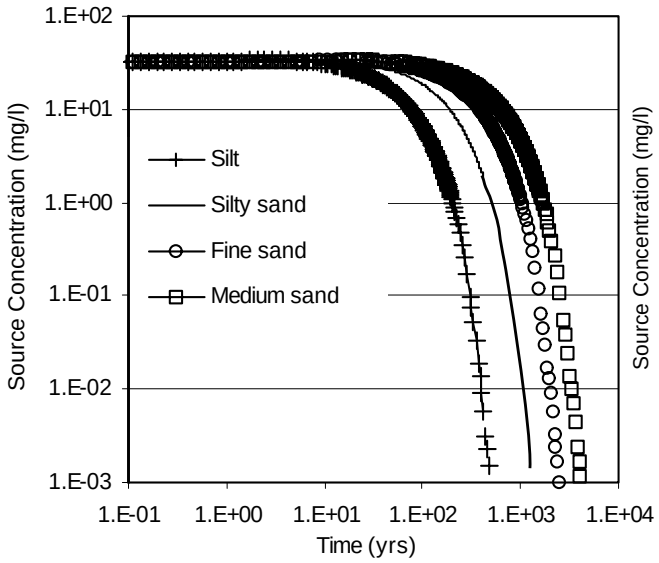

Figure E-2a. Source depletion of benzene from gasoline where the regional flow is the same for each soil (no biodecay in the source zone).

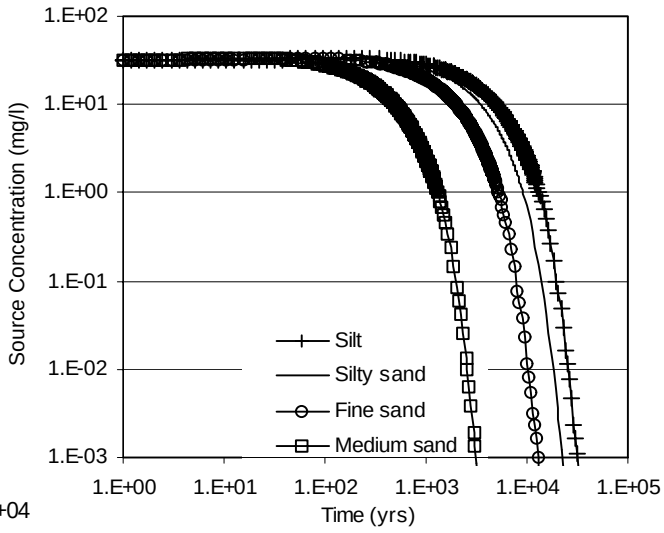

Figure E-2b. Source depletion of benzene from gasoline where the hydraulic gradient is the same for each soil (no biodecay in the source zone).

assumed for all soils, then the flow through the finer-grained units is small and the source depletion time is long (Figure E-2b). Therefore, the soil type exerts a strong influence on source residence time with or without cleanup. These estimates do not include volatilization from the LNAPL, which will be discussed below.

Effect of LNAPL Thickness

The mass distribution of LNAPL and the related source longevity for any compound of interest are exponentially related to soil and fluid capillary properties, and to capillary pressure, which can, in turn, be related to the LNAPL thickness observed in a monitoring well at vertical equilibrium (VEQ). For a range of thicknesses from 0.25 to 2.0 meters in a fine-sand, the volume varies over nearly two orders of magnitude (Figure E-3). This has a very large impact on the chemical component depletion from the LNAPL under natural groundwater flow conditions (Figure E-4).

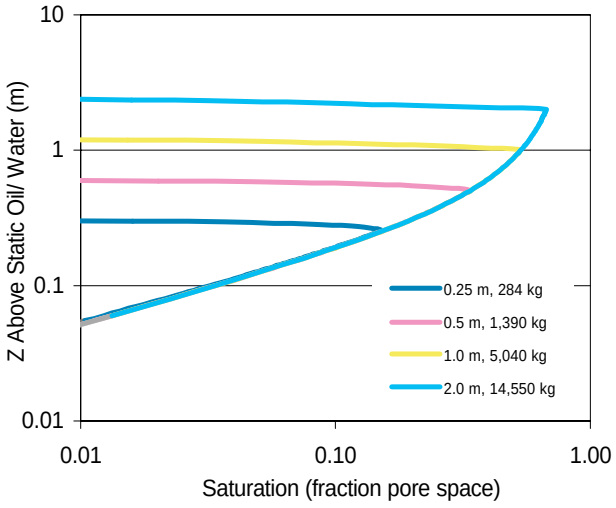

Figure E-3. Equilibrium gasoline profiles at various well thicknesses, plotted log-log to expand scale.

Effect of LNAPL Residual Saturation

LNAPL residual saturation is the smallest saturation remaining in the formation against applied hydraulic recovery and is the theoretical endpoint of LNAPL hydraulic recovery. It is also a highly optimistic endpoint because real hydraulic variability, well efficiency, well interference, aquifer heterogeneity and other factors all combine to diminish actual recovery and leave more LNAPL in the formation. For instance, for an initial

gasoline thickness of 1 m, we find that the benefit of LNAPL removal decreases and the source benzene concentration residence time approaches that of a non-remediated condition as the residual gasoline saturation increases from 5 to 30% for a sand soil (Figure E-5). Since one cannot hydraulically reduce LNAPL saturations below residual saturation, this factor is very important for any site where hydraulic recovery may be considered of potential benefit.

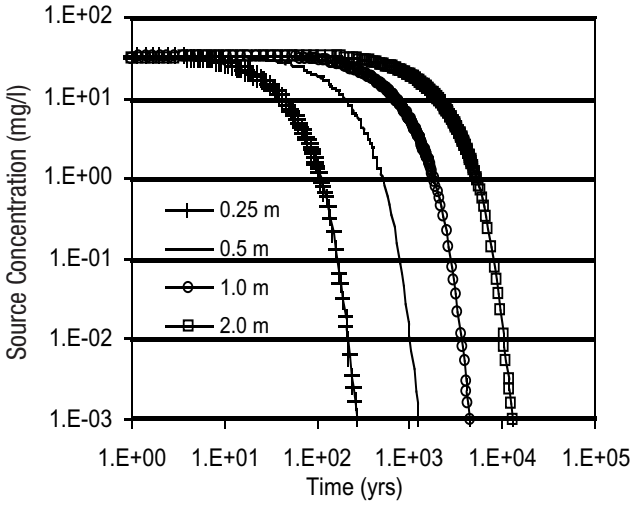

Figure E-4. Depletion curves for benzene associated with the vertically equilibrated (VEQ) profiles from 0.25 to 2.0 m.

Contrast in Components of Concern

The effective solubility and mole fractions of the various compounds in fuels have a significant effect on the longevity of the compounds within the source. For example, we have compared MTBE and benzene in gasoline with naphthalene in a diesel for 2 m of observed thickness in a fine-sand (Figure E-6). Because the effective solubility of MTBE and benzene are high relative to naphthalene, the source longevity between the components is separated by several orders of magnitude, with naphthalene present for tens of thousands of years for the conditions considered (Figure E-7).

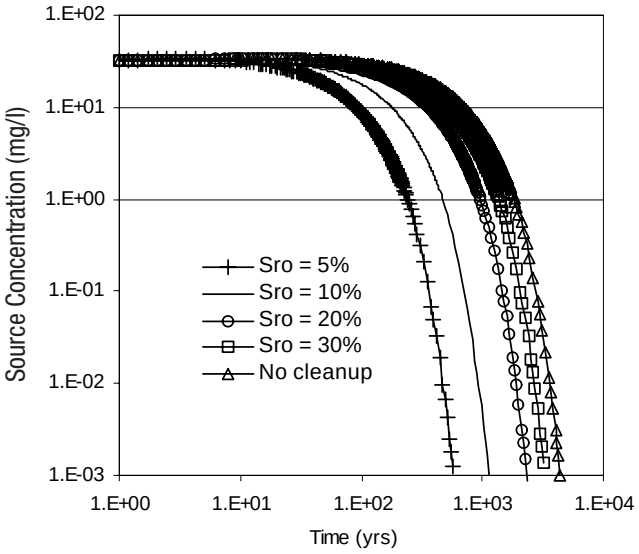

Figure E-5. Benzene source depletion calculation for various gasoline specific retention values in a fine-sand. The actual value for many sands in this class would be 15 to 30%.

Component Volatilization

Volatilization is another potential mass loss mechanism from the LNAPL source depending on fuel volatility and site subsurface conditions. Using the example above, we have looked at free volatilization from the source. MTBE and benzene both have substantially higher vapor pressures than naphthalene. Comparison of Figure E-7 (source depletion without volatilization) to Figure E-8 (depletion with volatilization) demonstrates that inclusion of volatilization as a mechanism of source depletion causes a reduction in the potential source longevity of MTBE and benzene, but naphthalene longevity remains essentially unchanged. Be aware that free volatilization from the LNAPL source in the water table zone is rare. There are almost always impeding horizons such as surface covers and geologic conditions to be considered.

This is not to say that component losses in the vadose zone are not significant as the LNAPL spill migrates downward to the water table region, particularly for volatile compounds like MTBE.

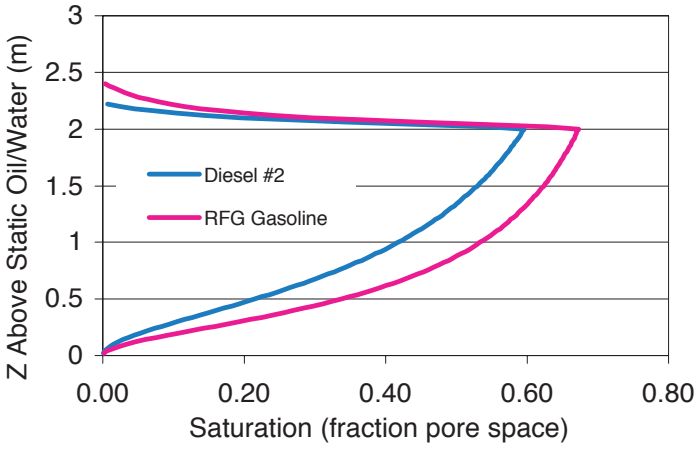

Figure E-6. Saturation profiles for 2 m observed fuel thickness, gasoline and diesel, in a fine-sand.

Remediation as a Function of Soil Type

There is a large contrast in the potential gains of hydraulic free product removal between coarse- and fine-grained soils, all other things being equal. Although fine-grained soils have lower LNAPL masses for the same observed LNAPL thickness condition, this lower saturation condition also significantly limits hydraulic recovery compared to coarser-grained soils. The same may be said for the air-phase if considering remediation by vacuum-enhanced methods. A comparison between source longevity for hydraulically remediated and non-remediated conditions in a finer-grained soil shows remediation impacts source longevity only slightly (Figure E-9). In contrast, for the same initial condition of 2 m of gasoline, remediation of coarser soils results in a more significant decrease in source longevity.

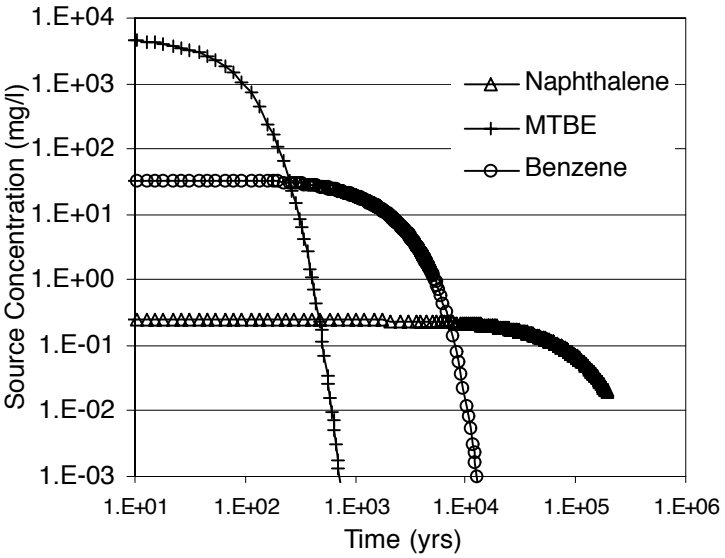

Figure E-7. Comparison of different fuel components and their longevity in the source under ambient conditions.

Effect of Regional Groundwater Flow Rate

The regional groundwater flow rate controls the source depletion rate in the absence of volatilization because it is responsible for the mass partitioning from the LNAPL. Therefore, one observes more rapid source depletion and more rapid decreases in the downgradient extent of a dissolved-phase plume more quickly in cases of high flow for the same

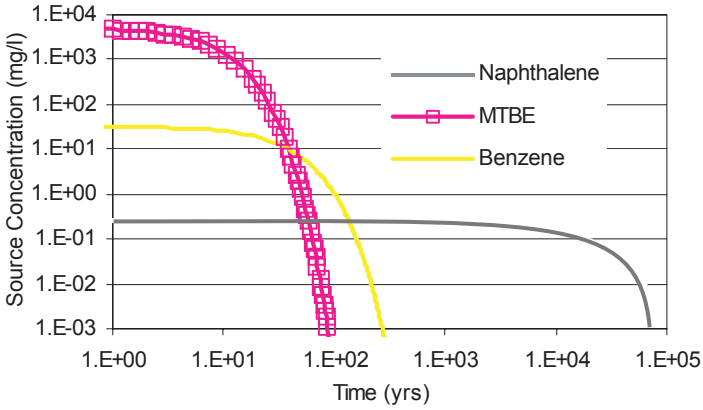

Figure E-8. The estimated source depletion graph for MTBE, benzene, and naphthalene allowing free volatilization from the source.

initial LNAPL mass distribution. The regional groundwater flow rate also impacts the potential downgradient extent of a given constituent concentration in a dissolved hydrocarbon plume, as does the specified biodecay rate.

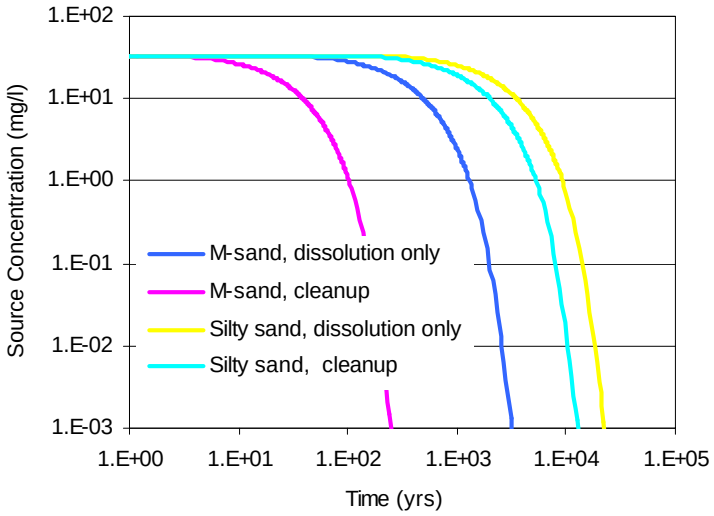

Figure E-9. Comparison of hydraulic LNAPL recovery cleanup versus intitial conditions for a silty sand and a medium sand.

Because the mass of LNAPL is very large compared to the solubility of its constituents, the longevity of the source is typically large compared to the time it takes for a dissolved phase plume to reach field equilibrium as a function of dissolution, transport, and the rate of biodegradation. Therefore, the downgradient extent of a given constituent concentration in a dissolved plume is almost entirely independent of the LNAPL source area conditions (Figure E-10). Possible exceptions are highly soluble compounds or very small LNAPL mass distributions in the source area.

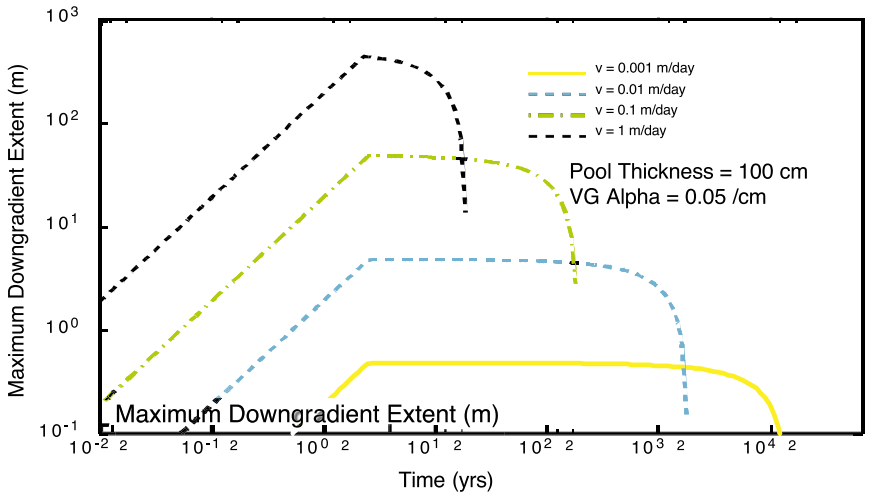

Figure E-10. The effect of groundwater velocity on the downgradient extent of benzene at a uniform decay rate.

It should be noted that dissolved-phase plume studies show that the extent of a stable, dissolved phase plume undergoing biodegradation, is not strongly dependent on groundwater flow velocity. This is likely due to the fact that biodegradation is often limited by the mass flux of oxygen and other electron receptors to the zone of biodegradation, which in turn is affected by groundwater flow velocity. This suggests that one might estimate higher biodecay rates in high flow settings, with a resultant diminishment in the dimishment in the downgradient extent of the plume.

KEY POINTS

From the points above and those developed in the body of this report, several summary observations and conclusions can be drawn. These observations and conclusions are derived from theory supported by lab and field data from the environmental field and many decades of petroleum production experience. The term “risk magnitude” is used as a relative indicator of risk potential based on the expected concentration of

a compound in groundwater or in the LNAPL phase. Whether or not a "risk" exists depends not only on concentration, but also on the nature of the potential receptors. Risk "longevity" refers to the time frame over which the risk magnitude remains relatively static.

1) For the groundwater and vapor exposure pathways, risk magnitude is strongly dependent on the chemical characteristics of the LNAPL source and the nature of potential receptors, whereas the risk longevity is strongly dependent on the mass distribution in the formation. The mass distribution depends strongly on soil properties and the characteristics of the LNAPL release. The zones of greatest LNAPL saturation within the source zone usually control the risk magnitude and longevity of groundwater and vapor impacts.

2) Under most conditions, hydraulic removal of LNAPL does not reduce the magnitude of risk in groundwater or vapor exposure scenarios, although there is a risk longevity reduction when mass is recovered. In permeable soils and under best-case conditions, the risk longevity reduction may be about an order of magnitude, or possibly a little more in rare cases. In lower permeability soils, risk longevity may be reduced only a few percent.

3) Hydraulic LNAPL recovery is not generally effective at mitigating existing groundwater risks unless both LNAPL and groundwater containment are successfully achieved. Hydraulic recovery has virtually no risk benefit in most cases with respect to the vapor phase exposure pathway. Under most conditions, free product containment intervention for the free phase must occur near the time of the release before excessive spreading and mobility reduction has occurred. Recovery and containment of dissolved-phase plumes are viable risk management options to mitigate groundwater receptor pathways, but will do little to treat the LNAPL source zone.

4) Any process that decreases the LNAPL saturation will decrease its mobility and recoverability. This means that LNAPL plumes become less mobile and recoverable through time as spreading results in smaller saturations. The pool becomes immobile when the LNAPL gradient is less than the capillary forces resisting further water displacement. This also means that LNAPL remediation is a self-limiting process since reducing saturations reduces the potential for further recovery.

5) In situ removal of specific chemicals of concern in LNAPL, using approaches such as vapor extraction, heating, or other enhancements, when feasible, reduces the risk magnitude of the release in approximate proportion to the corresponding mole fraction reduction in the source. The effectiveness of most cleanup technologies, however, depends on the ability to thoroughly contact the LNAPL with the remediation stream throughout the source area. Therefore, understanding of the LNAPL source characteristics and distribution is meaningful to any risk reduction strategy.

6) There is a widely held belief that the measured LNAPL thickness in a monitoring well exaggerates the thickness of LNAPL present in the formation adjacent to the well. However, fluid physics theory indicates that, at vertical equilibrium, the thickness of the LNAPL-affected interval in the aquifer will be greater than the LNAPL thickness observed in the well. In a few instances in the field, however, there may be situations where the LNAPL thickness appears greater in the well than the LNAPL-affected formation outside of the well. Heterogeneity and conditions where vertical equilibrium does not exist may produce this apparent thickness exaggeration.

From a corrective action perspective, it is important to recognize that the thickness of LNAPL in a well may exaggerate the *volume* of in-place and recoverable LNAPL in the formation. LNAPL exists at a variety of saturations in the formation over the vertical interval suggested by the thickness of the LNAPL in the well. However, substantial amounts of the LNAPL outside of the well will occur at low saturations that renders it immobile within the formation and unrecoverable.

7) For most conditions, observable plume thickness in observation wells and risk are unrelated, particularly under small observable LNAPL accumulations. However, large accumulations of LNAPL that return quickly to a well after bailing can imply local area mobility of the free phase product. Transport of the free phase LNAPL can often have undesirable outcomes and present a significant risk.

8) For the same capillary pressure conditions, LNAPL saturations are substantially smaller in fine-grained soils than in coarse-grained soils, all other things being equal. This effect combines with the low intrinsic permeability of fine-grained soils to produce very low mobility and potential recoverability in fine-grained materials. When the regional groundwater flow and volatilization from the fine-grained materials is small, the lifespan of LNAPL in these materials can be long.

9) LNAPL viscosity varies significantly for various petroleum products and crude oils and is inversely proportional to the effective LNAPL conductivity. Thus, for the same soil and product saturation, a fuel oil pool may be up to 50 times less mobile and recoverable than a similar pool of gasoline.

10) Industry and regulatory experience indicate that it is rare for hydraulic LNAPL removal schemes to recover more than 30% of the oil in place, although exceptional instances may yield 50-60%. When groundwater is produced, the ratio of product to water is usually less than 0.01 and typically decreases further with time.

11) For biodegradable constituents, the downgradient extent of the dissolved-phase plume is largely unrelated to the LNAPL mass distribution, unless the mass is very small. The maximum extent of the dissolved-phase plume is controlled by the groundwater velocity and degradation rates, which may be

related. Typical biodegradable plumes are expected to become stable in less than a few years.

12) The expected groundwater residence time of some compounds from LNAPL sources is on the order of decades to thousands of years. The residence time increases for larger pools with high LNAPL saturation and as the component solubility and its mole fraction in the source becomes smaller. Therefore, low volatility and solubility fuel components such as polynuclear aromatic hydrocarbons may persist at low concentrations for very long times. However, these same chemical attributes, coupled with bioattenuation and other factors, often buffer the risk magnitude of plumes from the long-lived sources.

13) From a technical standpoint, risk in a given exposure scenario depends on the points of compliance selected. If plumes are long-lived but also attenuated at some distance, there is obvious potential risk from direct contact within a certain radius of the plume, but no risk outside that zone. Therefore, the public, responsible parties, and regulators may benefit from a technical consensus on how to define and maintain compliance zones.

Section 1.0

ABSTRACT

Light nonaqueous phase liquids (LNAPL; *a.k.a.* petroleum fuels, "product" and crude oil) are common sources of hydrocarbons in both water and vapor phases, with all phases presenting potential health, resource, and environmental risks. Ample environmental and oil reservoir data have shown that complete recovery of oil from geologic formations is not generally feasible. Even at residual saturation (trapped and immobile), the LNAPL phase has a mass that is typically several orders of magnitude greater than normally present in sorbed, water, or vapor states, implying the potential for long-term impacts.

Regulatory agencies usually require a responsible party to "remove free product to the maximum extent practicable." Lacking in ways to easily assess the mobility and long-term risks of LNAPL pools from site to site, arbitrary maximum LNAPL thickness in wells (e.g., 0.1 feet) is often adopted as endpoints for free product recovery. However, observed LNAPL thickness in wells has little or no relationship to the magnitude of risk presented before or after cleanup attempts. Often, free product recovery efforts are undertaken with little understanding of how much product can be recovered, how long the recovery will take and whether the site conditions will change significantly after the recoverable product is removed. This report is intended, in part, to assist in evaluating these issues.

This study provides quantitative theory and tools to evaluate LNAPL sources, their chemistry, and the effects various remediation strategies may have on groundwater and vapor exposure pathways. These exposure pathways are often a critical component of quantitative risk assessment. The study was designed to link the multiphase and chemical processes controlling *in situ* LNAPL distribution, mobility, and cleanup to quantify estimates of the time dependent concentrations within and downgradient of the LNAPL source. This work considers active flow of groundwater through the LNAPL impacted interval, which has generally not been considered in other analytic evaluations.

The results of this work suggest that the physical limitations to hydraulic free-phase recovery using current technology are such that significant health or resource risk reduction is gained only within a narrow range of chemical and geologic conditions. The greatest risk reductions, as measured by concentration reduction along an exposure pathway, occur in highly permeable soils and for volatile and soluble fuel components. The least effective risk reductions occur in low permeability materials and for fuels that have small volatility and solubility. Under many conditions, it is likely that LNAPL-sourced dissolved and vapor plumes will be present for decades to centuries unless treatment options improve significantly. The evaluation methods presented here can be used to show that the field endpoint, both chemical and physical, of any given cleanup method controls the long-term residual risk.

Section 2.0

INTRODUCTION

This report provides a series of linked analytic methods (or tools) to evaluate light non-aqueous phase liquids (LNAPLs) and their impacts in the water table region. The LNAPL conditions may be conceptualized under a range of conditions, including application of simplified cleanup strategies, under equilibrium conditions, and under user-defined conditions. The purpose is to assist in building conceptual site models that account for key processes and properties affecting the longevity and magnitude of chemical impacts associated with LNAPL spills in the water table region. As human and ecological risks are in part dependent on the chemical concentrations reaching receptors and the timing of those impacts, this technical methodology can assist in risk-based comparisons of various site LNAPL scenarios, including remediation endpoints. The metric of this evaluation method is concentrations in groundwater as a function of the LNAPL source conditions through time, with or without volatilization. There are no explicit risk calculations, as those are site and receptor dependent.

The report is focused on multicomponent petroleum products, although many of the principles apply to other NAPLs, including dense non-aqueous phase liquids (DNAPLs). Throughout the report, the term LNAPL will be used to describe petroleum fuels, crude oil, and other water immiscible compounds having a density less than water.

The impetus for developing this methodology has been decades of petroleum recovery experience coupled with more recent environmental experience that clearly demonstrates significant limits exist to complete LNAPL recovery from geologic materials. This suggests it would be useful to consider the various factors controlling LNAPL distribution and recovery and link those to the associated differences in the magnitude, longevity, and distribution of groundwater impacts. Obviously, LNAPL mass reduction seems inherently good, but the question is how to technically define “good.” If, for instance, a risk to groundwater is presented by a fuel release and we find that our common recovery technologies do not mitigate that risk, we would probably all agree that this is not “good.” Conversely, if mass removal reduces fuel mobility and risk longevity in a meaningful way, we would also probably agree that this is “good.” The intent of this toolkit is to help the user to distinguish, in a site specific context, between effective and ineffective remediation using concentration reduction as a consistent benchmark.

The building of this LNAPL screening method depends on several related attributes of LNAPL spills affecting the water table region. First, the multiphase hydrogeologic aspects of LNAPL in the water table region is considered for a range of possible initial conditions. Second, the partitioning and transport of chemicals from the LNAPL in groundwater is linked to the mass distribution and chemical composition of the LNAPL. Volatilization of compounds from the LNAPL may also be

considered. Because the screening evaluation method is based on several linked methods or "tools," the term "toolkit" will be used throughout this report to refer to one or more of the various technical aspects. The "toolkit" is also organized in a software utility called API-LNAST (**LN**APL Dissolution **a**nd Transport **S**creening **T**ool), which will be discussed subsequently. The LNAST program is primarily an organizational tool to aid the user in performing the linked dissolution, volatilization, and solute transport calculations. Use of the program is not necessary, as all the pertinent information, equations, and methodologies are also provided in this report.

The remainder of this introduction will develop an overview of concepts important to the LNAPL problem in the groundwater system, touch briefly on risk concepts, and discuss what this methodology considers. Following this overview, the report will discuss geologic, fluid, and chemical parameters important in the underlying description of the problem. Remediation aspects will also be developed to assist in bracketing the possible LNAPL conditions as a function of the cleanup strategy applied. Following this background and description of the important controls and parameters, a User's Guide is developed for the included software utility API-LNAST. Example problems are also provided to assist in showing how evaluations might proceed.

Throughout this manual, the active use of equations will be minimized and graphical examples will be used instead wherever possible to keep the focus on the principles, with some simple equations presented for elucidation of key ideas and concepts. Comprehensive development of necessary equations is provided in Appendices A and B. Appendix C provides a synopsis of parameter ranges for the various inputs needed for the calculations. Appendix D provides a brief overview of field "reality" checks that might be of assistance when considering the best application of the toolkit and the appropriate input parameters. Appendix E shows example input and output files.

2.1 LNAPL SPILL CONTEXT AND METHOD OVERVIEW

The body of field observations, supported by multi-phase fluid and chemical partitioning theory, indicates that the release of a fuel hydrocarbon will undergo the following evolution:

1. An LNAPL release begins with vertical drainage of LNAPL under gravity and capillary gradients (Figure 2-1a). The drainage is strongly influenced by soil characteristics and occurs most rapidly in dry, high permeability soils, and more slowly in wet or low permeability soils. As the LNAPL moves downward through the vadose zone it will be subject to physical and chemical process that include volatilization, entrapment of part or all of the LNAPL as residual phase (immobile), and dissolution of LNAPL components into soil pore water.

2. If the release is sufficiently large to exceed the residual retention capacity of the vadose zone soils, the LNAPL will eventually encounter the capillary fringe above the water table (Figure 2-1b); this also occurs for perched water table zones. As LNAPL encounters pore spaces completely or partially saturated with water near the water table, the weight of the LNAPL causes it to displace pore water until hydraulic equilibrium is achieved. At the same time, the large vertical gradient through the vadose zone dissipates into a lateral gradient in the capillary and water table zones. The lateral gradient is often semi-radial because of mounding of free product due to the resistance of the water wet materials to freely transmit the oil. The result is a free product mound, with a gradient that often has little relationship to the groundwater gradient.

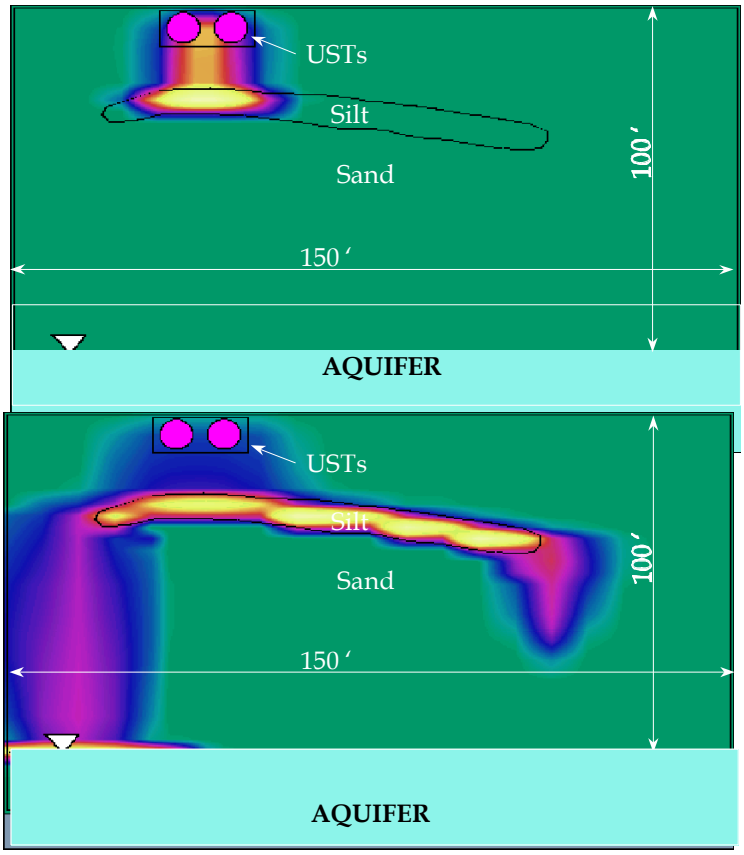

Figures 2-1a & b. Multiphase calculation showing downward LNAPL spill propagation in cross-section at 2 weeks and 1 year. Notice deflection of oil by the silt bed & later-time mounding in the water table region.

3. Once the release of free product stops, the LNAPL in the water table region will eventually cease to move as the resistive forces in the water wet sediments balance the driving forces in the LNAPL pool. An absolute endpoint of this movement is when the LNAPL reaches field residual saturation, a condition where the effective hydraulic conductivity of the LNAPL is zero. This leaves a mass, often large, of LNAPL for secondary dissolved and vapor-phase transport (Figure 2-2). When immobile, the LNAPL presents a risk only as a source of dissolved-phase and vapor-phase compounds to the environment. It is important to understand that in the interval below the top of the oil capillary fringe, LNAPL and water *coexist* in a zone often characterized by observed free product in a monitoring well (the theory will be discussed subsequently). In this zone, both water and product "fight" for space, and interact chemically as well (Figure 2-2).

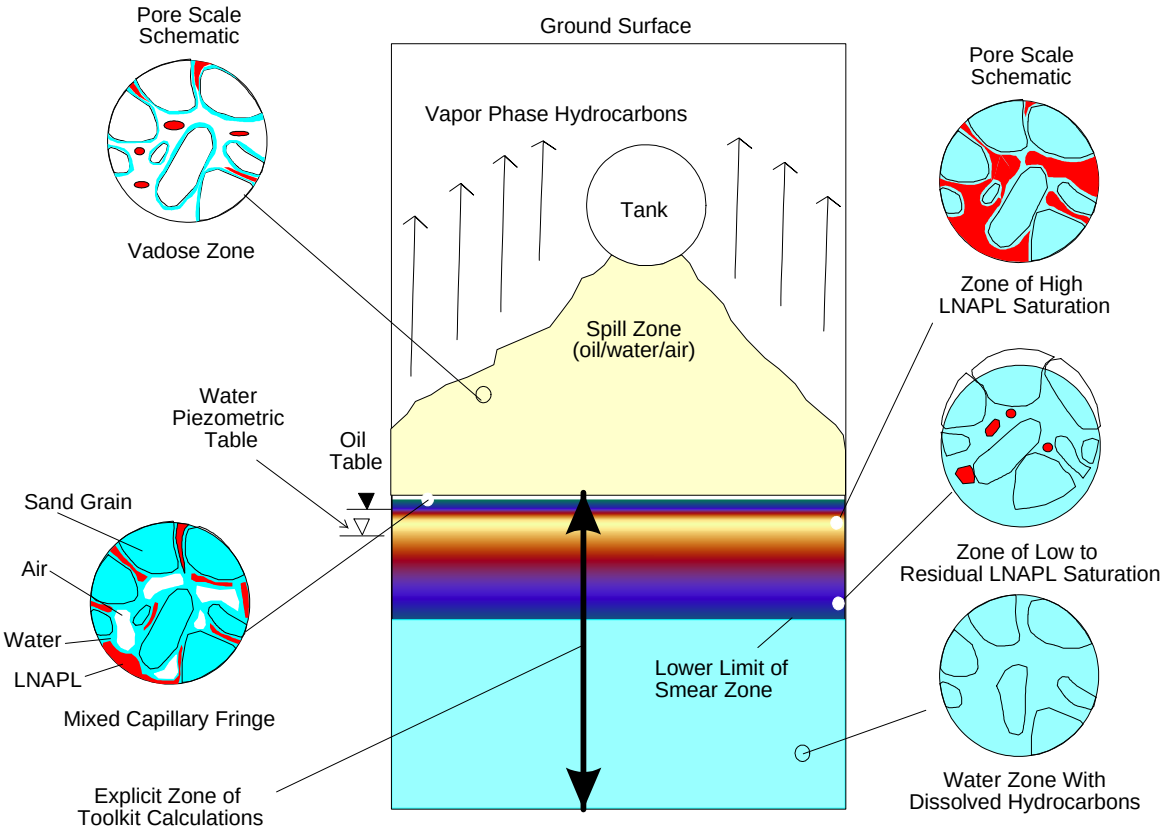

Figure 2-2. Schematic of an LNAPL spill showing different zones of impact from the source, in this case an underground storage tank (modified after White et al., 1996).

4. During the evolution of the LNAPL lens, external hydraulic factors may act to re-distribute all or portions of it. For example, water table fluctuations will tend to smear LNAPL vertically throughout the range of hydraulic variation, and often below the normally observed oil/water interface in a monitoring well.

5. As soon as the LNAPL encounters groundwater at or below the top of the groundwater capillary fringe, dissolution of soluble components of the LNAPL by groundwater moving below and through the LNAPL impacted interval begins. Thus a dissolved-phase plume starts to develop and, with time, grows in the downgradient direction.

6. For biodegradable constituents, the dissolved phase groundwater plume continues to grow until equilibrium is established between the rate of dissolution of the soluble LNAPL constituents and the rate of biodegradation. At this point, the plume stabilizes spatially. For non-biodegradable constituents, the dissolved-phase plume continues to expand until equilibrium is reached between the rate of dissolution from the LNAPL source area and the rate of dispersion (spreading) and dilution.

7. As dissolution and volatilization of soluble and volatile LNAPL compounds continues, the LNAPL becomes increasingly depleted of these compounds, resulting in decreasing concentrations of these constituents in the source area and a resulting contraction of the dissolved phase plume. This continues until the LNAPL is completely depleted of a constituent, and the dissolved-phase plume for the constituent disappears.

Overall chemical transport pathways (i.e., risk factors) potentially associated with this process include: (1) Volatilization of compounds from LNAPL in the vadose zone and upward migration of the resulting vapors to the surface; (2) Impacts to groundwater from dissolution of soluble compounds in LNAPL in the vadose zone (leachate); (3) Lateral movement of LNAPL in the water table region; (4) Volatilization of compounds from the LNAPL lens in the water table region and upward migration of the resulting vapors; (5) Dissolution and transport of soluble LNAPL constituents by groundwater moving through and below the LNAPL; (6) Potential volatilization and upward migration of vapors directly from the dissolved-phase groundwater plume. Remediation is designed to mitigate one or more of the risk factors above. When LNAPL is present, most remediation stratiegies target LNAPL mass reduction or changing the LNAPL chemistry such concentrations in the dissolved and/or vapor phase are reduced. Risk management and institutional control strategies may elect to address transport pathways without attempting to mitigate LNAPL impacts directly.

This technical methodology explicitly addresses items 4 and 5 above, with combined consideration of simplified aspects of remediation. Site specific parameters (estimated or measured) may be used to: (1) Evaluate the potential for LNAPL mobility; (2) Estimate the longevity and strength of the dissolving LNAPL source under conditions ranging from ambient conditions to those after some period of remediation; and (3) Simulate the behavior of the associated dissolved plume over time and distance downgradient of the source, in response to the selected degree of source removal. The method may be viewed as a site conceptual model that is mathematically based. As mentioned, the focus of the toolkit methods will be primarily on chemical concentrations in groundwater as a function of various LNAPL source and chemical conditions. However, the toolkit can also be used to evaluate simple mass reduction strategies, which could be a goal independent of groundwater concentrations or risk.

Human and ecological risks are in part dependent on the concentration reaching receptors; therefore one goal of this technical methodology is to assist in risk-based comparisons of various site cleanup options. The reader is reminded that the purpose of this work is not risk quantification, as that is strongly site and receptor dependent. The purpose is to provide links between LNAPL source conditions and resultant concentrations in groundwater under a range of scenarios that can be compared with independently estimated cleanup targets, risk-based or otherwise. If a specified condition fails to meet chemical target levels within a zone of compliance or time, then one would typically look at alternative strategies.

The technical method developed in this report allows the user to specify LNAPL conditions (e.g., saturation and spatial distribution) in the water table region for any combination of homogeneous soil and fluid properties. The LNAPL conditions in the water table region may then be acted upon by remediation, or left under the user specified ambient conditions. The toolkit also allows user prescribed conditions for simple layered systems without explicit hydraulic recovery estimates. Whichever path is taken by the user results in an estimated distribution of oil in the formation. That distribution then controls the dissolution of hydrocarbons out of the LNAPL into the groundwater and vapor phases. The user can specify the chemical compounds of interest within the LNAPL, and the time dependent concentrations of those compounds are calculated based on the initial mass and the progressive depletion of mass from the LNAPL source zone. Biodegradation of the LNAPL source is not considered, but biodegradation is allowed to act on the dissolved-phase plume, as specified by the user.

The vertical interval considered in the calculations is from the top of the oil capillary fringe to the lowermost occurrence of LNAPL in the formation. This includes: (1) the interval from the top of the oil capillary fringe to the oil/air interface in a monitoring well, where oil, water and air co-exist in the pore space; (2) the interval from the oil/air interface to the oil/water interface in a monitoring well, where oil and water coexist in the pore space and the oil may have significant mobility; and (3) the zone below the oil/water interface, where immobile oil may be trapped at residual saturations due to a rise in the water table. Some workers refer to the entire interval described above as the "smear zone". However, the term "smear zone" has been used by a variety of hydrogeologists and engineers to mean different things. A search of the use of the term "smear zone" on the internet reveals that the term is most commonly applied to the portion of the vertical profile above the water table where variations in the water table elevation has "smeared out" LNAPL in the vadose zone. For example, the U.S. Environmental Protection Agency (Office of Solid Waste and Emergency Response) defined it as;

"Smear zone is the area immediately above the groundwater table, which, in this application, was the area from the top of the well screens to the water table, and which was contaminated by hydrocarbons."

A similarly common definition was the zone below the oil/water interface in a monitoring wells where LNAPL has been smeared out due to water table fluctuations, such as the following definition;

" the zone of seasonal or climatic groundwater fluctuation"

Many workers included both of the above intervals in their definition, but in virtually all cases it was stated implicitly or explicitly that the "smear zone" was due to seasonal or climatic water table fluctuations. Because we wish to make it clear that LNAPL is distributed below the water table without any water table fluctuations, and because we are specifically not dealing with the portion of the vadose zone above the oil capillary fringe, we will avoid the use of the term "smear zone", and simply refer to the vertical interval of interest as the "hydrocarbon impacted interval" or "LNAPL source zone."

The LNAPL source zone treated is a simplified one, consisting of a rectangular box through which groundwater flows in contact with variable vertical saturations of LNAPL, as determined by the user's specifications. Unlike most previously published methods, this toolkit considers groundwater transport *through* the LNAPL zone. Groundwater flow is one dimensional with dispersion and reactions in all directions. The geologic medium is homogeneous, as is the distribution of other related fluid and hydraulic properties. Simplified soil layering may also be implemented. Mass balance is accounted for in the partitioning from the LNAPL source to the water and vapor phases – that is, the total LNAPL mass as well as that of each of the soluble constituents within the LNAPL is recalculated for each time step. However, as mass is depleted from the LNAPL through dissolution and volatilization, the distribution (saturations) of the LNAPL is not recalculated from the initial condition, nor is the groundwater flux through the source zone re-calculated as the zone is depleted of LNAPL. Therefore, while the method considers relatively complicated multiphase and multicomponent cleanup and transport issues, it is critically important to remember that the homogeneity and simple dimensionality assumed by the toolkit are generalizations of a much more complicated system. The intended use of the toolkit is to bracket a range of physical and chemical expectations using site specific ranges of data. This manual provides guidance and field back-checks on the key assumptions, where possible.

There are many uncertainties and assumptions involved in use of this toolkit, and the user is cautioned to be fully aware of these before using the results for planning purposes. One prevailing source of uncertainty is site characterization, where generally sparse data sets must be broadly interpreted across the site. It is also common to find key multiphase parameters unmeasured, necessitating user estimation of one or more key factors. It is of fundamental importance to test toolkit assumptions against available field data and site specific parameter measurements to ensure that the scenario outcomes considered are generally realistic. As a conceptual screening tool, part of the analysis process should be to generate realistic conceptualizations of site conditions that can be extended to make site management decisions. Because of the potentially infinite variability in geologic and chemical parameter distributions, the toolkit can only address one set of parameters and distributions at a time. The toolkit is not a numerical model where highly complex site conditions can be reasonably represented. However, even at complex sites, the principles and estimates of the toolkit can be used to bracket a range of risk and cleanup expectations to guide corrective action strategies.

We have touched briefly and generally on the inherent assumptions in this evaluation method. A comprehensive list of assumptions is provided in Section 5, the User's Guide. The assumptions will be better understood once all the linked hydraulics and chemistry factors are described. Realizing that the intent of this method is to assess the benefit of various source treatment actions, it is very important that the assumptions and limitations are fully understood.

2.2 RISK BACKGROUND

Risk is a global term encompassing potential threats from contaminant releases to humans, resources, and the environment. Risk assessment practices allow clear identification of the potential chemical receptors, such as groundwater users, and the protection goals that may be appropriate. Risk is only one basis for setting target cleanup goals, as regulatory standards, public policy, business liability, and other factors may all be relevant. What one does with the concentration estimates derived from the toolkit depends directly on the context of the site and the applicable environmental restoration goals.

Many of the modern corrective action assessment frameworks have streamlined risk assessment practice by integrating site characterization, initial response action, exposure assessment, and risk management (e.g., Risk Assessment Guidance for Superfund, EPA, 1995; Risk-Based Corrective Action, ASTM, 1995). Regardless of the framework used, most quantitative risk assessment is based on four main components:

1. *Hazard identification* entails a qualitative assessment of site conditions and operating history to identify potential compounds of concern. For typical gasoline station operations, these compounds could include aromatic hydrocarbons and fuel oxygenates such as methyl tertiary-butyl ether (MTBE).

2. *Dose Response* entails defining the chemical hazard and toxicologic properties of the compounds of concern identified in the previous step. The result is a quantitative relationship between chemical dose and potential health hazards for either acute or chronic effects.

3. *Exposure Assessment* involves assessing the potential contaminant receptors and calculating the potential chemical concentrations at receptor points of contact. Receptors can include both people and environmentally sensitive habitats and animals. Chemical fate and transport calculations are included in this component. The points of contact often coincide with regulatory points of compliance.

4. *Risk Characterization* is the quantitative synthesis of the preceding steps under which the nature of the contaminant, its pathways, and receptors are combined to estimate specific risks of potential deleterious effects from the contaminant release.

Of the four risk assessment components above, exposure, chemical fate and transport (F&T), and remediation assessment often have the widest latitude for site specific scientific evaluation. This is because both hazard identification and dose response aspects are derived from epidemiological studies characterizing the potential environmental impacts to humans and other receptors of various chemical compounds. These studies are often statistically difficult and may involve inferences from one receptor to another that may or may not be valid in all instances (e.g., mice to people). Toxicologic studies are also time consuming and expensive and open to significant interpretation. Therefore, the general practice is to use standard chemical toxicity information provided by the U.S. EPA or other qualified sources.

For the reasons discussed, the degree of risk for a given site strongly depends on the results of receptor and fate and transport evaluations. Fate and transport evaluations are also the cornerstones of remediation planning and system design, since natural and artificial transport (i.e., cleanup) are both controlled by the same processes. This is reflected in the remediation selection aspects of risk-based frameworks.

When a risk reduction is suggested to be necessary, or when target thresholds are exceeded, the chemical concentrations reaching receptors must be reduced, or pathways eliminated, and methods should be selected based on their capability to effectively reach the desired goals. Risk reduction and current cleanup technology are often not synonymous because cleanup limitations often preclude significant risk reduction. In these cases, other risk management techniques are as protective of environmental and human health. The focus of this work is to aid users in deciding if common cleanup technologies will meet the site specific risk-based goals or other targets that may apply.

Section 3.0

HYDROGEOLOGY OF LNAPL FLOW IN THE SUBSURFACE

The fundamental principles of LNAPL hydraulics are identical to basic groundwater hydrogeology, but the devil is in the details. The differences between the flow of a single fluid in porous media and the flow of multiple fluids in the same media are significant, and directly impact mobility, recoverability, and risk associated with all phases (water, air, LNAPL). Every complexity of standard hydrogeology is magnified by the presence and interaction of multiple fluid phases. Often these effects are synergistic. For example, where there is a three order of magnitude range in the mobility of water between a medium-grained sand and a silt, there will be as much as a six order of magnitude difference in the mobility of an LNAPL under typical conditions. In the interest of time and sanity, we have attempted to bring some of the most salient concepts together in this section about LNAPL hydrogeology. Since whole volumes of work are dedicated to the subject, it is obvious that we must skip over many of the finer points in order to develop the technical story required to make this toolkit work. The bibliography scratches the surface of the works available in multiphase fluid mechanics and related disciplines; for those wishing more insight, however, it is a good place to start.

The main points of multiphase fluid hydrogeology can be highlighted in a few sentences, and are therefore not conceptually difficult. (1) Fluids flow downgradient – LNAPLs and water frequently have different gradients and gradient directions, so directions of groundwater movement and LNAPL movement must be assessed separately. (2) For a fixed set of fluid pressures, the size of the pore space controls the relative percentage of the pore space (phase saturation) occupied by each fluid – LNAPL and air displace water more readily from large pore spaces than from small pore spaces. However, once LNAPL has invaded a small pore space, it is more difficult to displace it with water than from a large pore space. (3) Fluids flow less readily when other fluids block their way – as LNAPL saturation increases, the mobility of LNAPL increases and the mobility of water decreases.

These are several of the key concepts necessary to build an understanding of multiphase flow. The following sections provide the individual pieces that link a description of the LNAPL source distribution to chemical transport from that source.

3.1 DISTRIBUTION OF LNAPL, WATER, AND AIR

The first controls of importance in the problem are the distribution of LNAPL, water, and vapor in the pore space. From these distributions come the mass of the impacts in the conceptual zone of interest, the relative mobility of each phase in the presence of others, and related factors like residual saturation. The following sections develop the fundamental hydraulics of multiphase fluid conditions.

3.1.1 Capillary Theory

The first subject deserving consideration in a multiphase fluid system is how to describe the distribution of the various phases (LNAPL, water, and air) in the subsurface. Granular soil may be view as an assemblage of tortuous pore tubes. In any small pore, capillary forces are usually a key element to the distribution of multiple phases in that pore, and therefore can be expected to play a critical role in multiphase hydraulics. Capillary forces are derived from the attraction of the surface of a liquid to the surface of a solid, which either elevates or depresses the liquid depending upon molecular surface forces. For most silicate granular soils, water rises in pore spaces in proportion to the interfacial tension of the water and inversely with the pore throat diameter, as discussed below. We will develop key concepts using the capillary tube analogy, and expand from there to natural granular soils. Only background is provided here; more expansive treatments can be found in the bibliography to this report (key capillary equations are in Appendix A).

Capillary tubes are a well-known physics/chemistry experiment. When a small diameter glass tube is placed in an open water bath, the water will rise in the tube due to capillary forces (Figure 3-1) exerted by the interaction of the pore wall material with water molecules (for this example). Since the water level in the bath is at atmospheric pressure, as is the surrounding air, it follows that the water that has risen in the tube must be held under tension. The capillary pressure at the top of the water column will be a function of the radius of the capillary tube (r) and the air-water interfacial tension, or surface tension (σ_{aw}), as given by $P_c = 2\sigma_{aw}/r$. Capillary head, or equivalently the height of the water rise (h_c) in the capillary tube, is simply the pressure divided by the unit weight of water, or $H_c = 2\sigma_{aw}/\gamma_w r$. Therefore, the capillary pressure and the height of capillary rise in a pore space are proportional to the interfacial tension and inversely proportional to the pore throat radius.

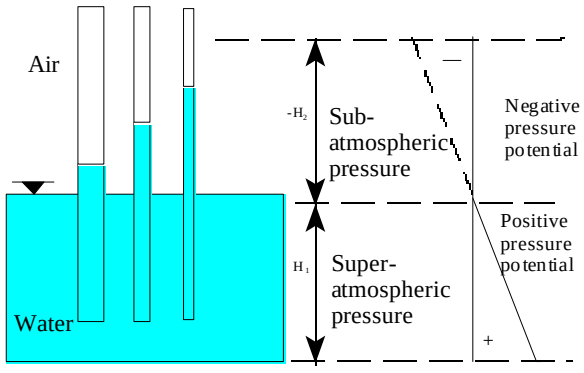

Figure 3-1. Schematic of a capillary tube bath. The water in the tubes is less than atmospheric above the open water table of the bath.

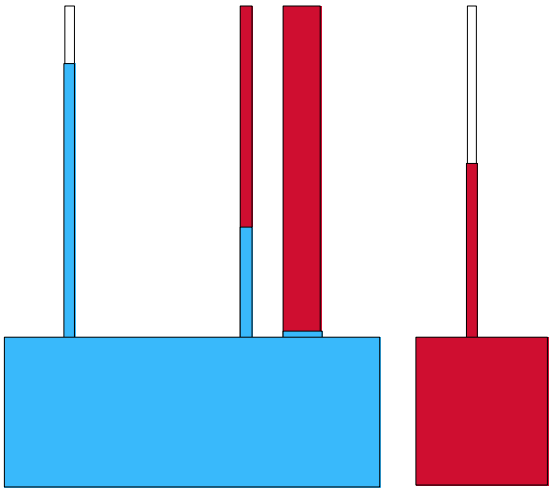

Figure 3-2. Capillary bath for 3 fluid phase couplets, water in blue, oil in red, air in white.

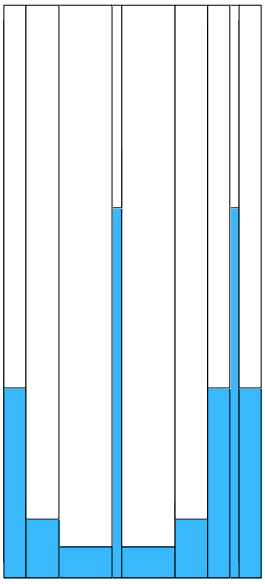

Figure 3-3. A schematic of mixed capillary rises for different pore-throats (i.e., tube sizes). In typical soil, a variety of pore-throat sizes are present resulting in this kind of variable saturation distribution.

Water and air, like water and LNAPL and LNAPL and air are immiscible, so it is not surprising to find there is analogous capillarity to LNAPL/water and LNAPL/air systems (Figure 3-2). In fact, the capillary pressure at the LNAPL/water (P_c^{ow}) and LNAPL/air (P_c^{oa}) interfaces in a capillary tube of radius r can be scaled to the capillary pressure at the air/water interface by recognizing that $P_c^{ow} = 2\sigma_{ow}/r$ and $P_c^{oa} = 2\sigma_{oa}/r$, where σ_{ow} and σ_{oa} are the oil-water and oil-air interfacial tensions, respectively. Because the radius r is a common factor, all capillary couplet systems can be related and scaled to a common system, usually the air-water system for convenience.

Extending these principles, soil can be viewed schematically as a suite of tortuous capillary tubes of differing pore diameters, with each size "packet" causing a different capillary rise (Figure 3-3). The usual graphical representation of the pore throat distribution (or capillarity) is often called the soil characteristic curve, the shape of which depends on the distribution of pore sizes for each soil (Figure 3-4). At equilibrium in a homogeneous media, these curves represent the water content as a function capillary pressure, or equivalently for the water-air couplet, elevation above the water table. As one moves upward in elevation above the water table (i.e., increasing capillary pressure), only the smaller pore throats hold water and the average moisture content decreases as air saturation increases.

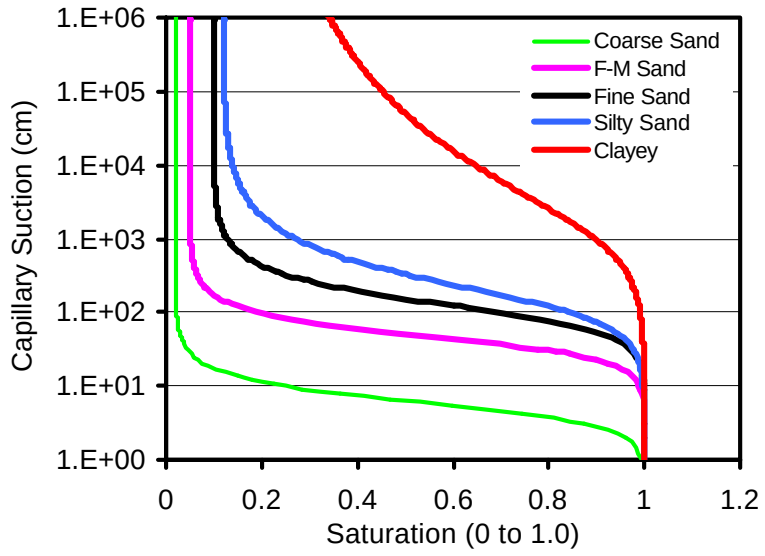

Figure 3-4. Capillary characteristic curves for typical soils. The curves represent the distribution of pore throat sizes.

As long as the fluid phases are continuous, the relative saturation of each is controlled by the capillary pressure and pore radius distribution. Capillary pressure (P_c) is simply the difference between the fluid pressure of the nonwetting fluid (P_{nw}) and the fluid pressure of the wetting fluid (P_w), or $P_c = P_{nw} - P_w$. Intuitively, if one applied enough driving force to a nonwetting fluid, such as air or LNAPL, the nonwetting fluid could

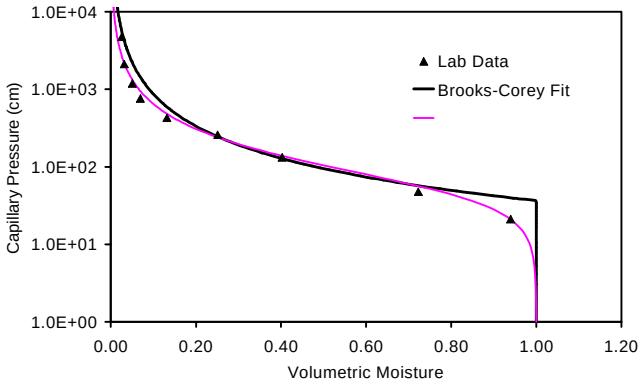

Figure 3-5. Lab data & best fit curves using both Brooks-Corey and van Genuchten models.

displace water from any pore space. But under natural conditions, it is observed that soil pore distribution has a significant impact on LNAPL, water, and air saturation under any pressure or gradient regime.

Given the description above, one can sense that high permeability materials with generally larger pore throats typically hold less capillary water (a small capillary fringe) than low permeability materials (a large capillary fringe) under equilibrium or for the same gradient conditions. These capillary descriptions of fluid saturation are the underpinning of all the remaining linked multiphase theory. As might be expected, complications to capillary properties and theory occur in soils with clays that shrink and swell, fractured materials, in pore structures undergoing certain types of chemical alteration, and under other atypical conditions. These conditions can result in a pore matrix that varies with time, making quantitative capillary description difficult. The interested reader is directed to the bibliography for other works touching on capillary theory and complexities.

It is worth mentioning that two commonly used capillary models differ in a key underlying assumption. The Brooks-Corey (BC) capillary function assumes a sharp capillary fringe height (step function) and a threshold immiscible phase entry pressure (Figure 3-5; Appendix A). That is, below a certain capillary pressure, it is assumed that water (or another wetting phase) will not be displaced or intruded by the nonwetting fluid. The van Genuchten (VG) function is continuous, and assumes that displacement of water by a nonwetting phase is possible at small capillary pressures, though the corresponding saturation of the nonwetting phase may be very small. It has been our experience, based on fitting many lab-derived capillary data sets (e.g., Figure 3-9), that the VG function generally provides a more representative fit, but there are cases where the BC function does an equally good and sometimes better job. The functions essentially converge for conditions where the “pore entry pressure” is exceeded, but vary significantly at pressures below the theoretical entry pressure value. This may not seem particularly important, but it has strong ramifications to the expected distribution of hydrocarbon in the source zones and the linked flow and chemical transport conditions. In this work, the VG capillary equation is used since the BC equation is essentially equivalent except at low pressures. One exception to this is the incorporation of an analytic hydraulic recovery screening model by others that uses the BC function (Charbeneau, 1999), as will be discussed in following sections with supporting equations in Appendix B.

We have noted above that all immiscible fluid couplets (e.g., LNAPL/water, water/air, air/LNAPL) respond to capillary forces in proportion to interfacial tension and pore throat radii. For the case we are considering, water, LNAPL, and vapor coexisting in the aquifer and capillary zone, capillary definition is needed for each couplet system. It has been observed that the soil capillary curves and properties are generally scalable between fluid pairs by the ratio of the interfacial tensions between the couplets of interest (Leverett, 1941; Parker, 1987). Often, lab measurements of capillarity are performed using air and water for agricultural and geotechnical applications, or measurements using air and mercury in some oil reservoir work. Each of the different test methods generates a two-phase capillary curve that represents the underlying pore throat distribution and fluid retention as a function of capillary pressure. These relationships can be scaled to other couplet systems using the interfacial tension ratios so that all three capillary couplets of interest here are defined (Figure 3-6; equations in Appendix A).

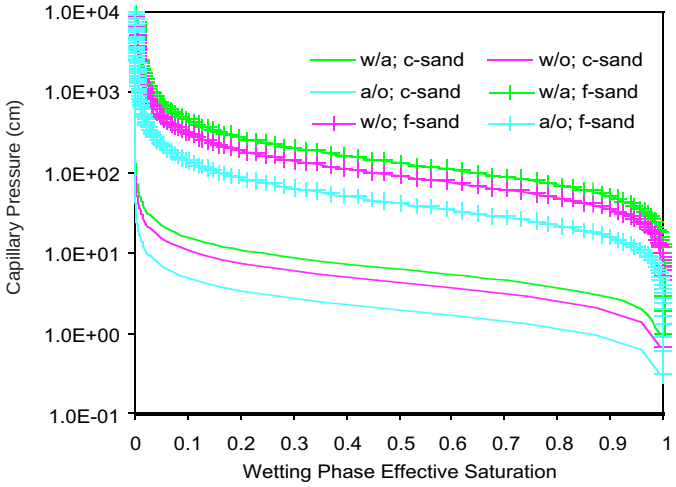

Figure 3-6. Characteristic capillary curves for 3 phase couplets in 2 sands. The shapes are identical, the offsets caused by the differences in interfacial fluid tension (IFT) and fluid density.

3.1.2 Distribution of Fluids Under Vertical Equilibrium

The relationships above can be extended to estimate field fluid saturation of LNAPL, water, and air in the capillary and water table regions. The sections below will first develop these relationships for homogenous soils, and then discuss how the same principles may be applied to heterogeneous systems. The full mathematical development is provided in Appendix A.

3.1.2.1 Homogeneous Soils. For environmental conditions, it has been observed that if sufficient time is allowed for the LNAPL to come to vertical equilibrium (VEQ) the LNAPL thickness observed in a well can be used to determine the capillary pressure relationships between the various phases (Farr et al., 1990; Lenhard & Parker, 1990). VEQ implies the vertical gradient in each phase (water/LNAPL) is zero throughout the mixed saturation profile. That is, there is no vertical gradient for LNAPL or water to move vertically in the equilibrated system. In such a system, the oil-water capillary pressure (P_c^{ow}) is zero below the oil-water interface in the formation or monitoring well, and is a function of the relative density of the LNAPL ($\rho_{ro} = \rho_o/\rho_w$), where ρ_o is the LNAPL density and ρ_w is the density of water and the height above the oil/water interface (h_{ow}). Similarly, the oil/air capillary pressure (P_c^{oa}) is zero below the oil/air interface in a monitoring wells and is a function of

the LNAPL relative density and the height above the oil/air interface (h_{oa}). These capillary pressures under VEQ, respectively, are: $P_c^{ow} = (1-\rho_{ro})\ h_{ow}$ and $P_c^{oa} = \rho ro\ (h_{ao})$.

Once capillary pressure is defined, it is combined with capillary soil and fluid properties to result in the saturation profiles of each wetting phase of interest (Fig. 3-7). This is analogous to oil/brine/gas boundary relationships defined in the oil production industry (Bradley, 1987; Chatzis et al., 1983). Specifically, above the

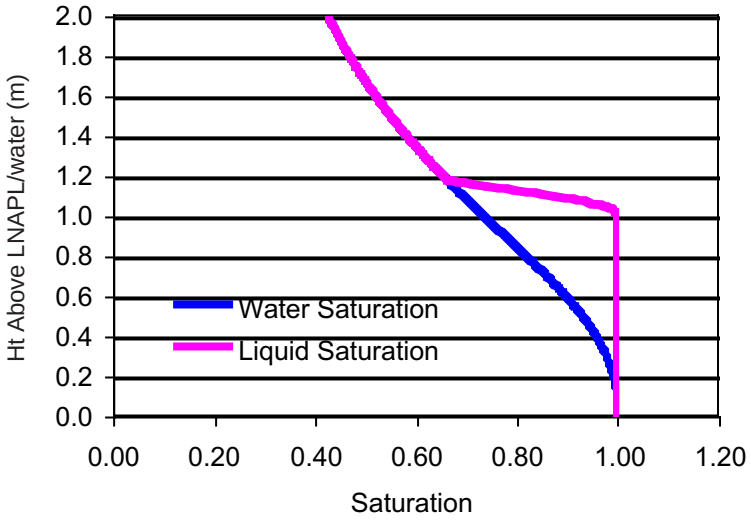

Figure 3-7. Wetting phase saturations, water below the LNAPL/air interface in the formation for 1 m of equilibrated LNAPL, and total liquid saturation above. The sum of all phases (air, water, LNAPL) is always 1.0, so by subtraction, all saturations can be defined.

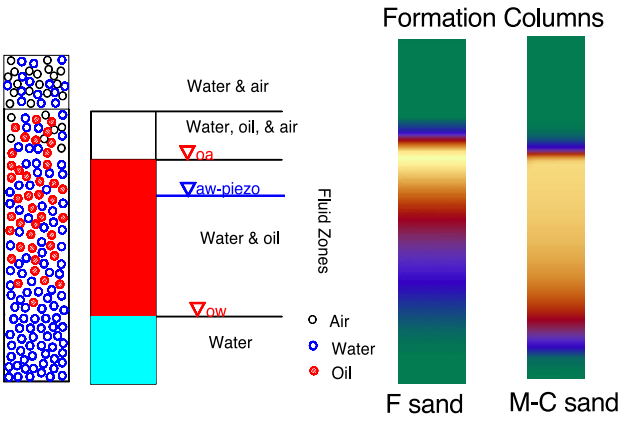

Figure 3-8a. Schematic of pore and well distribution of free product (after Farr et al., 1990) and calculated formation saturation columns.

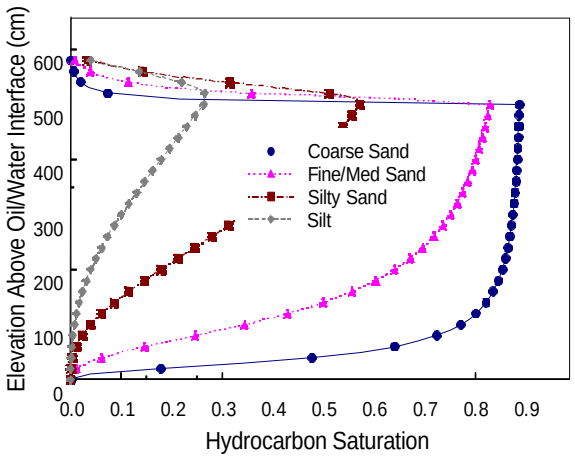

Figure 3-8b. Oil saturation estimated for various soils based on capillary properties and VEQ for 500 cm thickness.

oil/water interface and below the "oil table", the water (wetting phase) and LNAPL (nonwetting) saturation is controlled by the LNAPL/water capillary pressure. Since the total saturation = 1.0, the LNAPL saturation is simply 1 - S_w. Above the oil/water liquid table, the liquid (S_l) and air saturation (LNAPL & water) are controlled by the oil/air capillary pressure. The air saturation is (1-S_l). From these definitions we can now describe the equilibrium LNAPL saturation profiles in the formation for any known set of soil, fluid, LNAPL thickness and associated capillary pressure conditions (Figures 3-8a & b). These profiles are usually plotted as height above the LNAPL/water contact because this is the datum where the capillary pressure differential begins. Keep in mind that this elevation is not the same as, but simply related to, the capillary pressure (see equations above, and in Appendix A).

The capillary relationships are exponential, and therefore very sensitive to soil type (pore size distribution) and equilibrated LNAPL thickness, or equivalently the LNAPL pressure head in the formation. In fact, as will be demonstrated subsequently, capillary properties are more important than intrinsic permeability or hydraulic conductivity. Because of this sensitivity, site-specific values of capillary properties are important in the analysis. Direct measurement of those capillary properties is preferable to values inferred from soil texture descriptions.

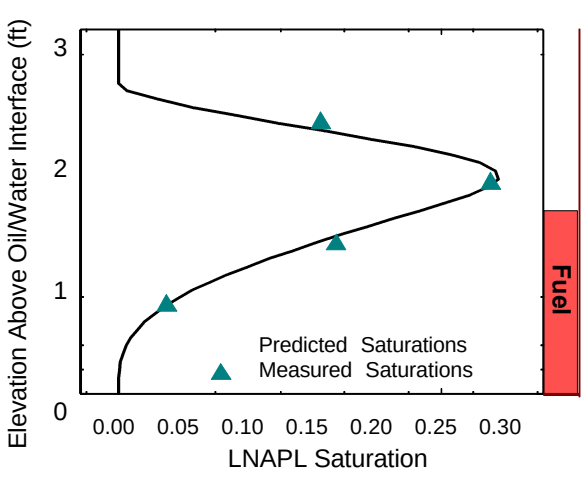

Figure 3-9a. Comparison of the capillary model to fuel saturation data collected at a dune sand site.

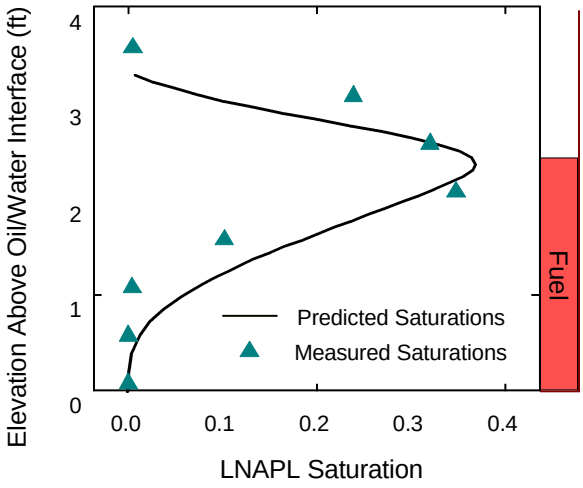

Figure 3-9b. Saturation data from the same site, but with a larger observed well thickness.

Experience has indicated that where the hydrostatic equilibrium assumption is satisfied, field and lab measurements strongly agree with capillary theory (Figures 3-9a and b). Like any sound physical model (and this model has 50 years of practical oil field use to back it), when the assumptions are met, the principles explain real observations. In contrast, several published lab experiments appear on the surface to conflict with capillary theory applied to environmental situations until one recognizes that the necessary VEQ boundary conditions have not likely been satisfied (e.g., Ballestero et al., 1994; EPA, 1995). Again, capillary theory has worked well for decades in the petroleum industry, and the analogy to environmental LNAPL conditions is fairly clear (Jennings, 1987; Farr et al., 1990). While disequilibrium

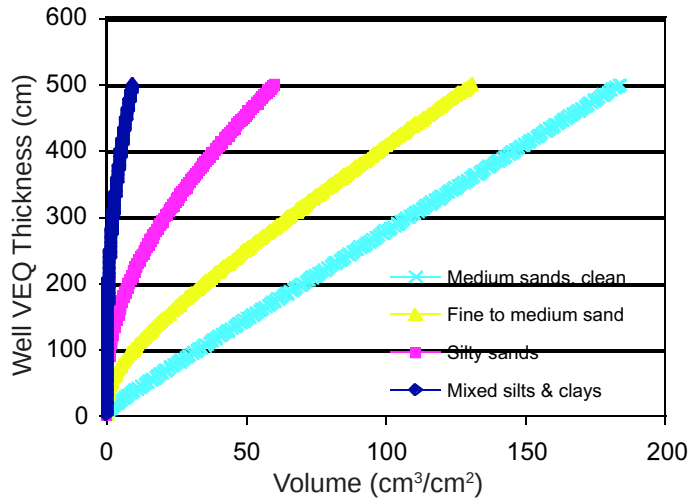

Figure 3-10. Integrated VEQ formation LNAPL volume as a function of theoretical observed well thickness for several soils.

conditions clearly complicate matters, as will be discussed subsequently, capillarity remains a fundamental cornerstone of fluid mechanics and is *required* to explain virtually any multiphase condition. Like all scientific endeavors, improvements to the theory are expected through time but, without a doubt, phase saturations are related to pore size distributions, fluid properties, and fluid pressures.

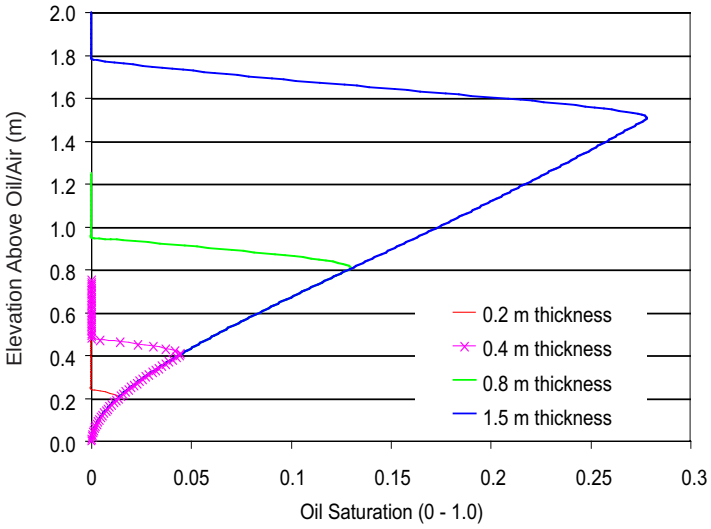

Figure 3-11. LNAPL saturation profiles for different equilibrated thicknesses in a silty sand showing nonlinear dependency on capillary pressure as related to thickness.

Perhaps the easiest way to picture the in situ LNAPL "floating within" the water table is by analogy to an iceberg. Most people recognize that the iceberg is 90% submerged because ice is less dense (0.9 g/cc) than water (1 g/cc). For an LNAPL thickness at equilibrium with a density of 0.75 g/cc, about 25% of the thickness will be above the water table, and 75% below. However, because the smaller pores will retain water against the weight of the LNAPL, the displacement in soil is volumetrically less than 100%. So, while there is no *thickness* exaggeration, there is an apparent *volume* exaggeration between observed thicknesses and volume in the formation. The volumetric fraction of LNAPL at and below the water table is strongly dependent on soil capillary characteristics, with coarser soils usually have much larger sub-water table impacts than fine materials (e.g., Figures 3-7 through 3-10).

The LNAPL saturation profile in the formation, when vertically integrated, provides a volume per unit area which, as we have seen, depends on the capillary pressure (or correlated equilibrated thickness) and the capillary properties (Figures 3-10 & 3-11; Appendix A). The area integration of the LNAPL volume per unit area estimates for all wells in a plume exhibiting free product results in an estimate of the total plume volume. Be aware that if the system is not under ideal VEQ conditions, or if there is a significant "smear" zone, the volume estimate will be in error, as is discussed later. Also recognize that since the local area volume is reported in units of volume per unit area (e.g., ft^3/ft^2; cm^3/cm^2; gal/ft^2, etc.), the dimensions reduce to units of length. This is often misinterpreted as a thickness exaggeration, which it is not. The data and theory covered above clearly show that the LNAPL-impacted vertical interval is always greater than the equilibrated thickness observed in a monitoring well under VEQ conditions. This is critically important because the volume of impacted aquifer material, as well as the LNAPL distribution within that volume, are key controls over cleanup, dissolution, biodegradation, and risk. Note that there are field conditions where product can be perched and a thickness exaggeration is possible due to the well acting as a local drain, as well as transient (non-equilibrium) conditions where thickness exaggeration is also possible.

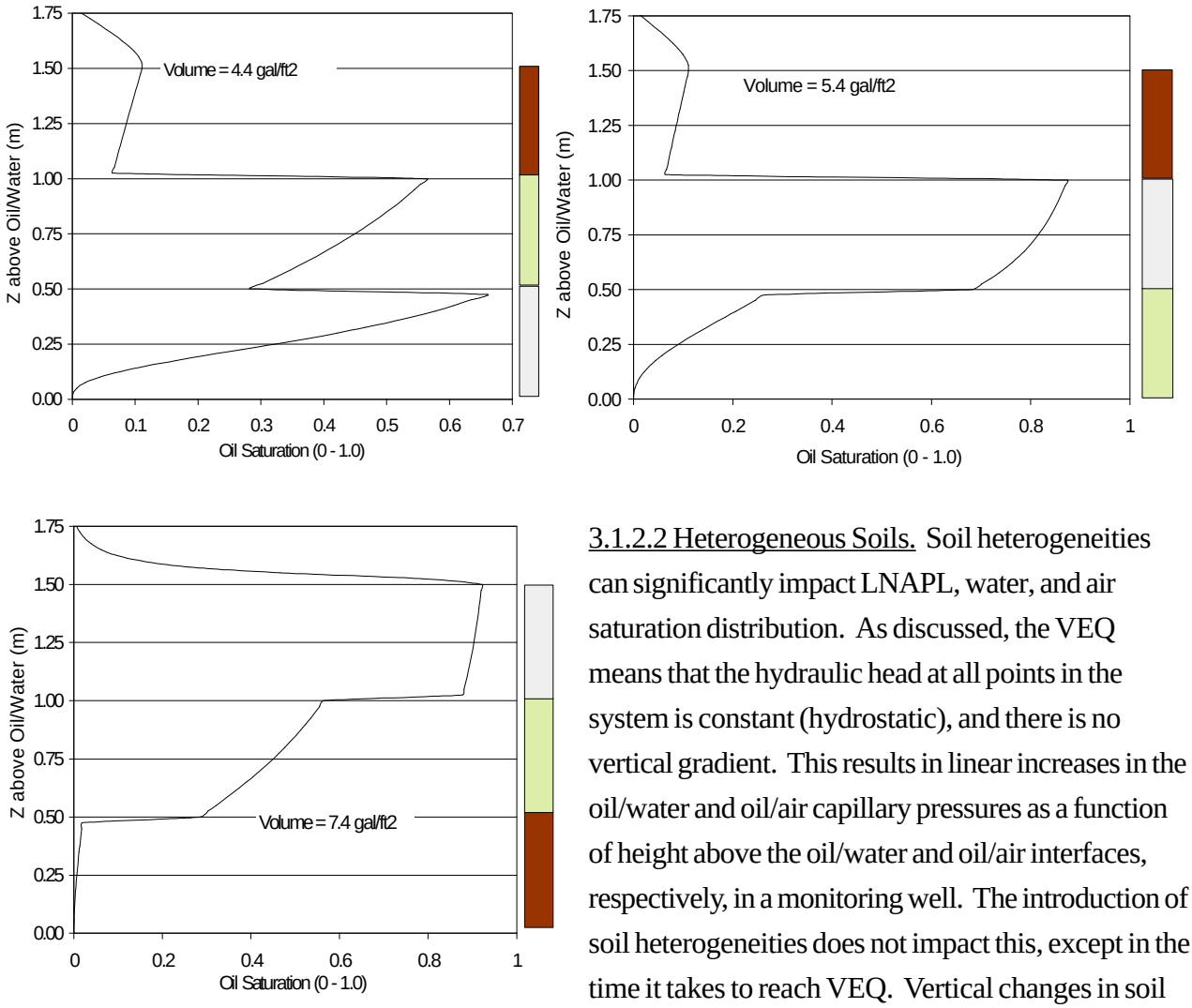

Figure 3-12a, b, and c. The VEQ distribution of gasoline as a function of stratigraphic position through the LNAPL zone. Medium sand = speckled; fine sand = white; silty sand = grey.

3.1.2.2 Heterogeneous Soils. Soil heterogeneities can significantly impact LNAPL, water, and air saturation distribution. As discussed, the VEQ means that the hydraulic head at all points in the system is constant (hydrostatic), and there is no vertical gradient. This results in linear increases in the oil/water and oil/air capillary pressures as a function of height above the oil/water and oil/air interfaces, respectively, in a monitoring well. The introduction of soil heterogeneities does not impact this, except in the time it takes to reach VEQ. Vertical changes in soil capillary properties, however, result in a heterogeneous LNAPL distribution. This heterogeneous fluid saturation profile can be calculated simply by using the capillary pressure calculated under VEQ and the appropriate soil capillary curve for each soil type in the vertical sequence. For most vertically heterogeneous sequences, the maximum saturation and mass are controlled by the coarsest beds (lowest capillarity), although vertical position in the impacted zone can be important. For instance, if we juxtapose three beds of different soil types and equivalent thickness (0.5 m; Figures 12a-c), we see that the LNAPL saturation profiles vary significantly as a function of position. The soils contrasted are a clean medium-grained sand, a fine-sand, and a silty sand. Notice that the formation LNAPL distribution varies significantly depending on the ordering of the beds, and that the total volume associated with each stacking is different. The greatest volume is where the medium sand is at the top of the LNAPL column, resulting in about 7.4 gals/ft^2 under the curve.

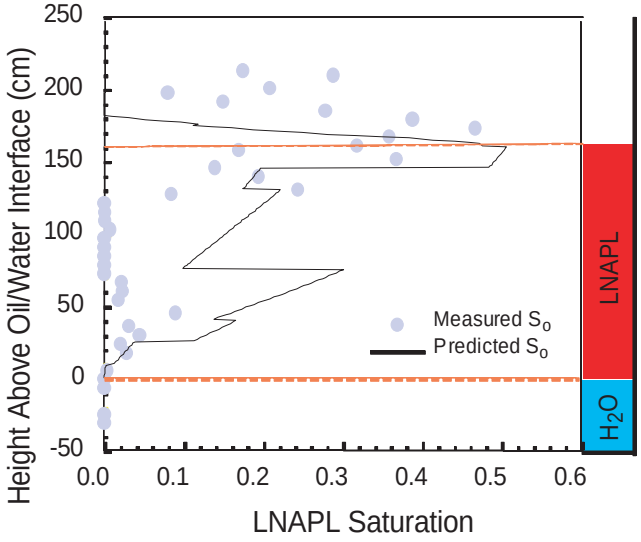

Figure 3-13a. Predicted versus measured LNAPL profile in an interbedded sand and silty sand formation in San Diego (Huntley et al., 1994). Note transient stranding above the current liquid table.

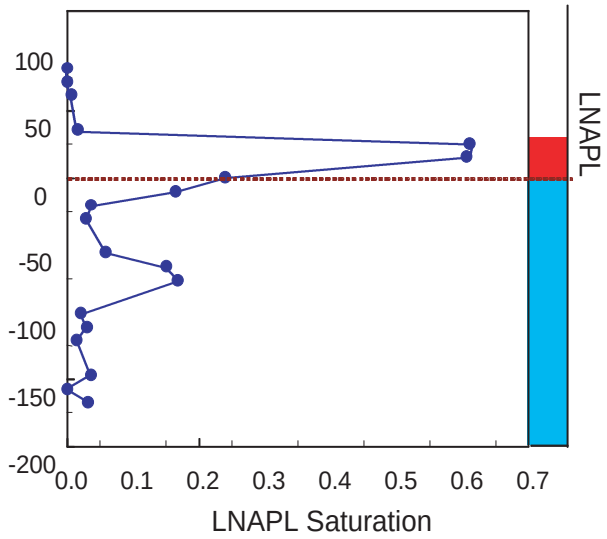

Figure 3-13b. Measured LNAPL saturation in a fine sand following a rise in the water table. Note stranding below the water table, and transient compression of the small thickness LNAPL zone.

It is useful to look at heterogeneous field conditions for comparison to theory. A detailed field study (Huntley et al., 1994) of fuel distribution in a widespread LNAPL plume showed that LNAPL distribution was strongly controlled by the vertical distribution of capillary properties relative to observed LNAPL in observation wells (e.g., Figure 3-13a). The example site exhibited highly variable LNAPL saturations that were generally, but not specifically, represented by the capillary model. The LNAPL saturation and soil data indicate there is a tendency for coarser materials to more closely match the capillary predictions than fine-grained materials. Although more study is needed, a logical explanation for this observation is that fine-grained materials require significantly longer equilibration times, and in practicality may never equilibrate fully. Similarly, one also finds "stranding" or "entrapment" of LNAPL below the water table in the field after the water table has risen (Figure 3-13b). This effect is caused from hysteresis and disequilibrium effects and contrasts in the effective conductivity of the water versus the LNAPL (discussed subsequently).

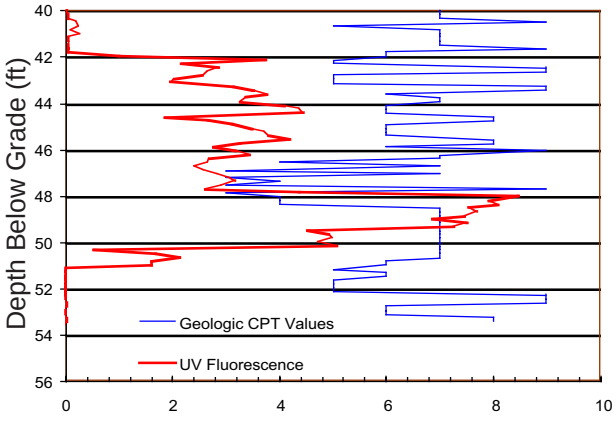

Figure 3-14. Downhole cone penetrometer and fluorescence logging showing inch-scale variability in geologic properties and LNAPL saturation (proportional to fluorescence log).

We see these same occurrences in indirect measurements of saturation, such as induced laser or ultraviolet fluorescence logging (Figure 3-14). In fact, geophysical logging may be one

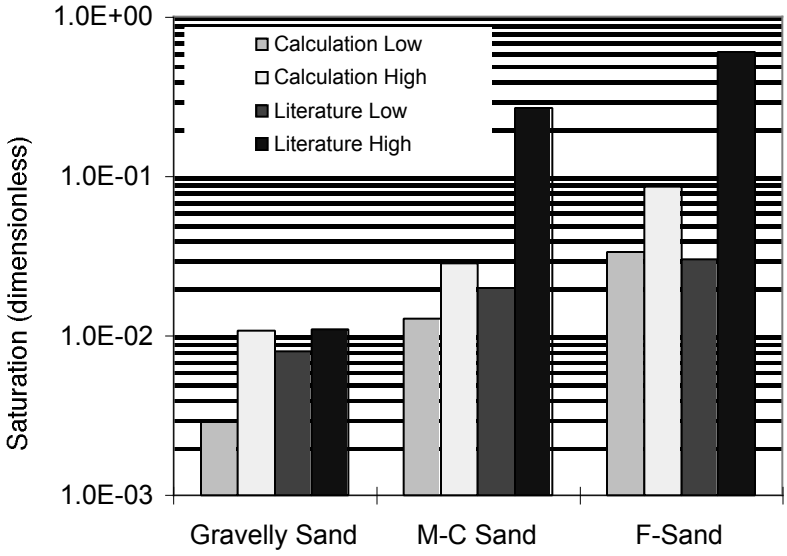

Figure 3-15. Range of residual gasoline saturation for 3 soil types (from Mercer & Cohen, 1990). Calculated ranges from Parker (1987; see Appendix A).

of the few techniques capable of cost-effectively detailing small-scale variability in geologic bedding and LNAPL distribution. In any case, when conditions are heterogeneous, expect idealized equilibrium capillary theory to encounter difficulties, not because the theory is flawed, but rather because thorough definition of the system is difficult and equilibrium is often not established. As shown above, if the scale of interbedding is known, heterogeneous LNAPL saturation profiles can be estimated. This is one option available for the LNAPL source description in the accompanying software utility, which is then used for calculations of groundwater dissolution and volatilization. Keep in mind that equilibrium conditions, by definition, do not account for complications of water table fluctuation and other transient LNAPL migration events. The vertical equilibrium assumption should be invoked and trusted only when justified by field conditions and data.

3.1.3 Hysteresis and LNAPL Entrapment

The capillary characteristics discussed above focus on the relations between capillary pressure and LNAPL saturation under conditions where LNAPL is displacing water from pore space, that is where LNAPL is invading a water saturated area. Important differences occur when the reverse happens, when water displaces water from pore spaces, such as occurs during any hydraulic remediation or water flooding exercise. Laboratory and field measurements indicate that porous media have a relatively large capacity to hold fluids, including LNAPL, against natural drainage forces. For instance, in water driven oil reservoir conditions, it is common for retained LNAPL to be present at saturations, called residual saturations, from 20 - 60% (in Bradley, 1987). Residual gasoline saturation in sands has been documented to range from as low as 2% to as high as 60% under a range of

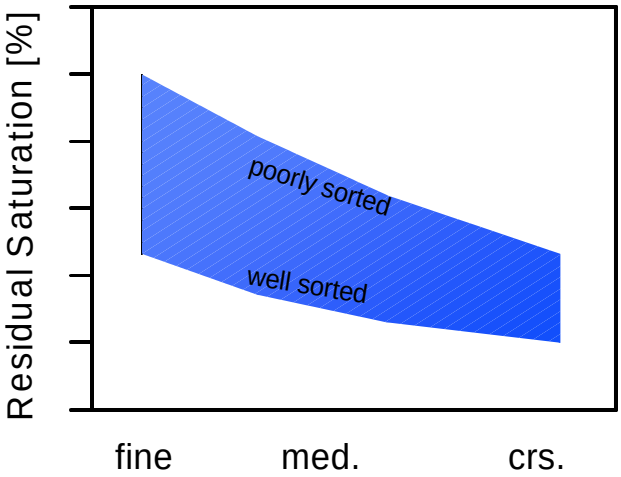

Figure 3-16. Schematic from available data ranges for residual LNAPL saturation in reservoir materials showing dependency on sorting and tortuosity.

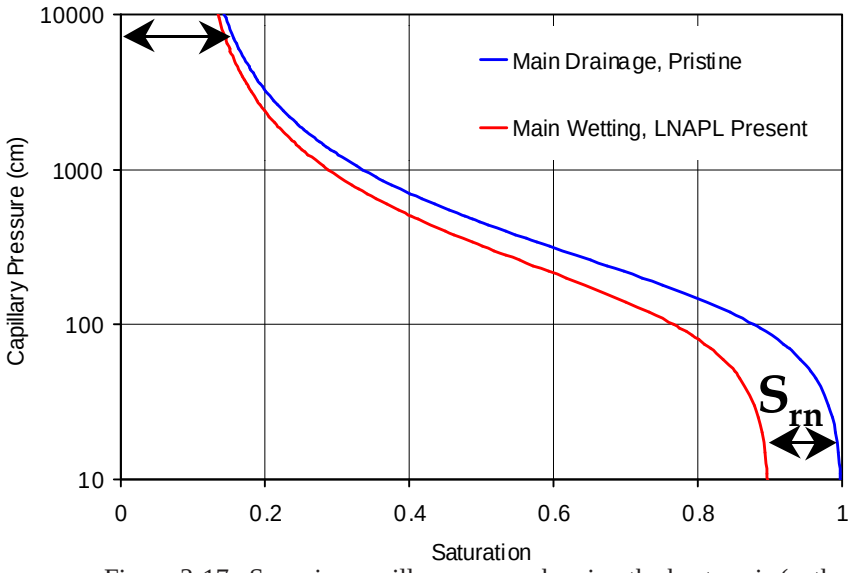

Figure 3-17. Scanning capillary curves showing the hysteresis (path dependency) effect for the wetting phase (water) displaced by LNAPL. Residual LNAPL saturation (approximately 15% in this case) fills pore space formerly occupied by water in the pristine system. The curves are plotted against capillary pressure head (cm) of the LNAPL/water system.

lab and field conditions (Figure 3-15; Mercer & Cohen, 1990).

Residual saturation tends to increase as soil becomes finer-grained, porosity decreases, and pore heterogeneity increases (Figure 3-16; Beckett & Lundegard, 1998; Chatzis et al., 1983). The LNAPL interfacial tensions and viscosity can also have some effect. Because of a limited environmental database, it is necessary to combine the residual saturation findings from agriculture and petroleum production to broaden the range of applicable values. Databases of LNAPL parameter values are needed to assist in further constraining the range of residual saturation for environmental conditions.

The explanation for residual saturation lies in the complexity and tortuosity of discrete pore pathways and the closely related concepts of hysteresis and entrapment. As a result, the capillary curve controlling water saturations are different for LNAPL displacing water (Drainage curve, Figure 3-17) compared to water displacing LNAPL (Wetting curve, Figure 3-17). This difference between the wetting and drainage curves is called hysteresis, and has been documented for many decades in agricultural (Stephens, 1996; Corey, 1986). The most important implication of hysteresis to the subject at hand is that the re-wetting curve (Figure 3-17) never achieves a water saturation of 1.0. This means that no matter what fluid pressures are applied in a water flooding operation, or how long we attempt to recover LNAPL hydraulically, water will not displace all of the LNAPL from the pore space, resulting in entrapped residual LNAPL. The difference between the maximum water saturation under drainage conditions (1.0) and the maximum water saturation under re-wetting (Figure 3-17) is the nonwetting phase residual saturation (S_{rn}, Figure 3-17). The entrapment occurs because the continuous pore pathways for

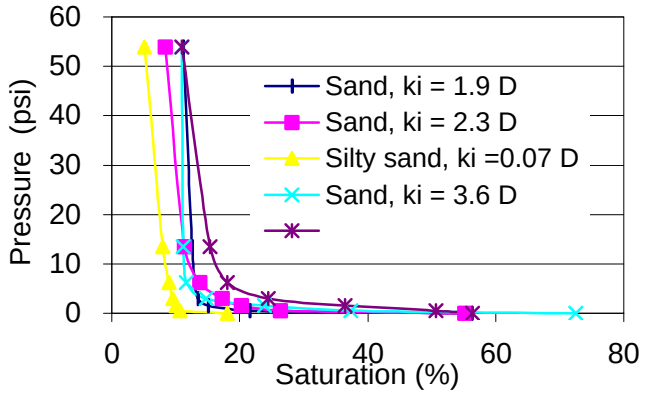

Figure 3-18. Lab measurements of LNAPL saturation versus applied pressure for different soil (permeability given in Darcys [D]); endpoints are residual LNAPL saturation, field LNAPL capacity is somewhere near the inflection of the curves.

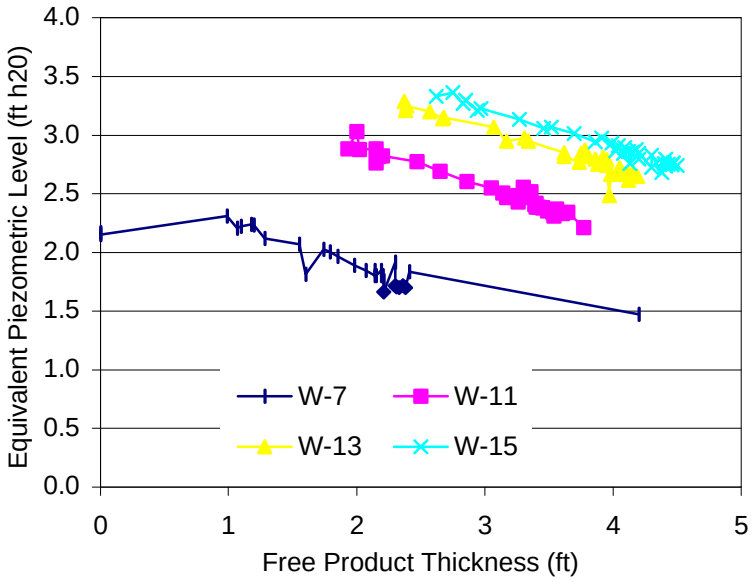

Figure 3-19. Data showing the inverse relationship between free product thickness and piezometric pressure over six years of monitoring. The individual measurements are from variable times, as shown in Figure 3-20.

LNAPL get cut off when the LNAPL saturation falls below a certain threshold. Not surprisingly, the more heterogeneous the pore or grain-size distribution, the greater the LNAPL stranding capacity of the particular soil (Figure 3-15). Nor is it surprising that the residual LNAPL capacity is often greater in the saturated zone than in the vadose zone (Lenhard & Parker, 1988).

It is important to distinguish between true residual LNAPL saturation, which is a lab measurement under ideal two-phase conditions, and ***field residual saturation***, which is invariably a larger value due to the influence of field scale heterogeneity. Heterogeneity can trap LNAPL in zones where, although present above true residual, it is immobilized by the surrounding materials. The field residual saturation is the best-case endpoint of any hydraulic recovery scheme, and is a key factor used in cleanup and chemical depletion calculations herein.

Lab measurements of "residual LNAPL saturation" are variable and may not really measure the hysteresis effect that causes true residual saturation. Drainage of LNAPL from core samples to residual saturation is generally very slow. Therefore, labs may estimate "residual LNAPL saturation" under an induced pressure gradient (e.g., centrifugation, pressure permeameters, etc.). Many of these tests are 3-phase, with air under pressure used to drive both water and LNAPL out of the pore space. These tests allow rapid screening of retained LNAPL under these conditions, but are not a true residual measurement (e.g., Figure 3-18). True residual LNAPL saturation values are usually larger, so this variety of lab values called "residual saturation"

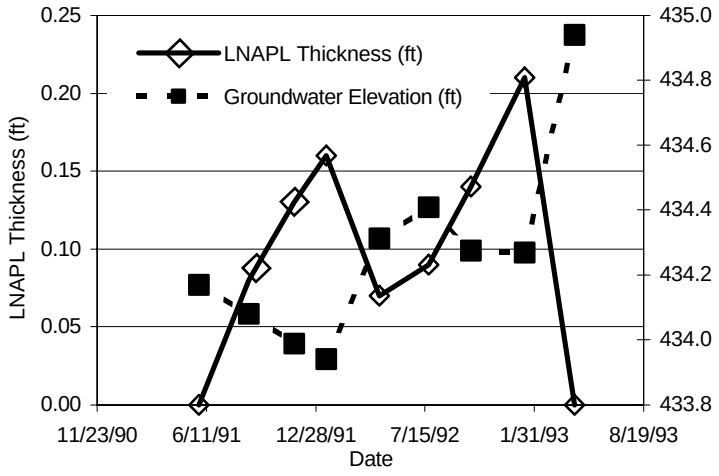

Figure 3-20. Data showing time series graph of product diminishing and increasing dependent simply on groundwater elevation.

should be used with caution. These types of measurements are of value for evaluating vadose zone residual (a 3-phase system) saturations and air-based cleanup schemes where vacuum or pressure is applied.

In addition to the residual saturation controlling the best-case endpoint to remediation using hydraulic approaches, the concept of residual saturation has significant implications with respect to the distribution of LNAPLs in the subsurface under conditions of a rising water table. Once LNAPL has invaded a pore space, increases in the fluid pressure of the wetting phase, such as that produced by a rising water table, will act to displace LNAPL out of that pore space. This displacement of LNAPL by water is, again, limited by the residual saturation of the LNAPL. Therefore, a rising water table will act to entrap LNAPL below the oil/water interface in a monitoring well, producing what many workers refer to as a "smear zone". This process is enhanced by the low mobility of LNAPL compared to that of water, as will be discussed later.

This LNAPL entrapped via this mechanism will not be amenable to any form of hydraulic remediation, but will contribute significantly to the dissolved-phase plume downgradient of the source area. This is a significant impact in areas where water tables have risen due to basin management or natural hydrologic system changes. For instance, in Southern California, salt water barrier projects and changes in basin pumping have caused groundwater levels to rise several tens of feet in some areas, stranding significant quantities of product below the current water table. In addition, if the surface source of an LNAPL has been eliminated, this rising water table will redistribute a fixed mass of LNAPL over a larger vertical interval, resulting in a decreased thickness of hydrocarbon in a monitoring well (Kemblowski & Chiang, 1990). The result is that LNAPL thickness can vary significantly with changes in groundwater elevation. We often observe that free product thins or "disappears" from observation wells with even modest rises in the water table, only to reappear when the water table falls (e.g., Figures 3-19 and 3-20). This is a good example where the presence of, or lack of, observable free product in a well is often irrelevant to risk, since under these "stranding" conditions the source for risk is unchanged. As we will see, the change in product thickness in observations wells is, of itself, often a poor indicator of risk or risk benefits associated with cleanup efforts.

3.1.4 Implications of LNAPL, Water, and Air Distribution

The mass and distribution of LNAPL is the control over rates of dissolution and source longevity. Though the equilibrated thickness of LNAPL in an observation well is always less than the thickness of the impacted aquifer zone (no thickness exaggeration), the volume of LNAPL in the formation is always less than that indicated by the equilibrated thickness in the monitoring wells and the formation porosity (volume exaggeration). Therefore, the formation LNAPL volume is smaller and the volume of impacted aquifer material larger than implied by the thickness of LNAPL in a monitoring well.

A rising water table, water flooding, or hydraulic recovery all act to entrap LNAPL in pore space because of hysteresis and related effects, including those of effective conductivity contrasts that will be discussed in the following sections. The implications of these processes and the resultant entrapment are several-fold. First, it implies that, for a fixed mass of LNAPL, the thickness of LNAPL in a monitoring well may vary significantly without any remediation whatsoever. Second, significant mass of LNAPL may be found below the oil/water interface in a well, acting as a source of dissolved-phase hydrocarbon, but not removable by any hydraulic remediation approach.

Finally, it is important to emphasize that no liquid-phase hydraulic recovery scheme can recover beyond the field residual LNAPL saturation, regardless of how efficiently designed or operated. Further, well interference and other recovery inefficiencies will almost always be present, causing actual LNAPL saturation endpoints in the formation to be much larger than residual saturation. This is important, in that the mass left in place after remediation, together with the distribution of that mass, ultimately controls the longevity of the source area as a source of dissolved-phase contamination, and therefore the success of the remediation. Ultimately, the link between risk reduction and remediation is dependent on the degree of mass removal and the distribution of residual mass of LNAPL chemicals of interest. For conditions of high residual LNAPL saturation, one correctly suspects that LNAPL recovery has little effect on risk magnitude since a significant source will still remain at the endpoint of hydraulic cleanup. Fundamentally, the ***field residual LNAPL saturation*** will be one of the most important input parameters in the quantitative evaluation of the source area and its link to dissolved and vapor-phase concentrations and risk.

3.2 LNAPL AND WATER MOBILITY

The mobility of LNAPL and water in the presence of each is important to the problem of LNAPL in water table region. The mobility of groundwater in the presence of LNAPL determines, in part, the partitioning and transport of soluble components from the LNAPL. The mobility of the LNAPL will determine is recoverability, as well as whether the analysis of a "static,, LNAPL source is warranted. As discussed previously, one of the potential risks in an LNAPL scenario is direct transport of the LNAPL phase to a receptor. Therefore, understanding phase mobility will assist the user in using the principles and analytic methods herein.

3.2.1 Relative Permeability and Effective Conductivity

We have already noted qualitatively that fluids flow less readily when other fluids share the pore space. From the section above, we now know how to estimate the fraction of one fluid versus another in the formation. We will now develop the fundamentals of the relative permeability concept that describes limitations to flow as a function of phase saturation.

Darcy's law for a multiphase system is:

$$q = k_r k_i \frac{\rho_f^g}{\mu_f} i \quad \text{Equation 3-1.}$$

where $\mathbf{q}$ *is the specific discharge of the fluid of interest,* $\mathbf{i}$ *is the hydraulic gradient of that fluid,* ρ_f *is the density of that fluid,* $\mathbf{g}$ *is the acceleration due to gravity,* μ_f *is the viscosity of that fluid,* $\mathbf{k}_i$ *is the intrinsic permeability of the soil, and* $\mathbf{k}_r$ *is the relative permeability of the soil with respect to the fluid of interest.*

This expression is often shortened to $q = K_e\, i$, *where* K_e *is the effective hydraulic conductivity of the soil with respect to the phase of interest, defined as;*

$$K_e = k_r k_i \frac{\rho_f^g}{\mu_f} \quad \text{Equation 3-2.}$$

Most of these expressions are familiar to even those unfamiliar with multiphase flow. The expressions simply state that the rate of flow is proportional to the gradient, the intrinsic permeability of the soil, the density of the fluid and inversely proportional to the viscosity of the fluid. The term added to the expression for multiphase flow is k_r, the relative permeability. Relative permeability is simply a

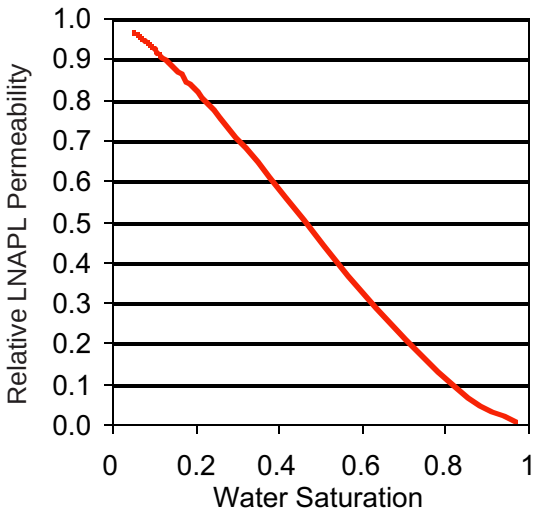

Figure 3-21a. Relative LNAPL permeability in a sand as a function of wetting phase saturation (Mualem function, 1976).

scalar ranging from 0 to 1.0 that describes the decreasing mobility of any phase with decreasing phase saturation (Figure 3-21a). The phenomenon of relative permeability has long been recognized in the oil production industry and is responsible for limits on practical recovery even when significant petroleum remains in the formation (Chatzis et al., 1983; Tyler & Finley, 1991).

This decrease in relative permeability with decreasing phase saturation is due to the fact that, as the phase saturation (of any fluid) decreases, the flow capacity also diminishes, as the flow path becomes more tortuous and disconnected. Flow is impeded by the presence of other immiscible phases blocking the pathways. Except for large LNAPL thickness in formations and in coarser materials, LNAPL saturation under most environmental conditions is relatively small (recall Figure 3-12) and, therefore, the relative permeability toward LNAPL is also often small. There are many functions used in agriculture and petroleum engineering that describe relative permeability as related to phase saturation (e.g., Stone, 1973; Honaphour, 1988; Mualem, 1976; Burdine, 1952; Gardner, 1956). In this work, the Mualem form is used (Appendix A), but for all the functions, the relative permeability of each phase varies exponentially with saturation, which in turn varies according to capillary properties, as previously discussed.

Because relative permeability is sensitive to phase saturation, which in turn depends exponentially on capillarity and pressure, the relative permeability increases with increasing height above the oil/water interface under VEQ conditions (Figure 3-21b), and the maximum relative permeability increases with the observed thickness of LNAPL in a monitoring well (Figure 3-21b). The effect of soil type is even more marked because, as discussed earlier, LNAPL saturations are greater in coarse-grained formations than in fine, and because the intrinsic permeability of coarse-grained formations are greater than that of fine-grained formations, the effective conductivity of the LNAPL phase in coarse-grained formations is much, greater than that of fine-grained formations for the same equilibrated thickness in a monitoring wells (Figure 3-22).

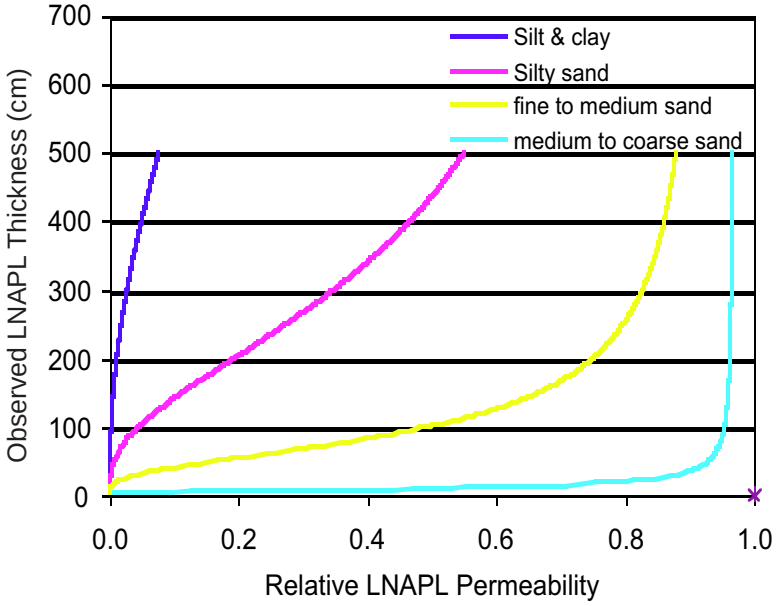

Figure 3-21b. Relative LNAPL permeability as a function of observed oil thickness. Recall that the LNAPL saturation is an exponential function of thickness per capillarity.

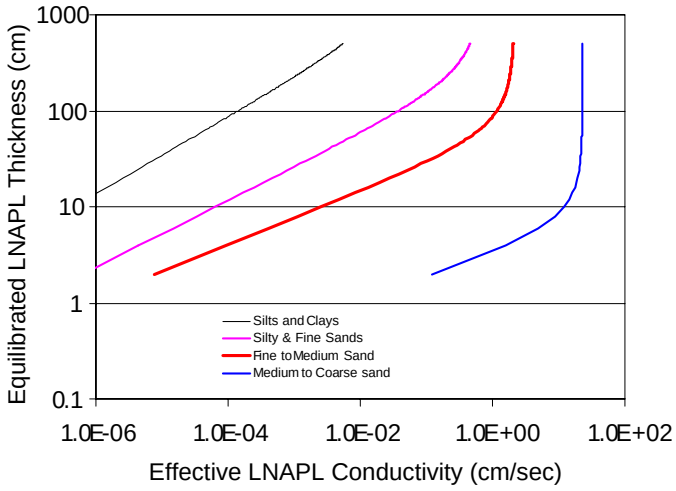

Figure 3-22. Effective LNAPL conductivity for JP-5 in different soils and under a range of observed thickness conditions.

Closely related to permeability and phase conductivity is the effective LNAPL transmissivity, which is simply the vertical integral of the effective conductivity profile (Appendix A). The effective transmissivity governs the bulk flow of fuel (or any other phase for that matter) under prevailing gradient conditions, including hydraulic recovery. Like conductivity, the effective transmissivity is similarly sensitive to soil type and LNAPL thickness, saturation, etc. (Figures 3-23a & b). Notice at some thickness threshold the effective transmissivity begins to decrease exponentially. Also, because different fuels have different density, viscosity, and interfacial tension properties, the effective transmissivity curves vary by fuel type, sometimes significantly (Figures 3-23b and 3-23c). For pure phase mobility, viscosity is the fluid variable having the greatest effect on the conductivity of any particular LNAPL type (Figure 3-23c).

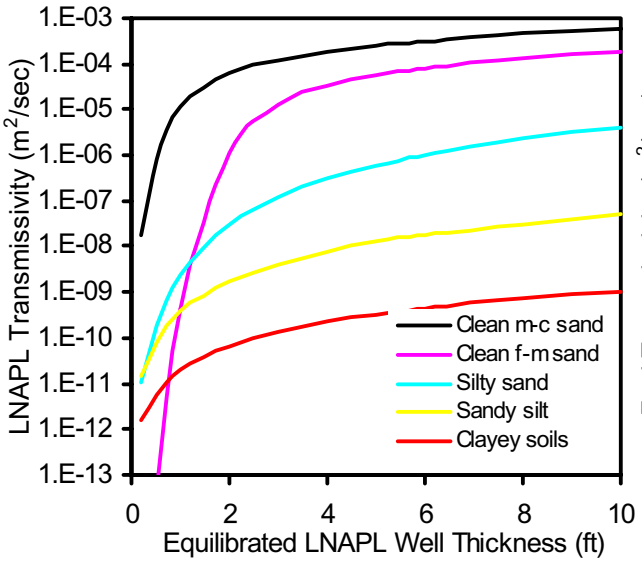

Figure 3-23a. Effective LNAPL transmissivity against equilibrated well thickness for gasoline in 5 soils.

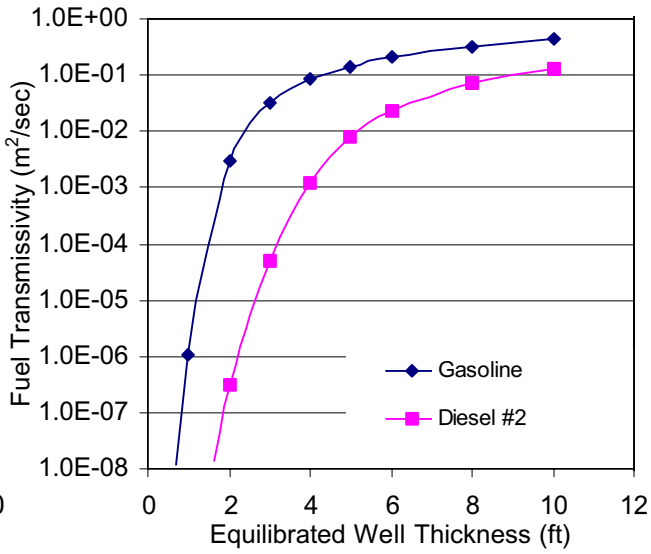

Figure 3-23b. Effective fuel transmissivity for same soil, but two different fuels (gasoline vs. diesel #2).

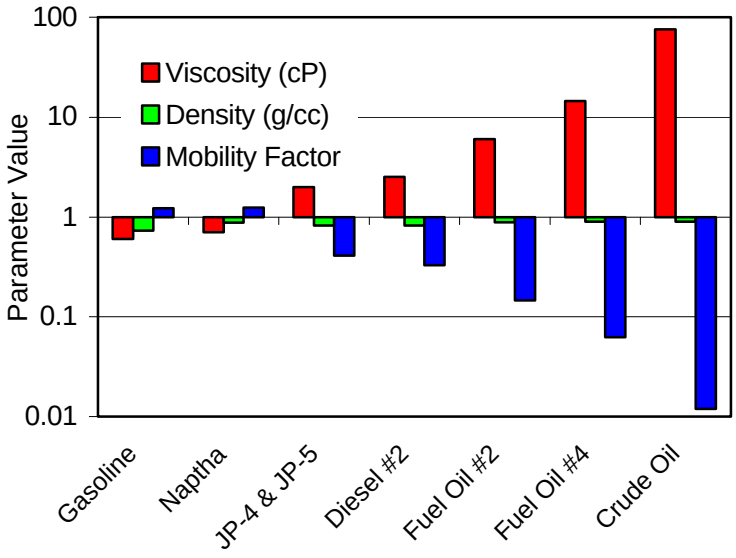

Figure 3-23c. Effective mobility of various LNAPL grades versus pure water with a mobility factor of 1.0. Notice that all other things being equal, viscosity plays the greatest role in changing pure phase mobility (where saturation is 100%).

3.2.2 Lateral Mobility of LNAPL

One of the important risk factors associated with the presence of an LNAPL is the potential for LNAPL to move and discharge directly to a receptor. Because of lateral, vertical, and temporal changes in LNAPL saturation, this lateral mobility of the LNAPL varies in both time and space. During the early stages of a typical release, LNAPL flows downward under gravitational and capillary gradients. If the vadose soils are relatively dry, the effective conductivity of the soil toward LNAPL is high because the relative permeability to LNAPL is high when the water saturation is low (recall Figures 3-21a and Figures 2-1a & b). Given a sufficient release volume, under the high gradient and effective conductivity the LNAPL advances quickly toward the water table. The LNAPL will also tend to deflect around fine-grained zones which often have both high water content, decreasing the relative permeability with respect to LNAPL, and low intrinsic permeability. Once the LNAPL encounters the capillary fringe, the resistance to LNAPL movement greatly increases because high water contents result in low relative permeability with respect to LNAPL. Water is displaced vertically and laterally and LNAPL partially infiltrates the water table zone according to the driving hydraulic head, capillarity, and effective conductivity. At the same time, the gradient toward LNAPL dissipates from gravitational (downward) to lateral (or semi-radial), with the net effect being a large decrease in the effective mobility. As a finite volume of hydrocarbon spreads outward to occupy a larger area and aquifer volume, the LNAPL saturations decrease resulting in a decrease in relative permeability and effective LNAPL conductivity. Under most conditions, a finite release will ultimately come to a field steady-state distribution with no further measurable movement. The ultimate resting place of an LNAPL release above or within the water table zone depends greatly on the volume and characteristics of the release, as well as the related soil and relative permeability characteristics.

It should be clear that LNAPL pools do not have a uniform mobility, but rather have a spectrum of potential velocities, exhibiting maximum values near the release area and minimum values near the pool boundaries (Figure 3-24). Again, the minimum conductivity values at the pool boundaries are responsible, in large part, for effective immobilization of most LNAPL pools. This is probably best shown by large plume studies in California and Texas (Mace et al., 1997, Rice et al., 1995). These studies found most dissolved-phase plumes to be stable, which implies that the LNAPL source area is not expanding. Similarly, downgradient observation wells would eventually fill with free product

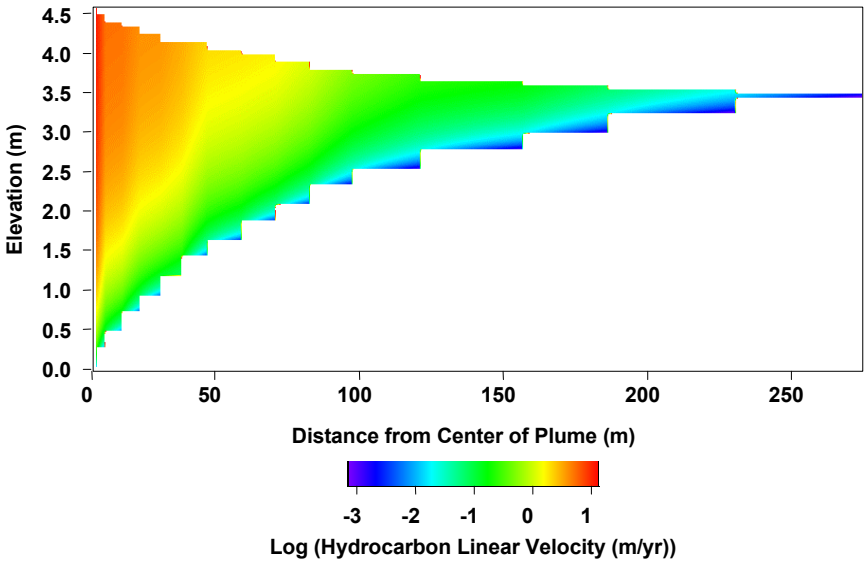

Figure 3-24. Cross-section of the velocity potential profile through a hydrocarbon plume. The site was characterized with soil and fluid capillary properties and fluid levels through time & distance.

for a spreading source. These attributes were not evident in the data from these studies, and the large majority of LNAPL pools were at field steady-state. This is not to imply that under a changed hydraulic condition, discrete remobilization could not occur in some cases.

The LNAPL mobility is a function of the effective conductivity discussed above, and the gradient. One may determine the LNAPL gradient in the same manner as for groundwater by noting that the elevation of the LNAPL/air interface in observation wells is at atmospheric pressure. This pressure surface can be contoured to result in a depiction of the lateral LNAPL gradient (Figure 3-25), where one often sees zones of LNAPL mounding even several decades after a release. Remember that the effective conductivity has implications with respect to vertical as well as lateral mobility, since the vertical hydrocarbon distribution is nonuniform. This means that the velocity and mass movement of LNAPL are related to position within the source zone. Vertically integrating the effective conductivity profile at each location results in the effective oil transmissivity, from which the total mass movement (i.e., flux) across a unit area of LNAPL can be estimated (Appendix A).

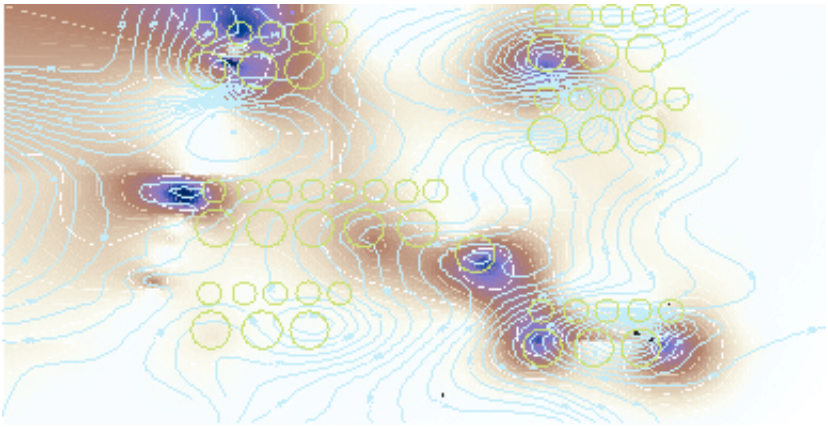

Figure 3-25. LNAPL contours of equal pressure (LNAPL table), overlain on a graded contour map of LNAPL volume per unit area, with dark zones having about 6 gal/ft^2, and the lightest color zones about 0.25 gal/ft^2.

Like many geologic processes, time is an important factor as the LNAPL mobility creeps toward zero in a progressively slowing mode. One could argue theoretically that product plume mobility is never truly zero, but simply approaches insignificance in an asymptotic fashion following a release. At some threshold, the rates of dissolution, vaporization, and degradation will exceed the lateral

transport rate and the product plume will be truly stagnant or retreating. Real-world conditions such as water table fluctuation can effectively end all meaningful movement through a combination of LNAPL entrapment and redistribution. While this is true, it is also true that every LNAPL spill has a period of spreading, so do not assume a priori that a particular plume is immobile without supporting field information.

One approach to assessment of the risk factor related to mobile LNAPL is the development of a mobility threshold, below which it is reasonably safe to assume LNAPL immobility. For instance, a hydraulic conductivity of 10^{-6} cm/sec is often used as a threshold for soil water immobility (e.g., some impoundment and landfill design). It is sensible that a similar hydraulic mobility limit could apply to LNAPL pools. Therefore, when the effective conductivity (Equation 3-2) is 10^{-6} cm/sec or less, the LNAPL might be considered effectively immobile (e.g., Brost & Beckett, 2000). The effective conductivity can be field verified through hydrocarbon baildown tests (Huntley, 2000; Appendix D), lab relative permeability tests, and other correlated data. If the pool is immobile, it is removed from risk calculations pertaining specifically to LNAPL phase transport. Further, any daughter risks that may be present would be spatially associated with the footprint of the immobile LNAPL pool. A related implication is that mitigation strategies could be designed to reduce the effective LNAPL conductivity to fully immobilize the separate liquid phase at sites where that has a positive benefit.

While a mobility threshold is clearly evidenced through data and theory, recognize that the discrete average pore velocity (q_p/n_{ep}, where n_{ep} is the effective phase filled porosity) can be important under certain conditions. Therefore, a mobility criterion should not be blindly used without being put into site specific context. LNAPL sentry wells downgradient (with respect to LNAPL, not necessarily groundwater) of the plume may be used as a prime piece of supporting evidence for the lack of phase mobility in a practical plume sense. Many sites have groundwater sampling wells outside and downgradient of the LNAPL source zone, and most sites being considered for risk evaluations have a history of data collection to support evaluations of potential pool mobility.

3.2.3 Time to Reach Vertical Equilibrium (VEQ)

Another important implication of LNAPL mobility is the time required for equilibration of product in observation wells. Intuitively, wells in the center of LNAPL pools should equilibrate more rapidly than wells near the boundary, which may never fully equilibrate. One can approximate the relative time for wells to equilibrate as a function of formation thickness by comparing the effective transmissivity across the vertical interval draining into a well (Figure 3-26). This approximation is for comparative purposes and underestimates the “filling” time because the gradient actually decreases through time; numerical simulations are necessary to accurately depict the complete process. As

seen, even under these best-case ideal conditions, wells in areas of thin LNAPL thicknesses, such as near the pool boundary, may require years to approach hydrostatic equilibrium. Therefore, one must be cautious about using the "appearance" of free product as the sole indicator of lateral LNAPL movement. The late-time accumulations of free product in wells may simply reflect slow equilibration times.

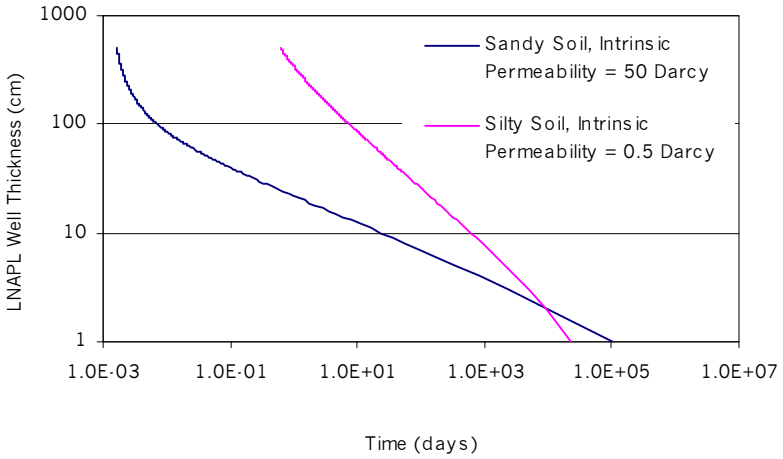

Figure 3-26. Approximate equilibration time between the well and formation for gasoline in 2 soils. More viscous fuels require proportionately longer equilibration times (recall Figure 3-23c).

As discussed previously, water table fluctuations will also often cause the ephemeral occurrence of free product in wells, particularly during low stands. A fluctuating water table can act both act to throw a system into disequilibrium and can entrap LNAPL below the oil/water interface (recall Figure 3-13b). As discussed previously, this entrapment below the oil/water interface is primarily due to the residual saturation of the LNAPL phase, but it is enhanced because the effective conductivity toward water is often far greater than toward the LNAPL, acting to trap additional fractions of LNAPL below a rising water table

3.2.4 Effect of Heterogeneity

As discussed in the capillary section, geologic heterogeneity has a marked impact on the relative permeability and effective conductivity of LNAPL. Looking at the same three stratigraphic sequences used as an example in the capillary section, we see that the effective conductivity varies over six orders of magnitude (Figure 3-27a-c). More generally, for materials with a range of intrinsic permeability of several additional orders of magnitude, the effective conductivity contrast can span upwards of ten orders of magnitude. The effect in the field is likely permanent disequilibrium in the low permeability materials incapable of equilibrating in the timeframe of typical hydrologic events, such as a seasonal water table fluctuations.

Geologic structures may aid or restrict LNAPL flow. Fractures, for instance, can facilitate LNAPL flow rates and cause significant contaminant spreading and persistence through LNAPL transfer to potentially porous walls of the fracture (Figure 3-26). Fractures are also problematic because it is difficult to measure and characterize their distribution and capillary properties. If the fracture aperture is large enough, capillarity is negligible within that zone and product can often move readily under a high effective conductivity. The work presented here is intended for intergranular porous

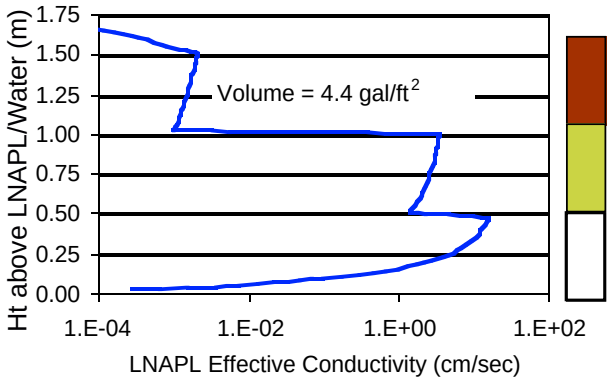

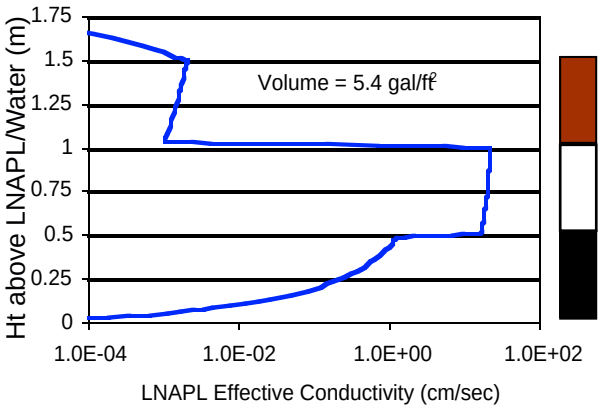

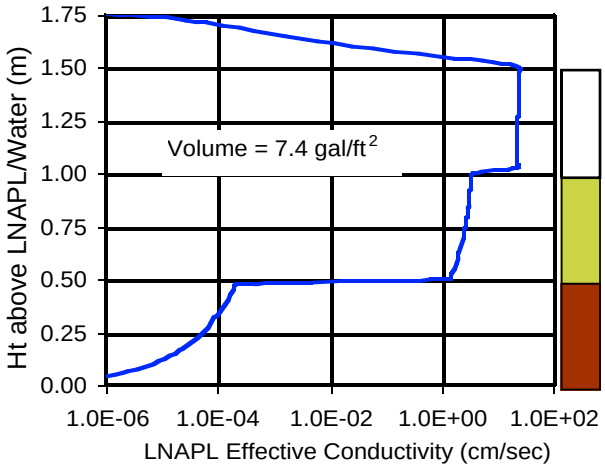

Figure 3-27a, b & c (top left, right, and bottom, respectively). The VEQ distribution of effective permeability ($k_i \cdot k_r$) as a function of stratigraphic position through the LNAPL zone. Medium-sand = speckled; fine-sand = white; silty sand = dark.

media only. If fractures are present, it may be possible to treat the formation as an equivalent porous media (e.g., Rouleau, 1988), but data justification would be needed first.

3.2.5 Mobility of the Air and Water Phases

Recall that relative permeability applies to all fluid phases. This principle is required to calculate groundwater flow through the LNAPL source zone (Appendix A). This calculation is a fundamental part of the mass partitioning analysis method presented herein and is a key component of the contaminant transport module in the included software utility. Water table zones that have high LNAPL saturations must, by implication, have low water saturation and therefore low effective groundwater conductivity. The principle is equally important for air-based cleanup methods where the effective air conductivity and flow is strongly influenced by liquid phase saturations throughout the target zone in the formation. Recalling that the relative permeability of air is small when water saturation is high, we would

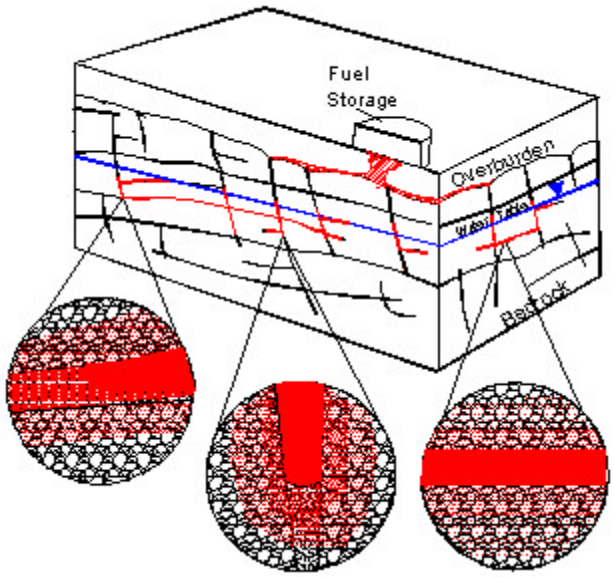

Figure 3-28. Schematic of NAPLs in fractures and various impacts (after Pankow & Cherry, 1996).

expect the rate of vapor flow to be low in the capillary fringe region or wherever soils are wet. These factors will be discussed in context in later sections. Ultimately, it is the interactions of various fluids in the variably saturated media that determine cleanup and transport of chemicals from the LNAPL source.

3.3 CHEMICAL TRANSPORT FROM THE LNAPL SOURCE

The period that an LNAPL source area provides chemical constituents to the dissolved and vapor phases at concentrations above some desired limit (the longevity of the source area) is a function of the original mass of the constituents of interest, their chemical properties, and the associated rate of dissolution and volatilization of those constituents. Thus far, sufficient background in multiphase hydraulics has been provided so that a general understanding of the factors that influence the distribution of LNAPL, and therefore its mass, are evident. There are two primary and linked components to chemical mass flux (Appendix A): 1) The advective flux that is the product of the rate of fluid flow (q_f) and the concentration in that discharge stream (C), integrated over the area perpendicular to the direction of transport ($q_f C$); 2) Diffusive flux processes that occur from chemical gradients even in the absence of fluid flow. Since soil vapor does not actively flow under most ambient conditions (no advective flux; barometric gradients & man-made factors excluded), it depends primarily on diffusion, and is somewhat less complicated to consider than water-phase transport. Therefore, we will develop the chemical concepts influencing water-phase transport first, and then move through vapor-phase transport by analogy, where applicable.

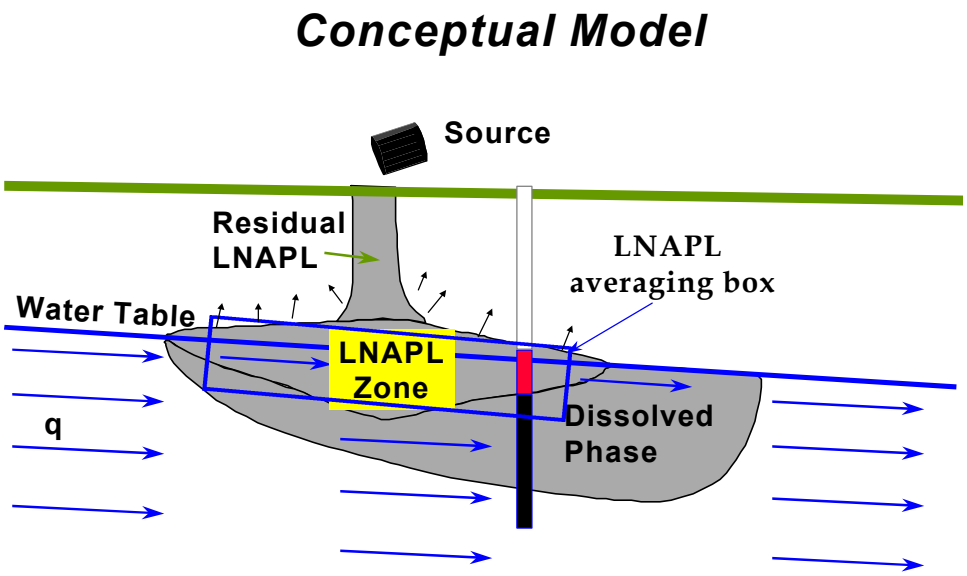

Figure 3-29. The conceptual calculation model, where groundwater flow through and below the LNAPL interval, along with volatile losses, controls the flux out of the source area.

3.3.1 Dissolved (Water) – Phase Mass Flux

As stated above, the rate of dissolved-phase mass loss from dissolution of the LNAPL source compounds is simply the mass flux leaving the source area in the dissolved phase, which is the product of the rate of groundwater flow (q) and the concentration distribution provided from the LNAPL, both within and below the source zone (Figure 3-29). This groundwater chemical flux occurs from the groundwater potentiometric surface (or corrected water table) to below the bottom of the LNAPL impacted interval (LNAPL/water interface). The approach used in the toolkit is to define a simplified source area geometry consisting of a three-dimensional rectangle of length (L) parallel to the direction of groundwater flow, width (W) perpendicular to the direction of groundwater flow, and a height or thickness of the LNAPL (Figure 3-30). The total mass of LNAPL in this rectangular domain is the product of the vertical integral of the product of the LNAPL saturation (S_o), the formation porosity (n), the LNAPL density (ρ_o), and the area (L x W). This source geometry must be simplified as such to allow the application of analytic solutions. The longevity of the LNAPL source will be controlled by the longest zone (parallel to the direction of groundwater flow) with the greatest vertical concentration of mass. Therefore, screening evaluations should consider this portion of the site specific field plume. The use of that "worst-case" section through the LNAPL plume in the direction of groundwater flow will usually result in a total estimated mass than is likely present or

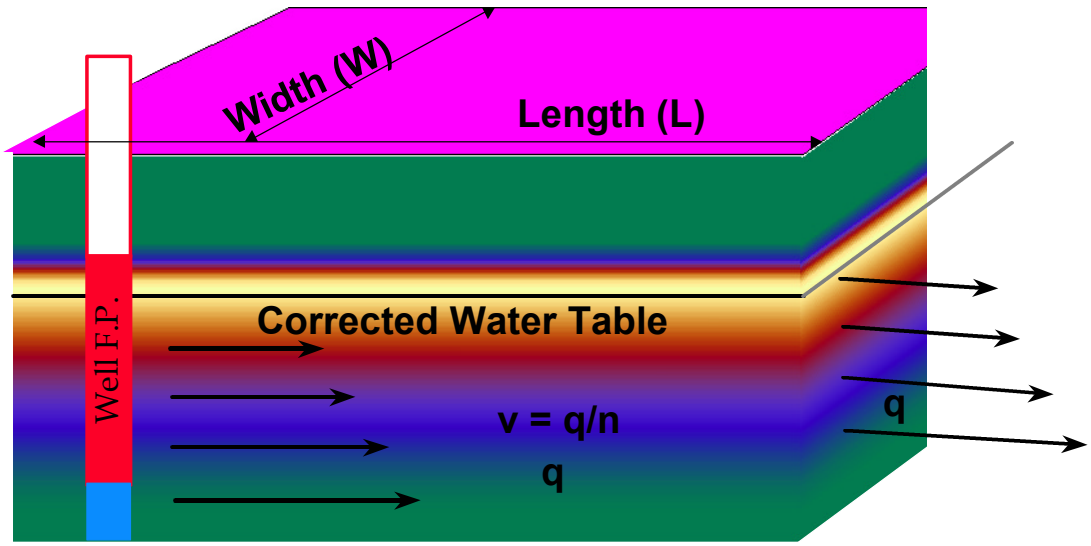

Figure 3-30. Three-dimensional box showing simplified LNAPL geometry with variable vertical distribution, according to the capillary theory discussed previously. The groundwater flow vectors are smaller in the LNAPL interval because of lower effective water conductivity.

than would be estimated by more spatially rigorous evaluations. Put another way, this analytic calculation method is not specifically concerned with accurately estimating the total LNAPL plume mass, but rather in evaluating a conservative (worst-case) distribution selected by the user, and mass values should be regarded accordingly.

The groundwater flow rate is defined by Darcy's Law, both above and below the LNAPL impacted interval (Appendix A). The concentration of each soluble constituent is taken to be the effective solubility of that constituent within the LNAPL impacted interval, and is calculated using the concept of vertical transverse dispersion for the zone below the LNAPL impacted interval, as discussed below. The effective solubility of each soluble constituent specified is calculated as the product of the pure-phase solubility and the mole fraction (Raoult's Law, discussed in the following sections and Appendix A). Therefore, as compounds are dissolved from the LNAPL, resulting in a decrease in their respective mole fraction, their effective solubility decreases, and the rate of dissolution decreases correspondingly.

3.3.1.1 Groundwater Mobility. The dissolution of the soluble components from LNAPLs depends on groundwater moving through and below the LNAPL source (vapor losses are covered subsequently). Rates of dissolution will be directly proportional to the groundwater flux. Beneath the bottom of the LNAPL impacted interval, where LNAPL saturation is zero, groundwater flux is simply governed by the gradient and water-saturated hydraulic conductivity of the aquifer materials. Above the groundwater potentiometric surface, horizontal groundwater movement is assumed negligible, as water pressures are less than atmospheric and movement is primarily vertical. Between the bottom of the LNAPL impacted interval and the effective groundwater potentiometric surface, however, groundwater movement occurs but is restricted to varying degrees by the presence of LNAPL occupying portions of the pore space. This is simply the concept of relative permeability again, as applied to the water phase. Zones of higher LNAPL saturation imply lower water saturation and, therefore, lower relative permeability with respect to water. As discussed previously, LNAPL saturation is not uniform between the LNAPL/water and LNAPL/air interfaces, rather it is represented by a saturation profile, most commonly with low LNAPL saturations near the lowermost LNAPL/water interface, increasing upward. Conversely, water saturations in this zone are represented by a profile with highest water saturations near the LNAPL/water interface, decreasing upward. This results in decreasing groundwater conductivity, velocity and flux, from the LNAPL/water interface upward to the corrected groundwater piezometric level and beyond to the LNAPL/air interface.

The decrease in the relative permeability, and therefore the groundwater flow rate, with height above the LNAPL/water interface is function of the vertical changes in LNAPL and water saturation. Recall that LNAPL more readily displaces water from coarse-grained materials than from fine-grained soils for the capillary pressure. Therefore, for the same VEQ thickness (or capillary pressure distribution) above the LNAPL/water interface, coarse-grained soils will have higher LNAPL saturations (and lower water saturations) than fine-grained soils, resulting in lower relative water permeability and relative flow (Figure 3-31a). In contrast, the fine-grained soil will have lower LNAPL

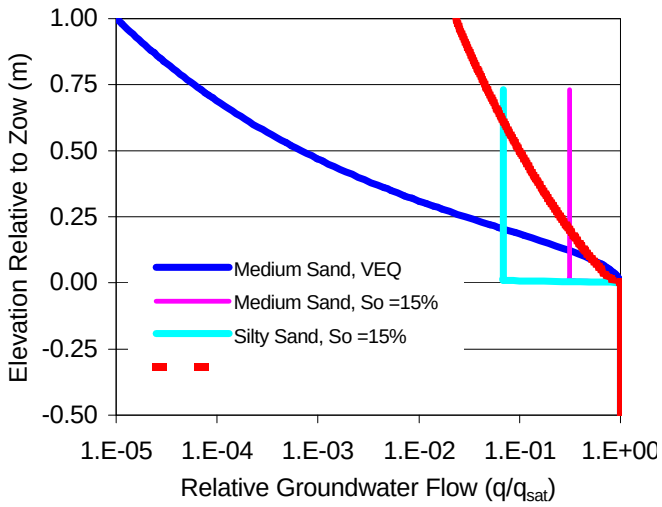

Figure 3-31a. Relative groundwater flow rates below (negative elevation) and above the LNAPL/water interface in the formation for 1 m of free product in a silty sand versus a clean sand.

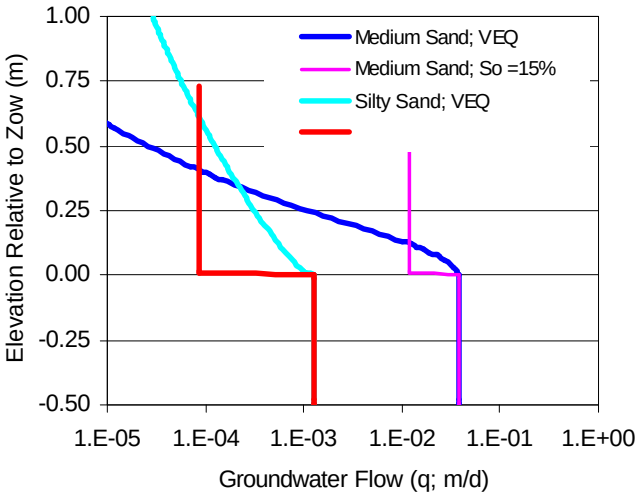

Figure 3-31b. Groundwater flow rates below (negative elevation) and above the LNAPL/water interface in the formation for 1 m of free product.

saturations and higher relative water permeability than the coarse material, resulting in higher relative flow as compared to the background regional groundwater flow rate. Conversely, for the ***same LNAPL saturation*** in a coarse and fine material, the differences in relative permeability are usually minor and the coarse material will generally exhibit a greater groundwater flow (higher effective conductivity) than the fine material under the same regional groundwater gradient condition (Figure 3-31b). As seen, the primary factors controlling water movement in the LNAPL zone are the LNAPL/water saturations, the corresponding water relative permeability, the hydraulic conductivity, and the groundwater gradient.

3.3.1.2 Concentrations. As noted above, within the LNAPL impacted interval, the dissolved-phase concentrations are assumed to be equal to the effective solubility of the constituents of interest (Appendix A). Below the LNAPL source zone, the component concentration profile is governed by the vertical dispersion of chemicals below the source zone. Biodegradation may play a role in this zone, but in many cases, this area is anaerobic with slow degradation rates. This potential degradation component below and within the LNAPL source zone is not considered herein as a con-

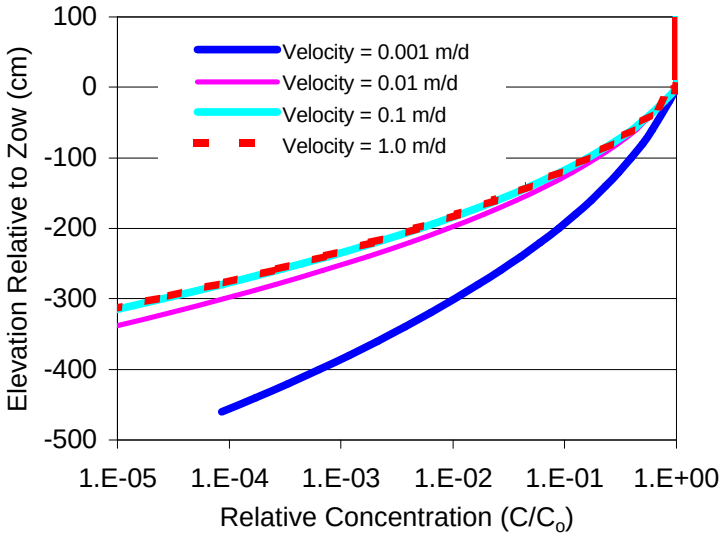

Figure 3-32. Relative concentration profile above and below the LNAPL/water interface (elevation = 0). Notice above the interface the relative concentration is 1.0 (equilibrium).

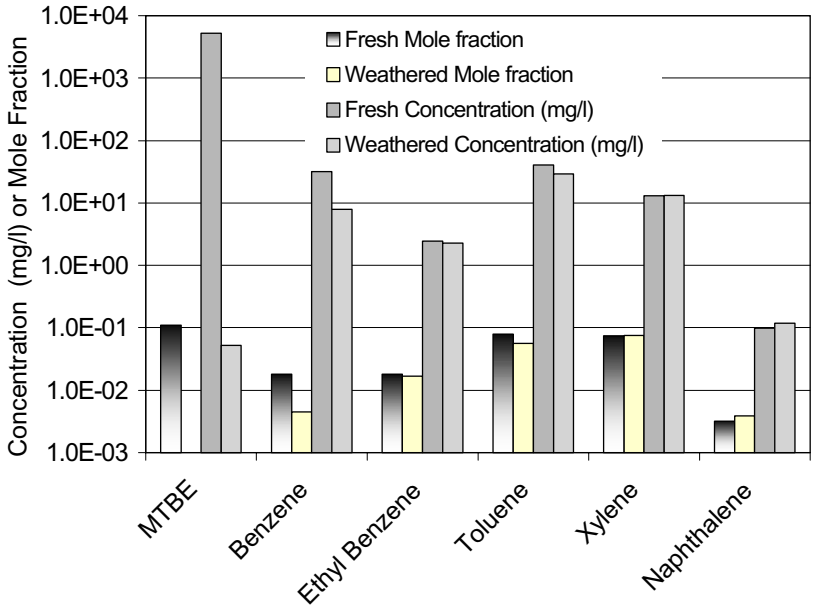

Figure 3-33. Comparison of mole fractions and associated groundwater concentrations for common gasoline compounds of concern. The "fresh" composition is an average of compositions typically found at the pump, and the weathered is estimated based on partitioning principles discussed herein.

servative assumption in analytic modeling, but may be important under certain conditions. The dispersive concentration profile below the LNAPL is exponential, and the depth of propagation depends on the dispersivity, which is in turn dependent on flow rate (Appendix A), and on the concentration at the upper boundary, which again is assumed to be equal to the effective solubility of each chemical of concern. In general, for all but very small pore velocities (less than 0.001 m/day) or very high dispersivity values, the dispersive concentrations decrease several orders of magnitude within about two to three meters below the LNAPL/water interface (Figure 3-32). Recall again that if field conditions are not at LNAPL equilibrium, or if heterogeneous soil and LNAPL distributions exist, these observations need to be altered accordingly.

The effective solubility of the constituents of interest is, as noted above, governed by Raoult's Law (Figure 3-33; Appendix A), which states simply that the effective solubility is the product of the pure phase solubility and the mole fraction of that constituent. Therefore, as clean groundwater moves into the LNAPL source area (Figure 3-33) from upstream, different constituents are picked up by the water as it moves along in proportion to their pure-phase solubility and molar fraction in the LNAPL. More soluble components with a high mole fraction in the source will dominate the groundwater contaminant composition in the short term. Constituents like MTBE and aromatic hydrocarbons, such as benzene, are examples of chemicals that are likely to have a strong presence in groundwater for as long as the source mass of that particular component is present, as discussed subsequently. These soluble compounds are also generally the first to be lost or "weathered" from the LNAPL source.

This type of chemical partitioning assumes equilibrium conditions prevail at a certain macro scale. The driving force toward equilibrium is the concentration gradient from the source LNAPL to the initially clean groundwater, but time is required to reach equilibrium. Laboratory experiments have demonstrated that equilibrium is generally a valid assumption provided that there is sufficient con-

tact time over a travel path of groundwater in contact with source LNAPL. Some workers have defined this as the ratio of path length over groundwater velocity, and have determined a rule of thumb ratio of 1 day that applies to gasoline and some other fuels (Rixey et al., 1997). There are conditions where high groundwater velocities, small LNAPL source width, or channeled flow or bypassing can invalidate this assumption, as demonstrated by laboratory studies. However, for most groundwater flow conditions in porous media, chemical equilibrium generally applies at the scale of individual beds. At a larger scale, that of multiple beds with different flow and LNAPL characteristics, apparent dissolved-phase disequilibrium is often exhibited. This apparent disequilibrium can be caused by rapid dissolution of the most soluble components of LNAPL in coarse-grained, permeable units, while dissolution of LNAPL from the finer-grained soils is limited by slow rates of groundwater flow and/or vertical diffusion (Figure 3-34). Other field conditions may exist having the same general effect, like variable LNAPL saturation distribution in different beds. Under these conditions, while discrete scale equilibrium may be present, higher groundwater flow through depleted zones will primarily gain chemical mass from adjacent beds diffusing into the more permeable zones. This distributed chemical partitioning can be considered in gross-scale by using the simple layered analysis provided in this analytic evaluation method (Appendix A).

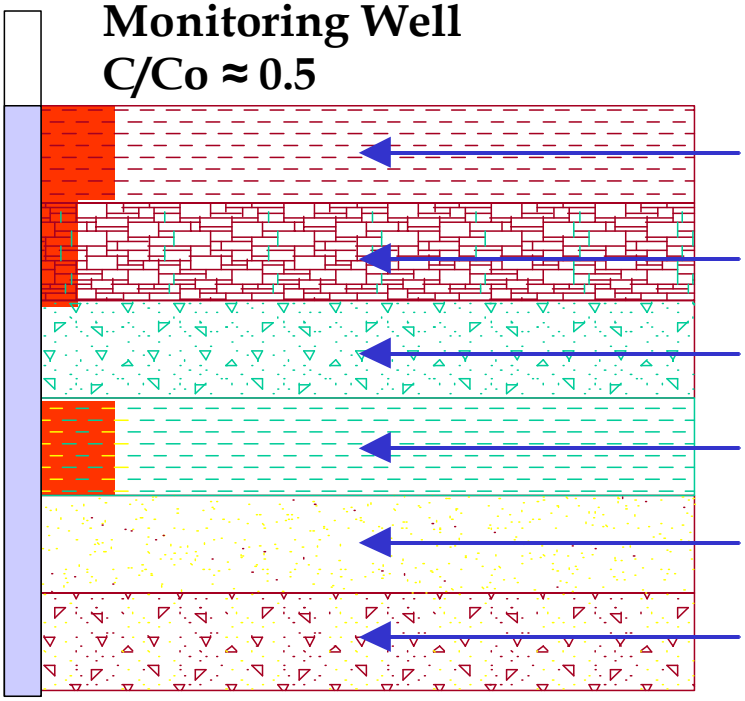

Figure 3-34. Schematic of a layered geologic condition where groundwater flowing in from the right encounters some beds with LNAPL (red), and some without, for a net concentration at a well less than predicted by equilibrium.

It should be noted as well that you will not see dissolved-phase component concentrations at their maximum effective solubility in LNAPL zones unless the groundwater monitoring

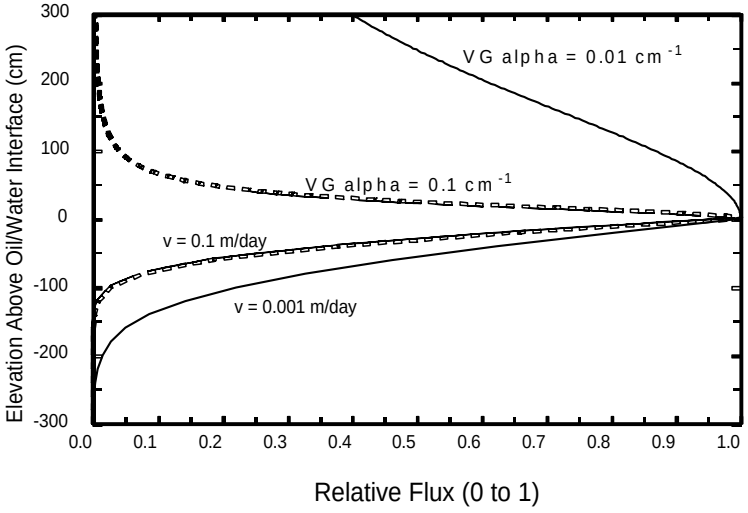

Figure 3-35. Relative dissolved-phase flux above and below the LNAPL/water interface (elevation = 0).

interval coincides precisely with the source interval. Where groundwater pathways are complicated with respect to the LNAPL source, dissolved-phase concentration variability and dilution are expected at some scale. The interesting questions this raises with respect to contaminant cleanup targets, health based or otherwise, and their points of measurement are left to the reader to consider.

3.3.1.3 Mass Flux (Dissolution). As noted above, the resultant chemical mass flux is the product of concentration and flow rate. From the discussion above, it is apparent that there are two components of groundwater mass flux from the LNAPL zone (Figure 3-35). One is from discrete water movement through the LNAPL at concentrations equal to the effective solubility, but with the flux scaled by the relative permeability toward water in that interval. The other component of flux is due to dissolution and dispersion below the LNAPL zone, where the relative permeability with respect to the water phase is 1.0, but the concentration decreases rapidly with depth below the bottom of the LNAPL impacted interval. The sum of the fluxes through and below the LNAPL source zone provides the net groundwater mass flux. Both the flux profiles above and below the LNAPL/water interface are exponential, but for completely different reasons. The flux above the LNAPL/water interface is exponentially controlled by the relative permeability function toward water, as we have seen in prior sections. The flux below the LNAPL/water interface is controlled by the exponential decrease in dissolved-phase concentrations. We can see that the maximum contaminant flux occurs at the LNAPL/water interface (Figure 3-34) where the concentration is equal to the effective solubility and the relative permeability to water is effectively 1.0.

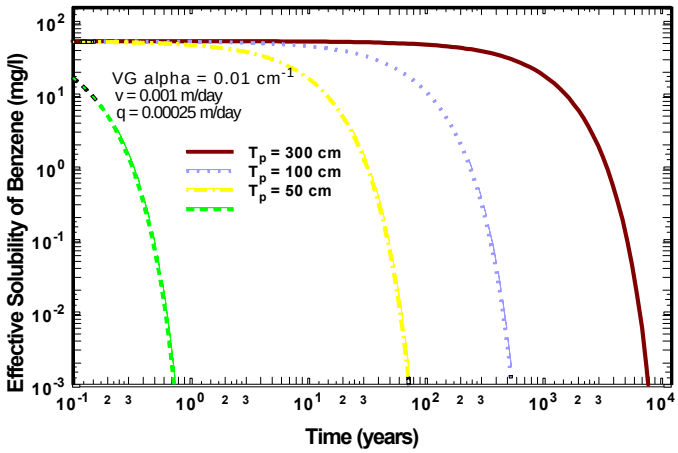

Figure 3-36. The effective solubility of benzene within the LNAPL source, showing the depletion through time as a function of initial pool thickness (T_p) for a sand soil. Notice the exponential effect of capillarity and thickness to depletion.

The calculation of the dissolution of an LNAPL source, and its resulting longevity, then depends on the discrete water flow rate through that zone and the dispersion properties beneath the source zone. Each “slug” of clean water moving into the source zone picks up mass in proportion to the component solubility and mole fraction remaining in the source. Once a “slug” of water is loaded at equilibrium with dissolved components, it moves through the remainder of the LNAPL source zone without picking up additional mass, and exits at the downgradient edge of the source zone at parti-

tioned equilibrium. This scenario produces depletion that starts at the upgradient edge of the source zone and migrates downgradient through time until source depletion begins to be manifest in decreasing groundwater concentrations of individual components at the leading edge of the source zone (Figure 3-36).

3.3.1.4 Downgradient Processes. Beyond the leading edge of the LNAPL source zone, the groundwater transport is governed by the groundwater flow rate, dispersion, retardation, and biodecay (for most compounds). This toolkit is not intended to give a comprehensive treatise on groundwater fate and transport principles; while the details are complicated, it is relatively simple to understand conceptually. Chemicals in groundwater will flow in response to both the hydraulic and chemical gradients, which interact to some degree. Obviously this implies three dimensions of consideration in the real world. The component transport may be slowed in all directions by sorption of organic components onto mineral surfaces or organic detritus in the soil matrix. While of significant scientific interest, this slowing (retardation) is often of little practical interest when the LNAPL phase is present. The retardation acts like a buffer, slowing the advancing dissolved-phase front of a particular component, but since the mass magnitude of the LNAPL source itself is often exceedingly large compared to the sorption capacity of most soils, the long-term effect of retardation is negligible for most LNAPL cases. This is particularly true for lower weight molecular components in fuels such as benzene and MTBE, with generally low affinity for partitioning to soil solid matter.

Probably the most important and fundamental attenuation mechanism in the dissolved-phase transport of most petroleum products is mass loss by biodegradation (Wilson et al., 1993; Wiedemeier et al., 1995). Biodegradation is largely responsible for the observed stabilization of the dissolved-phase plume with respect to distance from the source. Analysis of many UST release sites in California and Texas have demonstrated that most dissolved-phase BTEX plumes are stable or receding, with a small percentage still in the expansion stage (Rice et al., 1995; Mace et al., 1997). This simply could not be so without a mass loss mechanism. The biodegradation of the petroleum hydrocarbons works very much like a septic system, with naturally occurring microbes digesting hydrocarbons for energy under various states of oxidation and reduction potential. While aerobic degradation generally proceeds at the highest rate, anaerobic reactions are important and the net system has a "halo" effect with different biochemical processes versus distance from the source (Wiedemeier et al., 1995). While alkyl ethers such as MTBE have been shown to be generally less biodegradable than the nonpolar aliphatic hydrocarbons, less is currently known about the degradation mechanisms affecting these compounds. There is good evidence that natural degradation of oxygenated hydrocarbons occurs under some conditions, but these conditions are not present in all natural environments (Salinitro et al., 1994, 1999).

The software utility included as part of this toolkit calculates downgradient dissolved phase concentrations using the Domenico (1987) solution for one dimensional advection combined with three-dimensional dispersion. First-order biodegradation is assumed for the dissolved phase, subject to user-input biodegradation rates. The rate of groundwater flow used in the Domenico is simply the product of the regional groundwater gradient and the water-saturated hydraulic conductivity. For the case of vertically heterogeneous soils (layered case), the thickness weighted average hydraulic conductivity is used. The Domenico (1987) solution uses a concentration boundary condition, which is provided by the source area dissolution calculations. The concentration used in the Domenico solution is the groundwater flux-weighted average concentration through the source area.

3.3.1.5 Dissolved-Phase Partitioning Implications. In the case of water transport through the LNAPL, the synergy of multiphase fluid mechanics again causes interesting mass transfer conditions that may not be intuitively apparent. For instance, one finds that transport through the LNAPL zone is actually less efficient in coarse-grained materials than in fine-grained soil for the same equilibrated well thickness. This is because the fine-grained materials hold much less product than the coarse-grained soils for the same equilibrated thickness condition, leading to much higher relative water flow in fine materials compared to coarse (recall Figure 3-31a & b). In addition, the smaller mass means a smaller number of pore volumes are needed to deplete the source in fine-grained materials for a similarly observed thickness of product. Thus, fine-grained soils would be stripped of their soluble fractions more quickly than coarse-grained materials if all other groundwater flow conditions were comparable and fluid equilibrium prevailed. Conversely, at the same LNAPL saturation and regional groundwater gradient, many more pore volumes of groundwater will pass through and below the LNAPL impacted interval in a permeable material as opposed to fine-grained units. Thus, the depletion and weathering of the source under these conditions would highly favor the coarse grained units, leaving residual “stranded” for long periods in the fine-grained materials.

It is of interest to note that in most prior work, dissolution and diffusion ***below*** the LNAPL zone were thought to be the primary mechanism of dissolved-phase depletion of the source (Hunt et al., 1988; Johnson & Pankow, 1992). The work presented here clearly shows that transport within the source zone is at least as important as diffusion below, and that the relative contribution of each is highly soil and LNAPL condition dependent (i.e., site specific). The following observations are a direct result of this linking of multiphase flow to the dissolution of the LNAPL source:

1. The maximum chemical flux in groundwater occurs at the formation LNAPL/water interface, where the dissolved phase concentration is equal to the effective solubility and the groundwater flux is equal to the regional groundwater flux. Above and below the interface, the mass flux decreases rapidly. Below the interface, the mass flux decreases because the concentration decreases rapidly with or without biodegradation (while the groundwater flux remains

constant); above the interface, the mass flux decreases as the relative permeability and groundwater flux decreases (while the concentration remains constant). In general, for the same overall hydrogeologic conditions, LNAPL is depleted most rapidly from zones containing the smallest initial LNAPL saturation.

2. The mass flux above the LNAPL/water interface (associated with groundwater flow through the LNAPL) is of the same magnitude or greater than that below the interface, with the precise proportions depending on soil, fluid, and LNAPL distribution properties. When LNAPL saturation is small, the relative mass flux within the smear zone is large.

3. Except for very small regional groundwater velocities, most of the chemical mass flux below the LNAPL/water interface occurs within 1 m of the interface and downward dispersion is relatively unimportant within a small vertical distance beneath the source. Because of the exponential dispersive decay, the vertical chemical gradient in groundwater is itself a very good indicator of source distribution in the formation.

4. For coarse-grained soils (capillary fringe < 0.10 m), significant mass flux above the LNAPL/water interface is limited to a zone within about 1 m of the interface.

5. For fine-grained soils (capillary fringe > 1.0 m), the mass flux above the LNAPL/water interface is much greater than that below, and continues to heights of more than 300 cm above the interface in the saturated zone, assuming sufficient thickness of LNAPL.

6. The residence time of any chemical is proportional to the initial mass of LNAPL in the source zone and the distribution of that mass, the chemical's mole fraction and chemical properties, and the time dependent rate of flux out of the LNAPL impacted interval. A small mass at high LNAPL saturation will last longer than a large mass with overall low LNAPL saturations, other things being equal. The impact of this attribute can only be evaluated on a site-specific basis.

3.4 VAPOR-PHASE TRANSPORT

As mentioned in the prior section, there are strong analogies between vapor phase transport from the LNAPL and groundwater transport. Equilibrium chemical and hydrostatic conditions are again assumed, and while perhaps valid for some conditions, will not suit all. Chemical partitioning follows Raoult's law for the vapor phase. The vapor flux out of the source zone depends on the distribution of the LNAPL, water, and vapor in the pore space (capillary properties), the chemical gradient and properties of the compounds of concern. The primary conceptual difference between the water and vapor phase is that only vertical diffusion is considered for the vapor phase since there is generally no active vapor flow through or above the LNAPL zone under ambient conditions.

Many components in fuels, particularly gasoline and other highly refined or low molecular weight products, are volatile. Analogous to the water-phase, vapor-phase compounds will partition into non-impacted zones in proportion to the pure phase vapor concentration and molar fraction of the particular component (Figure 3-37). This is again Raoult's Law, but applied to vapor partitioning rather than water-phase partitioning (Appendix A). Under ambient conditions, vapor-phase flux generally follows the concentration gradient from areas of high concentration above the source zone to areas of low concentration at land surface, as governed by Fick's Law for 1-dimensional steady-state vapor diffusion (Appendix A). Fick's Law states that the chemical mass flux in the vapor phase is the product of the concentration gradient and the air diffusion coefficient. At steady-state with no degradation, the vertical mass flux from the lower boundary to the land surface is constant with elevation, which requires that the concentration gradient varies inversely with the effective air diffusivity. The Millington-Quirk equation (1959) (Equation 3-3), empirically determined based on laboratory experiments of vapor flux and chemical concentration distribution as a function of water- and air-filled porosity, suggests that the effective diffusion vapor coefficient (D_{eff}) is a sensitive to the total and air-filled porosities (Q_a and Q_t, respectively) as well as the free air diffusion coefficient (D_a). Fundamentally, zones of wet soil impede diffusive vapor migration.

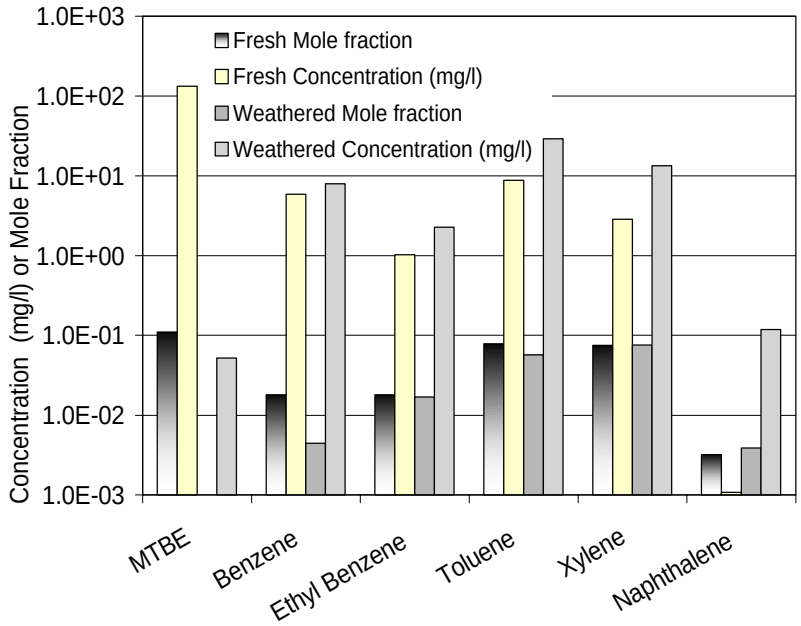

Figure 3-37. Comparison of mole fractions and associated vapor concentrations for common gasoline compounds of concern. The "fresh" composition is an average of compositions typically found at the pump, and the weathered is estimated based on partitioning principles discussed herein.

$$D_{eff} = D_a \frac{\theta_a^{10/3}}{\theta_t^2}$$

Equation 3-3

As the diffusion coefficient varies significantly with air-filled porosity and therefore pore fluid content (eq. 3-3), it is clear from prior discussion that the effective vapor diffusion coefficient must decrease with height above the oil/water capillary fringe due to decreasing liquid saturation (at equilibrium). The chemical gradient must also be discretely variable accordingly to remain mass balanced. That is, the vapor flux crossing some imaginary horizontal boundary near the LNAPL/water capillary fringe (low D_{eff}) must equal the flux crossing another horizontal boundary above that zone (higher D_{eff}). The average vapor flux, in the absence of biodegradation losses and at steady state, is the product of the average vertical concentration gradient and the average vertical diffusion coefficient (Appendix A), with mass therefore conserved. The inclusion of volatilization in this evaluation method is optional and must be used with caution, as discussed later, or plumes in sandy materials will be suggested to simply "evaporate" over a short timeframe, something that is not often observed in the field.

The method here is only concerned with volatilization as it relates to rates of component mass losses from the LNAPL source, in turn affecting groundwater chemical transport and longevity. The transient chemical characteristics of the LNAPL source due to mass losses can be used separately to calculate potential vapor flux to ground surface or another receptor. In this work, no attenuation mechanisms (e.g., biodegradation) are considered along the path between the LNAPL source and the land surface. Under conditions where biodegradation is present, the LNAPL mass loss rate would be expected to increase. Hydrocarbon vapor concentration profiles collected in the field often show significant concentration reductions toward ground surface, along with a coincident increase in the biochemical oxidation state as indicated by fixed gas chemistry changes (Ririe et al., 1998; API, 1999). These vadose zone processes are not part of this work, but the link to the source LNAPL provided here should be kept in mind by the user.

Now, let's bring the effective vapor diffusion into context with multiphase fluid mechanics. There are certain conditions where one would naturally expect high liquid content; in the

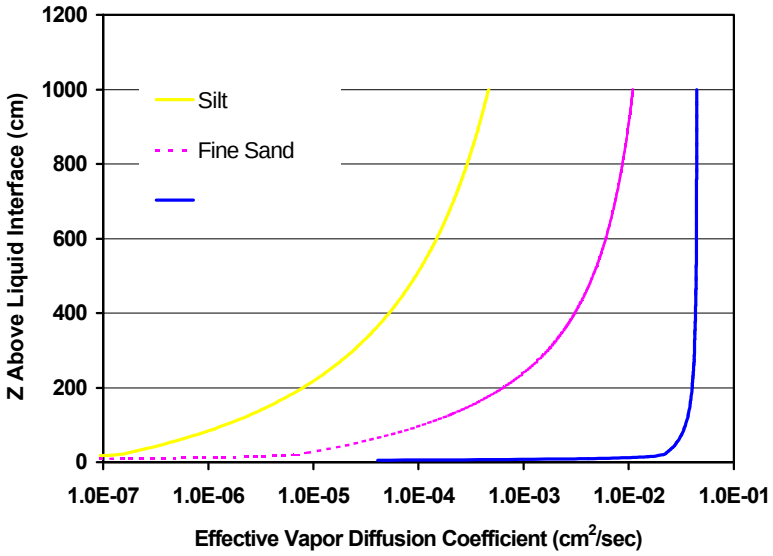

Figure 3-38. The effective vapor diffusion coefficient versus elevation above the liquid table.

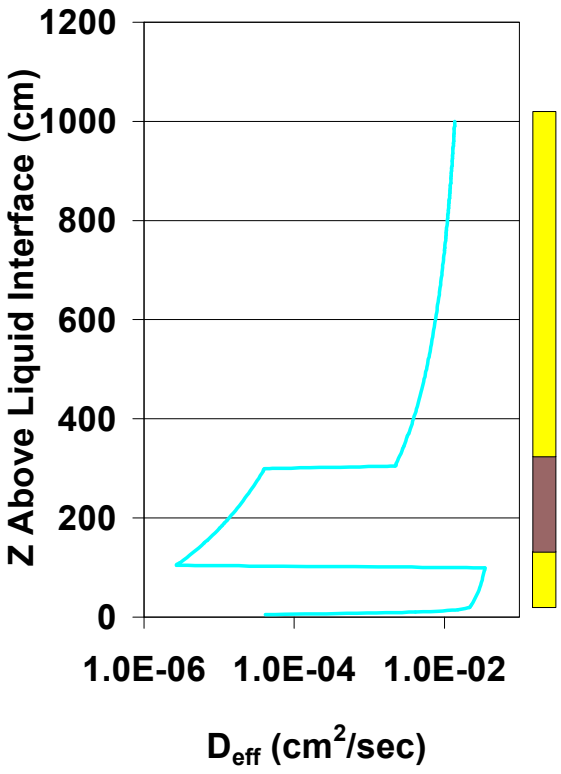

Figure 3-39. The effective vapor-diffusion coefficient (D_{eff}) with elevation above the liquid interface for a heterogeneous system of sand, overlain by silty sand, overlain by fine sand.

capillary fringe or where fine-grained soils are present between coarser materials, both resulting in zones of small effective vapor diffusion coefficients (Figures 3-38 and 39). This suggests that the capillary zone of an LNAPL spill impedes vapor transport from that source to varying degrees depending on the soil characteristics. Further, any fine-grained materials overlying the source zone in a layered system would similarly impede vapor transport, as would competent surface covers with negligible porosity. Regardless of soil type, the liquid capillary fringe zone has effective vapor diffusion coefficients that are several orders of magnitude smaller than values in the dryer zones (Figure 3-38). Not surprisingly, the transition from low to high effective vapor diffusion coefficients is most significant in coarse-grained soils, with fine-grained soils normally exhibiting a more gradual change. Therefore, even in a homogeneous, coarse-grained soil, we have a vapor flux limiting zone in the capillary fringe caused by multiphase fluid aspects. In general, flux limiting zones are one key reason why LNAPL plumes do not quickly evaporate from the subsurface as they would at ground surface.

In addition to variable air saturation in different soil zones, fluctuating water tables, surface water infiltration, and other events can also reduce the vapor diffusion from the LNAPL source. Essentially, any wet zone for any hydrogeologic reason will impede vapor transport. Under wet conditions, the vapor diffusion coefficient is negligible and chemicals in vapor must partition slowly through the water phase. When there is a highly water wetted vapor “barrier”, the vapor flux is controlled first by partitioning from the vapor to the water phase, and then by Henry’s Law for partitioning back from the water phase to vapor above the wetted zone. As discussed previously, the effects of transient hydrologic conditions are not explicitly considered in the calculation method, but need to be conceptualized on a site specific basis by the user before performing estimates of vapor partitioning from the LNAPL.

The calculation method developed in this toolkit handles the effective diffusion and diffusion limiting horizons in two ways. First, for any soil and fluid capillary conditions, the weighted effective diffusion coefficient is calculated by integrating across the interval between the oil/air interface and the land surface (Appendix A). Second, where vapor flux limiting zones are present, a volatilization efficiency factor may be defined by the user to better reflect the "slowing" of volatile losses from the LNAPL source. The User's Guide (Section 5) develops a procedure for considering and using the vapor efficiency factor.

While the main driving force of vapor transport is diffusion in response to the chemical gradient, the transport is still subject to the other factors we have discussed in the preceding sections that are not part of this calculation method that deals specifically with the LNAPL zone in the water table region. For instance, as vapor is transported upward into "clean" zones, it will partition into the water and soil phases where biodegradation and sorption may occur. Even without any reactions, the water in the soil is a temporary mass sink for compounds passing from LNAPL, to vapor, to soil pore water. As the vapor phase partitions and is acted upon in the aqueous state, hydrocarbon mass may be removed from the vapor phase system, reducing concentrations reaching ground surface (or some other point) and also affecting the net chemical gradient. Some mass may also return to the saturated zone by groundwater recharge from the surface. If the rates of mass transfer and biodegradation are sufficient, the net effect is a vapor plume of limited vertical extent above the LNAPL source, analogous to biodegraded groundwater plumes reaching some maximum distance from the source. Vapor profile data collected above free product plumes often exhibit attributes of these phenomena (Ririe et al., 1998). Therefore, we see that the primary transport mechanisms are analogous between the vapor and water phases, but that the vapor phase moves predominantly under the diffusion gradient, whereas groundwater usually experiences an active flow gradient. The remaining differences reside primarily in the differences in the magnitude of transport parameters for each phase.

3.4.1 Implications

The implications of vapor partitioning trend opposite those discussed for water phase partitioning, because the efficiency of vapor partitioning decreases as water content increases (opposite that for the water-phase partitioning). The potential rate of LNAPL vaporization is orders of magnitude greater in low capillarity soils (generally coarse) than in finer-grained materials. Even so, the LNAPL mass present in those low capillarity soils is usually much greater than in fine-grained sediments for the same observed fuel thickness or capillary pressure condition. Because of the exponentially of vapor diffusion rates as a function of soil capillarity, the user needs to select reasonably representative conditions for the screening evaluations discussed subsequently. If one is not careful, plumes will be predicted to vaporize in relatively short periods. More on this is provided in the user's guide.

Section 4.0

SOURCE CLEANUP

This section provides an overview of LNAPL source removal and remediation by designed or natural *in situ* processes in context with the theory presented in Section 3. There are many different strategies and reasons for implementing site mitigation. Terms like active remediation, passive remediation, engineering controls, and institutional controls all have different meanings and contexts, and this manual makes no distinction between them, just as the manual makes no specific site risk calculations. This evaluation method allows the user to consider a range of mitigation actions, regardless of context, to look at potential benefits of one method versus others. It is up to the user to define the goals of source reduction and then use the technical principles herein to evaluate the likelihood of achieving those goals for any particular strategy based on the site specifics of LNAPL smear zone. Caution should be used in evaluating cleanup conditions, as simplified models and screening approaches generally overestimate the degree of cleanup because heterogeneity and well field aspects are not explicitly considered. There is more on this in the user's guide (Section 5).

Theoretical and field experiences are combined in this section to show some key relationships between common remediation strategies and concentration reduction in the LNAPL source zone, particularly as it pertains to using this toolkit. As a reminder, the source we are concerned with is LNAPL in contact with groundwater and the capillary fringe. Vadose zone aspects are not considered. Hydraulic recovery methods are discussed first, followed by chemical aspects of remediation by partitioning methods and biodegradation. For any particular site, risk diminishment is achieved through the time and space dependent reductions in LNAPL source concentrations caused by the remediation mechanisms. This report is not intended to provide a thorough background of the principles of remediation. The interested reader is referred to the many excellent remediation references provided in the bibliography of this report.

The myriad of LNAPL remediation options works primarily through three processes, singly or in combination: 1) Hydraulic free-phase and fluid recovery, enhanced or otherwise; 2) Hydrocarbon mass depletion through volatilization and vapor recovery or other chemical/physical changes; 3) Mass reduction through naturally occurring biodegradation or enhanced biodegradation through nutrient and oxygen addition. The discussion below focuses on commonly applied remediation methods, but the principles are also applicable to more technically advanced strategies such as heat flooding, surfactant application, oxidation, and other hybrids. The fundamentals still come down to a description of the initial target mass in-place, the geologic materials in which it resides, the rate of action of the remediation mechanism, and the final endpoint distribution of mass and chemical characteristics. For technologically intensive methods, the user will need to estimate the time and space dependent source reduction outcomes independent from this toolkit and then use those esti-

mates as input to the toolkit. For instance, if vapor "stripping" is a component important to a particular LNAPL remediation, the user will need to independently calculate the associated mass and chemical component reductions in time and space. Another example might be *in situ* air sparging (IAS), where multiphase and multicomponent aspects are both important, but not directly addressed in this manual. Parts of this section will discuss some of these more complex attributes to assist the user in understanding various remediation mechanisms, but the associated calculation methods are not simple analytic expressions and are outside the scope of this screening method.

All LNAPL smear zone remediation methods, at their heart, are multiphase phenomenon controlled by interactions between the LNAPL source and the mass removal mechanisms. That interaction, which is heavily influenced by the geologic system, determines remediation effectiveness. Without consideration of the source and its distribution, predictive targeted remediation design is not possible, nor is there any yardstick by which to assess potential benefits. In this section we will show some of the relationships between remediation and the actual changes in concentration in the subsurface. We will see that common methods of evaluating remediation success, such as asymptotic behavior or observed LNAPL thickness diminishment, are of limited use unless placed in context with the LNAPL source and the risk implications.

The general goal of all remediation methods is to reduce the concentration of hydrocarbons below a target concentration, be it a statutory or a risk-based standard. While standards are typically applied to the water or vapor phases, the prior discussions make it clear that the components of concern (COC) in the LNAPL source itself must decrease for goals to be reached in the other phases. If site COC concentrations at present or future receptors are below a risk-based or other applicable standard, remediation is presumed unnecessary. The key to remediation design is adjusting remediation actions consistent with subsurface conditions such that concentration reductions and/or other targets are met. If specific remediation methods are incapable of achieving the desired goal, either due to technologic or cost limitations, then an alternate management action is suggested. All remediation methods have physical and chemical limitations that, when combined with geologic complexity, make cleanup of LNAPL smear zones to pristine conditions improbable under most conditions.

The search for effective active remediation strategies has often led to promulgation of new methods ahead of complete understanding of the physical and chemical principals controlling that method. This has sometimes led to application of new methods to inappropriate source distributions or geologic settings, or to the inefficient use of these methods, limiting the true potential of some remediation systems. For instance, in situ air sparging (IAS) was thought by many to cause air bubbles in aquifers that would rise in an ever widening cone until the water table was intercepted. Under that thinking, one would simply place deep sparge zones for good areal coverage and effec-

tiveness. However, soil and petroleum physics predict that discrete bubbles usually have insufficient buoyancy to infiltrate water saturated pore throats in most soils. Instead, the air stream is expected and seen in lab studies to move in continuous pore channels under a sufficient gradient (Ji et al., 1993; Johnson et al., 1993). The actual IAS air distribution and mass removal rates are significantly different from that visualized by the incorrect inverted bubble cone model. Thus, both the successes and failures of this and other cleanup methods are often viewed from an incorrect physical and chemical perspective, which may limit the appropriate uses of various technologies.

The following subsections will discuss the multiphase attributes of several commonly used remediation techniques and relate those attributes to the remaining source at the effective endpoint of remediation. This background discussion is intended to assist the toolkit user in later assigning source input parameters to this toolkit screening method. This toolkit does provide some assistance in explicitly screening the potential effectiveness of several hydraulic recovery methods, but does not calculate mass or chemical removal for more complicated systems involving chemical stripping and other enhanced factors. We will however, provide some diagnostic suggestions in the user's guide that may assist in that endeavor. Bottom line, you will again need to account for multiphase LNAPL conditions in the smear zone when considering remediation or there will be no way to link chemical changes in the source zone to potential risk benefits.

4.1 HYDRAULIC RECOVERY

Hydraulic recovery relies on LNAPL flow to a recovery well, trench, or other in situ collection device under an induced hydraulic gradient. The product flows toward the well in response to the induced gradient at a rate controlled by the effective conductivity. As LNAPL is recovered, there is a decrease in the remaining mass and saturation, which causes a progressive decrease in the LNAPL effective conductivity. With finer-grained soils, this effect, concentrated near the recovery well, can act as an impediment to recovery from further distances (Figures 4-1a & b). In coarser-grained material, one may reasonably expect the formation to respond more uniformly, with less of this attribute. (Figures 4-2a & b). However, at some point and regardless of soil characteristics, the effective conductivity of LNAPL becomes negligible as does any further recovery through any hydraulic approach. These factors cause the well-known asymptotic LNAPL recovery response for virtually any condition except a continuing release.

By definition, in no case can hydraulic recovery reduce the LNAPL source to below the field residual oil saturation of the formation. Whether or not this best-case endpoint is approached, depends greatly on the subsurface operating efficiency of the recovery system. Wells placed and pumped without appropriate design or planning are likely to either interfere with one another or simply have insufficient coverage to attain an endpoint close to field residual saturation. Natural hydrologic

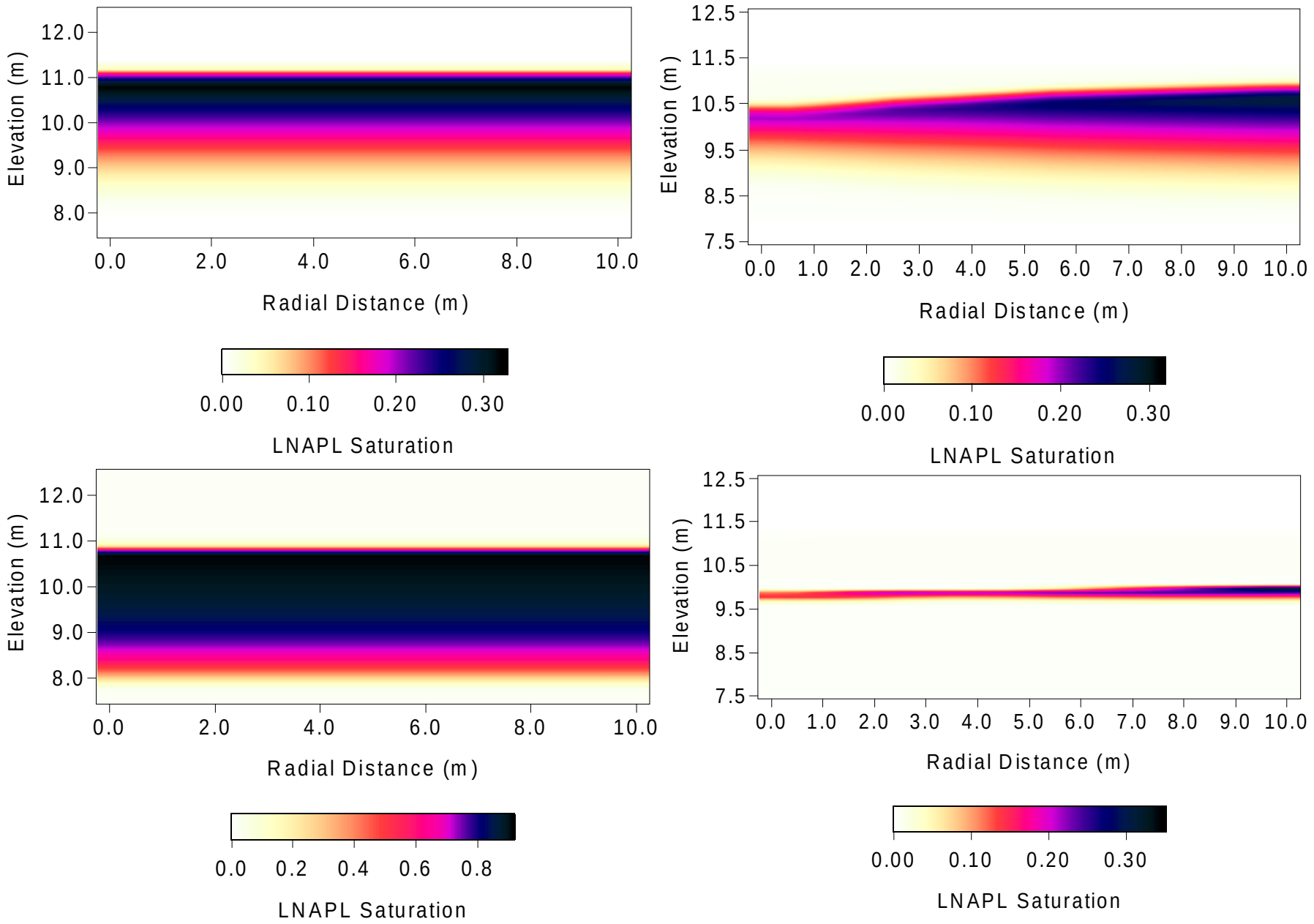

Figure 4-1a & b (top left and right) and 4-2a & b (bottom left and right). Cross section of a radial modeled smear zone (8 - 11 m elevation) containing gasoline LNAPL at equilibrium conditions on the left, and remediated conditions after 3 years of aggressive hydraulic recovery on the right. The top model is a silty sand (4-1a & b), the bottom coarse sand (4-2a & b) (after Beckett & Huntley, 1998).

variability can also strongly affect the mobility of the source zone, with periods of high water tables generally reducing the availability of recoverable product, although natural enhancements to recovery are also possible in certain conditions.

4.1.1 Summary of Hydraulic Recovery Experiences

It is illustrative to consider oil field and environmental experiences in context with the physics of LNAPL mobility discussed in Section 3. These experiences and data clearly indicate the real limits to the complete recovery of NAPL from geologic formations. Once in place, a fraction of the oil tenaciously holds onto its pore space. The magnitude of this residual fraction and its physical and chemical characteristics are key to site specific risk.

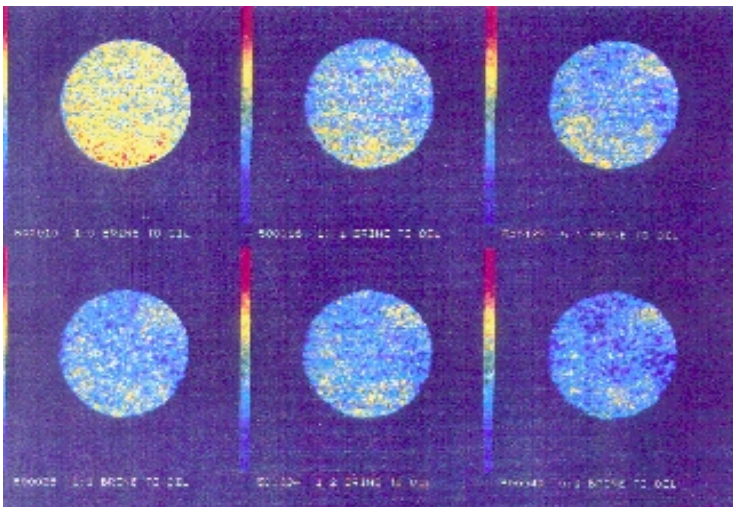

Figure 4-3. "Slices" of a reservoir core under CAT scan showing different water (brine, yellow) and oil (LNAPL, blue) flow conditions. The upper left shows 100% brine flow (residual oil saturation), and the lower right 100% oil flow (residual water). Courtesy of Terra Tek, Salt Lake City, Utah.

In the oil industry there is economic incentive to optimize oil recovery efficiency. Consequently, many field and laboratory investigations of the controls on oil mobility and recovery have been undertaken that are relevant to environmental LNAPL recoverability. When oil displacement is carried out by flooding the reservoir with water, air, or steam, capillary forces are responsible for trapping some fraction of the oil initially in place. Studies of oil reservoir rocks have shown that the residual oil left behind at the conclusion of water flooding typically ranges from 25 to 50% of the pore volume (e.g., Chatzis et al., 1988; Melrose and Brandner, 1974) (Figure 4-3). Pore structure and wettability are two properties that strongly influence residual oil saturation. A tendency has been observed for residual oil saturation to be greater where porosity is lower and the pore size (or grain size) distribution is wider, as discussed in Section 3 (Figure 3-26). As a reminder, the environmental case is one where water is normally the wetting phase, except within certain types of geologic deposits. The same is not true in oil reservoirs, where the wettability sequence depends on the specifics of each reservoir setting.

Oil left behind in reservoirs can exist either as an immobile residual or as an unrecovered mobile fraction. Unrecovered mobile oil in large, well-managed reservoirs can range from just 20 and up to 70% of the initial mobile oil in place (Tyler and Finley, 1991). Unrecovered mobile oil exists because of heterogeneities in the reservoir and the limitations of well recovery efficiency. In comparing oil reservoirs to environmental conditions, it is important to consider that oil reservoirs typically have greater initial oil saturations and mobility than observed in environmental release conditions. Further, oil reservoirs are typically under confined conditions allowing more effective application of standard pumping and enhanced recovery techniques such as heating, water flooding, and chemical treatment methods. Offsetting factors are that crude oils have viscosities that are typically higher than refined products (reducing flow), and reservoirs often have intrinsic permeabilities that are smaller than unconsolidated alluvial sediments prevalent in the environmental case. Thus, the reservoir comparison is for illustrative purposes more than as a refined quantitative comparison. In general, the hydraulics of recovery and initial oil conductivity are far better in reservoirs than for small volume LNAPL spills in unconfined, unconsolidated sediments. However, other factors limit total recovery in reservoirs that may be less restrictive under environmental release conditions.

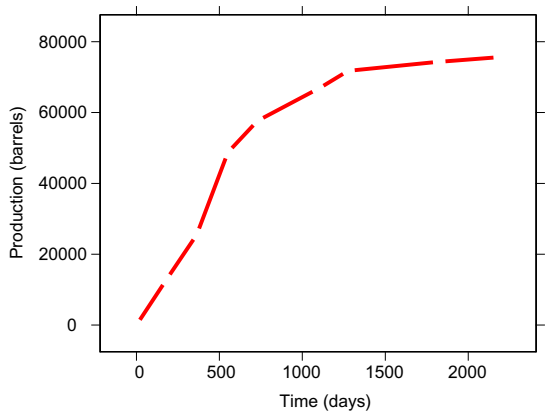

Figure 4-4. Cumulative fuel recovery at a site with outwash sands and gravels where LNAPL affects an adjacent stream channel.

Field and laboratory observations of environmental LNAPL recovery are different viewpoints of the same multiphase phenomena observed in petroleum production. However, measuring detailed subsurface LNAPL responses with respect to time and distance over the life of a remediation project is rare for typical environmental operations. The cost is high and interpretation of results is often difficult. Still, a few well-documented LNAPL remediation examples summarized in the following paragraphs provide insight to the further limitations that real-world conditions exert on LNAPL recovery.

4.1.1.1 Case Study; Fuel LNAPL Recovery in Outwash Sands. A former refinery in the central U.S. has been extensively studied because LNAPL has migrated over a significant area and potentially threatens a groundwater resource and an adjacent stream. Pumping large amounts of groundwater is required to achieve hydraulic control of the groundwater system to mitigate potential impacts at the stream. Soil saturation and petrophysical measurements, laser fluorescence, cone penetrometer, and hydraulic tests have been combined to produce a comprehensive data set. From these data, oil company scientists have estimated the original LNAPL volume to be approximately 4 to 6 million gallons in predominantly permeable outwash sand and gravel sediments. The high permeability outwash sands and gravels puts this site in the upper percentiles of probable LNAPL recovery success.

Of the LNAPL in-place at the former refinery, about 3.3 million gallons have been recovered through aggressive groundwater and product pumping over 13 years, approximately 2.9 million of which was recovered over the first 31/2 years of operation (Figure 4-4). The cost of the system installation and operation has been approximately $8.5 million, for a current net cost of a little less than $3 per gallon recovered. However, because product recovery has diminished through time, consistent with theory, the cost per gallon has increased from about $1 over the initial recovery period to about $50 currently. The future cost per gallon recovered is expected to increase as a greater percentage of costs are allocated to operation and water disposal per gallon of LNAPL recovered.

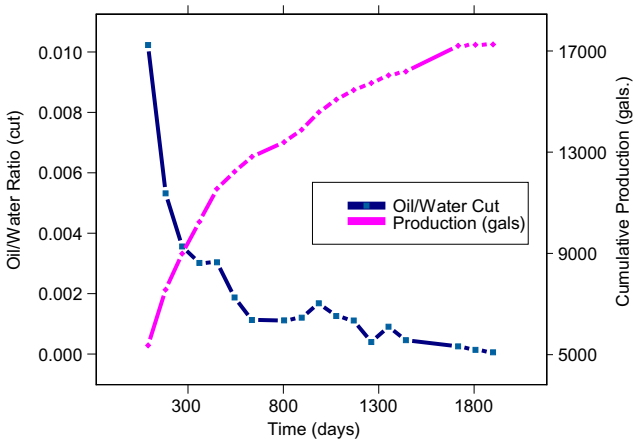

Figure 4-5. Cumulative total recovery as well as fraction of oil to water through time at a site recovering diesel range fuel in a dune and beach sand.

Despite the good percentage of LNAPL recovery versus the estimates of initial in-place volume, the adjacent stream could still potentially be impacted by the LNAPL beneath the site during certain hydrologic events (e.g., a low water table stand). Consequently, containment and alternate recovery strategies are being considered since product recovery has not completely addressed the key impacts and potential risks of concern. This example shows that limits to LNAPL recovery can sometimes preclude risk mitigation goals even in permeable materials.

4.1.1.2 Case Study: Diesel Range Fuel in Dune Sand. Another example of LNAPL recovery comes from a large diesel plume in unconsolidated dune and beach sand that exhibits a permeability of approximately 10 Darcys. The fuel is similar to diesel #2 and #2 fuel oil with a relative viscosity of about 11 as compared to water.

The LNAPL plume was found beneath an area of about 400,000 square feet, and was contained on the downgradient side by a bentonite and polymer wall to both limit migration and to enhance product recovery by dual phase pumping. The five-year history of product recovery shows rapidly diminishing efficiency (Figure 4-5). The fraction of LNAPL in the recovered liquids decreased steeply from an initial high of 0.01, and over the lifetime the project averaged just 0.002. Excavation and test cores taken after 4 years of recovery showed that large amounts of LNAPL remained in the soil even though recovery wells were no longer removing any significant LNAPL. LNAPL saturation at the capillary fringe was still 10 to 20% in most areas in the free product pool. At an average total solubility of about 15 mg/l, the remaining residual plume will reside for at least several thousand years if no other actions are taken.

4.1.1.3 Case 3. In downtown San Diego, an LNAPL plume known as the "blob" has historically exhibited hydrocarbon thicknesses in observation wells up to 10 feet. The plume is estimated to have an approximate volume of 64,000 gallons (Huntley et al., 1994). However, free product pumping has resulted in only limited recovery, with less than a few thousand gallons collected over several years by the various area hydraulic remediation systems. In various locations, where residential or other units have been constructed, excavation of LNAPL affected soil has been required where recovery efforts have failed to meet regulatory requirements for LNAPL recovery.

4.1.1.4 Summary of Case Studies. In summary, for most of the hydraulic recovery cases evaluated from literature and in our own records, the total LNAPL recovery was less than 30% of the original volume in-place with the upper end being as high as 60%. A few other case studies are summarized by the EPA and others (Table 4-1) and are consistent with the theory and examples above. The implication is that for most sites, recovery of more than 30% of the LNAPL in-place would be the exception rather than the rule. In finer-grained materials, recovery of more than 15% of the LNAPL in place would be unusual. These generalizations are for overview purposes and certainly should not be arbitrarily applied to specific sites. However, it is useful to remember these ranges to assist setting up calculations of the risk benefit of recovery actions. A method of approximating potential hydraulic recovery is provided in the next section.

Case	Fuel	% of Spill Recovered	Average oil/water (%)
1	JP-4	25	<1
2	gasoline	23	?
3	gasoline	30-60	0.0025
4	gasoline	28	0.04
5	mixed	27	0.06

case 1-4 EPA/530/UST-88/001

Table 4-1: Case Studies of LNAPL Recovery

The limited success demonstrated by these examples speaks to the theoretical LNAPL recovery limits discussed earlier. It is through no lack of effort that LNAPL plumes persist. Plumes persist because of the physical limitations to recovery of an immiscible-phase liquid in water-wet pore space and from inefficiencies in the hydraulic recovery systems.

4.1.2 Hydraulic Recovery Approximation

Through the years, several analytic groundwater recovery equations have been defined for specific aquifer settings. The equations generally relate an applied pumping rate or drawdown to changes in aquifer drawdown as a function of transmissivity and storage coefficient. One of the simplest approximations relating drawdown to pumping rate in a confined aquifer is the steady-state Thiem equation (1906). Using a correction for the unconfined aquifer conditions (Dupuit assumptions,

1863), the Thiem equation can be applied as a simple approximation to many unconfined environmental LNAPL recovery conditions. If one holds drawdown constant, the equation can be rearranged to estimate the steady-state flow rate as a function of drawdown, conductivity, and radius of influence. This is the basis for the oil and water recovery approximation provided in this toolkit based on work by Charbeneau, 1999 (Appendix B).

To approximate LNAPL recovery in the water table region, modifications to the Thiem equation are required with additional assumptions. Assuming VEQ conditions prevail and that uniform conditions exist within the product radius of capture, we can estimate the effective transmissivity with respect to LNAPL for those conditions. This is accomplished by vertically integrating the relative permeability profile for a given set of LNAPL thickness, soil type, and fluid properties and then combining with the values of permeability, density, and viscosity (Appendix B). Product recovery over some incremental period, that will reduce the mass and saturation of the LNAPL remaining in-place. This new smaller saturation profile can then be used to recalculate the correspondingly smaller effective transmissivity, and oil recovery can then move on through the next time increment. And so on until there is no recoverable oil remaining.

Based on the modified work of Charbeneau (1999; Appendix B), this approximation method as included in this toolkit considers: 1) LNAPL-only skimming; 2) dual-phase recovery of water and LNAPL; 3) hydraulic recovery effects of applied vacuum to the prior methods; 4) trench recovery. While this approach is simple, it does account for some of the key aspects of oil recovery. The approximation is also not valid for layered heterogeneity, as the transmissivity does not change uniformly between different layers containing different capillary properties and initial LNAPL saturations. Some of the important aspects to the approach are discussed below.

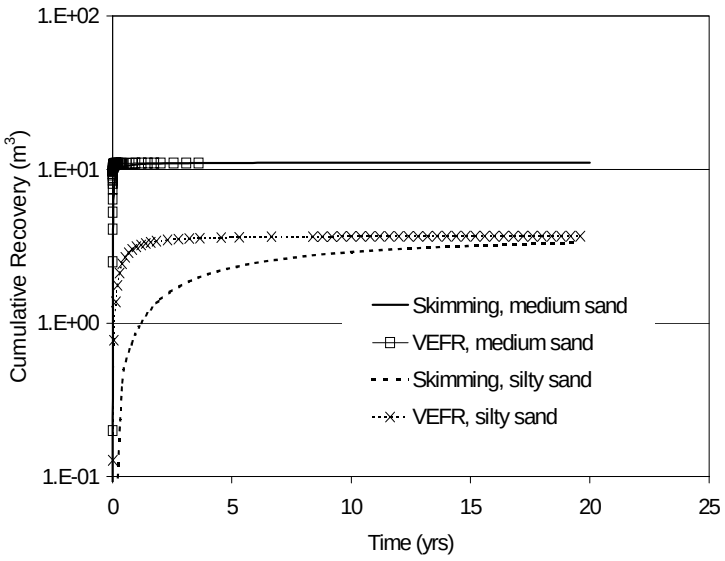

Figure 4-6. Comparison between aggressive remediation using vacuum enhanced fluid recovery (VEFR) versus skimming for 2 soils. For each soil, the cumulative recovery converges to the same endpoint for both cleanup methods.

First, oil will not be recovered below the field residual saturation. In fact, this is the theoretical endpoint for any hydraulic recovery strategy using the above approach. Only the time required to reach the endpoint varies by method (Figure 4-6). Second, the change in LNAPL mobility through recovery is taken into account through the ever diminishing saturation, thickness and transmissivity relationship, producing an asymptotic curve. Third, one can consider the time benefit of

different recovery strategies using different applied gradients and pumping configurations. Again, only the hydraulic aspects of recovery are considered, so vacuum-enhanced recovery does not include the volatile mass recovery of the method, which is often more important than the fluid recovery.

In invoking this approximation for trench and radial pumping recovery, several assumptions are required: 1) Transient pumping conditions are ignored; 2) VEQ is always maintained; 3) Smearing of LNAPL is not considered; 4) The decrease in hydrocarbon volume from recovery is assumed to result in a uniform change in saturation throughout the radius of LNAPL capture; 5) Heterogeneity and anisotropy are not considered; 6) Well interactions are not considered, except in as much as recovery multiple wells is assumed to be additive. Although this analytic approach greatly simplifies the underlying multiphase processes, it compares reasonably well with numerical simulations of multiphase recovery when soils are relatively permeable (k_i > 1.0 Darcy), the pore sorting parameter is not too large (VG beta < 2.5; BC sorting index < 1.0), and the soil capillarity is small (VG alpha > 2 m^{-1}). Because of the constraints of the approximation, it is best used for comparative screening of hydraulic recovery outcomes, but not for comprehensive or complex conditions. When the approximation is in error, it appears to underestimate the recovery time and overestimate the recovery effectiveness, and should be used as an optimistic screening tool only. This optimistic aspect of the recovery screening is due to several factors, including the averaging of the LNAPL profile uniformly across the radius of capture that is user-supplied rather than predicted, aspects related to the importance of vertical drainage, and other mathematical constraints inherent in analytic screening methods. Also, use of an artificially low field residual LNAPL saturation will result in optimistically incorrect results since the LNAPL residual saturation is the theoretical endpoint of any hydraulic recovery effort. If a suggested scenario has a specific risk benefit, then one should view the result skeptically and pursue further data collection or analyses to better constrain the information. Conversely, if the toolkit suggests minimal risk benefit for a specific recovery action, the result will almost certainly be conservative.

As mentioned previously, under these assumptions, the final endpoint of hydraulic recovery will always be the specific LNAPL retention, and it is unnecessary to calculate the endpoint using the approximation method if all remediation approaches are taken to this limit. However, the time required to reach this endpoint is a function of the remediation approach selected, so the comparative estimation becomes useful when time considerations are important. Recall in Section 3.4 the discussion of relative permeability and effective transmissivity decreasing as the formation LNAPL thickness decreases. Each hydraulic recovery method discussed herein decreases the LNAPL “thickness” (i.e., saturation) at different rates because the applied gradient is different. The larger the gradient toward the LNAPL recovery well, the faster the formation approaches field residual saturation.

4.2 CHEMICAL PARTITIONING REMEDIATION

This section presents an overview of chemical partitioning remediation , the fundamentals of which are based on the combination of multiphase hydrogeology and multicomponent chemistry concepts discussed in Section 3. While there is certainly a chemical component associated with hydraulic recovery, that component is small and not the focus of those remediation methods. The focus here will be on vapor partitioning methods including *in situ* air sparging (IAS) and soil vapor extraction (SVE), with some discussion of biodegradation and heat enhancements. The intent of this section is to provide a multiphase and chemical perspective to remediation to assist the user in assigning related parameters to the LNAPL evaluation toolkit. The actual estimation of changes in LNAPL mole fractions of various compounds due to chemical partitioning remediation is not within the scope of this work. However, the principles can greatly assist in the interpretation of past remediation outcomes or the potential benefits of proposed chemical cleanup strategies.

The key principle for chemical partitioning remediation is the designed subsurface delivery of the selected cleanup mechanism in a manner consistent with the distribution of the LNAPL source and the pertinent chemical properties to be able to meet the desired time, concentration, and other related goals. Particularly in the water table "smear" zone, the multiphase interactions are usually an important consideration to the efficient delivery of the remediation mechanism. Some discussion of chemical partitioning "efficiency" will be provided in context with the multiphase conditions in the smear zone.

4.2.1 Multicomponent Partitioning

In Section 3, the principles of partitioning were discussed with respect to both the water and vapor phases. The fraction that partitions from the free phase source at any point in time depends on the pure phase solubility (for dissolution into groundwater) and vapor pressure (for partitioning into the vapor phase) of the compound, which are then scaled by the mole fraction within the source at that time. For instance, if a pure phase component had a solubility of 1,000 mg/l and a mole fraction of 0.01 in LNAPL, the effective dissolved-phase solubility would be 10 mg/l. The same prin-

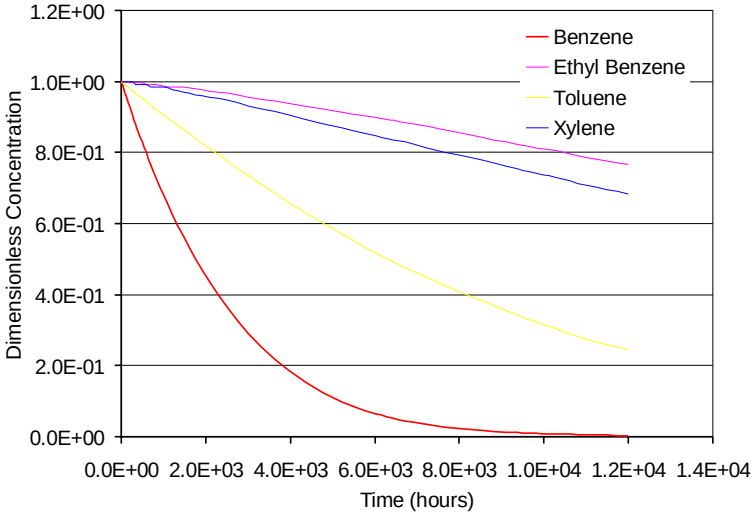

Figure 4-7. Aromatic compound partitioning from gasoline under soil vapor extraction (SVE), with partitioning based on Raoult's Law.

ciple applies to the vapor phase (Raoult's Law; Appendix A).

From this, we can envision that any chemical partitioning remediation, like SVE or IAS, should produce a chromatographic separation of compounds from the LNAPL source (Johnson et al., 1990; Figure 4-7). Similarly, other enhanced vapor recovery methods such as heating, will increase the volatility of some compounds. So, even with efficient subsurface remediation design, different compounds will respond differently through the time of cleanup. The least chemically amenable compounds of concern (COC) will control the total remediation time. For vapor phase partitioning methods, the least amenable compounds are generally those with small mole fraction, low vapor pressure, and higher molecular weight. For instance, the vapor pressures of MTBE, benzene, and naphthalene span three orders of magnitude. The expectation for the relative rates of mass partitioning during vapor-phase remediation for each compound is fairly obvious (Figure 4-8).

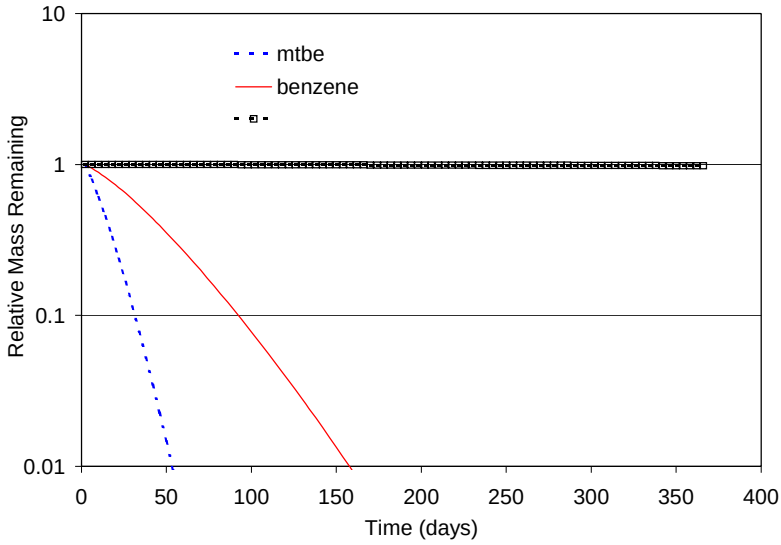

Figure 4-8. SVE simulation showing the relative amenability to vapor stripping of MTBE, benzene, and naphthalene. Clearly, it is of no benefit to attempt naphthalene stripping under ambient conditions.

4.2.2 Remediation Delivery Efficiency

Subsurface remediation efficiency encompasses the idea that the more direct the delivery of the cleanup mechanism, the more efficacious and timely the period of action. Efficiency can be viewed in two broad categories, remediation pathway efficiency and chemical efficiency. It is perhaps most illustrative to discuss each by example, as follows.

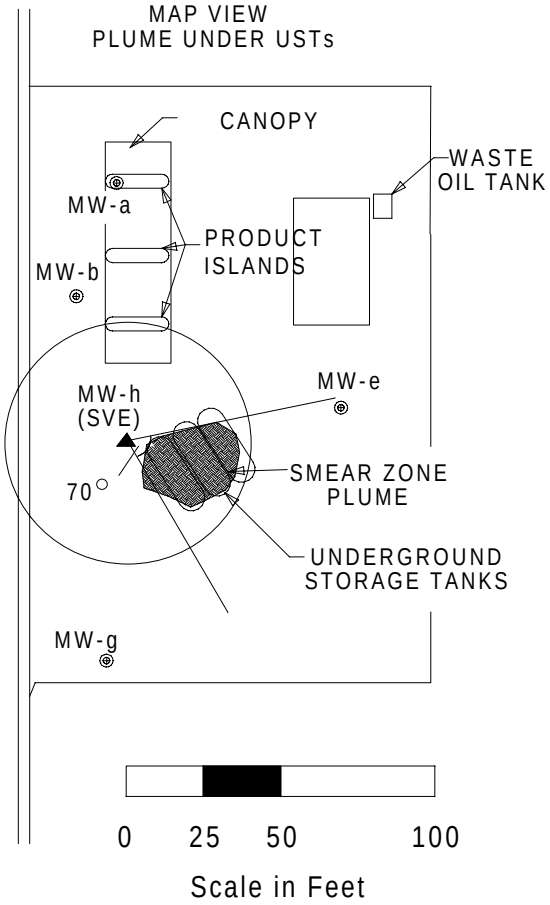

Figure 4-9. Map view of tank plume with an SVE well installed outside the cavity area for 70 degrees of coverage.

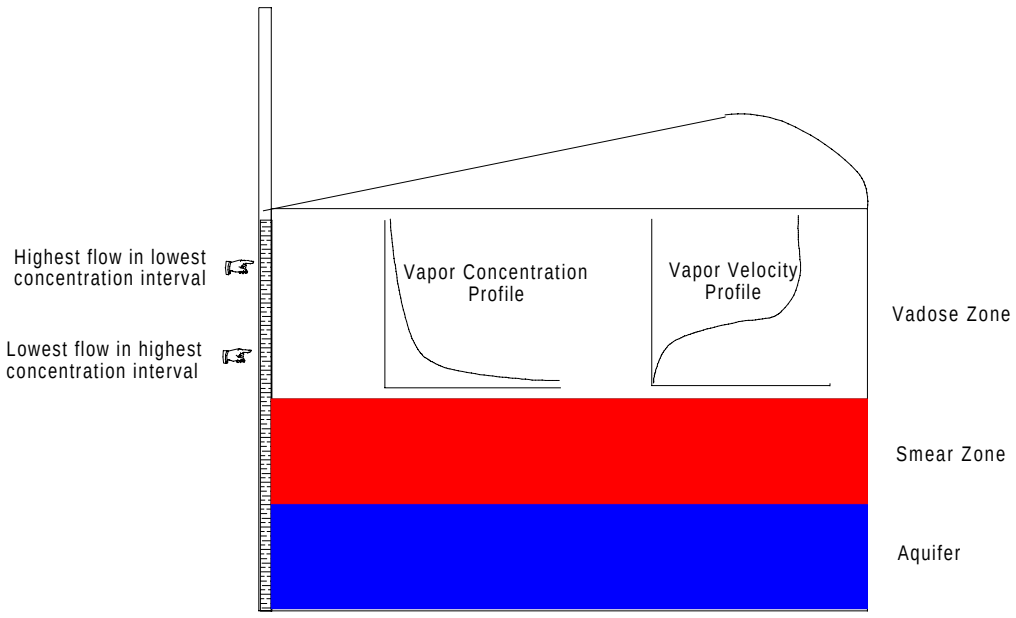

Figure 4-10. Radial section schematic showing the 2 key principles of vertical efficiency.
1) Relatively low vapor flow above the smear zone because of high liquid content;
2) Low vapor concentrations in upper zone of higher flow.

4.2.2.1 Remediation Pathway Efficiency. Envision a condition where a LNAPL plume exists in the smear zone and where site underground tank locations require the placement of a monitoring/recovery well alongside the plume, instead of in the center of the plume (Figure 4-9). The radial vapor recovery efficiency, the fraction of dilution caused by the lateral well positioning, is the ratio of the wedge through which impacted vapor is contacted compared to full radial flow across the whole plume. The impacted flow "wedge" is about 70°, for a radial efficiency of 70/360, or about 20%. Accounting for chemical diffusion above the product and the relative slowing of vapor flow due to higher moisture content near the capillary fringe, the vertical component of efficiency is estimated to be about 20% (Figure 4-10). The resultant total SVE efficiency is about 4% (20% x 20%). Knowing the vapor concentration present above standing LNAPL, one can use field concentration observations to test this efficiency or dilution factor. If the equilibrium vapor concentration of the LNAPL were 100,000 ppmv, the observed field concentration under the given conditions would be estimated at about 4,000 ppmv. This is an example of how remediation data and observations can be used as a form of characterization information to assist in constraining the site conceptual model.

In contrast to the condition above, if one had managed to install a well in the center of the plume, perhaps by slant drilling or maybe pushing a guide casing between underground tanks, the radial flow efficiency would be close to 100% (360°/360°). If that were coupled with an efficient well screen of limited length, designed to force air flow within and just above the source, one could

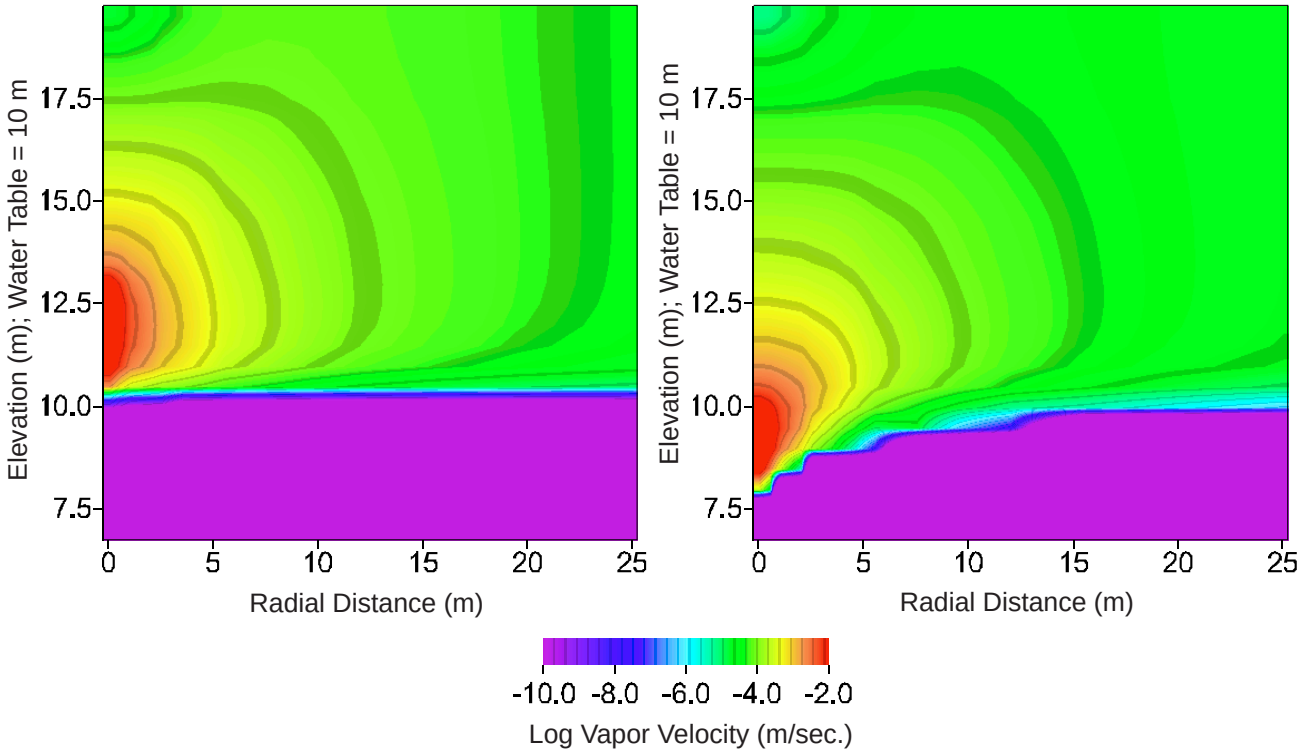

Figures 4-11a & b (left and right). Examples of cleanup efficiency where on the left, SVE is applied without groundwater drawdown, and on the right drawdown is applied to dewater part of the smear zone (original water table = 10 m elevation). One can see the logarithmic air velocity increase associated with the opening up of the smear zone to vapor flow.

expect a vertical efficiency of 50% or more, for a total SVE efficiency of about 50%. In this idealized scenario, each constituent would reach it's remediation goal about 12 times faster for this more efficient design than for one with a 4% efficiency. Achieving good cleanup efficiencies in the field is obviously more challenging.

It is worth noting that both efficient and inefficient remediation curves are asymptotic, indicating that asymptotic behavior alone has no risk relevance. Most remediation actions will go asymptotic; those designed to be efficient with respect to the formation and source will have a better likelihood of reaching mitigation goals and get there more quickly than inefficient systems. Cleanup designs that do not fully consider the depth and lateral distribution of LNAPL (target zones) will have a low certainty for reaching mitigation goals.

Flow efficiency can be further increased by considering the multiphase effects on the vapor flow path. As an example, recall that in the smear zone, all phases interact in complex interdependent ways and air does not readily flow through liquid wet pores. Let's expand the simple SVE scenario above to include the designed vapor delivery to the smear zone by a combination of groundwater drawdown and screen design. For an average sand (permeability = 25 Darcy), we will consider the SVE efficiency ramifications for the groundwater drawdown and a well screen design that forces air through the smear zone by drawing from below the original water table. We will ignore the liquid recovery aspects and simply

focus on the stripping potential in the smear zone associated with each. The calculations are performed using a multiphase simulator (Huyakorn et al., 1994). The results indicate a significant gain in efficiency by forcing air flow through the NAPL interval. A prime indicator of remediation effectiveness is the distribution of air flow relative to the source interval. Where significant flow bypasses the source, the remediation efficiency is low. Note that because the mass recovery happens from the outside in, the total airflow path is important, not simply the discrete flow rates that are exponentially higher close to the extraction zone. For the SVE-only from a 10-ft well screen, none of the flow directly crosses the smear zone, and we are left with the same condition discussed above where the vertical efficiency is about 20% or less (Figure 4-11a). In contrast, virtually all the vapor extracted crosses some portion of the smear zone for the focussed SVE with drawdown condition (Figure 4-11b). Notice, not surprisingly, that one must also plan for the right amount of dewatering to open up sufficient smear zone for vapor flow and cleanup.

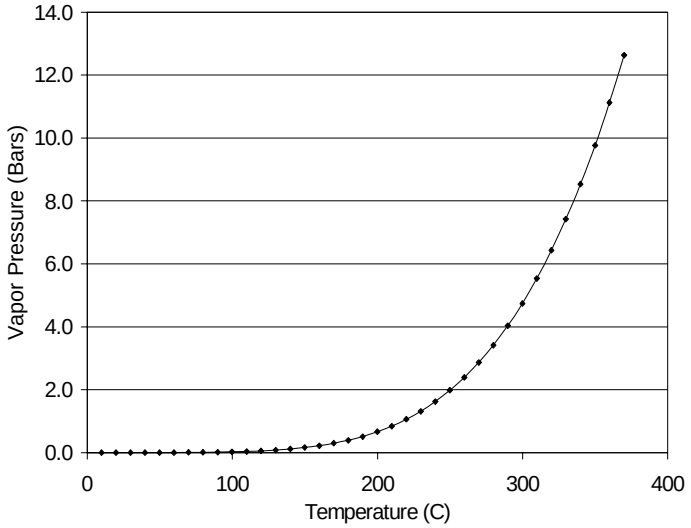

Figure 4-12. Naphthalene vapor pressure as a function of temperature. Note that the sharp increase in vapor pressure occurs above 200ºC.

Another interesting aspect of the smear zone is that both water and LNAPL will upwell in response to the applied vacuum. When the LNAPL upwells, it is still available for more efficient partitioning to the vapor phase because a contact interface is maintained. This aspect has been seen in laboratory experiments of venting above free product (Frank & Huntley, 1997). However, many conditions, such as heterogeneous soil layering or low effective conductivity toward the phase may preclude significant LNAPL upwelling with a loss in stripping efficiency. When water upwells and bypasses the LNAPL source, the vapor phase partitioning is limited by the aqueous diffusion from the source through groundwater and into the vapor stream. This attribute is documented in the field where vapor phase concentrations and mole fractions of COC are smaller than the analogous concentrations in the aqueous phase. In other words, there is an apparent disequilibrium because of the separation of the source from the cleanup stream. Because aqueous diffusion is slow, it controls the rate of mass transfer from the source to the vapor phase when the source is occluded by groundwater.

4.2.2.2 Chemical Efficiency. We will briefly mention chemical efficiency, which is in effect the degree to which the volatility and other characteristics of a COC are amenable to mass partitioning. As we saw in the examples above, MTBE and benzene are recovered more efficiently from a chemical per-

spective than is naphthalene (Figure 4-8). If we look at other less amenable compounds, such as naphthalene, we see that it is relatively immaterial whether the flow efficiency is good or poor, naphthalene is simply not efficiently recovered by chemical partitioning methods at ambient temperatures.

However, increasing the temperature of the NAPL will increase the effective vapor pressure of organic compounds (Reid et al., 1987) and therefore also increase the potential recoverability. Heating will also usually decrease the viscosity and interfacial tensions of the multiphase fluids, making the liquid phase more mobile. Again using naphthalene as an example, one sees that the pure phase vapor pressure increases significantly once temperatures exceed 200° C (Figure 4-12). Whether or not this potential gain in chemical efficiency is worth the effort depends, as always, on the specifics of site concentration reduction goals. The example is merely used to show the principle of chemical efficiency. The partitioning of vapor from the water phase (Henry's Law) may or may not benefit from heating, because the increase in vapor pressure is usually competing against an increase in aqueous solubility. The relationship is nonlinear and not discussed herein (see Reid et al., 1987).

4.2.3. Enhanced Biodegradation

Last, a brief mention of biodegradation is in order. Biodegradation is another form of chemical mass reduction where enhancements to the rate of degradation may be expected by addition of oxygen and possibly nutrients to the system. Other enhancements are also possible, but not discussed (e.g., denitrification, methanogenesis, sulfate reduction, etc.). Many LNAPL COCs microbially degrade under aerobic and some anaerobic conditions. Some chemicals, like MTBE and highly branched aliphatic compounds, degrade less readily than other compounds like mono-aromatics (e.g., benzene, toluene).

The complex interactions of the microbiologic system are often simplified by the use of a pseudo-first order reaction, where the rate of reaction depends on the concentration of one component. Typically, this relationship is put in the form of contaminant decay rate, but it can as easily be considered on the basis of oxygen utilization. The solubility of oxygen in water is about 8 mg/l at 25 C, with solubility increasing with decreasing temperature. If ambient groundwater conditions are in the 1 to 2 mg/l range, oxygenation of the water to 8 mg/l may increase the rate of decay by as much as a factor of 8. Artificial oxygenation methods, such as peroxide injection, can further increase oxygen levels in groundwater, but at a certain level sterilization effects may occur and direct chemical oxidation rather than biodecay is underway.

While the increase in biodegradation rates from enhancements associated with aeration or other mechanisms is beneficial from a groundwater transport standpoint, the relative increase in rates of LNAPL mass reduction is often small. This goes back to the fact that the LNAPL mass is often very large compared to the associated mass in the dissolved-phase. Mass must partition from the LNAPL to the groundwater phase to be available for biodegradation, a process that has many limitations

including the groundwater flow rate into and through the source zone and rates of aqueous diffusion. For LNAPL plumes of small mass and low saturations, the flux of electron acceptors into the LNAPL source zone and the associated biodegradation can be a more important mechanism of chemical mass loss in the source zone (Sweeney et al., 1998).

4.2.4. Removal of LNAPL Constituents - Summary

In summary, reduction of specific LNAPL compounds is comprised of many factors including chemical amenability and multiphase interactions. While the myriad of potential complications and enhancements cannot be considered in a brief summary, certain generalizations will usually hold true:

1. Component mass reduction will be most efficient when the delivery stream intercepts the complete interval of hydrocarbon impacts, lateral and vertical. Incomplete or inefficient delivery will doom a mass recovery strategy regardless of the underlying amenability of the method for a particular fuel source.

2. The source chemistry and attributes of the mass recovery method must be linked to evaluate the probable effectiveness of any particular remediation method.

3. When properly designed, methods that alter the source chemistry will generally have a more significant risk benefit than recovery through hydraulic means where the mass is reduced, but without significant chemical alteration.

4. To consider the site specific risk benefit of any particular mitigation method, one must set a concentration goal ahead of time. Since cleanup to pristine conditions is physically infeasible at most sites, a risk-based method to determine the safe and necessary concentration goals is clearly useful. When geologic and/or chemical conditions preclude meeting such goals, other risk management strategies become necessary and can be immediately defined.

5. Mole fraction chemical analyses of specific compounds are the most useful tools to evaluate the real effect of a particular site mass removal strategy. Mole fractions will “chromatographically” shift through time unless the chemical remediation is not accessing the full source zone or there is diffusion limiting geologic horizons.

4.2.5 Reducing Source Zone Uncertainty

Probably the greatest determinant of active remediation success is the good spatial definition of the LNAPL source, both laterally and vertically. Lateral definition is relatively straightforward from direct and indirect data from groundwater monitoring wells and borings. Vertical definition, however, can sometimes be more problematic for several potential reasons. First, soil sampling below

the water table is difficult and source definition data are often incomplete in industry standard assessments. Second, site investigation and remediation responses to subsurface releases are rarely coincident with the timing of release. Therefore, the full hydrogeologic variability of the system is often unknown. Oil flows more readily under a water drainage condition, and if sufficient LNAPL mass is present it will "trail" the historic water table during lowering conditions. Therefore, the variability we see over a short time of environmental monitoring may not reflect the full variability of the system during the release history. There are also man-made artifacts, such as salt water barrier projects that have locally overprinted deeper zones of LNAPL release. Third, the scale of NAPL movement in a heterogeneous setting is often smaller than the scale of sampling, making solid conceptual interpretation difficult.

There are several potential methods that may reduce vertical source uncertainty. The need to reduce this uncertainty depends on the remediation goals, the contrast between those goals and site conditions, and the time and financial aspects of the potential chemical remediation method. These suggested methods are not comprehensive, but may provide a starting point for enhancing the predictions of risk reduction associated with specific actions:

1. Groundwater profiling using discrete sampling techniques can be used to assist in evaluation of the vertical zone of impacts crossing monitoring well screens (Kaplan, et al., 1991). Recall from Section 3.6.2 that the groundwater concentration diminishes sharply beneath the lowermost oil/water interface in the formation. A range of calculations suggests that the underlying diffusion rind is often insignificant more than about 2 m below oil interface. Therefore, groundwater profiling can sometimes document the presence of source NAPL across the saturated well screen interval. If a strong source is present to the total depth of a well, it is possible that the zone extends downward. If strong vertical attenuation is noted, the source distribution can be inferred with relative ease and accuracy.

2. Laser and ultraviolet fluorescence methods can detect petroleum hydrocarbons in situ by the fluorescence properties of those compounds. The laser method can be closely calibrated to a range of fuel types and provide data that can be used to delineate source distributions. These tools often include a cone penetrometer log that can be correlated to geologic materials, providing a second important and often underassessed data set. Both fluorescence and penetrometer logs have a high vertical sampling density, often on the order of inches.

3. Other geophysical methods are available based on nuclear magnetic resonance, dielectric properties, resistivity, and others. Many of these methods require significant interpretation and are sometimes impractical because of tool size and cost.

4. Continuous core soil sampling is another possible method to characterize source zones beneath the water table. However, there are real limits to the collection integrity of most commonly used samplers when materials are fully liquid saturated. Suction or downhole freezing can mitigate some of these problems, but as in general practice, advanced core sampling techniques will be unavailable to many projects.

Section 5.0

LNAST USER'S GUIDE

This chapter provides guidance on how to use the toolkit software utility (LNAST; **LN**APL Dissolution **a**nd Transport **S**creening **T**ool) to evaluate LNAPL impacts to groundwater under a range of conditions. First, an overview of the program menus and structure will be given. The reader will then be guided through data input, with a discussion of the parameter selection process. Chapter 6 will provide some example problems and recommendations will be given for execution of a site screening.

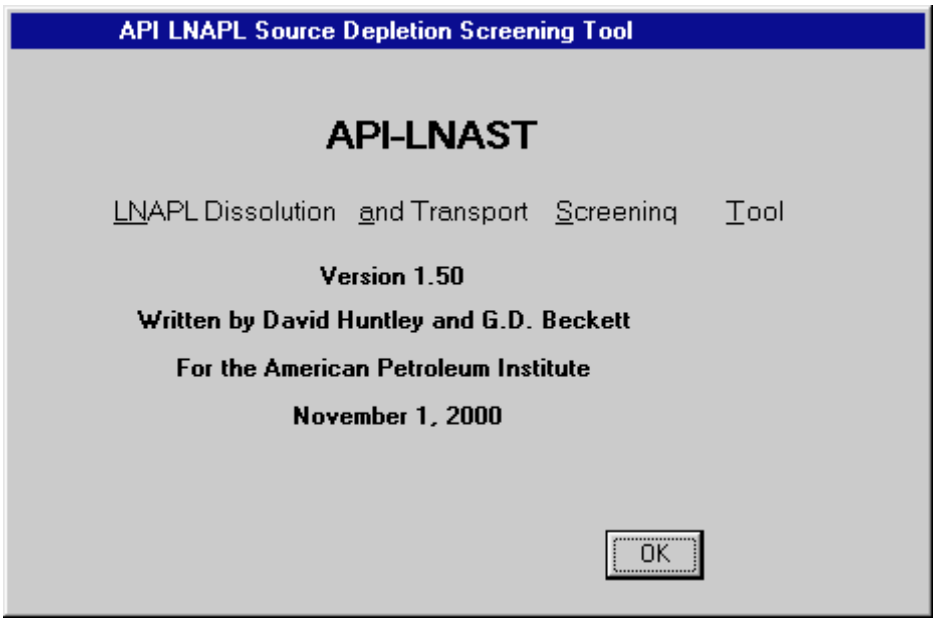

Figure 5-1, LNAST introduction screen. Select **OK** to start the program.

It is recommended that you open up the LNAST software utility for viewing as you read this section. The first window displayed is a software title screen giving version and date information (Figure 5-1). Clicking the **OK** button will take the user to the input and execution menus of the utility (Figure 5-2). Again, details of the entries and execution will be given after the general overview below.

5.1 SOFTWARE UTILITY OVERVIEW

As discussed above, the LNAST software utility was written to calculate (1) the depletion of soluble or volatile components from a multicomponent LNAPL source area, followed by (2) the downgradient movement of a dissolved phase, subject to biodegradation and dispersion. The sequence of steps the user must undertake is critical to the successful use of the program.

First, the user must select and input the appropriate soil, groundwater, and LNAPL physical and chemical properties. This is done through a series of five input tabs in the LNAPL utility, identified as "Soil Properties", "Groundwater Conditions", "Source Area Parameters", "LNAPL Properties", and "Solute Transport Properties".

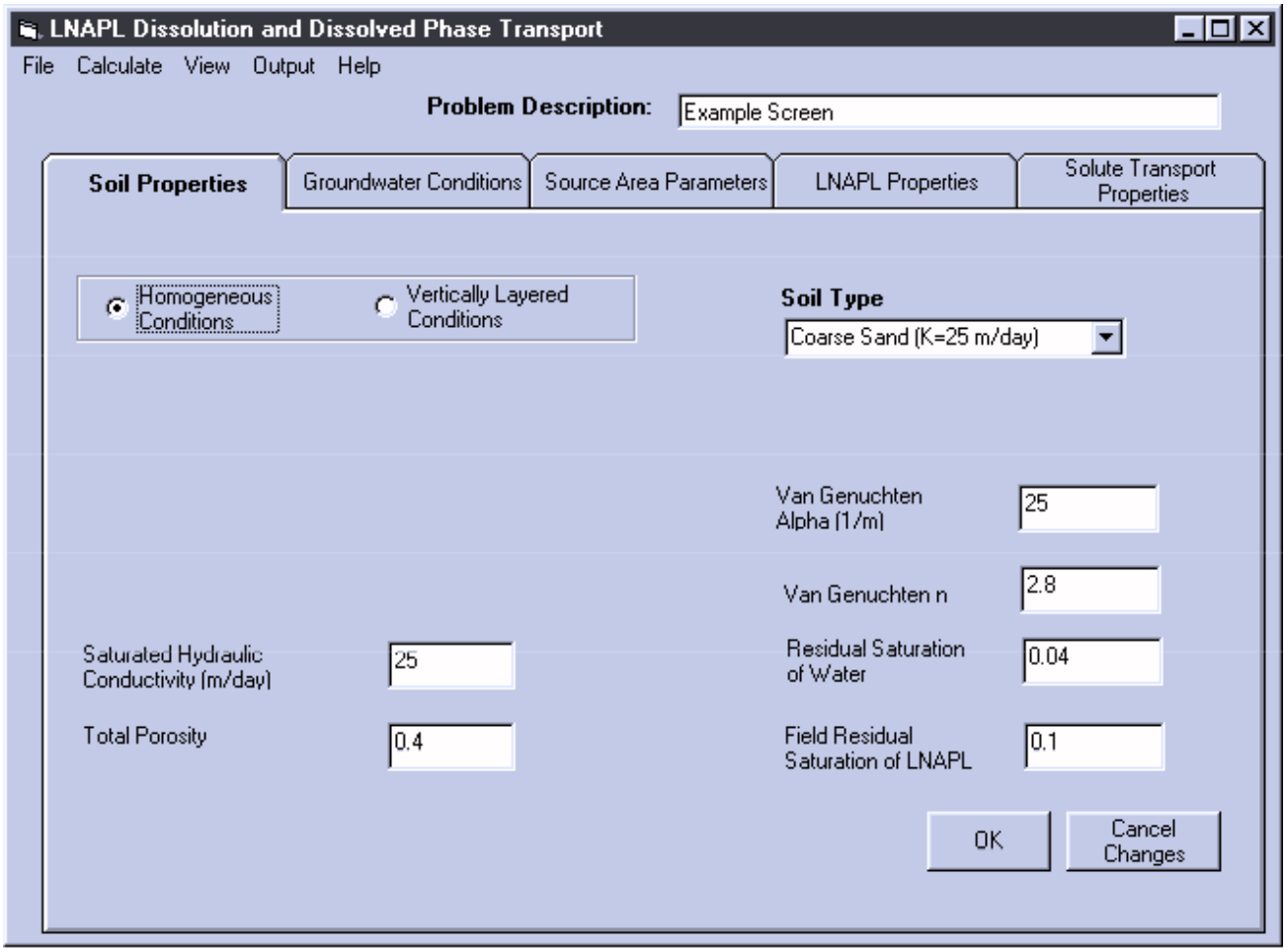

Figure 5-2. **The Soil Properties** Tab, with a homogeneous conditions and coarse sand selected.

Second, the user must direct the program to calculate the depletion of LNAPL source through dissolution and/or volatilization. This is done by selecting LNAPL Source Depletion found under the CALCULATE menu option. Based on the data previously input, the software utility first calculates LNAPL mass, distribution, and the fractions of chemicals of concern. Multiphase fluid mechanics are used to calculate the groundwater flow through the LNAPL zone, and chemical transport principles are linked to estimate advective and dispersive chemical losses from the LNAPL source. The result of this series of calculations is the dissolved phase concentration of each of the specified LNAPL components in the source area (i.e. in contact with the LNAPL) as a function of time. These results may be displayed, printed, or copied as either a table of values, a graph, or both.

Third, the results of the LNAPL source depletion calculation are used to calculate the resulting downgradient dissolved phase concentrations for each of the soluble components using the Domenico (1987) analytic solution to the three-dimensional solute transport equation under one-dimensional groundwater flow conditions. The user initiates this step by selecting Downgradient Dissolved Phase, again found under the CALCULATE menu option. It is important to note that the user must first select calculation of the LNAPL source depletion before the downgradient dissolved

phase calculations can be done. In addition, if any soil, groundwater condition, source area parameter, or LNAPL property is changed, the LNAPL source depletion calculations must be completed before any downgradient dissolved phase calculations are undertaken. The output from the source area depletion calculations are used as input to the downgradient dissolved phase calculations. As for the LNAPL source depletion calculations, the downgradient dissolved phase calculations may be displayed, printed, or copied as either a table of values, a graph, or both.

5.2 LNAST MENU OPTIONS

The LNAST software utility is organized as a standard Microsoft Windows program. Five pull-down menu options (**File**, **Calculate**, **View**, **Output**, and **Help**) are found along the top of the active window (Figures 5-2 and 5-3). The **File** menu (Figure 5-3) selection allows the user to start a **New Project**, to **Open** (an existing) **Project,** to **Save Project** using the existing file name, to **Save Project As** a new file name, or to **Exit** the program. Starting a **New Project** sets all of the parameters to their default values. This is automatically done when the user starts the program, but the user may wish to do this after completion of a series of calculations as a fast way to re-initialize everything before entering a new data set. **Open Project** will initiate a standard file open window, which allows the user to find and open a project file that has been previously saved. It is not necessary or appropriate to do this when initiating a new project. **Save Project** and **Save Project As** are the standard file save menu options in the Windows environment. **Save Project As** opens a file directory window, that allows you to specify a new file name (and directory location) to save your project information. The option **Save Project** simply saves the project under the last filename used. Finally, the **Exit** menu option is self-explanatory.

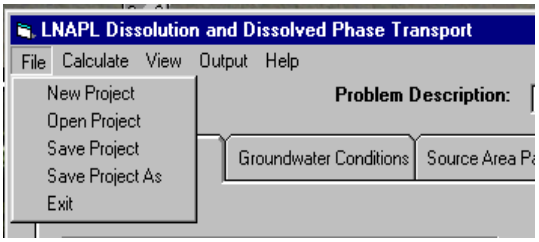

Figure 5-3. The **File** pulldown menu has several options for managing and saving calculation input files.

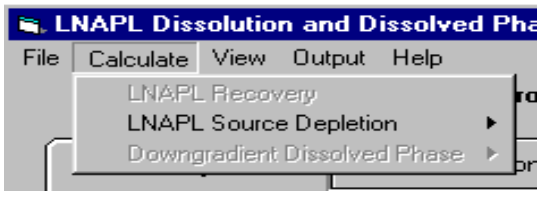

Figure 5-4. The **Calculate** menu.

The **Calculate** menu option (Figure 5-4), as discussed above, is where the user initiates calculation of the LNAPL source depletion and the downgradient dissolved phase calculations. In addition, if the user wants to calculate LNAPL source depletion (by dissolution and/or volatilization) after LNAPL recovery, the user will first select **LNAPL Recovery** from the **CALCULATE** menu option prior to calculating LNAPL source depletion. Both the **LNAPL Source Depletion** and the **Downgradient Dissolved Phase** menu items provide further choices for the user. The **LNAPL**

Source Depletion calculation may be done with or without volatilization. Under **Downgradient Dissolved Phase**, the user has the choice of either calculating **Downgradient Extent** or **Concentrations at Selected Distances.** In the first case (**Downgradient Extent**), LNAST calculates the maximum downgradient distance where each dissolved phase compound exceeds a *target concentration*, which is a user-input variable, as a function of time. In the second case (**Concentrations at Selected Distances**) the concentration/time history is calculated at up to 20 user-selected distances from the source area. In both cases, concentrations are calculated along the centerline directly downgradient of the center of the source area at the water table. Because of this, the concentrations and downgradient distances calculated by the software utility are often higher than concentrations typically observed in the field because those are often measured in wells screened across intervals that exceed the thickness of the source area and may or may not be located exactly along the axis of the plume.

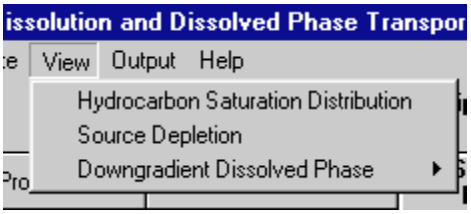

Fig. 5-5. The **View** Menu

The **View** menu option (Figure 5-5) allows the user to go back and view the results of the active calculations. These results are displayed as tables, but graphs may also be created from the **Graph** menu selection found at the top of each table. The user may view **Hydrocarbon Saturation Distribution** and/or **Source Depletion** results only after calculation of the **LNAPL Source Depletion** calculations (under the **Calculate** menu option). The user may view **Downgradient Dissolved Phase** results only after the downgradient dissolved phase calculations are complete.

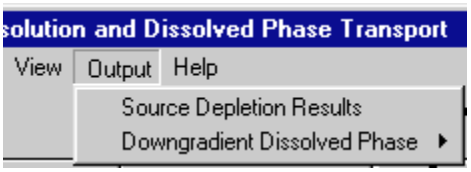

Fig. 5-6. The **Output** Menu

The **Output** menu (Figure 5-6) option allows the user to save tabulated results of either the LNAPL source depletion calculations or the downgradient dissolved phase calculations as a tab-delimited file.

For the current LNAST version (1.50), the **Help** menu option only brings up the starting screen, the window that supplies the date and version number of the program, for reference (Figure 5-1).

5.3 DATA INPUT

Users familiar with multiphase fluid mechanics and fate and transport principles may not require much guidance, but we still recommend reviewing parameter definitions used here as they may be slightly different from those you have used in the past. Screening models like this toolkit can simplify the evaluation of complex multiphase flow, multicomponent partitioning and associated chemical transport. It should be kept in mind, however, that highly erroneous results can be generated if you fail to account for parameter uncertainty and the sensitivity of the results to your input assumptions and site conceptual model. Almost certainly you will need to consider a range of site conditions to gain a full spectrum of reasonable results. Similarly, you will need to think carefully about the applicability of certain assumptions inherent in the definition of the LNAPL source term and all the other related factors. We will do our best to give you a feeling for the most critical aspects in general, but it is most important that you recognize how to place results in site context. For instance, if site groundwater concentrations exhibit characteristics indicative of a depleting LNAPL source, it would be inappropriate to select a source term that results in a large mass and correspondingly extensive long-term impacts. In other words, always ask "Does this make any sense at all with what we see at the site?" If the answer is no, it does not mean physics and chemistry have failed you, it means that one of the critical assumptions or interpretation of the results are not representative and require reevaluation.

Lastly, you will clearly have a better idea of where to start and how to assign input parameters if you measure key data at the site. A first cut of screening evaluations can certainly be performed using judgment and inferential information, and this is often a good step to defining the data most important for more refined evaluations. Given the large number of linked parameters, one may be able to generate a site conceptual model that appears representative, only to find on measurement that some key factors require revision. Solutions from multivariate models are usually non-unique, meaning more than one set of parameters can result in similar results.

As with any scientific calculation, use of consistent units is mandatory. A shareware program called "UNITS" is available on the World Wide Web that can assist in unit conversions (**http://www.steamesteem.com**, select the units conversion frame).

As noted above, the software utility calculations are based on the assignment of five linked categories of data: 1) Soil petrophysical characteristics; 2) Prevailing groundwater flow conditions; 3) Description of the LNAPL source distribution in the formation; 4) Chemical and physical properties of the LNAPL and its components of risk concern; 5) Solute transport properties. The user tabs of LNAST coincide with the 5 parameters groups defined above, and will be described in order in the sections that follow.

5.3.1 Soil Properties

Soil parameters may be input assuming either that the soil is homogeneous, or by subdividing the vertical LNAPL impacted zone into up to five layers. The user makes this choice by selecting either the ***Homogeneous Conditions*** (Figure 5-7) or the ***Vertically Layered Conditions*** (Figure 5-8) option button on the **Soil Properties** tab. If the user selects ***Homogeneous Conditions***, a single value of *Soil Type*, *Saturated Hydraulic Conductivity*, *Total Porosity*, *Van Genuchten Alpha*, *Van Genuchten n*, *Residual Saturation of Water*, and *Field Residual Saturation of LNAPL* (Figure 5-7) are entered.

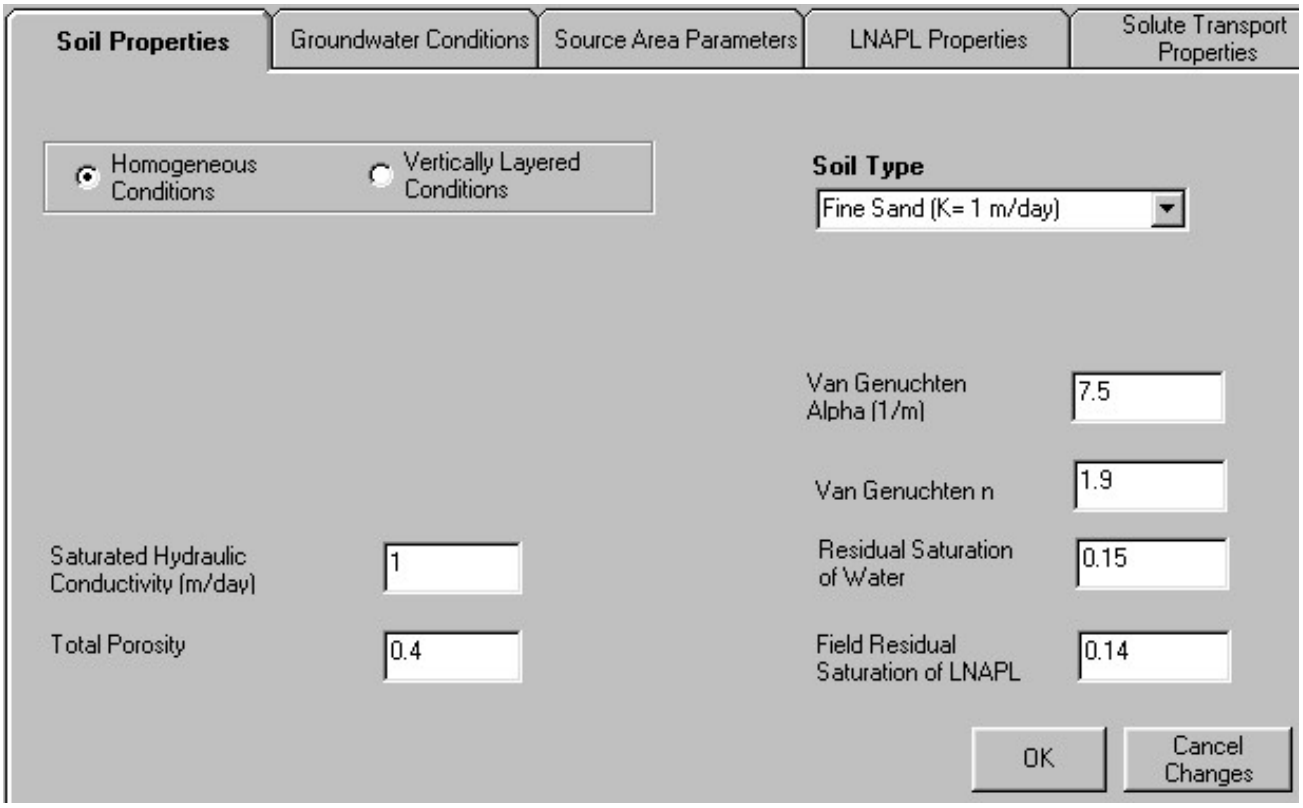

Figure 5-7. The **Soil Properties** Tab, with ***Homogeneous Conditions*** selected for a fine sand.

If the **Vertically Layered Conditions** option is selected (Figure 5-8), values for each of these parameters must be selected for each of the different layers. Prior to entering the parameters for each layer, the number of layers and the thickness of each layer must be entered. This is done by first entering a value between 2 and 5 under *Number of Soil Layers*. Then, in the adjacent box, each layer number is selected sequentially, starting with layer 1, the lower-most layer, and ending with the upper-most layer. As each layer is selected, the thickness of that layer is entered. Note that the elevation of the bottom of layer 1 is fixed at 0.0 (Figure 5-8) and that the elevation of the bottom of each subsequent layer is the sum of the bottom elevation and the thickness of the previous layer. The soil parameters *Soil Type*, *Saturated Hydraulic Conductivity*, *Total Porosity*, *Van Genuchten Alpha*, *Van Genuchten n*, *Residual Saturation of Water*, and *Field Residual Saturation of LNAPL* may be

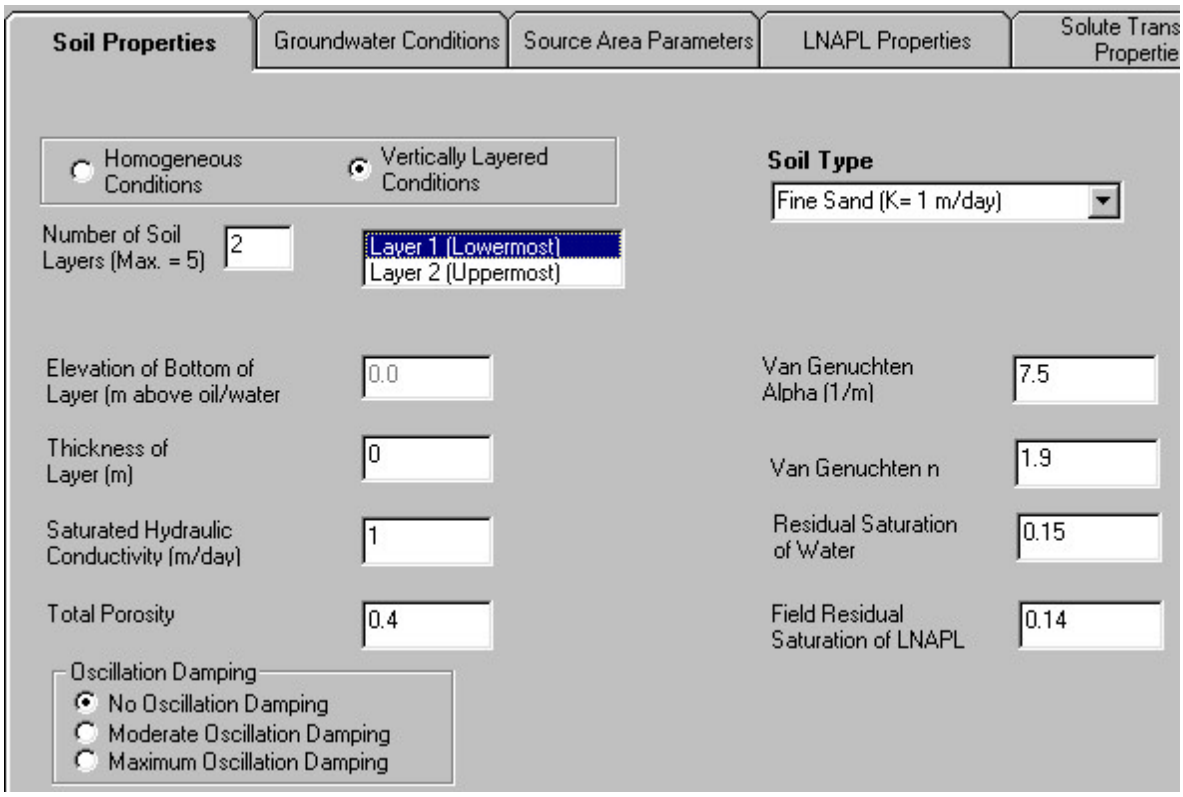

Figure 5-8. The **Soil Properties** Tab with *Vertically Layered Conditions* selected for 2 layers.

entered at the same time the thickness of each layer is entered, or the user may scroll through the layer numbers and enter those parameters separately.

The user needs to be aware that source area LNAPL depletion by groundwater dissolution only occurs between the oil/water interface and the potentiometric surface, where the piezometric surface elevation is calculated as $\rho_r t$, where t is the thickness of LNAPL and ρ_r is the relative density of the LNAPL. If, for example, the user specifies three layers, each 1 m thick, and the thickness of LNAPL is less than 2.25 m for an LNAPL with a relative density of 0.75, the uppermost layer will be entirely above the potentiomentric surface and there will be no depletion by groundwater dissolution. Similarly, any layer which is entirely below the oil/water interface will not be depleted by volatilization. This is a necessary modularization of the problem to keep the solutions analytic.

5.3.1.1 Soil Type. A soil type needs to be selected from amongst the choices available under the list box identified as **Soil Type** (Figures 5-7 & 5-8). Included within those choices is the soil type "Custom" which, after selecting, can be edited and characterized by any description desired. The soil types are provided as a descriptive indicator of changing soil texture, resulting in a range of conductive and capillary properties. The LNAST utility has been programmed with example soil

conditions from literature (Carsel & Parrish, 1988) that depend on the initial soil type selected. Though selection of a **Soil Type** results in example values of *Saturated Hydraulic Conductivity*, *Total Porosity, Van Genuchten Alpha, Van Genuchten n, Residual Saturation of Water*, and *Field Residual Saturation of LNAPL* in the **Soil Properties** tab, each of those values can be changed by the user by simply typing a new value in the appropriate input box and clicking on another box of on the **OK** button. As on all of the screens that contain **OK** and **Cancel Changes** buttons, changes in soil parameters can be canceled by clicking on the **Cancel Changes** button, which causes all values to revert to the last value entered since before clicking on the **OK** button. As prior discussions have suggested, use of site specific parameters is always preferred, whether derived through measurement or interpretation.

Each soil type is described primarily through the hydraulic conductivity, which is the basis for comparison with other selected parameters. In general, a high conductivity is correlated with coarser-grained materials and a small capillary rise. Although conductivity is a reasonable and often available correlative parameter, recognize that the calculation outcome is actually more sensitive to capillary parameters. We recommend ignoring visual or texture descriptions in favor of measured or inferred capillarity or hydraulic conductivity whenever possible. Physical soil descriptions from boring logs can be highly misleading with respect to the controlling parameters. For instance, a predominantly coarse-grained material may in fact have a large capillary rise if there is a significant fraction of interstitial fine-grained materials. Similarly, partially cemented materials will typically have both smaller porosity and pore throat size (higher capillary rise).

5.3.1.2 Saturated Hydraulic Conductivity. The hydraulic conductivity of the soil is a measurement of the relative ability of a particular fluid to flow under a prevailing gradient. As discussed previously, the hydraulic conductivity is proportional to the intrinsic permeability and the specific fluid properties (Section 3, Appendix A). LNAST requires a saturated conductivity value for water, which is ultimately used in the groundwater transport calculations both inside and outside the source zone, as well as in certain liquid recovery estimates. Example values for the textural descriptions of various soils are provided from literature.

The hydraulic conductivity for water can be estimated by various lab and field tests. Single well and aquifer pump tests provide hydraulic conductivity values at a field scale and are probably the best measurements one can obtain. In certain situations, hydraulic conductivity measurements from core samples may be viable values. Laboratory measurements of intrinsic permeability or hydraulic conductivity are essentially interchangeable since the standard properties of water are known and apply at most environmental sites. However, lab measurements can suffer from three inherent difficulties. First, small discrete samples may not be representative of the majority of the formation. This potential impact can be minimized by collecting several measurements and by using good

selection judgment in the sampling process. Second, some test methods are run at conditions not analogous to field conditions and one must use caution in interpreting and using results. For instance, a constant head permeameter test may give misleading results if not run at a confining pressure similar to where the sample was collected. Third, and perhaps most important, it can be difficult to collect undisturbed samples in many environments. These primary lab limitations generally apply to any petrophysical test. However, as will be discussed, for some parameters lab testing is often the only realistic option.

5.3.1.3 Total Porosity, Effective Porosity, Residual Water Saturation. The total porosity, effective porosity, and residual water saturation are related terms with respect to the volume of the pore space and the fraction occupied by fluids. All are entered in the program as decimal quantities, taking on values from something greater than zero but usually much less than one (never greater than one). Total porosity is the total volume of voids divided by the total sample volume. The total porosity may be calculated if one knows the bulk and dry grain density . Since many sediments are quartz rich, the grain density can often be assumed to be approximately 2.65 g/cc, leaving bulk density as the only unknown, which is a common measurement.

The effective porosity is that portion of the pore space available for transmission of fluids. It is discussed here because of its relationship to porosity and residual water, but is an input in the last LNAST tab **Solute Transport Properties**. It is smaller than total porosity because some fraction of pore water is usually held as an immobile layer adjacent to pore walls (Hillel, 1982; Corey, 1986) and some pores may be unconnected. The effective porosity is used in calculation of the dissolved-phase solute transport. LNAST allows input of the effective porosity term or approximates it by subtracting the product of the residual water saturation times the total porosity from the total porosity (Stephens, 1996). In general, this underestimates the effective porosity, as it assumes all water retained at residual saturation is a result isolated pores which will not reach chemical equilibrium with fluids moving through the remainder of the pore space.

Residual water saturation is the fraction of water held to be irreducible under natural conditions. Residual saturation is related to residual moisture content and total porosity by $S_r = \theta_r/\theta_t$ (Appendix A). Unfortunately, there are several ways to define residual water saturation, depending on the geologic specialization using the information. In agriculture, residual water content is often taken to be the retained fraction below the wilting point, or the saturation threshold below which plant roots cannot acquire further moisture from the soil (~ 15 bars capillary pressure; Stephens, 1995). For some applications, residual water content is taken to be the retained water under field drainage conditions, also called specific retention or field capacity, which is a higher value (~ $^1/_3$ bar capillary pressure; Stephens, 1995). Regardless of the definition used, the residual water fraction generally increases as the fraction of fine-grained materials increases. We recommend using a residual water

content larger than the willting point because capillary pressures in the field in the LNAPL zone are far below the order 15 bars. The residual water saturation, in occupying volume in the pores, affects the volume of LNAPL that might be present for any particular set of conditions. The higher the residual water saturation, the smaller the LNAPL volume, all other things being equal.

5.3.1.4 Van Genuchten Capillary Parameters. The van Genuchten (VG) capillary function (1980) is used for all toolkit calculations except for the hydraulic recovery approximations where that function is converted to the Brooks-Corey (BC) capillary function (1964) (Appendices A & B). There are 2 primary parameters associated with the VG function, the parameter α that is inversely related to the capillary fringe height, with coarse materials generally having large α values and fine-grained soils having small values; the *n* parameter, which is a function of the pore throat distribution, with high values indicating high pore size uniformity. The residual water saturation (described above) is related to capillarity in calculations of pore volumes and saturation.

When capillary values must be assumed, literature values may be used (Appendix C) as qualitatively correlated to hydraulic conductivity. Note that many literature values for unconsolidated materials are from agricultural studies and that native soils might not have the same properties. Agricultural soils are usually disaggregated, tilled, and not in native depositional state. If there was an error in assuming those values based on soil class description, it would usually be to overestimate the pore throat sizing (i.e., capillary α too large), in turn resulting in overestimation of LNAPL mass, longevity, and related conditions.

One may infer some capillary generalities from pore distribution and conductivity. High conductivity often implies a larger pore throat sizing and therefore larger α value. Exceptions to this rule of thumb are formations of well-sorted materials (i.e., having similar grain sizes) that have a high conductivity and simultaneously a small α value. In general, the capillary parameters will be skewed toward the fine-grained fraction in many mixed soils when the fraction of fine material exceeds 15 to 20%. There are also methods of

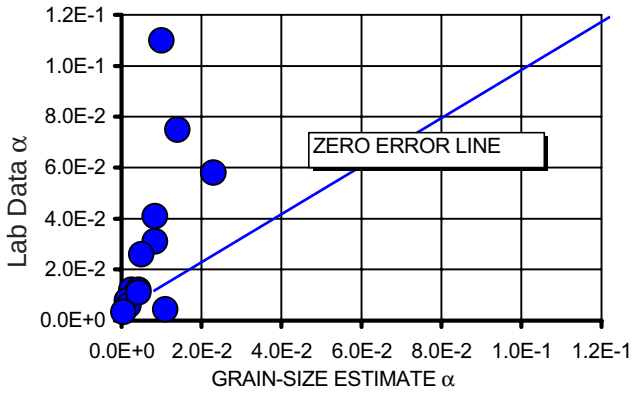

Figure 5-9. Lab versus grain-size estimated α values.

analytically constructing capillary approximations from grain-size distributions (Arya & Paris, 1981; Mishra et al., 1989). These methods can assist in making a preliminary determination of the possible range of capillary values. However, experience has shown that these methods are usually inaccurate and, because of the LNAPL sensitivity to capillary properties, should not be arbitrarily used for refined analyses (e.g., Figure 5-9).

5.3.1.5 LNAPL Field Residual Saturation. This term is analogous to residual water saturation, except it pertains to the LNAPL phase. As discussed in Section 3.4, the residual LNAPL saturation is caused by hysteresis and pore entrapment. The *field residual LNAPL saturation* is the minimum saturation that will remain at the endpoint of hydraulic LNAPL recovery. As such, it is a primary control over the residual risk impacts after hydraulic recovery has gone as far as possible. It is also important because it effectively determines the relative benefit of various hydraulic recovery strategies. For instance, if initial LNAPL saturation averaged 30% at a site and the field LNAPL residual saturation was 20%, then one can immediately see that a best-case mass recovery is about 1/3 of the original mass and 2/3 will remain in place. As will be shown subsequently, the risk magnitude will not have changed and the risk longevity will have been reduced by a similar factor (approximately 33%).

Because the field residual LNAPL mass is so important in the screening calculations, one must use caution in applying lab values that are not really measurements of residual due to hysteresis (see discussion in Section 3). There are several potential methods of approximating field residual saturation values. One is to review soil sampling data from the LNAPL impacted zone at several locations in an near the known occurrence of free phase product. The greatest saturations not associated with the occurrence of free product in a nearby well would be an indicator of the field residual saturation. For instance, in downtown San Diego, a diesel #1 plume was investigated and it was determined that at field LNAPL saturations below about 10 to 15%, no free product was observed in adjacent monitoring wells for those particular soils (Huntley et al., 1991).

Another method of estimating residual saturation is with water displacement tests whereby a soil core is first drained to residual water by forcing LNAPL through the core under pressure. Then, the LNAPL is redisplaced by water forced into the core. The oil remaining after this test is the lab residual saturation of the LNAPL smear zone. Extrapolation of lab values to field scale is always difficult and must be done with good geologic judgment. As discussed previously, lab residual saturation values will almost always be less than field residual saturation due to heterogeneities and other field scale conditions. Lacking either of the data sets above, one must rely on literature values (Appendix C) as a starting point. Recall that the LNAPL residual saturation is often related to the type of hydrocarbon spilled, with more viscous products often having greater residual saturation. Soil type and pore sorting is also important. In addition, the residual saturation in the vadose zone is often smaller than in the aquifer zone (Mercer & Cohen, 1990), and it is the aquifer zone with which we are concerned in this work. Remember that

the calculations do not apply to a mobile NAPL plume, though certain aspects may be useful in evaluation. Choose the residual saturation parameter carefully or misleading results will occur.

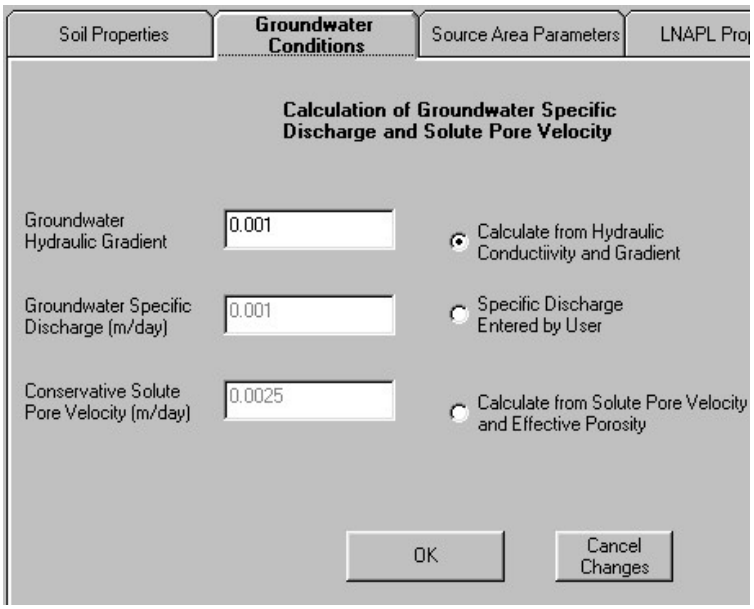

Figure 5-10a. **Groundwater Conditions** Tab for a homogenous soil.

5.3.2 Groundwater Flow Conditions

Following the **Soil Properties**, the next user Tab in the LNAST utility is **Groundwater Conditions**, which identifies the regional groundwater flow rate. The groundwater flow rate is necessary for the calculation of the depletion of the LNAPL source and for the downgradient dissolved phase transport calculations. For a single material, the groundwater flow rate can be determined by several methods, all based on Darcy's law (Figure 5-10a). For multiple soil types, the regional flow through each unit is based on a single regional gradient and the conductivity for each layer (Figure 5-3b). The flow and transport conditions are constrained by the single selected regional groundwater flow parameter. For example, if specific discharge is selected and entered, the utility uses previously entered values of hydraulic conductivity and effective porosity to calculate gradient and pore velocity. If pore velocity is selected and entered, previously entered values of effective porosity and hydraulic conductivity are used to calculate specific discharge and gradient. Finally, if hydraulic gradient is selected and entered (as it must be for multilayer conditions), previously entered values of effective porosity and hydraulic conductivity are used by the utility to calculate the regional specific discharge and groundwater pore velocity.

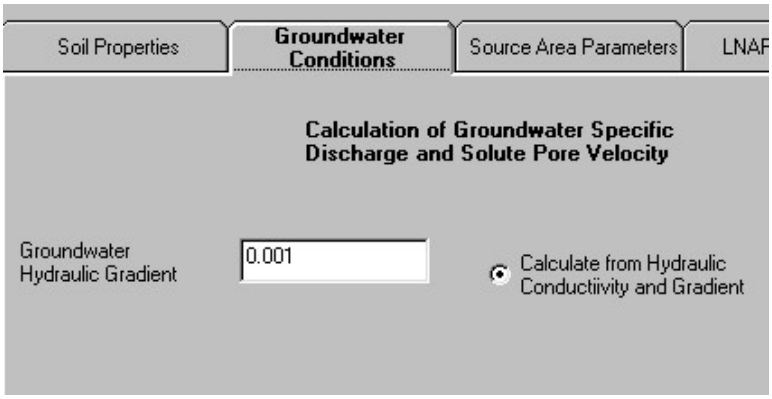

Figure 5-10b. **Groundwater Conditions** for layered soil problem.

As discussed previously, this regional groundwater flow rate is used to calculate chemical transport through, below, and beyond the source zone. Within the source zone, the flow rate is scaled by the relative permeability toward water and the resultant effective conductivity throughout the LNAPL source profile.

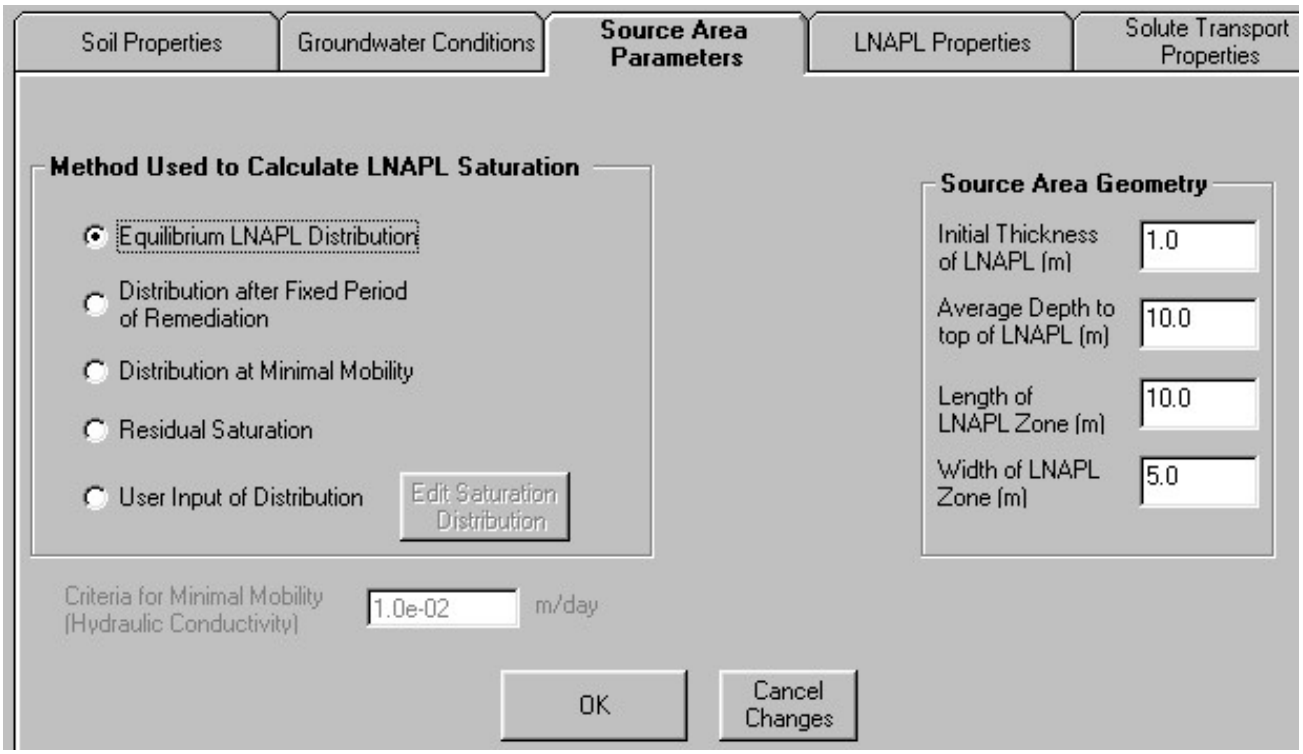

Figure 5-11. **Source Area Parameters** Tab to set LNAPL distribution and geometric conditions.

5.3.3 Source Area Parameters

The next Tab, **Source Area Parameters** (Figure 5-11), form the fundamental basis for the various possible distributions of LNAPL mass considered by the screening model that, when combined with hydrogeologic and chemical properties, result in a quantitative estimate of the potential source depletion and coincident chemical transport in groundwater and soil vapor. The right side of this Tab includes overall geometry that must be specified for all problems. The left side of the Tab determines the methodology used to calculate the vertical distribution of LNAPL within the specified geometry.

Following is a general overview of this properties Tab, followed by a more detailed discussion of each option. Starting with the geometry of the LNAPL, the **Source Area Geometry** menu includes the *Initial Thickness of the LNAPL*, the *Average Depth to the Top of the LNAPL*, the *Length of the LNAPL Zone*, and the *Width of the LNAPL Zone*. For all methods used to calculate the LNAPL saturation distribution except the user-input distribution, the *Initial Thickness of LNAPL* is the equilibrated thickness of LNAPL present or assumed to be present in a representative monitoring well in the plume area under consideration. For the user-input distribution, the *Initial Thickness of LNAPL* will be the total thickness input by the user, as discussed further below. The *Average Depth to the Top of the LNAPL* is used in the estimation of volatile losses to groundsurface, when this mechanism is considered by the user. The *Length of the LNAPL Zone* is measured in the direction of (parallel to) groundwater flow. The longevity of the source area is proportional to this length. The *Width of the LNAPL Zone* is the dimension of the source area perpendicular to the direction of

groundwater flow. Though the total mass of LNAPL in a problem is linearly related to the width of the source area for any geometry, so is the groundwater flux and therefore the rate of dissolution. Therefore under the analytic conditions of the calculations, the width of the source area has no impact on the rate of depletion of the source area, and only slightly affects downgradient dissolved phase concentrations through its effect on transverse spreading of the plume. Under "real" conditions, narrow plumes would deplete more quickly because of transverse depletion in the source zone. In these calculations, transverse spreading is not considered until groundwater transport occurs after the leading edge of the LNAPL pool. Therefore the model is conservative in this respect, and underestimates source depletion to some extent with respect to this factor.

It is apparent that the above *Source Area Geometry* describes a box, and since LNAPL plumes are not boxes, one needs to think about how to best prescribe the geometry. The prevalent control over risk and longevity are zones containing the greatest saturations of LNAPL and the longest dimensions of the source area parallel to the direction of groundwater flow. As discussed earlier, under VEQ the LNAPL source mass increases non-linearly with increased observed well thickness. So our first suggestion is to focus on areas of thickest LNAPL impacts as the zone of primary interest. Take a representative observed thickness across that area for input to the calculation. If one wished to be more refined, a contouring algorithm could be run on your observed thickness data points in the "worst-case" area to derive statistical parameters (average, mean, deviation, etc.) to identify a range of selections. Keep in mind that the LNAST utility will generate a source distribution, contaminant mass, and the distributed groundwater flow rate through the LNAPL plume. Because of the focus on conservative averaging and a host of other complications, we strongly suggest not using this mass estimate as a basis for estimating the volume of the spill. To be reasonably representative, a spill volume is estimated by accounting for source area heterogeneity, water level fluctuations, historic LNAPL thicknesses across the area of impact, and the residual saturation under 2-phase and 3-phase conditions. This type of calculation is not the intent of the toolkit screening evaluations. However, if such an estimate has been made, that LNAPL distribution and averaged mass may be input directly by the user as described in Section 5.3.3.5.

Once the source area geometry is defined, you may select from a variety of **Methods Used to Calculate LNAPL Saturation** including *Equilibrium LNAPL Distribution, Distribution after a Fixed Period of Remediation, Distribution at Minimal Mobility, Residual Saturation*, and *User Input Distribution*. These source area stipulations are as important as soil capillary properties in estimating how LNAPL impacts may behave through time, and some careful thought is warranted when selecting the parameters of a particular screening calculation.

5.3.3.1 Equilibrium LNAPL Conditions. One possible LNAPL source approximation is to use the assumption of vertical equilibrium (VEQ) with respect to the LNAPL and water phases. When this is selected, a representative LNAPL thickness is specified and is used along with soil and fluid capillary properties to calculated the vertical distribution of the LNAPL source zone (see section 3.1 for background). It is important to remember that the VEQ assumption, while straightforward, may not be representative for many reasons (recall Section 3.2). VEQ is most likely to be prevalent in homogenous or coarser grained materials where groundwater fluctuations are minimal. There are cases where these assumptions do a good job representing field LNAPL saturation conditions (recall Figures 3-13a-b).

5.3.3.2 Distribution after Fixed Period of Remediation. The LNAST utility has modularized a multiphase recovery estimate method based on several simplifying hydraulic principles, as discussed previously. The multiphase recovery approximation techniques are fully documented by Charbeneau, 1999 (Appendix B). To calculate the *Distribution of LNAPL after a Fixed Period of Remediation*, the user selects the remediation option after specifying the soil, groundwater, and initial source distribution geometry. The selection button is 2nd from the top on the left-hand side of the **Source Area Parameters** Tab (Figure 5-11). When performing a calculation using this option, the user must click on the **LNAPL Recovery** option under the **Calculate** pulldown menu before proceeding to the depletion and downgradient extent calculations. When one executes this calculation, a second user screen will appear (Figure 5-12), and additional inputs will be required depending on the specific LNAPL recovery mechanism selected. The **Calculate** option is only selected after all five primary parameter input tabs have been completed. It is mentioned here because of its order of appearance in the parameter tabs.

As noted previously, LNAPL recovery calculations are estimates of hydraulic recovery only and do not consider the chemical changes that may occur during various cleanup actions. For each cleanup option, there is a specific set of required inputs, such as the radius of capture, drawdown, applied vacuum, screen length, and others depending on the specific option selected (Figure 5-12). Selection of more than one well results only in the multiplication of recovery rates from a single well. It does not consider issues of well interference or any other hydraulic complications or multiphase issues. The LNAPL pool must be bigger than the radius of capture to benefit from evaluating “multiple” well recovery. The selected inputs for each remediation condition, along with the LNAPL distribution and related mobility characteristics, determine the rate of cleanup for a particular option. The recovery calculations can be run for any user selected time to indicate whether a hydraulic recovery action will result in a desired concentration target or timeframe of impacts as a result of that specified period of recovery. As a reminder, all the provided cleanup estimates converge on the specified residual LNAPL saturation selected in the **Soil Properties** Tab, so the endpoint of all the recovery methods will be identical; only the time to reach the endpoint will vary.

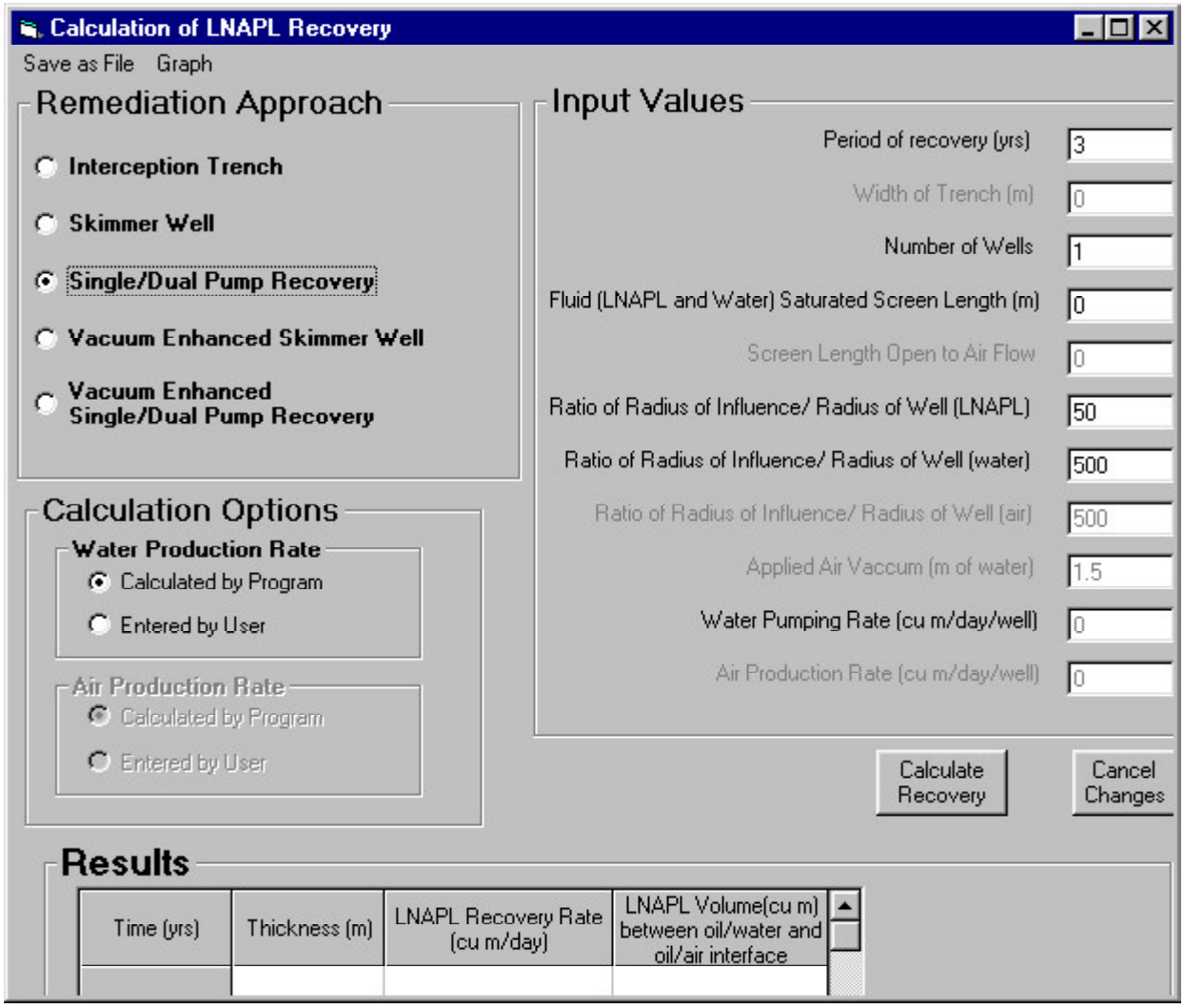

Figure 5-12. The Calculation of LNAPL Recovery screen that appears when this option is selected from the calculate menu. When recovery is considered, this calculation must be the first completed.

It is important to remember that the screening hydraulic recovery method is based on the Brooks-Corey capillary description of LNAPL distribution (Appendix B; Charbeneau, 1999). In that description, product is theoretically not present or mobile at observed thicknesses less than the corresponding oil entry pressure. This creates a mass calculation discrepancy between the continuous van Genuchten function used in this work for other related calculations as compared to the Brooks-Corey recovery function. In simple terms, the recovery function should be viewed as the recovery of the approximate mobile fraction of free product. The LNAPL recovery estimates are also optimistic and generally underpredict the time of recovery and overestimate the recovery effectiveness because of the assumptions inherent in simplifying the multiphase flow problem to an anlytic approach. The suggested use is for comparative evaluations of different strategies under different timeframes.

The specific remediation options are as follows, each requiring different user input. The required input is highlighted automatically by the LNAST utility on selection by the user of the option button corresponding to the specific remediation method. Each of the hydraulic recovery methods is described briefly in the following paragraphs, with the full equations and description provided in Appendix B (Charbeneau et al., 1999).

1. Interception Trench: The trench is assumed to passively collect LNAPL by ambient drainage. The gradient is the difference between the product/air interface and the groundwater piezometric surface (a.k.a., corrected groundwater elevation). This results in skimming with no groundwater production or drawdown. The solution is based on the analytic solution to a horizontal sink in a rectangular domain and on the width of that sink (Appendix B). Mathematically, the trench length must be less than or equal to the plume width.

2. LNAPL Skimmer Well: This is a radial pumping well solution based on the Thiem equation solution to a line-sink in a radial domain (Appendix B). The drawdown for LNAPL is the difference between the product/air interface and the groundwater piezometric surface (a.k.a., corrected groundwater elevation). The only other parameter required is the ratio of the radius of influence with respect to product to the radius of the well, including filter pack.

3. Single/Dual Pump LNAPL Recovery Well: Like #2 above, except that groundwater production is allowed beneath the LNAPL source zone to induce a larger gradient than under skimming conditions. Both the groundwater and LNAPL respond to that increased gradient. The solution for both groundwater and LNAPL recovery is again based on the Thiem equation solution to a line-sink in a radial domain (Appendix B). The program either calculates the water production rate based on the conductivity and screen length provided (i.e., effective transmissivity), or the rate can be provided directly by the user. In turn, the water production and radii of influence ratios determine the drawdown and gradient for the given hydraulic conductivity. In addition to the input parameters required for a skimmer well, the LNAPL saturated screen length (prior to pumping) is required as is, the ratio of the radius of influence with respect to water to the well radius. The groundwater pumping rate can either be entered by the user or be calculated by the utility. If calculated by the utility, it is assumed that both the piezometric surface and the oil/air interface are drawn down to same position (i.e., product thickness is maintained at zero in the recovery well during pumping).

4. Vacuum-Enhanced Skimmer Well: Like #2 above, except that a vacuum is applied to increase the net gradient. Although groundwater production is not explicitly calculated, there is an implicit assumption that the groundwater piezometric surface will be maintained at its static

level. Since applying a vacuum will cause fluid upwelling, groundwater production is implicitly required in this scenario, though that production rate is not calculated. This is not a comprehensive remediation calculation and only liquid phase recovery is considered. That is, there is no accounting for volatilization from the LNAPL source, which can be significant as discussed previously. The solution for these assumptions is simply a variant on the Thiem equation (Appendix B). Again, the vacuum extraction rate can either be entered directly by the user, or calculated by the program, given the applied air vacuum.

5. Vacuum-Enhanced Single/Dual Pump Recovery: A combination of #3 and #4 above, with no other explanation required.

Once the remediation alternative has been selected and the appropriate parameters entered, the recovery through time is calculated by clicking on the **Calculate Recovery** button. The recovery history table can be saved to a file by selecting the **Save as File** menu option, and as with all other results tables, this can also be plotted by selecting the **Graph** option. It is not necessary, however, to save the results to a file for the transport calculations to occur, as the results are saved in memory for access by the transport calculations. After completing the remediation calculation, return to the main part of the program by closing the LNAPL recovery window. The results and the effect on the LNAPL distribution in the source zone will be stored in memory by the program for use in the subsequent calculations of dissolution and transport, as discussed subsequently.

5.3.3.3 Distribution at Minimal Mobility. The third possible LNAPL distribution option is the *Distribution at Minimal Mobility* (effective LNAPL conductivity), where the LNAPL saturation corresponding to the specified effective conductivity is determined from the effective conductivity function (Section 3.3; Appendix A). When this option button is selected, the *Criterion for Minimal Mobility* box at the bottom right of the tab will now requires user input of the specific mobility threshold. For instance, one might select a threshold LNAPL conductivity similar to that used for leachate water

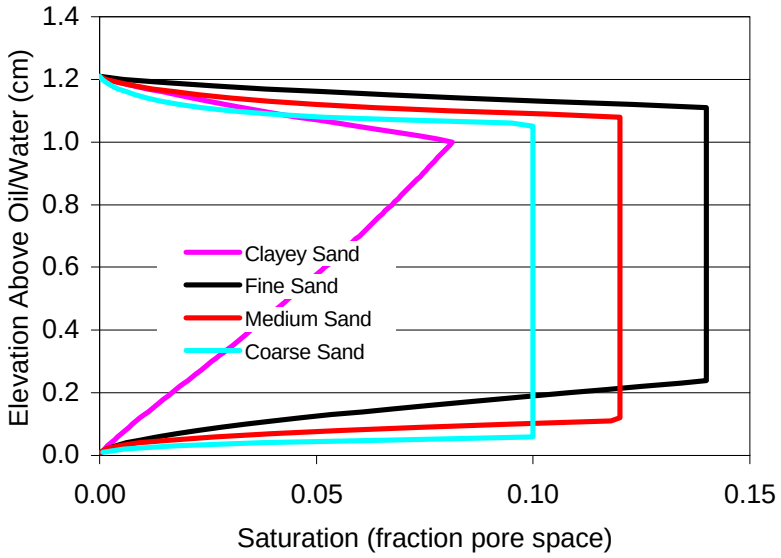

Figure 5-13. LNAPL profiles at minimum mobility, showing truncation once the criterion saturation threshold is reached. Notice that for the clayey material, the threshold is not anywhere exceeded and the profile is unchanged.

in certain regulated landfills, such as the 10^{-6} cm/sec (8.64×10^{-4} m/day). Alternatively, since landfill drainage is vertical and the LNAPL pool gradient is lateral, one could use the LNAPL gradient to scale the effective mobilty. Other mobility criteria can be generated by the user based on professional judgment, regulatory requirements, or other relevant factors.

Like all of the **Methods Used to Calculate LNAPL Saturation**, except the user-input distribution, the derivation of the minimum conductivity begins with a VEQ LNAPL saturation profile for the stipulated thickness condition. Then, the profile is truncated at the LNAPL saturation that corresponds to an effective conductivity equal to that specified by the user (Figure 5-13). This estimate method is therefore limited by the same conditions applying to VEQ, and, additionally, assumes that the relative permeability function (Appendix A) is a reasonable approximation of actual conditions.

5.3.3.4 Field Residual Saturation. This option assumes that the maximum LNAPL saturations in a profile are equal to the LNAPL residual saturation specified previously in the **Soil Properties** Tab. As for the other options (except user specified), it operates by first calculating a saturation profile under vertical equilibrium conditions. Where calculated saturations are below field residual, they are left untouched. Where calculated saturations are above residual, they are reduced to the field residual saturation value. This results in a truncated profile similar to those discussed above (see Figure 5-13). The resulting saturation distribution therefore depends upon the soil parameters and the specified thickness of the LNAPL-impacted interval.

Recall also that the endpoint of any hydraulic recovery scheme, given sufficient time, will be the field residual saturation. Therefore, selecting this option will provide a direct estimate of plume longevity and transport after any hydraulic recovery method, but without a time to reach the recovery endpoint. This calculation is useful when the conditions are such that the field residual saturation results in long-lived plume regardless of the hydraulic remediation strategy. In other words, one is able to say something tangible about the best case hydraulic recovery condition without going through the steps to calculate that recovery.

5.3.3.5 User Input LNAPL Distribution. This option allows the user to define the vertical LNAPL saturation profile based on data, interpretations, or other information. When selected, this option allows the user to pull up a submenu (by clicking on the *Edit Saturation Distribution* button) that allows incremental definition of the saturation profile (Figure 5-14). The number of depth intervals is based on your knowledge of the saturation distribution, derived either through assumption or measurement. Application of measured saturation values is self-evident; the user simply inputs results for each interval over which the data apply. The LNAST utility linearizes this data as a step function upward from the lowermost LNAPL/water interface in the formation. A value of zero saturation is assumed by the program at the base of the LNAPL (elevation = 0).

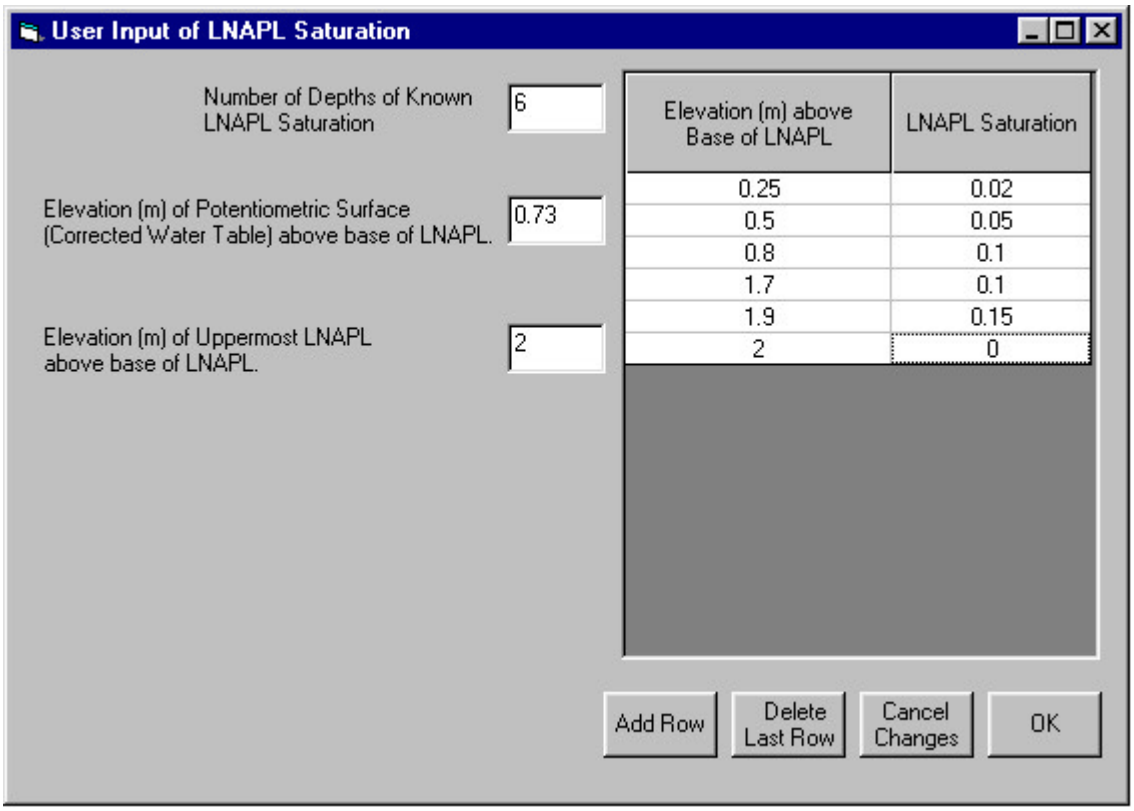

Figure 5-14. User defined input of LNAPL distribution for the smear zone example given in the text. Direct measurements can be similarly input.

A smear zone example is given to illustrate data entry. Suppose that the observed thickness in an observation well is currently about 0.3 m, and that the current water/LNAPL interface has risen about 1.7 m over some period. We know that the saturation profile of the current observed thickness does not represent the total zone of LNAPL impact because LNAPL will be stranded in the interval where the LNAPL/ water interface rose (Figure 5-15). The LNAPL in that zone will be at residual oil saturation, except for the base of the profile where LNAPL saturation is less than the residual (Figure 5-15). In our example then, the saturation profile would be piecewise specified from the base upward (Figure 5-14). The mass and relative groundwater flow through the profile is calculated by the utility as discussed previously.

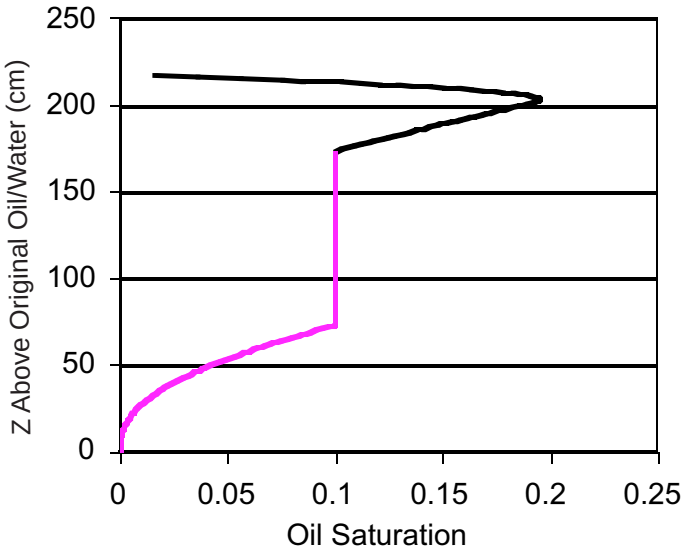

Figure 5-15. LNAPL smearing example due to a rise in the water table, creating a 200 cm (2 m) smear zone.

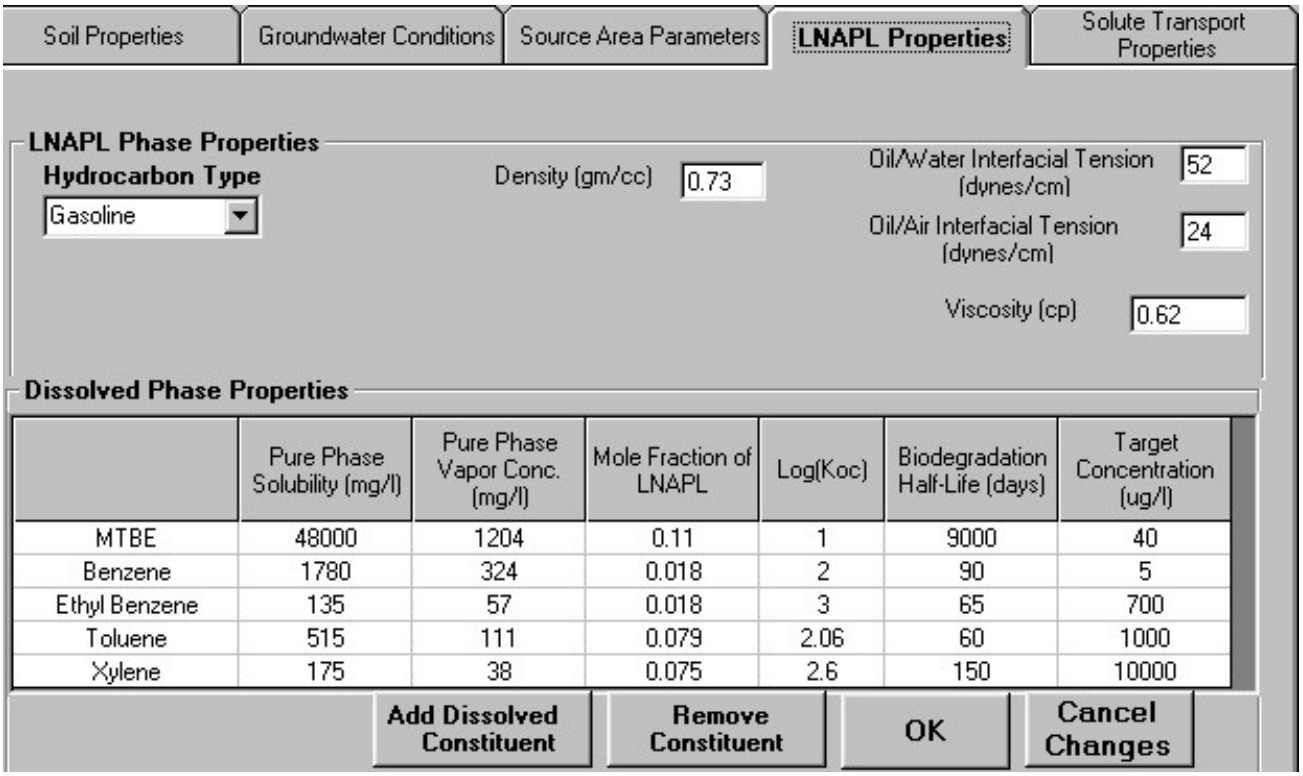

	Pure Phase Solubility (mg/l)	Pure Phase Vapor Conc. (mg/l)	Mole Fraction of LNAPL	Log(Koc)	Biodegradation Half-Life (days)	Target Concentration (ug/l)
MTBE	48000	1204	0.11	1	9000	40
Benzene	1780	324	0.018	2	90	5
Ethyl Benzene	135	57	0.018	3	65	700
Toluene	515	111	0.079	2.06	60	1000
Xylene	175	38	0.075	2.6	150	10000

Figure 5-16. The **LNAPL Properties** Tab.

5.3.4 LNAPL Properties

The fourth Tab in the LNAST utility is the **LNAPL Properties** (Figure 5-16) that includes both the physical and chemical attributes of the LNAPL source. The physical aspects combine with soil properties and are important in the mobility, recoverability, and saturation conditions of the source. The physical input values often vary, most particularly the interfacial tension value of the oil/water couplet.

The chemical parameters are a key element of the fate and transport outcomes of various components from the source, and ultimately of risk. Of all the parameters used in these LNAPL and groundwater transport calculations, the chemistry aspects are the most affected by regulatory guidance, particularly the *Target Concentration*. Further, fuels are chemically variable depending not only on the refined characteristics, which have been variable through time and different manufacturers, but also on the environment and characteristics of the spill itself. It is unlikely that LNAST's default chemical inputs will apply to many sites. Guidance on chemical inputs will be provided, but it is recommended that the appropriate regulatory standards be considered when the final values are selected for chemical screening. Each jurisdiction will likely have specific issues that cannot

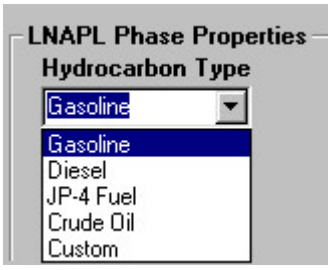

Figure 5-17. Hydrocarbon Type.

be addressed in a general document such as this. Examples of LNAPL physical and chemical properties, toxicology, and ranges of fuel compositions are provided in Appendix C. It may also be of interest for the reader to refer to the Total Petroleum Hydrocarbon Criteria Working Group documents for additional information on fuels, chemical fractions, and toxicology (AEHS, 1999).

The LNAST Tab for **LNAPL Properties** has a drop box for the primary description of the *hydrocarbon type* including gasoline, jet fuel, diesel, crude, or custom (Figure 5-17). The LNAPL need not be a petroleum fuel, as long as the physical and chemical properties are known and the basic assumptions made in the toolkit are applicable. Once the LNAPL drop-box item is selected, all the remaining parameter boxes in the tab fill with the suggested "default" parameters. Like all values used in the software utility, the values in the input boxes are user-editable. Do not use the default values if you know them to be non-representative of the site LNAPL of interest. They are intended as a general starting point only, and site specific values should be used whenever available.

The physical and chemical properties entered should be those properties of the LNAPL source as it exists in the subsurface (and in contact with groundwater), not at the fuel pump. Many changes in chemistry occur in NAPLs as they are transported through the vadose zone. The mole fraction of volatile constituents, such as MTBE and benzene, are likely to be much different at depth than in the original surface source (see the example problems in Section 6). In addition, there is sensitivity to the LNAPL physical properties, particularly field interfacial tension values. Chemical and physical analysis of site specific free product, or at a minimum, corresponding evaluations of dissolved-phase concentrations in groundwater is recommended to assist in making more representative calculations of chemical impacts.

5.3.4.1 LNAPL Physical Properties. The physical LNAPL parameters include interfacial tensions, viscosity, and density (in approximate order of relevance). The interfacial fluid tensions (IFT) are used to scale the air/water capillary parameters to the LNAPL/air and LNAPL/water systems (Leverett, 1941; Appendix C), as discussed in Section 3.2. These three capillary couplets are necessary to develop the multiphase description of the source, and these are relatively sensitive values. Note that IFT includes surface tension, a term typically used for liquid in contact with vapor. The viscosity is an important fluid parameter affecting the conductivity of the oil phase (recall prior discussions in Section 3). Density is also a component of conductivity, but is less important because the relative range of variability is small, generally between 0.7 and 0.9 g/cc. Typical ranges for these parameters for a variety of petroleum products can be found in Appendix C.

5.3.4.2 Chemical Properties of LNAPL. Up to this point, factors that control the distribution, mobility, and physical transport of the LNAPL have been discussed. This parameter section takes us into the chemical aspects of the LNAPL. There are three critical factors in this section: 1) Selection of

the chemicals of concern; 2) Selection of the molar fraction of those compounds; 3) Selection of the biodegradation rate. The remaining factors, such as pure phase solubility, organic carbon partitioning coefficient, and vapor concentration are well documented in literature or are easily derived. The target concentration is also straightforward and can be a risk-based standard, a cleanup guideline, an regulatory standard, or other applicable concentration. Federal drinking water standards have been used as the default here, and should not be used site specifically unless consistent with potential water use and applicable regulations. As discussed above, selection of a *Hydrocarbon Type* results in the creation of an example set of soluble compounds of concern. The individual chemical properties of these compounds of concern be edited, and compounds can be added or removed. Any chemical that is not present in your LNAPL source should be removed from the list, by clicking on the **Remove Constituent** button, and selecting the constituent you want removed from the list of constituents in the drop box. Alternatively, if you want to add a constituent, click on the **Add Constituent** button, which adds a blank line on the bottom of the **Chemical Phase Properties** table. The user must now manually enter the required data in that last line of the table.

5.3.4.2.1 Chemicals of Concern. Petroleum fuels are refined from crude oils that have different compositions and the specifications of refining have also varied through time with the changing formulations of the manufacturers (example fuels in Appendix C). Further, the subsurface weathering and degradation of fuels is also sensitive to many environmental variables. Because of this, the component makeup of fuels themselves is variable, therefore the utility user must use caution when selecting both the specific chemical components and their molar fractions within the fuel source. As mentioned earlier, the regulatory agencies associated with a particular site may also have specific guidance and expectations with respect to the specific compounds of concern in various LNAPLs.

In the work presented here, the default chemicals of concern and their maximum expected mole fractions were assimilated from the TPH Criteria Working Group Series (AEHS, 1999). In that work, a wide range of scientific input was sought regarding composition and risk properties of fuels, and a large example database compiled.

In the LNAST LNAPL Properties Tab, one can see that several example gasoline compounds and their physical properties are listed for each fuel type (Figure 5-9; gasoline example). If there are different compounds at the site being screened, the user can insert them for evaluation, as noted above. As mentioned, examples of fuel composition, properties, and toxicity information are provided in Appendix C. Selected parameters requiring user judgment are discussed below. Standard physical properties such as pure phase solubility, vapor concentration, log K_{oc}, and regulatory standards are not discussed as the user can simply input that information from a reliable source.

As an aside, pure phase vapor properties are often reported in terms of partial pressures or volumetrically. These may be converted to the units used in the LNAST utility through the ideal gas law ($pv = nRT$), where p = partial pressure of the compound, v = volume, n = moles, R = ideal gas constant, and T = temperature, all in consistent units. Further, note that ($n/v = p/RT$) is the molar concentration (moles/volume), and knowing the molecular weight of the chemical compound, one can convert to mass per volume units. For readers unfamiliar with these gas law calculations, any basic chemistry text will provide sufficient background.

5.3.4.2.2 Mole Fractions. As discussed, the mole fractions selected for evaluation have a large impact on the results. For instance, pure xylenes would dissolve in water to 175 mg/l, clearly above the federal maximum contaminant limit (MCL) for drinking water of 10 mg/l. However, at a mid-range gasoline mole fraction of 5%, xylenes would only attain an effective solubility of 8.75 mg/l, which is below the MCL. Therefore, whether or not xylenes are a threat above drinking water standards or other mitigation targets depends directly on the mole fraction input. Recalling the previous discussion of Raoult's Law (Section 3.7), it is straightforward to use measured water chemistry in or very near the source to assist in determining the mole fraction in the source (Appendix C). The primary caution in this approach is that dilution can distort the results, and biodecay and sorption can alter the groundwater plume chemistry with distance from the source. Therefore, it is important when gathering mole fraction information that only samples within or very near the source zone be used in the evaluation.

5.3.4.2.3 Organic Carbon Partitioning Coefficient. The organic carbon partitioning coefficient (K_{oc}) is a measure of a chemical's affinity for the organic matter that may be present in soil (Jury et al., 1986). The higher the K_{oc}, the greater the partitioning between the dissolved-phase groundwater and soil matter, all other things being equal. The soil partitioning coefficient (K_d) is the product of the K_{oc} and the fraction of organic carbon (F_{oc}), discussed in the Solute Transport Properties section below). Whereas K_{oc} is a constant for any given compound at standard conditions, the actual partitioning to soil depends on the F_{oc} and other physical soil properties. This factor is used in the groundwater transport calculation and accounts for the slowing (retardation) of compounds having a relatively high affinity for the organic phase.

The organic carbon partitioning coefficient is a common measure for organic compounds. Lacking this information, there are also relationships linking the octanol-water partitioning (K_{ow}) to the K_{oc} (Karickhoff et al., 1979).

5.3.4.2.4 Biodegradation Half-Life. Biodegradation is calculated by a pseudo-first order rate reaction within the groundwater transport module. First order reactions are described by half-lives, or correspondingly by decay constants. As mentioned in Section 3, biodegradation is the most important factor limiting the extent of many dissolved-phase petroleum constituents. While there are many indicators of biodegradation activity, the primary indication is a stagnant or receding dissolved-phase

plume. Literature half-life values for various LNAPL compounds span several orders of magnitude (Howard et al., 1991). The example values provided are in the typically expected range with the understanding that this is a site specific parameter.

To select a biodecay half-life, we recommend the user run several iterations of the calculation method to back into a degradation rate that makes sense for the plume dimensions at your site. Note that as a rate, biodegradation depends on residence time. Under high groundwater flow rates, a smaller half-life is required to result in a plume having the same length as under conditions of lower groundwater flow velocity. So if one evaluates a range of flow rates, an inversely proportional range of biodecay rates would also be needed to fit the same observed plume. As has been discussed, there is an apparent interdependency between groundwater flow rates and biodegradation rates such that this comparative approach is necessary. Based on field observations, one would generally expect higher decay rates at higher rates of flow.

5.3.4.2.5 Target Concentration. The target concentration is that which one would like in groundwater at any spatial point of concern. This could be a regulatory threshold, risk-based target, nuisance-based target, or other concentration based on the specifics of a particular site. When the LNAST program calculates the downgradient extent of a compound of concern, it defines the limit relative to this target concentration goal.

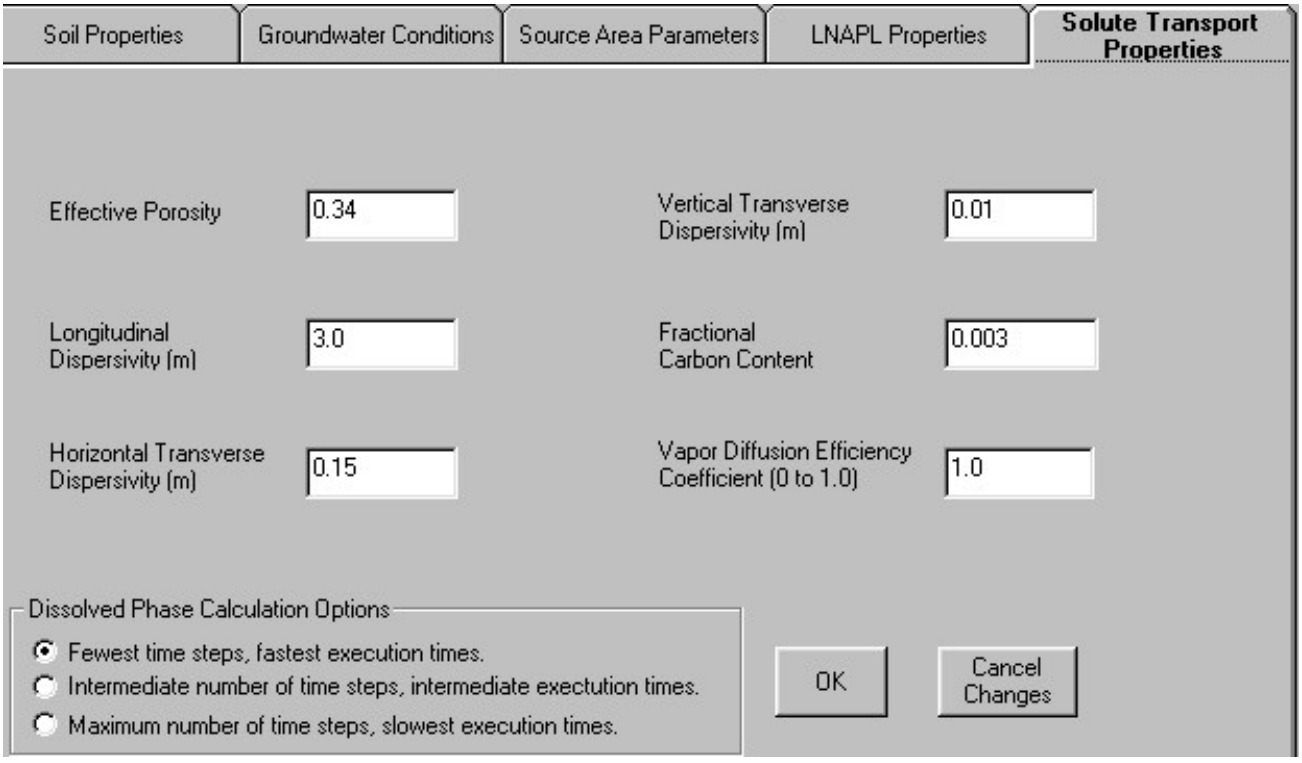

Figure 5-18. The **Solute Transport Properties** Tab.

5.3.5 Solute Transport Properties

The fifth and last Tab is for the **Solute Transport Properties** (Figure 5-18), where the remainder of the parameters needed to calculate groundwater transport of hydrocarbon compounds away from the source are specified. These are just the transport parameters that do not fit in well in the other parameter groups. However, as discussed, all of the properties specified in prior Tabs also influence solute transport outcomes directly or indirectly.

5.3.5.1 Effective Porosity. The effective porosity, as discussed previously, is automatically calculated to be the total porosity minus the residual volumetric water content (direct and indirect inputs in the first Tab, **Soil Properties**). One can also directly input a different effective porosity if desired. The effective porosity is used in the calculation of the average linear groundwater flow velocity, a key input in the groundwater transport equations.

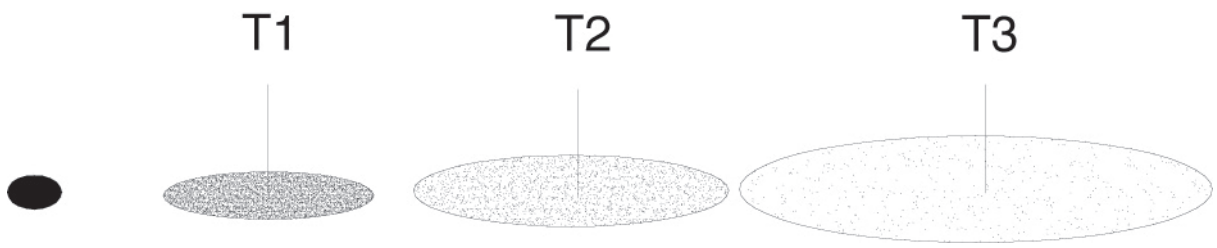

Figure 5-19. Schematic instant point source plume migration downgradient, showing the effects of dispersion, as the plume mass is unchanged but occupies a larger volume through increasing time T1, T2 and T3 (non-degraded conditions).

5.3.5.2 Dispersivity. The dispersion of plumes causes spreading and dilution away from the ideal centerline of movement. For an ideal, nonreactive (i.e., no biodegradation) point source plume, the total solute mass remains unchanged after elimination of the source, but occupies a larger and larger volume as dispersive travel progresses (Figure 5-19). There are three factors influencing dispersion: 1) Mixing in pore channels due to complex pathways; 2) Mixing in individual pore channels due to discrete contrasts in the fluid velocity profile; 3) Mixing from molecular diffusion of compounds following the chemical gradient. Of these, the mechanical mixing aspects are usually the most important, except in low permeability materials where diffusion plays an important role (Sauty, 1980, Pickens & Grisak, 1981). The term dispersivity refers to the coefficient of hydrodynamic mixing, with the total mechanical mixing being proportional to both the dispersivity and the velocity (Appendix A). Therefore, more plume mixing occurs at higher groundwater velocities. The dispersivity can be derived by measuring breakthrough curves for a solute passing through a soil core, and then fitting a type curve. However, several studies have determined that dispersivity is a scale dependent parameter (Pickens & Grisak, 1981; Sudicky, 1986; Xu & Eckstein, 1995). Therefore, applying a lab-derived value may be of little practical value, since the field-scale dispersivity would usually be significantly larger.

While field studies of dispersivity have produced variable results, some general rules of thumb have been identified based on the field scale of the plume: 1) Longitudinal dispersivity [α_l] 10% of plume length; 2) Horizontal or transverse dispersivity [α_t] 10 to 33% of α_l; 3) and vertical dispersivity 1 to 5% of [α_l]. For more refined estimates, one can calibrate to site observations. A wider plume than predicted might indicate a larger transverse dispersivity, a longer more diffuse plume could suggest a larger value of longitudinal dispersivity. While of general interest, the dispersivity is not the most critical parameter in the calculation results, although it clearly influences the net plume distribution.

5.3.5.3 Fractional Carbon Content. The fractional organic carbon content (Foc) is a measure of natural organic material in soil for which organic contaminant in petroleum have some affinity and will partition to during the spreading stages of dissolved-phase plume genesis. Fine-grained minerals can also act analogously, sorbing some fraction of the passing petroleum plume. When organic material is present, the sorption of individual compounds generally depends on the affinity for the organic phase as compared to the water phase. Usually, sorption of organic compounds increases with increasing molecular weight, polarity, and branched structure.

This parameter can be measured or inferred, as it has low sensitivity in the calculations when LNAPL mass is present. For most alluvial sediments, the value of organic carbon is typically low. However, deposition in many aquatic environments can include a significant organic content, in which case lab measurements are recommended. A caution for lab measurement is that certain ranges of petroleum contamination will be measured as organic carbon unless the lab is aware that the sample may be impacted and treats it accordingly.

5.3.5.4 Vapor Diffusion Efficiency. This vapor diffusion efficiency is a scalar from 0 to 1 (Appendix A) that is multiplied by the vapor flux to reduce the net flux exiting the LNAPL source. One may use this coefficient based on site specific measurement for any condition that can limit vapor transport from the LNAPL to ground surface. One such condition present at many sites is a low vapor permeability surface cover, like concrete or asphalt. Most risk assessment guidelines allow a vapor flux attenuation factor between 0.1 and 0.001 for such conditions (ASTM, 1995). Another condition that will limit vapor flux is any zone of high moisture content. We know from capillary discussions in Section 3 that fine-grained materials interbedded with coarse will usually have a much higher water content and lower effective vapor diffusion efficiency.

We recommend the user input vapor diffusion efficiency for surface cover as suggested in regulatory guidance and/or in a specific risk evaluation method. For soil zones of high moisture, it is recommended that the user determine the effective vapor diffusion coefficient using the moisture content and the Millington-Quirk Equation (Section 3.7). A rough approximation for the vapor efficiency

coefficient is to calculate the "new" effective diffusion coefficient (accounting for the high moisture horizon) and divide that by the original, while accounting for the zone thicknesses (Equation 5-1):

$$D^*_e \approx L_t/(L_m/D_{em} + L_d/D_{ed})$$

$$VE \approx D_e^*/D_{ed}$$

where ***L*** *is the particular zone thickness where the subscript* ***t*** *indicates total,* ***m*** *and* ***d*** *moist and dry,* $\boldsymbol{D_e}$ *is the new effective vapor diffusion coefficient, and* ***VE*** *is the vapor efficiency coefficient.*

A more thorough method for estimating vapor diffusion efficiency is to first calculate the stratigraphic moisture profile above the capillary zone for the two soil types you are evaluating, the dryer and the more moist. Then, construct a stratigraphic moisture profile by superimposing the moisture from each soil type into the proper elevation sequence (recall Figure 3-42). Calculate the effective diffusion coefficient (D_e*) using the summation equation in Appendix A, and divide by the original integrated value (D_{ed}) to define the vapor efficiency coefficient.

5.4 PERFORMING CALCULATIONS

This is an overview of the calculation procedure using the LNAST utility. The interested user may gain additional insight by reviewing the example problems in the following chapter where some of the thought processes are provided and the first example problem is a working tutorial. Through the five Tabs in the LNAST utility, the user has input soil, groundwater, source distribution, LNAPL properties, and transport parameters necessary to evaluate the time dependent concentrations within and associated with the LNAPL source under ambient and remediated conditions.

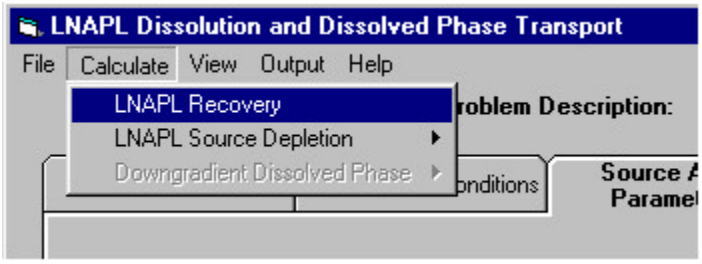

Figure 5-20. The Calculate drop menu. Source depletion is calculated from initial LNAPL conditions directly or, alternatively, the LNAPL distribution after a fixed period of remediation is calculated 1st, depending on the source area selection by the user.

The calculation sequence begins by pulling down the **Calculate** Menu (Figure 5-20). If LNAPL source distribution after remediation is selected, the first step is to calculate the source distribution for the cleanup parameters specified in the Source Parameters Option, and no other calculation option will be allowed by the utility (recall Section 5.5.2). If the LNAPL recovery option was not selected, one would proceed directly to the LNAPL Source Depletion calculation. The source depletion calculation *must* occur before downgradient groundwater transport calculations each and every time there is a change in any controlling parameter. The output from the source depletion calculations is the input into groundwater transport estimate, and must therefore be updated each time a new condition is considered. The source depletion estimates are stored in computer memory, and hence must be overwritten by explicit recalculation or old values will be used for the new problem, producing incorrect results.

The user has two source depletion options, with or without volatilization (Figure 5-21). Recall the discussion of the vapor efficiency coefficient that affects volatilization, if selected (see Section 3.7). When the utility is given the command, it will calculate the source depletion by dissolution and, optionally, volatilization. This is the required input to the groundwater fate and transport module. When the calculation of source depletion is complete, a table will be shown (Figure 5-22) that displays the individual component dissolved phase concentrations within the source zone. The user may save the file (**Save as File**), graph (select the **Graph** menu option displayed), or simply close this window; the calculation results are held in memory and

Figure 5-21. The source depletion calculation options, with or without volatilization from the LNAPL source.

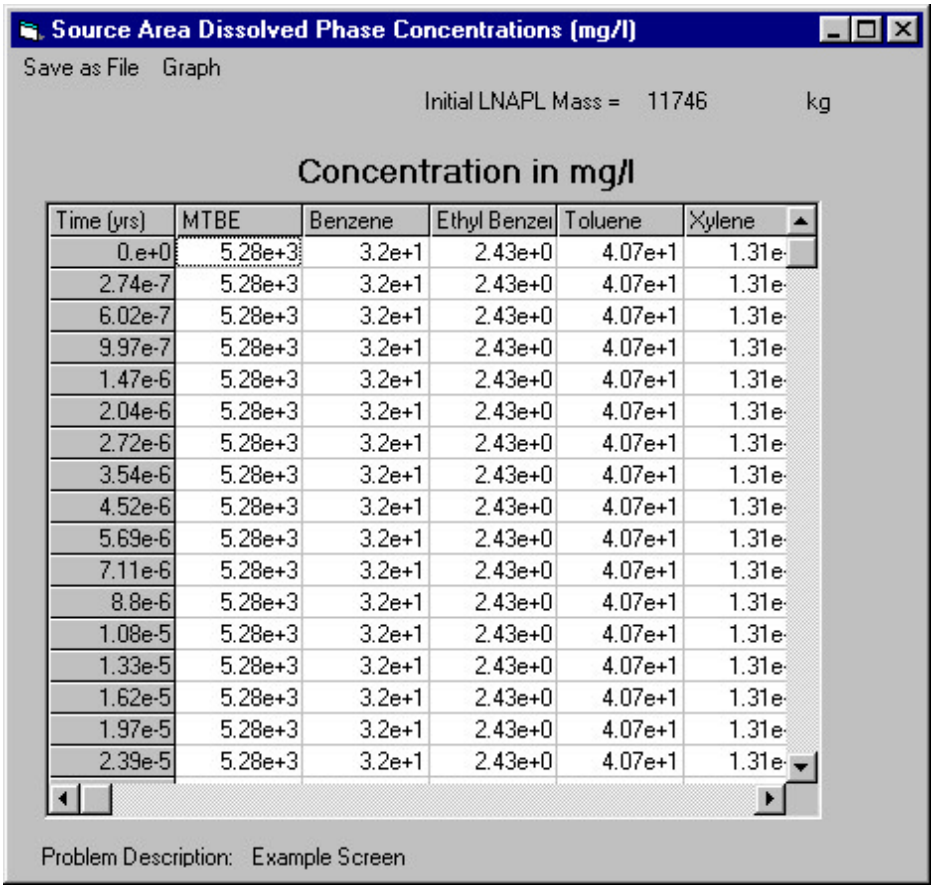

Time (yrs)	MTBE	Benzene	Ethyl Benzei	Toluene	Xylene
0.e+0	5.28e+3	3.2e+1	2.43e+0	4.07e+1	1.31e
2.74e-7	5.28e+3	3.2e+1	2.43e+0	4.07e+1	1.31e
6.02e-7	5.28e+3	3.2e+1	2.43e+0	4.07e+1	1.31e
9.97e-7	5.28e+3	3.2e+1	2.43e+0	4.07e+1	1.31e
1.47e-6	5.28e+3	3.2e+1	2.43e+0	4.07e+1	1.31e
2.04e-6	5.28e+3	3.2e+1	2.43e+0	4.07e+1	1.31e
2.72e-6	5.28e+3	3.2e+1	2.43e+0	4.07e+1	1.31e
3.54e-6	5.28e+3	3.2e+1	2.43e+0	4.07e+1	1.31e
4.52e-6	5.28e+3	3.2e+1	2.43e+0	4.07e+1	1.31e
5.69e-6	5.28e+3	3.2e+1	2.43e+0	4.07e+1	1.31e
7.11e-6	5.28e+3	3.2e+1	2.43e+0	4.07e+1	1.31e
8.8e-6	5.28e+3	3.2e+1	2.43e+0	4.07e+1	1.31e
1.08e-5	5.28e+3	3.2e+1	2.43e+0	4.07e+1	1.31e
1.33e-5	5.28e+3	3.2e+1	2.43e+0	4.07e+1	1.31e
1.62e-5	5.28e+3	3.2e+1	2.43e+0	4.07e+1	1.31e
1.97e-5	5.28e+3	3.2e+1	2.43e+0	4.07e+1	1.31e
2.39e-5	5.28e+3	3.2e+1	2.43e+0	4.07e+1	1.31e

Figure 5-22. Output table that is automatically displayed after calculation of the source zone depletion estimate. The concentration values represent the estimated concentration in groundwater at the leading edge of the LNAPL source zone. Vapor losses are considered, if selected.

the table and graph are available in the **View** menu until another calculation is run. The hydrocarbon mass in the geometric source zone is also provided but, as discussed earlier, should not be viewed as an actual plume mass estimate because of simplifying geometric conditions and because one would typically select worst-case areas for screening purposes. It is best viewed as an averaged mass in a type area. However, if this LNAPL mass is infeasibly large based on other site knowledge, that would indicate the site screening parameters need to be reconceptualized by the user. The averaged LNAPL mass is provided as a reality check for this reason. Obviously, this calculation method is constrained by mass and other relationships, and needs an estimated starting mass distribution for the type area as part of the conceptual model.

The simplest way to compare multiple site conceptualizations is to save the source depletion and transport calculation results from each run in separate files and import into a common analysis platform, such as a spreadsheet or database program. Selection of **Save as File** from the top of the output table window saves the output results as tab-delimited files ASCII file, which are easily imported into most analysis routines.

If one chooses to graph from this environment, by selecting **Graph** from the menu options at the top of the table, a plot of the concentration of all of the compounds specified in the **LNAPL Propertied** – *Dissolved Phase Properties* window will be plotted as a function of time. This graph may be manipulated in a number of ways. It may by printed to any of the printers recognized by the users

windows setup (**Print** menu option), the **Legend** may be turned on or off, the graph may be copied to another program, or the graph itself may be edited. To copy the graph to another program, select **Copy/Save** from the menu at the top of the graph, which opens a copy/export window. To copy and paste a graph directly to another program, select *Bitmap* as the Export type and *Clipboard* as the **Export Destination.** Executing the **Paste** command in any open program will then copy the graph into that open file. To save the graph as a file for import into another program in the future, select *Metafile* as the Export type and *File* as the **Export Destination.** Then click on the **Browse** button to open up menu that allows you to name the file to be saved. In addition, double-clicking on any of the graphs will bring a window that allows the user to change many of the aspects of the graph, including the title (and subtitle), the way the data sets are plotted (and which data sets are plotted), and the text fonts.

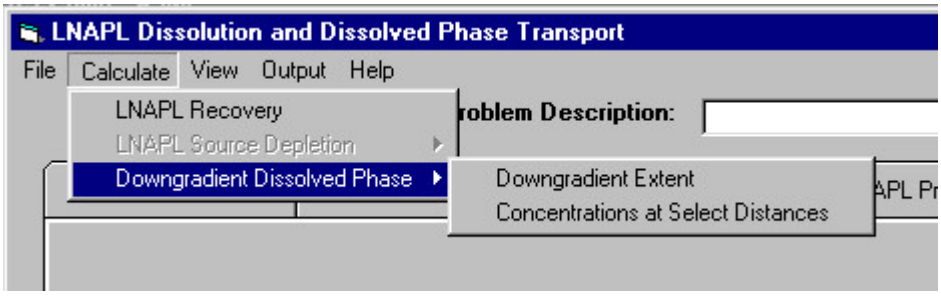

Figure 5-23. After the LNAPL source depletion is run, the Downgradient Dissolved Phase calculation can occur. Two options are provided:
1) Downgradient extent based on target concentration;
2) Concentration through time estimated at selected distances.

With the source zone depletion calculated, the user can now go on to calculate the time dependent groundwater concentrations associated with the prescribed soil and LNAPL source conditions. This action is also initiated by pulling down the **Calculate** Menu and choosing between a *Downgradient Extent* evaluation and *Concentrations at Selected Distances* (Figure 5-23). The *Downgradient Extent* evaluation calculates the downgradient movement and eventual contraction of dissolved components at their specified target concentration as a function of source depletion through time.

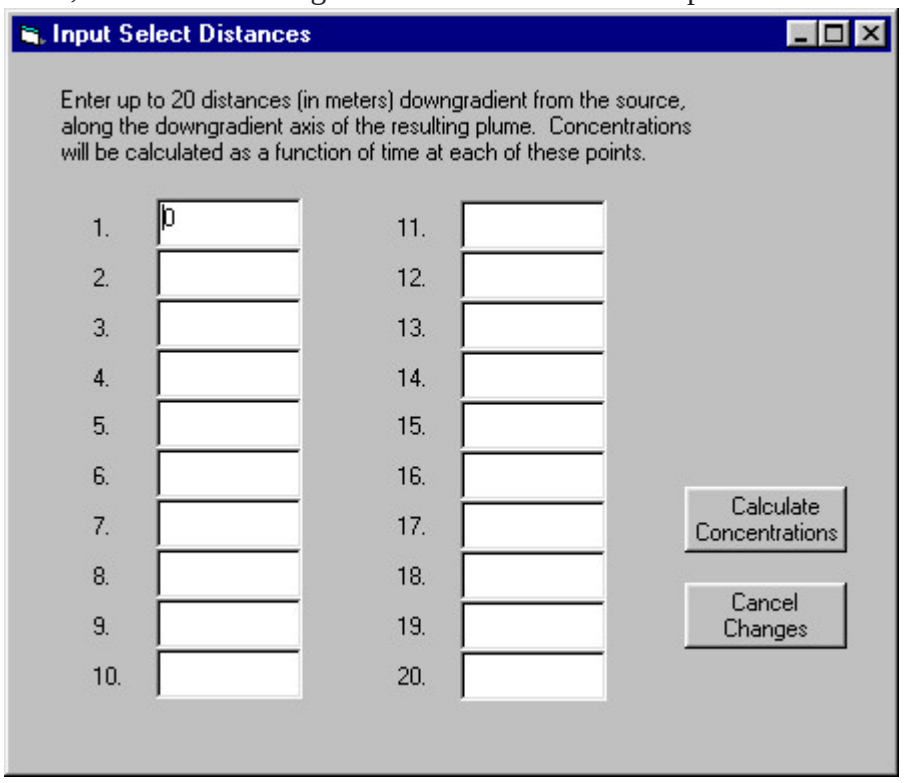

Figure 5-24. When the concentration at selected distances is selected, this screen appears prompting the user for the desired downstream locations along the central axis of the plume.

The *Concentrations At Selected Distances* are commonly known as breakthrough curves and the estimated concentration spectrum through time will be provided at the selected points (Figure 5-24). The user is prompted for the desired locations through a second drop-down menu that appears when that option from the **Downgradient Dissolved Phase** menu is selected. The execution time of the groundwater transport calculations depends on your computer CPU speed, the number of compounds selected, and the number of downgradient distances. For example, with five compounds selected, a 233 mHz computer will take approximately three minutes to execute downgradient extent simulation. A progress bar showing the degree of completion is displayed while the model is running. For any simulation, it is recommended that initial conceptual runs be done with a minimum of compounds and/or distances to "dial in" to reasonable site conditions. Then, the appropriate level of detail with respect to compounds of concern, distances, and other variable factors can be put into the final set of calculations. There is little sense in wasting time (yours and the computer's) on extensive preliminary runs investigating the probable range of site LNAPL conditions.

Once the groundwater transport is calculated, LNAST automatically displays output tables of interest. Again, these output data can be **Saved** or **Graphed** using the pull-down menu at the top of the output table. Similarly, after the runs are complete, tables and graphs can be regenerated by pulling down the **View** menu and selecting the output of interest.

5.5 KEY ASSUMPTIONS

Several key assumptions are critical in this toolkit (recall, there are several "tools" that are linked in the cleanup and transport evaluations). There are also other potential limitations stemming from unconsidered site specifics or general unknowns in the current base of scientific knowledge. Several technical considerations have been discussed in context with the subject matter of the preceding report sections. Keep the limitations in mind as you use the toolkit and you will generate better answers.

The assumptions in the list given below are ordered in relative importance, based on experience and scientific opinion, but the hierarchy of your particular site may be different. Further, certain limitations apply only when specific evaluation conditions are selected in the toolkit. The key assumptions are: 1) Homogeneous or uniformly layered soil conditions, and homogeneous fluid, and chemical conditions; 2) Capillary hysteresis is not explicitly considered, with only the residual oil factor considered; 3) Static LNAPL conditions with no active transport in the free phase outside the defined geometry; 4) Ideal remediation hydraulics under homogeneous conditions, no well interference, hydraulic inefficiency, etc.; 5) Equilibrium chemical partitioning; 6) First-order biodecay; 7) Macroscopic hydraulic and chemical interactions, no non-ideal conditions such as fingering, cutoff, etc.

Of these main assumptions, the nuances of heterogeneity cannot be overemphasized. We have already developed the primary concepts of multiphase synergy. So it is easy to imagine that aquifer

heterogeneities that cause order of magnitude changes in standard groundwater flow conditions, will now cause several orders of change for multiphase conditions. For instance, we often see field conditions where LNAPL is present in coarse-grained material near VEQ, but LNAPL is nearly absent in the interbedded fine-grained units (recall Figures 3-12 and 3-13). While complicated, it is easily explained in the multiphase context by observing that the time to equilibrium is short in the coarse materials and exponentially longer in the fine-grained zones. When coupled with natural hydrologic variability, this often means that fine-grained units will never come to equilibrium with LNAPL. Under these conditions, if one assumed the LNAPL saturation distribution to be at vertical equilibrium, the assumption would cause a larger source mass to be estimated than actually present, along with a longer source residence time than would be demonstrated in the field. The point is to keep the geologic setting and multiphase concepts in mind when using these screening tools so that the answers are in context with site conditions.

Section 6.0

EXAMPLE PROBLEMS

This section provides example problems to assist the user in understanding the use of the LNAPL partitioning and transport screening tool. The interpretive value of the evaluations depends on understanding the principles provided in prior sections, and the constraining assumptions of the calculation methods. Therefore, the primary focus is to *show the application of the principles* to site conceptual models. The importance of good hydrogeologic judgement in selecting parameter values and understanding the impact of their uncertainty has already been discussed. This screening model is intended to reflect general principles and processes, not highly detailed site specifics. You certainly can and should "dial" in parameter ranges using site specific observations, but attempts at highly detailed calibration are unlikely to better the results. You can get the big pieces right and still expect to have nuances that fall outside the range of the conditions considered. Piecing together and interpreting the results is the key to success.

In this evaluation process, one typically brackets site hydrogeologic and LNAPL conditions as they may pertain to specific regulatory, business, or public concerns. The facets of the evaluations applicable to those issues may encompass only a portion of the calculation output. For instance, if one were interested in the potential longevity of a chemical compound in fuel in a permeable horizon, one may use properties that represent that specific geologic horizon, but not surrounding materials. Thus, the results from the calculations would not be used directly to infer broader site conditions, but would rather be placed in context as one portion of overall conditions.

The first problems of this section are primarily tutorial, although they also give framework for thinking through the calculation process. The last problem is from a more complicated site to provide some insight into possible interpretive scenarios that might be developed. The permutations possible in the calculations are too extensive for complete treatment. The user will need to forge forward based on the understanding of the underlying physics, hydraulics, chemistry, and transport principles.

6.1 PROBLEM #1: TUTORIAL EXAMPLE

This first problem is highly simplified and has no site specific interpretive goals. The problem is setup for a homogenous fine-sand condition, with an equilibrium distribution of LNAPL in the source zone at an observed well thickness of 1 m (~3.3-ft). This baseline condition will be compared to the condition at the end of 3 years of simple LNAPL skimming. Example values for each property data set are used throughout most of this problem, with a few exceptions to show how user-defined inputs are added. The fuel for this example is gasoline without MTBE or other oxygenated compounds. The various parameters and operation of the program will be highlighted by API-LNAST screens, and it is suggested that you have the software running while you go through the problems.

A problem is started by opening the API-LNAST program. When the program is executed, an introduction screen showing the version and compilation data appears (Figure 6-1). Select the **OK** button, and the program will open the main screen, where the various properties tabs will show up (Figure 6-2). This example problem will proceed sequentially through

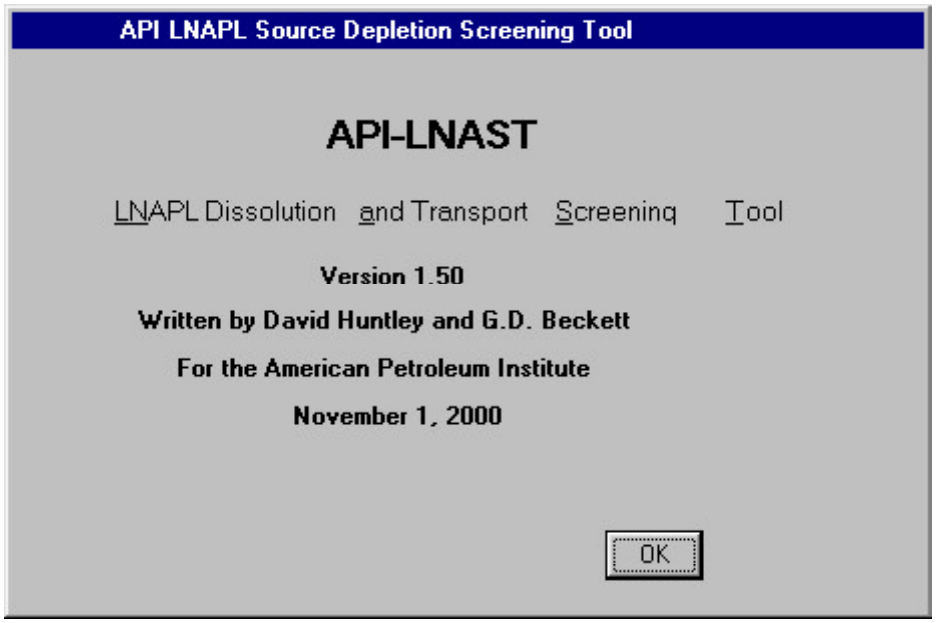

Figure 6-1, LNAST introduction screen. Select **OK** to start a problem.

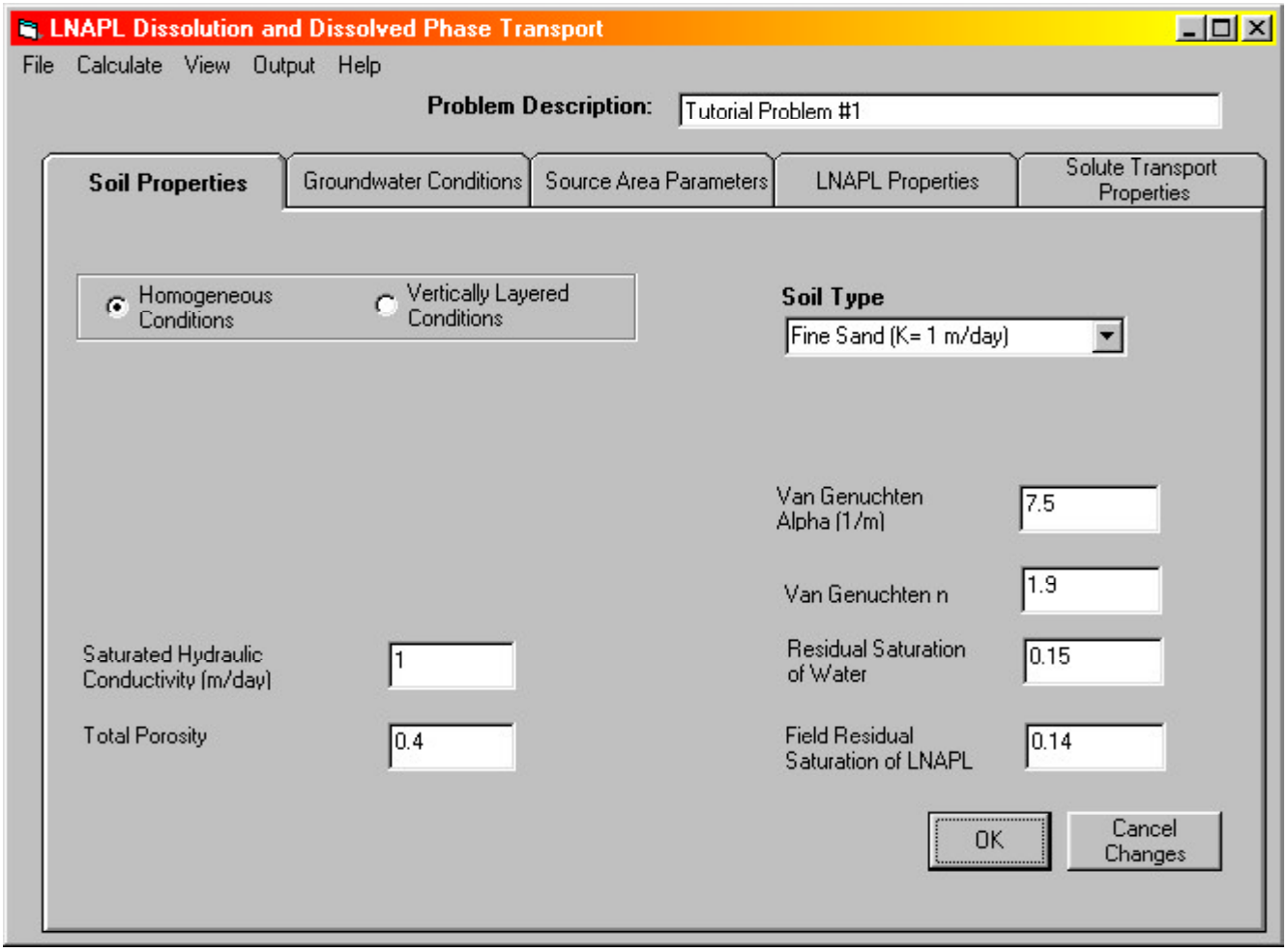

Figure 6-2. **Soil Properties** Tab for example Problem 1. A fine-sand has been selected from the **Soil Type Box**, and the example parameters are automatically provided.

the parameter screens from left to right. There is, however, no need to start with any one properties tab, but doing things in a systematic way typically decreases mistakes or confusion as analyses progress. The top menu line above the parameter input screens is used after the input selections are made, as discussed below.

First select the **Soil Properties** Tab. In that tab, there are several parameter requirements, as discussed in Section 5. For the purposes of learning, the **Homogeneous** conditions button will be selected. Later on in the problem sets, the layered heterogeneity condition will be used. Under the **Soil Type** drop box, select the fine-sand (Figure 6-2). Example parameters for this type of material will be placed in each entry box on the page, with a last reminder that the example parameters come from a variety of sources and may not apply to your particular site problem. You can replace any parameter with a site specific value by highlighting the input box with your cursor, and typing in the updated value. Remember that all data units must be consistent with those requested by the utility. For this page, length units are meters and time is in days. You may place a problem name and description in the Text Box that is present on the upper right of the utility frame.

The next Tab in the software utility (**Groundwater Conditions**; Figure 6-3) is for specifying regional groundwater flow conditions. Simply input the regional gradient, the regional specific discharge, or the average pore velocity. Each of these are related through Darcy's Law (Appendix B). Be aware that when one selects a layered condition, the only option is to input the regional groundwater gradient because the conductivity of each layer will be different and a uniform groundwater flow specification will not apply. For this example problem, we will input a hydraulic gradient of 0.005. Click the gradient selection button, highlight the input box, and type in the gradient value.

The Source Area Parameters Tab is selected next. As discussed previously, this Tab controls the geometry and physical distribution of the LNAPL source in the water table region. As noted above, this calculation will compare equilibrated LNAPL conditions for the default example thickness (1 m) to the ending conditions after 3 years of product skim-

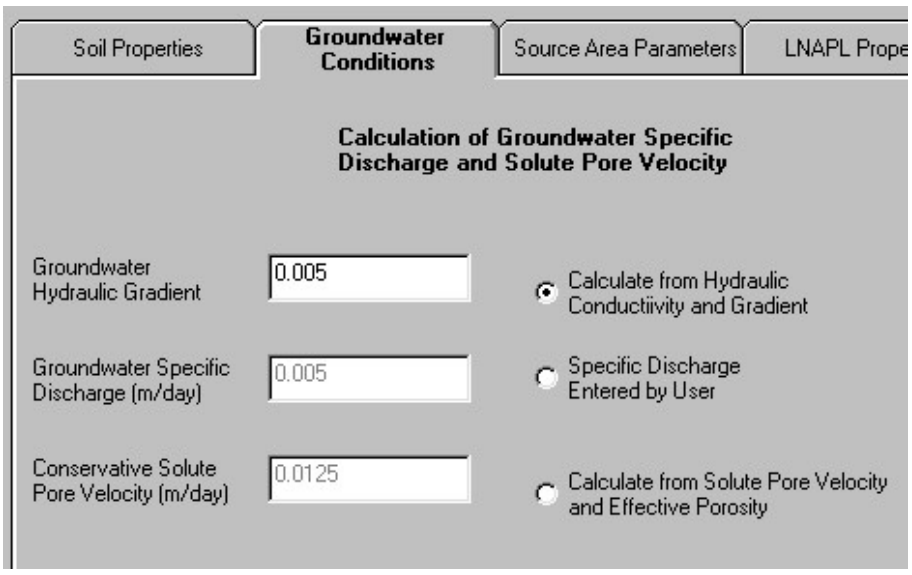

Figure 6-3. The hydraulic gradient options in the **Groundwater Conditions** Tab.

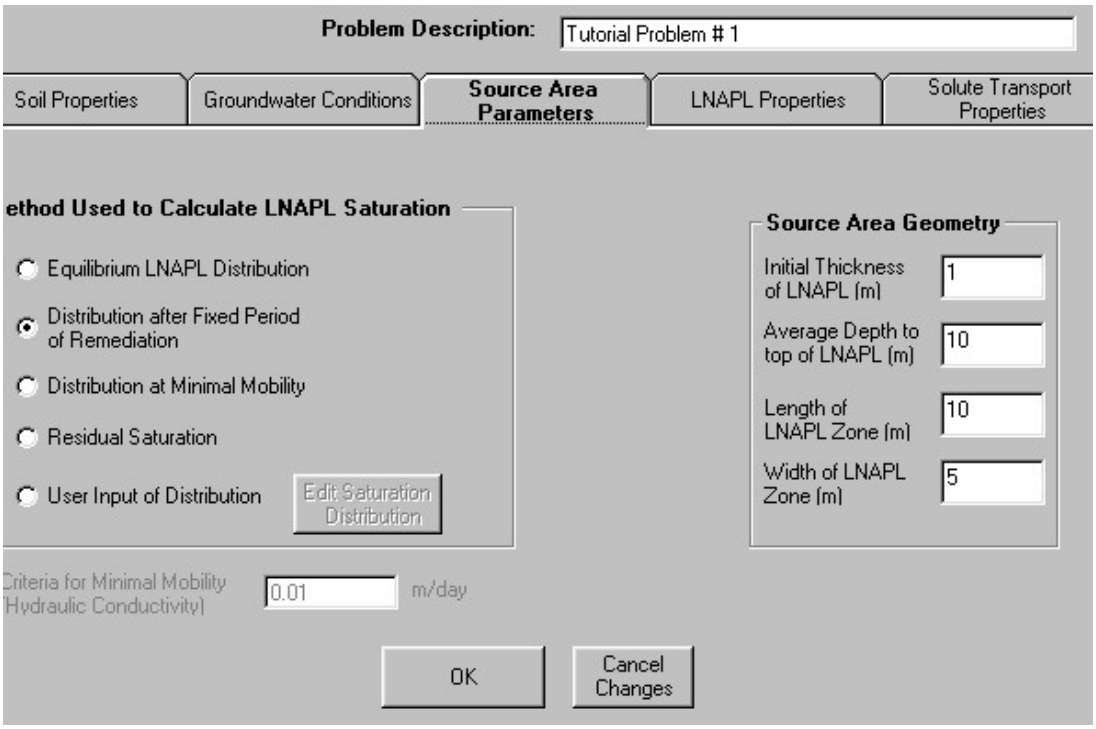

Figure 6-4. The Source Area Parameters Tab with the example selections for the first part of Problem #1. The LNAPL distribution is at vertical equilibrium, and the geometry as given on the right.

ming. Each problem for the comparison is run separately (VEQ versus skimming). So, for now, allow all example defaults on this page to remain unchanged (Figure 6-4). After the first problem has been executed, which will happen after we input the remaining information, we will come back to this page and change the source area description by adding skimming.

The next Tab in the utility is the LNAPL Properties selection. We will leave all values as given in the example screen for gasoline, except that we will remove MTBE from consideration, as the problem applies to gasoline without oxygenated additives. To remove MTBE from consideration, click on the "Remove Constituent" button on the bottom of the page. This action will bring up a selection box that provides the compound list under consideration. Highlight MTBE with the cursor, and a confirmation box will appear asking if the compound is really to be deleted (yes/no; Figure 6-5). Select "Yes", and MTBE will be removed from the table of compounds under consideration. The list of remaining com-

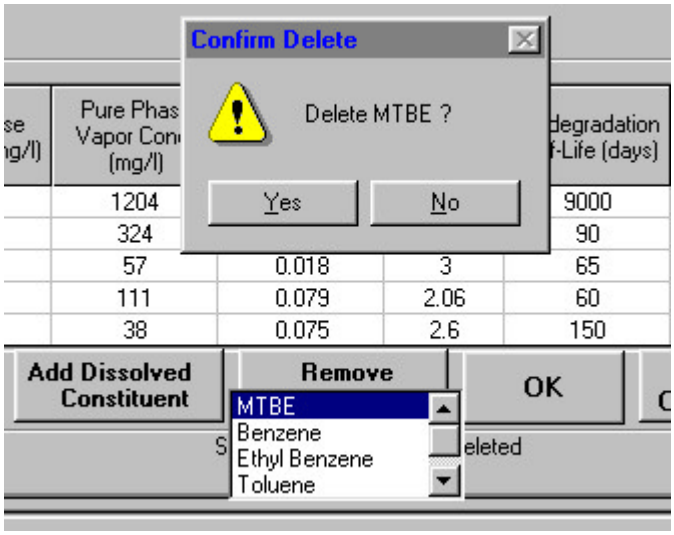

Figure 6-5. Remove MTBE by highlighting the compound in the Remove Constituent list, and confirm the deletion by selecting **Yes** in the confirmation box.

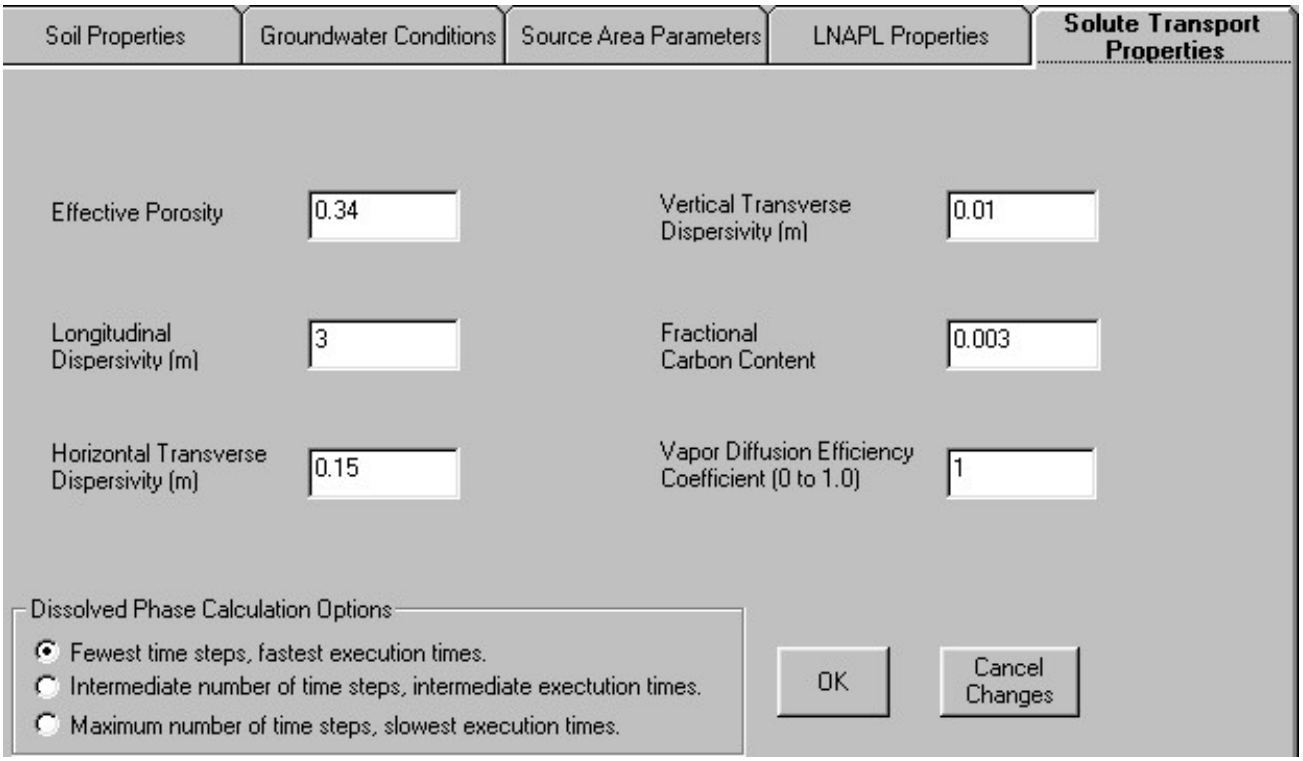

Figure 6-6. **Solute Transport Properties** Tab with the selected parameters for Problem #1.

pounds includes benzene, toluene, ethyl benzene, and xylene. The remaining LNAPL properties will stay unchanged for this example (Figure 6-4).

The last Tab in the LNAST utility is the Solute Transport Properties section where the groundwater and transport factors are input. We will use the example values in all fields for this tutorial problem (Figure 6-6). Notice that there is an option at the lower left for time stepping sensitivity. Fewer time steps result in shorter calculation times, but may loose some desired refinements. Typically, fuels with highly soluble compounds, like MTBE, alcohols, or other additives are more likely to benefit from time stepping refinements because the rate of mass loss of these compounds will be high relative to other low solubility species. The resulting contrast in the mass loss rates between compound can cause spiky output with fewer time steps.

The properties necessary to run a problem have now been fully specified, and the calculations can be performed. As noted in the User's Guide (Section 5), a calculation proceeds in the following step-wise manner. If remediation is considered as the specification for the LNAPL distribution, that must be run before other calculations (as discussed below in the second half of our example problem). Next, the depletion of soluble and volatile components from the LNAPL is calculated to determine the time dependent concentrations in the groundwater phase in the source zone. Last, the groundwater transport of the selected compounds of interest are calculated based on the output from the first calculation. In the case of a remediation measure, as in the second part of this problem, one must first perform the remediation estimate to determine the LNAPL conditions for the partitioning calculations. So for this first part, we will select Calculate from the top menu, and then select the Include Volatilization option (Figure 6-7).

The LNAST utility will calculate the depletion of the specific compounds of interest and display a table of results. One may **Graph** and/or **Save** the results by selecting either option on output table screen (Figure 6-8). Because we are performing a comparison problem, we will save the information to a tab-delimited file that we can later graph in a spreadsheet. Name the file with an extension that you will remember, for instance *.DEP signifying a depletion data file. We will save and name the output "PROB1A.DEP".

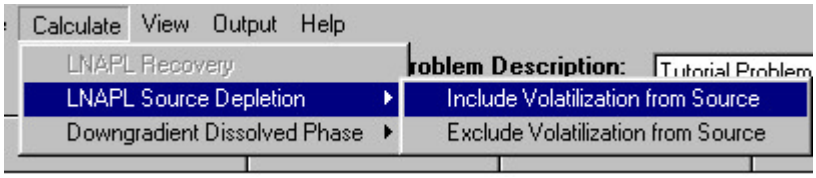

Figure 6-7. From the **Calculate** pull-down menu, select the **LNAPL Source Depletion** option, and then the **Include Volatilization from Source** sub-option.

If you wish, you can also **View**, **Save** and/or **Graph** the LNAPL distribution estimated for the properties that have been selected. To do so, go to the **View** menu at the top of the main program and select the **Hydrocarbon Saturation Distribution** option. When selected, this will show a table of the LNAPL distribution associated with the problem. This can be graphed or saved. Again, the Save option will be selected so that these conditions can be compared to the second half of the problem (save as PROB1A.SAT).

We are now ready for the second part of this first set of calculations. Again pull down the **Calculate** menu with the cursor, and this time select the **Downgradient Extent** option. There are 2 suboptions, one for the downgradient extent of the compounds of interest at the selected target concentrations, the second for calculating the time-concentration profile at user specified distances. For this comparative calculation, we will select the downgradient extent. A timer bar appears at the bottom of the screen while the calculation executes. This will take a few seconds to a few minutes depending on several factors including the number of compounds selected, the time stepping refinement, and your computer processor speed. Once the calculation is complete, a results table again appears with the same options as the last (graph and/or save). Because we will make a

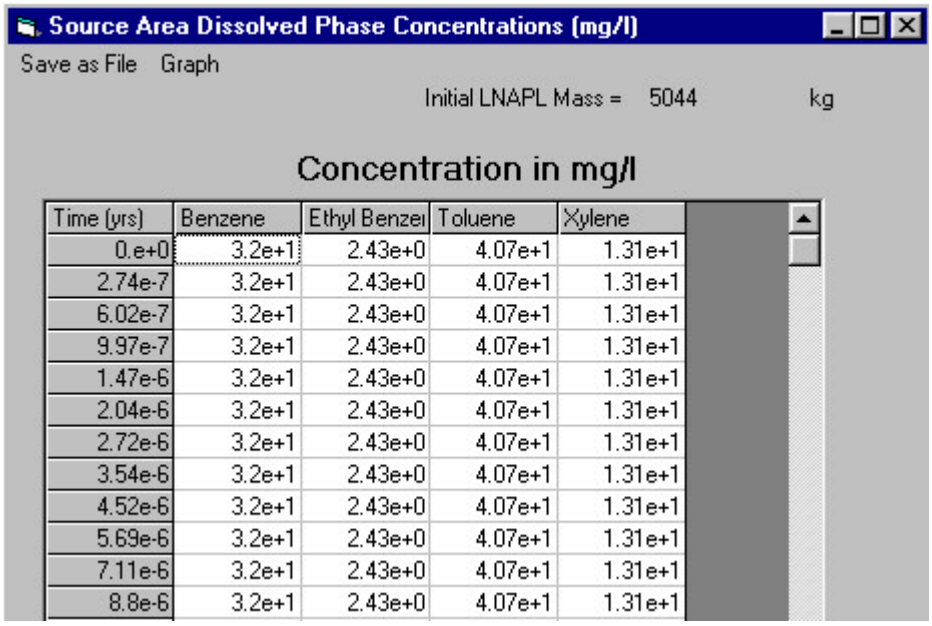

Time (yrs)	Benzene	Ethyl Benzei	Toluene	Xylene
0.e+0	3.2e+1	2.43e+0	4.07e+1	1.31e+1
2.74e-7	3.2e+1	2.43e+0	4.07e+1	1.31e+1
6.02e-7	3.2e+1	2.43e+0	4.07e+1	1.31e+1
9.97e-7	3.2e+1	2.43e+0	4.07e+1	1.31e+1
1.47e-6	3.2e+1	2.43e+0	4.07e+1	1.31e+1
2.04e-6	3.2e+1	2.43e+0	4.07e+1	1.31e+1
2.72e-6	3.2e+1	2.43e+0	4.07e+1	1.31e+1
3.54e-6	3.2e+1	2.43e+0	4.07e+1	1.31e+1
4.52e-6	3.2e+1	2.43e+0	4.07e+1	1.31e+1
5.69e-6	3.2e+1	2.43e+0	4.07e+1	1.31e+1
7.11e-6	3.2e+1	2.43e+0	4.07e+1	1.31e+1
8.8e-6	3.2e+1	2.43e+0	4.07e+1	1.31e+1

Figure 6-8. This output table is provided once the source area depletion calculation is complete. One may **Save** and/or **Graph** the output.

comparison between this result and that following simplified skimming, we will also save this file now as “PROB1A.DXT”, with the DXT extension indicating that this is the downgradient extent output file. Again, all files are stored as tab-delimited text. This would also be a good time to save the problem file itself by pulling down the File, Save option from the main pull-down menu at the top of the utility. This file is automatically saved with the extension “API” (PROB1A.API). This input file can be opened anytime to run a comparison against any other set of conditions.

The second half of this comparison problem can now be executed. Because all factors are the same except the change of LNAPL distribution to a post-skimming condition, all that is needed to rerun the problem is to go back to the **Source Area Parameters** Tab and select the Distribution after a Fixed Period of Remediation option (Figure 6-9). Now when the calculate menu is pulled down, notice that the first allowable calculation is for the remediation condition, because this is needed to describe the LNAPL distribution on which dissolution will act. Note that because the old problem is still in memory, jumping to the Downgradient Dissolved-Phase calculation would merely reproduce the prior result, and not the new result after skimming. Be sure to always proceed through the calculations in the correct order, which follows the listing from top to bottom in the Calculation menu options as discussed previously.

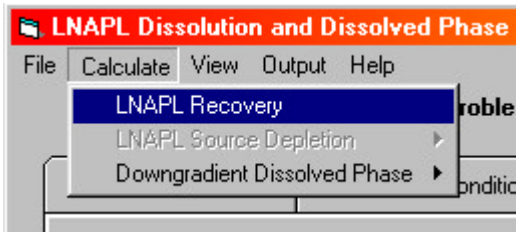

Figure 6-9. Calculate LNAPL recovery after resetting the Source Area Parameters to the Remediation option.

Once the LNAPL Recovery option is selected, a new screen will appear that contains all the input specifications needed for the problem (Figure 6-10). First select the Skimmer Well button. The software will then highlight the input boxes that require parameters. We will leave the inputs at the default example settings. Recall that a more thorough definition of the inputs and requirements is provided in the User’s Guide (Section 5), and in Appendix A that documents the remediation approximations by Charbeneau et al., 1999. The remediation estimate is run by selecting the **Calculate Recovery** button on the right, under the Input Values table. The output table will be filled with the results, which will remain stored in memory for the remaining two portions of the calculation (depletion & transport). As with all other output, you may save and/or graph the results by selecting those options at the top of the menu.

As mentioned, the next stage is to calculate the depletion of the selected compounds from the LNAPL source zone that remains after the skimming effort. The depletion calculation is done in the same way as before. Simply select the **Calculate** pull down menu, and **LNAPL Source Depletion** option, with the **Include Volatilization** sub-option. This will produce a table analogous to the first half of this tutorial problem, that may again be graphed and/or saved. Because we are making a

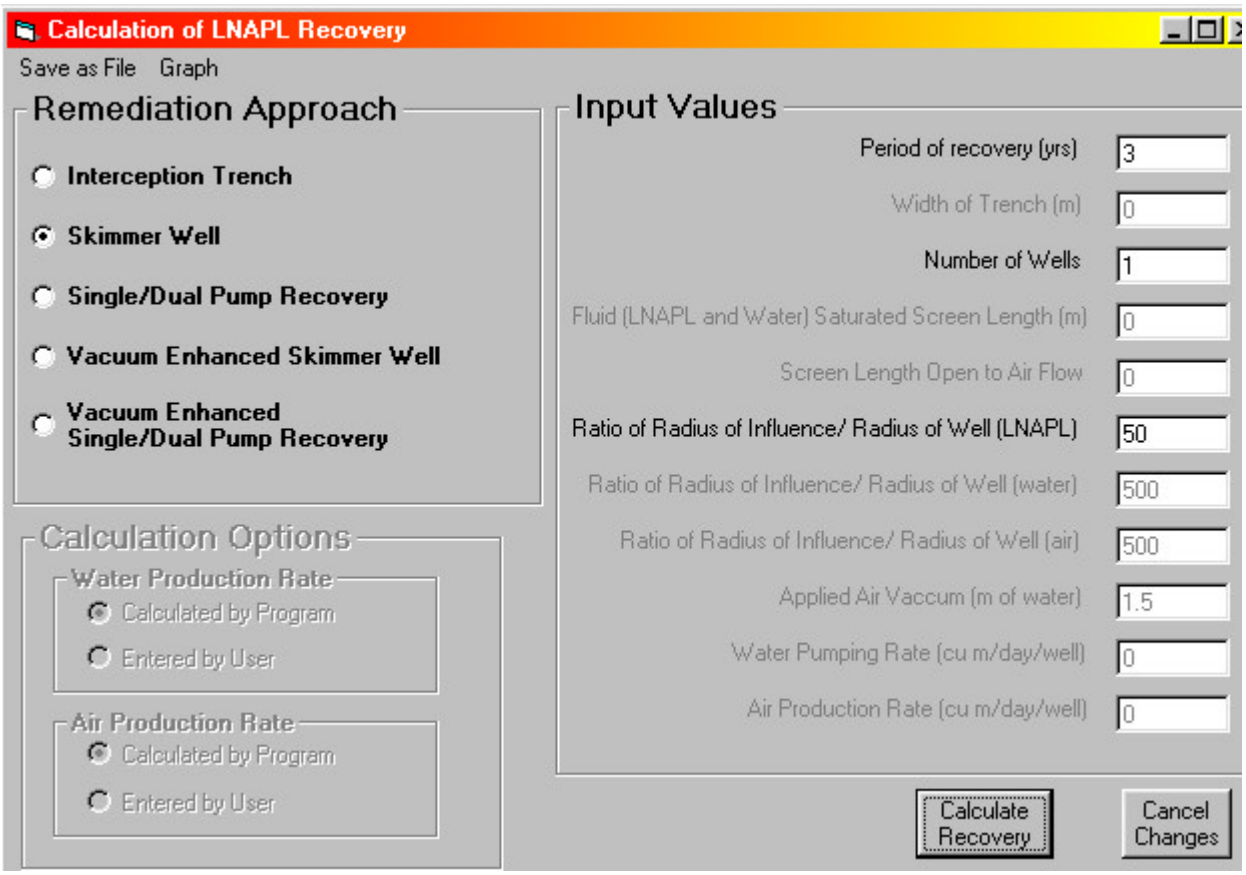

Figure 6-10. The remediation calculation screen with Skimmer Well selected, along with the inputs on the right that define the skimmer well operations.

comparison, we will save the output as “PROB1B.DEP” for later graphing in a spreadsheet. The LNAPL saturation distribution will also be saved from the View menu (PROB1B.SAT). Now the **Downgradient Extent** calculation may be run, again, exactly as in the first half of the problem. **Save** the output file as “PROB1B.DXT”.

Both halves of this simple tutorial problem are now complete. The key results will be graphed comparatively, as mentioned, using a spreadsheet program. Any graphing software may be used to construct these comparative charts. Alternatively, one could also just print key results from within the software routine for each calculation and visually compare the graphical results. The key is that the LNAST utility can only graph one set of calculations at a time. If is often more illustrative to combine different calculations into a single graph, as will be done here for explanatory purposes. Each of the output files can be brought into the graphing routine you have selected as a tab-delimited file. Three sets of output files have been saved; 1) Saturation (*.SAT); 2) Source depletion (*.DEP); 3) Downgradient extent (*.DXT). Each will be compared in order.

The LNAPL saturation distribution for each part of the problem, as discussed extensively in prior sections, controls the mass distribution and flux of chemicals from the source area. It is of interest then to compare the difference between the "ambient" condition of vertical equilibrium of the LNAPL to the condition after 3 years of skimming recovery (Figure 6-11). As seen, the profiles are similar for areas where the LNAPL saturation is below residual. The remainder of the ambient profile is the theoretically recoverable LNAPL. Recall again that these recovery approximations are usually optimistic compared to field conditions.

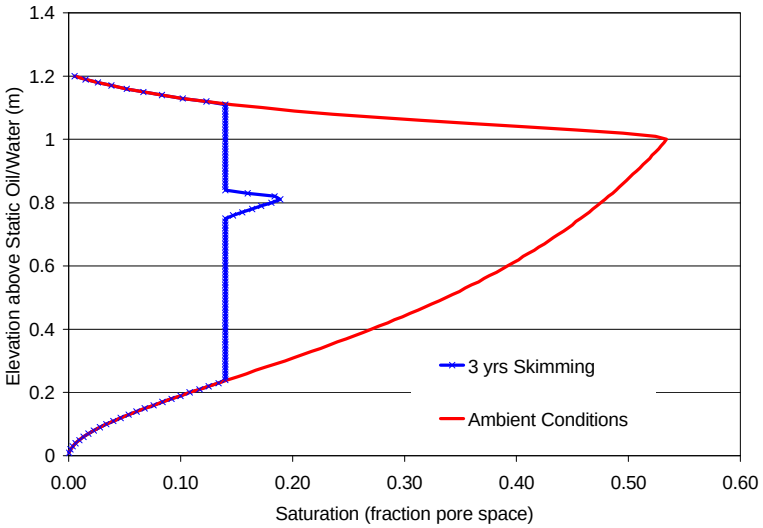

Figure 6-11. LNAPL saturation profiles for ambient and post-skimming conditions. The "nub" in the skimming profile is the remaining theoretically recoverable LNAPL.

It is also of interest to inspect how the depletion of LNAPL from skimming changed the relative permeability with respect to groundwater that is flowing through and below the zone of LNAPL impacts (given in the output file). As expected, the relative permeability to water increased due to removal of LNAPL (Figure 6-12). In turn, we might expect some degree of faster partitioning of compounds to the water phase as the flux through the LNAPL has increased accordingly. This comparison is given below.

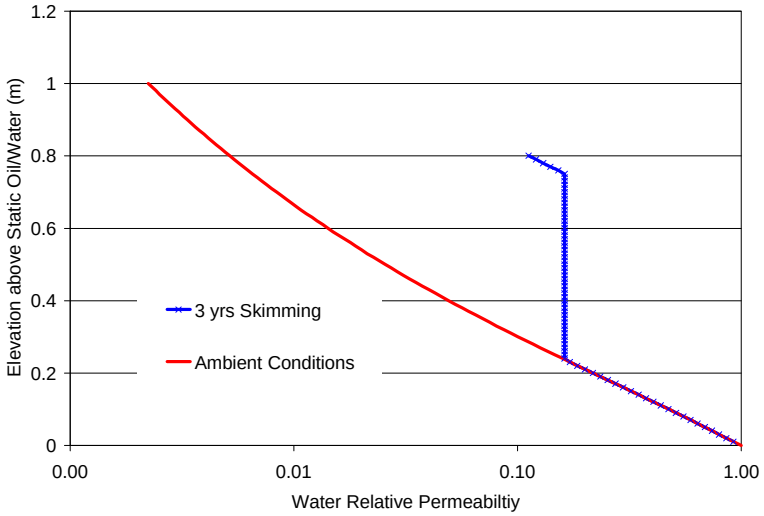

Figure 6-12. Water relative permeability under ambient and skimming conditions. Notice that skimming increased the relative permeability to water by removing LNAPL.

Next, the depletion of benzene and xylene is contrasted between the two problem halves, as well as contrasting compound specific outcomes. As seen, the "residence" time of benzene is suggested to be depleted by a little more than half, from about 90 years to 40. It is also clear that less soluble and volatile compounds, like xylene, will remain for significantly longer periods. The reason for the depletion gain is that, for this particular example, there was a significant recoverable fraction estimated from the LNAPL source zone (from about 5,000 kg to 2,100 kg in the source zone).

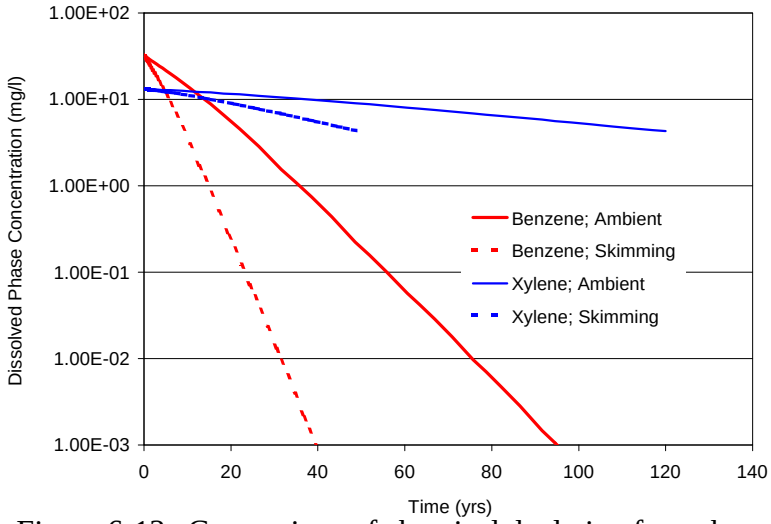

Figure 6-13. Comparison of chemical depletion from the source area for benzene and xylene.

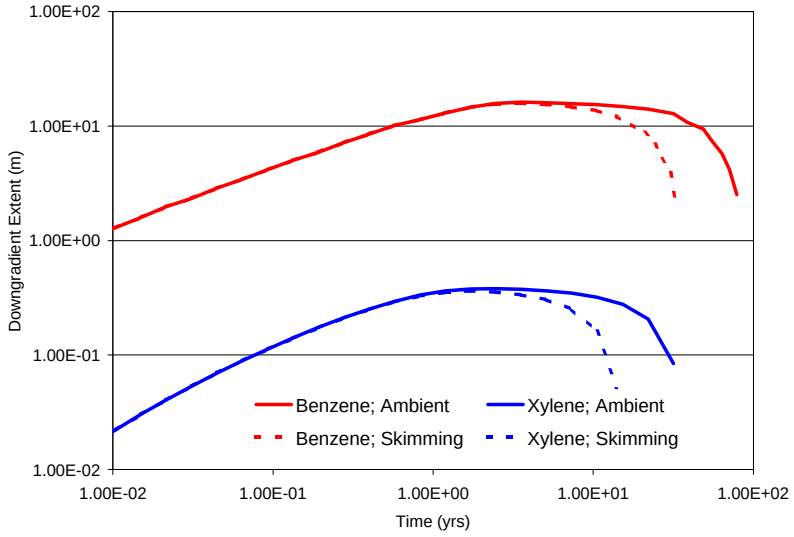

Figure 6-14. Estimated downgradient extent of benzene and xylene for each of the two LNAPL source conditions.

Last, the downgradient extent conditions can be compared for the same compounds and conditions (6-14). Recall that this calculation is based on the target concentration specified in the LNAPL Properties Tab. Therefore, the extent is a plot of the downstream migration at that particular concentration. It does not mean that detectable concentrations are not present beyond that distance, but simply that those detections would not be estimated to be above the selected target threshold. This is the primary reason, though not the only, that the downgradient extent of xylene is much smaller than benzene (about 0.3 versus 16 m, respectively). Notice also that the total downgradient extent is not affected by remediation for this case because the time of spreading downstream is much smaller than the depletion time of compounds of concern.

This example problem provides the tutorial background necessary to run the software. However, only simple interpretative evaluations were included as part of the problem. The next tutorial problem is relatively simple also, but is taken from our site database. A bit more time will be spent on the conceptualization of the problem, and interpretive aspects.

6.2 PROBLEM #2: GASOLINE IN A COASTAL DUNE SAND, AMBIENT EVALUATION

This problem is a relatively simple condition patterned in a general way after a real site, though the purpose here is not to go into site specifics, but rather to explain the concept of site bracketing. This problem extends the tutorial problem by showing how interpretations of soil parameter values can be used to extend and compare results. The problem will also show how using some interpretive common sense is necessary to producing meaningful results.

The site subsurface consists of coastal dune sands that are composed of uniform fine-grained sand, with a hydraulic conductivity of about 3 m/day. The water table is relatively stable about 10 m below grade with a gradient of 0.003 m/m. The LNAPL source is assumed to be gasoline without MTBE, and has been observed at thicknesses of 1.25 m in several wells within the heart of the source zone, with plume width and length averaging 10 m in the zone of significant product accumulations. For the actual site, we know the measured capillarity, but will assume that we do not so that we can show how one might go about a bracketing a screening estimate.

6.2.1 Defining the Problem

The dune sand condition suggests that we have a homogeneous geologic environment, so we will select that calculation option (i.e., no layering). We have been given hydraulic conductivity, but do not know any other geologic or fluid parameters. The *K* value given is between the fine- and medium-sand default values in LNAST, so we can compare the outcomes between the remaining properties associated with each of those example soils, plus one site specific soil estimate (key values, Table 6.1). So, although this is a homogeneous setting, we will need to bracket a range of possible soil conditions to gain insight into the problem and examine the which parameters appear most representative. We will use the default example soil parameters (except *K*, which was given) for the fine- and medium-sand selections, and compare with a site specific soil parameter estimate.

For this particular problem, the capillary properties are the most important unknown. For the site specific soil, one might suspect that the pore distribution of a very well sorted sand will be uniform, corresponding to a larger sorting index of approximately 4.5 (Van Genuchten *n* parameter). Recall that higher *n* values suggest more uniform pore sizing and grain sorting. Taking the grain-diameter associated with fine-sand, one also could estimate that the capillary rise parameter could be as small as 1.5/m. Three soil types are now described (Table 6-1) that will be used for each calculation set. Recall that these are placed into the calculation set through the **Soil Properties** Tab.

The hydraulic gradient was given, so we will use that input in the **Groundwater Conditions** Tab (not pictured). In the **Source Area** Tab (Figure 6-16), we will input the source geometry information provided and select Equilibrium LNAPL Distribution. We will assume the 1.25 m thickness

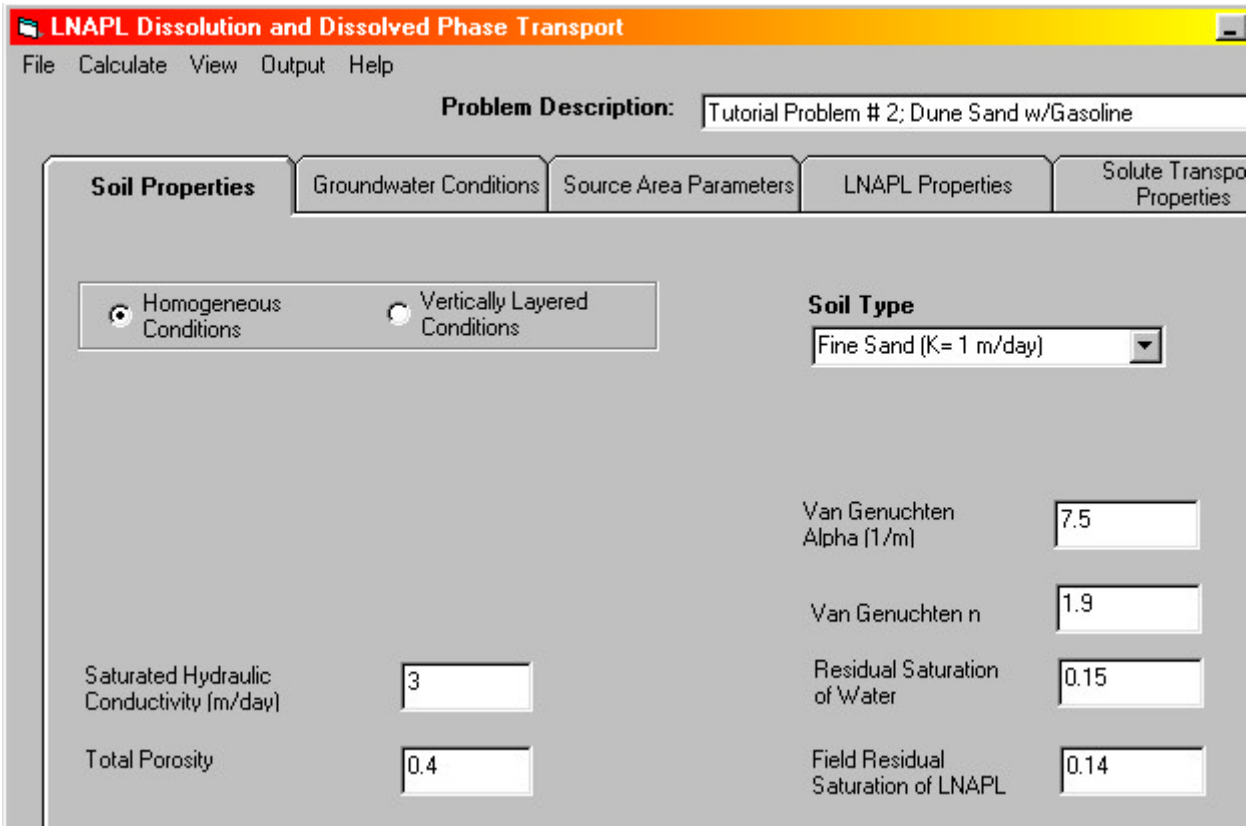

Figure 6-15. **Soil Properties** Tab showing a set of conditions for Case 1.

condition as given, and a plume width and length equal to 10 m. Finally, moving to the **LNAPL Properties** Tab (Figure 6-17), we will choose the default gasoline selection, but since there is no MTBE in the fuel, we use the **Remove Constituent Option** and remove MTBE as a constituent of concern. For instructional purposes, we will leave the remaining compounds. However, the real-world problem would be primarily concerned with benzene, as other COCs present a much smaller relative risk.

For comparison purposes, we will contrast the VEQ conditions for the 3 soils with a prescribed minimum LNAPL mobility condition equal to 8.64×10^{-4} m/day (1×10^{-6} cm/sec). This problem then will result in a comparison of 2 primary conditions, each with 3 different soil conditions (Table 6-1), for a total of 6 calculation sets.

6.2.2 Running the Problem

We have the 3 sets of soil inputs described above (Table 6-1) that will be run for VEQ (odd numbered cases) and minimum mobility conditions (even numbered cases). The program allows projects inputs to be saved to disk. Since all but a few parameters will remain unchanged for each calculation, it is suggested that a base project be saved that can then be updated for each additional run by systematically changing just the new parameters. Each run can then be saved as new project file, so a permanent record will exist for the full problem set.

TABLE 6-1
SOIL PROPERTIES FOR PROBLEM #2

Soil Parameters	Cases		
	1 & 2 fine-sand	3 & 4 medium-sand	5 & 6 site sand
Hydraulic Conductivity (m/d)	3	3	3
Porosity	0.4	0.4	0.4
Effective Porosity	0.34	0.364	0.34
VG alpha	7.5	14.5	1.5
VG *n*	1.9	2.7	4.5
Residual water saturation	0.15	0.09	0.15
Specific Oil Retention	0.14	0.12	0.14

Before executing any new run, make sure your new inputs are correct. When you type a value in an input box, hit enter or move the cursor after the entry. The **Cancel** button will reset values to the example parameter set up until the time that the **OK** button is hit. We will start with the fine-sand VEQ condition (Case 1) as our example, the remainder of the problem sets will not be explicitly discussed as the necessary changes are straightforward. Going to the **Soil Properties** Tab, we will select the fine-sand default parameters, with the exception of the hydraulic conductivity, which was given as 3 m/d (Figure 6-15). Next, we will input the given hydraulic gradient (0.003) in the **Groundwater Conditions** Tab (not shown). Now moving to the **Source Area Parameters** Tab, we select Equilibrium LNAPL Distribution as the method to calculate LNAPL saturation VEQ conditions and input the given plume geometry information (Figure 6-16). As discussed so long ago, one should generally not use averages in the plume geometry specifications because the zones of greatest LNAPL pool thickness and saturation control the risk outcomes. Said another way, given two otherwise identical plumes with respect to total mass and area of impact, the plume having areas of more concentrated mass will present the greater risk residence time. Moving on to the last Tab, **LNAPL Properties**, we will accept all default values for gasoline except that MTBE will be removed as a constituent for consideration (Figure 6-17).

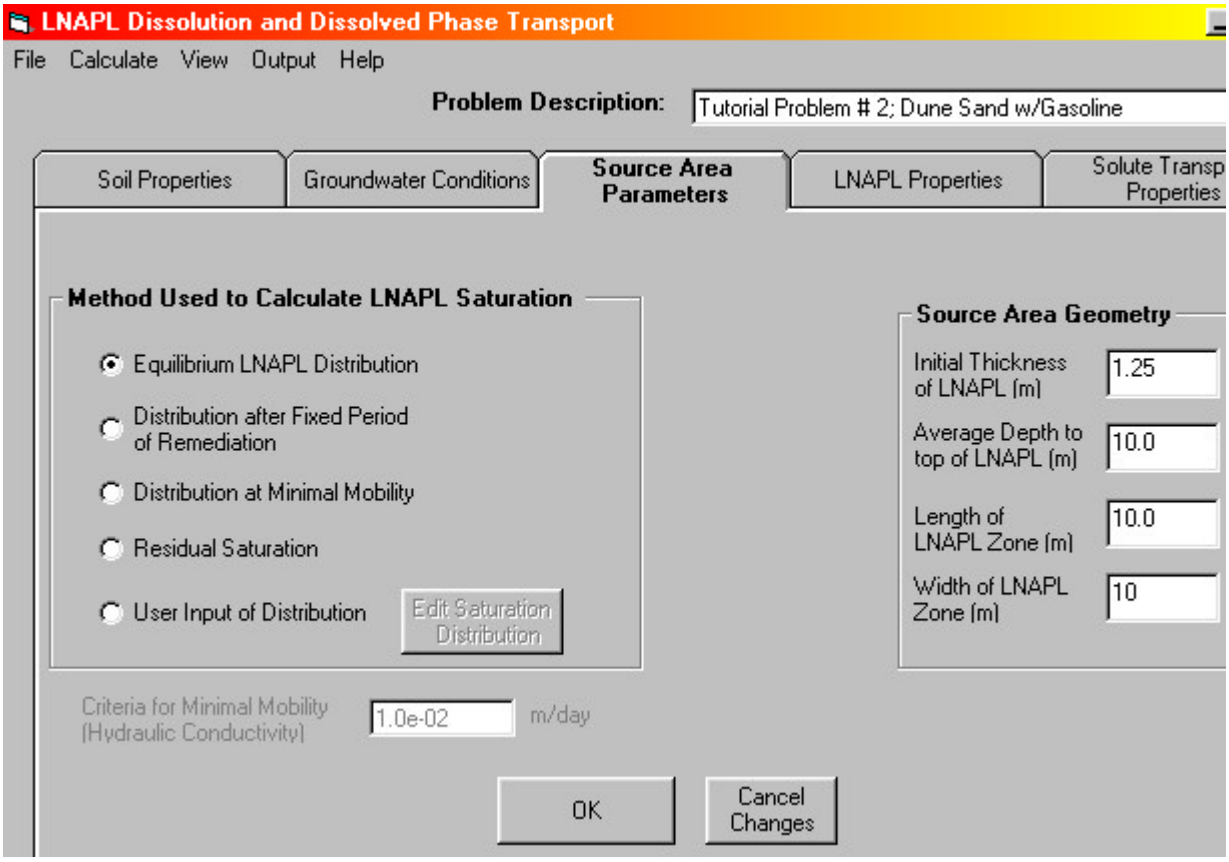

Figure 6-16. **Source Area Parameters** Tab for Problem #2 showing the LNAPL geometry conditions for Cases 1, 3, and 5. For Cases 2, 4, and 6, the Distribution at Minimal Mobility would be checked, with all other parameters remaining the same.

At this point, the problem is ready to run. Before doing so, save the project by selecting the **File, Save Project** option in the menu at the top of the LNAST utility screen (this menu is always available above the data entry tabs) and save the project to a file name of your choice. Now select the **Calculate** menu and then select LNAPL Source Depletion (note that this is the only option available at this juncture). Two options can be selected, source depletion with or without volatilization. Since this product is gasoline and there are no geologic conditions noted that would impede volatilization, it is appropriate to select the Include Volatilization From the Source option. Once selected, the program calculates the initial saturation profile and mass throughout the LNAPL impacted interval. Then mass is depleted by water transport through the LNAPL and vapor transport above the LNAPL. Once this calculation is done, a table of time versus water-phase concentration is produced; the table also provides the integrated mass of the simple geometric plume. Remember that because the calculation assumptions are directed toward conservative aspects of the problem, this mass is a “conservative type area mass” and not the total LNAPL mass present in the subsurface, as discussed previously. Methods of better estimating the LNAPL plume mass are based on the same principles provided here, but require a bit more work. First, one must estimate the volume per unit area about each observation location containing LNAPL (gals/ft^2, liter/m^2, etc.) and then integrate those results across the total area of the plume. One should also include oil stranding and entrapment effects from water level variations and heterogeneity effects, as discussed previously. In the case of our problem,

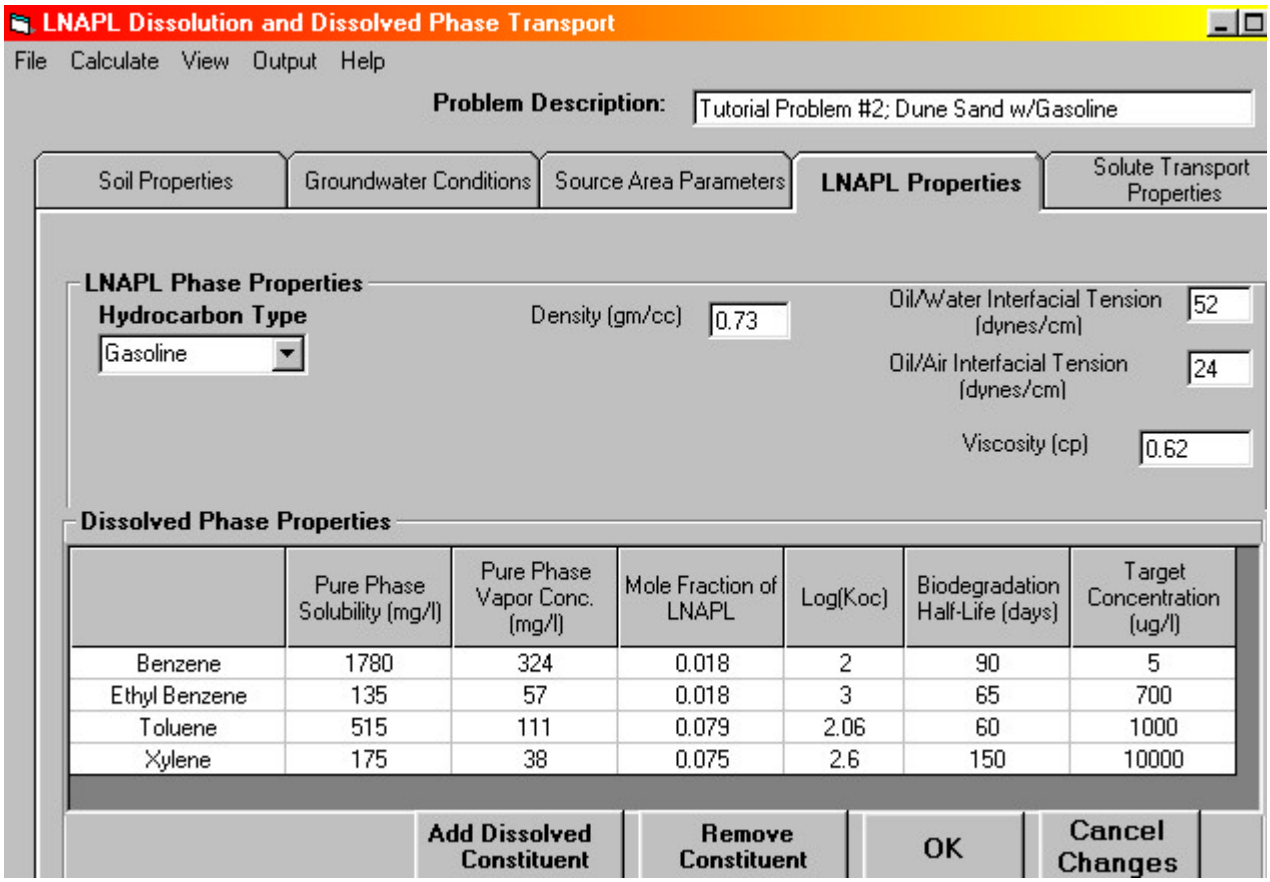

Figure 6-17. Screen showing the LNAPL properties selected for Problem 2.

we have used the worst-case thickness of 1.25 m across the areal domain for each of the soil and LNAPL saturation conditions, which should produce an overestimate of the volume in-place for each calculation condition, and thus result in worst-case plume longevity conditions.

The mass depletion results just calculated are stored in computer memory as automatic input into the groundwater contaminant transport calculations by the Domenico approximation (1987, 1990). Two options are available in the **Calculate** menu to make the next step in the process. One may ask the program to calculate the downgradient extent of dissolved compounds of interest based on the user selected target concentration, or the program can also calculate the time dependent concentration at individual locations directly downgradient of the LNAPL source along the center of axis. The results of these latter calculations are often termed “breakthrough curves”. We will use both options for our analysis of the results, first running the downgradient extent, and then calculating breakthrough curves at 5, 10, and 30 m downgradient.

6.2.3 Results

The most significant observation regarding this set of evaluations is the large difference created because of the range of soil capillary conditions that were estimated. Particularly, the mass and impact of the best-guess dune sand parameters were much less than the default conditions for the parameters we estimated to be more representative for the specific dune sand in question. The initial mass for the cases ranged from a low of approximately 1,690 for Cases 5 & 6, to a high of about 25,700 kg for Case 3 (Figure 6-18). Obviously, the range of capillary properties selected has a significant influence on the results. Equally obvious, the Case 5 conditions did not exceed the minimum mobility threshold, and therefore were identical to Case 6. So for this site, the hydraulic conductivity was relatively high, but did not correspond to a smaller capillary rises (larger α) that would have been expected using the "example" sands. The user should now recognize the problem with using the example parameter sets in Appendix C and the LNAST utility without site specific reasoning.

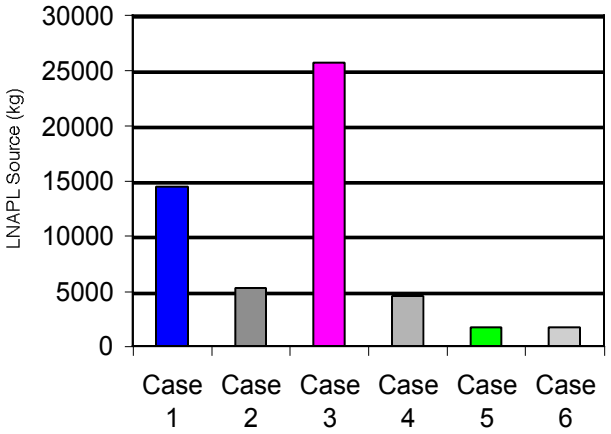

Figure 6-18. Comparison of initial mass conditions for the six cases in Problem 2.

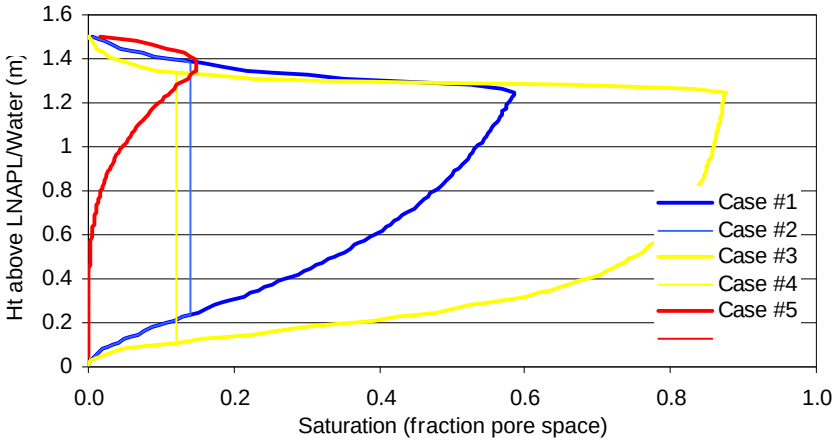

Figure 6-19. Initial LNAPL saturation profiles for the 3 soils and 2 initial conditions used for Problem #2.

The results of this evaluation can be best understood by first reviewing each of the initial LNAPL gasoline source profiles (Figure 6-19), which as will be recalled, control both the total mass and the relative groundwater flux through the source interval (Figure 6-20). The medium sand (Cases 3 & 4) exhibits the greatest ambient saturation, and therefore smallest groundwater effective conductivity and flow through the source (Figure 6-20), the fine-sand (Cases 1 & 2) the next smallest saturation and greater groundwater flow. Our best-estimate capillary conditions (Cases 5 & 6) exhibit the least oil saturation and therefore the greatest groundwater flow through the source interval. Notice for the minimum LNAPL mobility condition, both the example fine- and medium-grained sand conditions

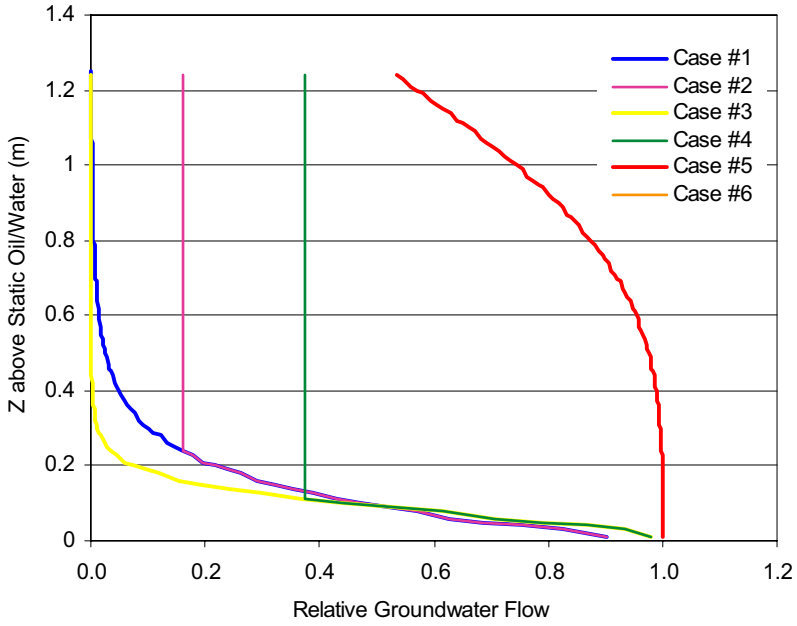

Figure 6-20. Relative groundwater flow through the gasoline interval. Since *K* is equal for all cases, the results show the important effects

(Cases 2 & 4) are truncated to meet that condition, whereas the best-estimate capillary conditions are below this threshold at ambient conditions (Figure 6-19). Among other things, this means that there would be no appreciable gain in attempting hydraulic recovery of the "best-estimate" condition (Cases 5 & 6) because the product would be at saturations below the lateral mobility threshold. At the same time, there was certainly LNAPL recovered for cases where the LNAPL saturation was greater than residual.

The source depletion of benzene from the LNAPL is highly sensitive to soil capillarity and initial conditions. However, the results are again interesting in their synergistic and non-intuitive aspects. With volatilization, the benzene source depletion for all conditions falls between about 20 and 150 years (Figure 6-21). This is at first surprising when we recall that each condition has the same regional groundwater flow rate and that soil condition #3 has significantly greater initial mass than the other conditions (Figure 6-18). For instance, the benzene depletion time for the best-guess fine-sand parameters is about the same as the depletion time for Case #3, the medium sand. Why? Recall that we selected the source depletion with volatilization option. The integrated effective vapor diffusion rate is several times greater for the medium sand than it is for the fine sand with best-estimate capillary parameters (Figure 6-22). This shows the potential importance of volatilization for coarser grained materials. If we look at source depletion without volatilization, we see results that make more intuitive sense (Figure 6-23). Aspects of volatilization to ground surface and into build-

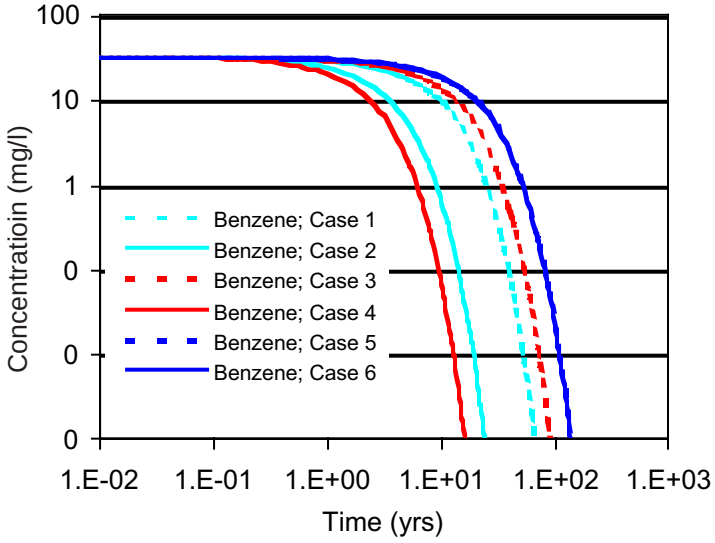

Figure 6-21. Benzene source depletion curves for Cases 1-6 including unimpeded volatilization from the source zone.

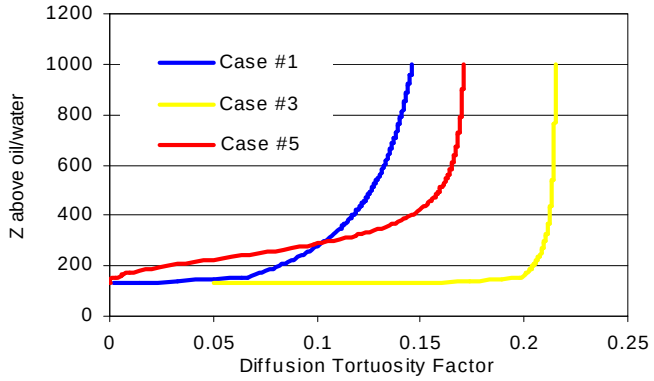

Figure 6-22. Vapor diffusion tortuosity factor for each soil condition based on the Millington-Quirk equation

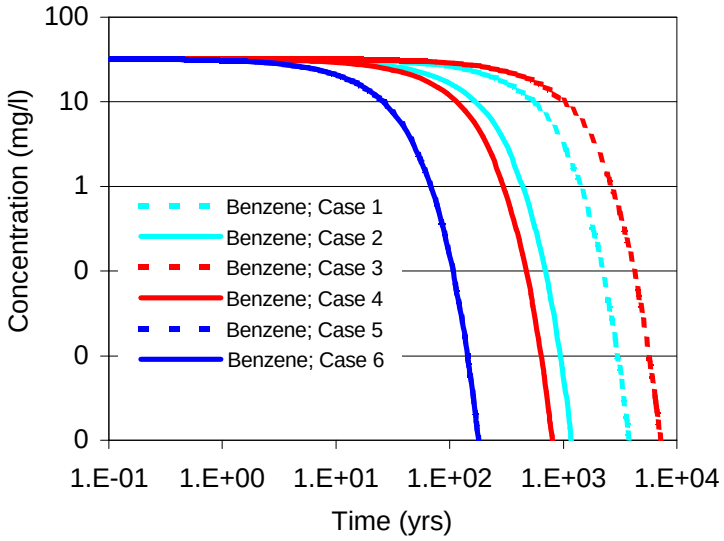

Figure 6-23. Benzene depletion curves without volatilization. Compare times to those in Figure 6-21.

ings are important to risk assessment. The reader could benefit by reviewing documents pertaining to vapor transport (ASTM, 1995; API, 1999).

Keep in mind that the key assumptions of homogeneity, moisture equilibrium, and connectivity to ground surface results in artificially large vapor flux to ground surface. In the author's experience, vapor flux limiting zones exist at most sites, be they simple site cover conditions, high soil moisture impediments or more complicated heterogeneities. Without high volatilization rates, one would expect the oil residence time to be significantly larger for Case 3 than for Case 5 & 6 (Figure 6-23). Under these vapor limited conditions, the medium-grained poolwould be resident about 50 times longer than the best-estimate fine-grained sand. So, without belaboring the point, it is very simple to see that results are highly dependent on good judgement. If there are vapor flux limiting horizons, use the guidance given previously to determine a reasonable vapor efficiency input factor.

Last, we can look at the downgradient extent characteristics under the different soil and initial LNAPL conditions. As expected based on prior discussions, the downgradient extent of benzene (and other compounds) is essentially the same for all 6 conditions considered (Figure 6-24a). This is because the mass of LNAPL is large and depletion is slow relative to the time necessary for the plume to reach the downgradient limits and field equilibrium conditions between transport and biodecay. The plume scenarios have much different residence and contraction times due to a combination of factors, but primarily the differing volatilization aspects discussed above.

The benzene breakthrough curves (concentration versus time) 5 m downstream of the source zone show similar early time shapes and peak concentration within about a 20% range (Figure 6-24b). Again, the volatile losses and soil characteristics of the example fine- and medium-grained sand soils suggest smaller peak concentrations and residence under the minimum mobility condition (Cases 2 & 4) for the reasons discussed above.

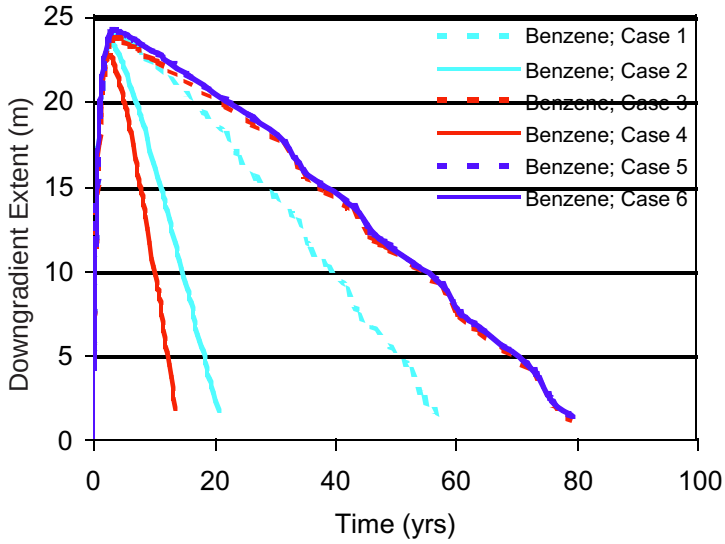

Figure 6-24a. Downgradient extent curves for benzene at MCL for soil and source condition.

In conclusion, this example problem shows the importance of site bracketing to investigate probable soil properties controlling the LNAPL mass, distribution, partitioning characteristics, residence time and downstream impacts. The importance of the selected capillary parameters is clear, as is the potential for incorrect estimates using the example parameters derived from literature. For a site-specific evaluation, one would look to any of the specific LNAST outputs and compare to the corresponding field conditions. For instance, which breakthrough curve(s) best represent the history of groundwater monitoring results? Do the predicted LNAPL zone saturations agree with soil sampling results or petrophysical analyses? Are the shapes and order of magnitude of the various curves consistent with field observations? The list goes on, but one can see that the purpose of the evaluations is to focus on key LNAPL aspects that control the risk related outcomes of interest.

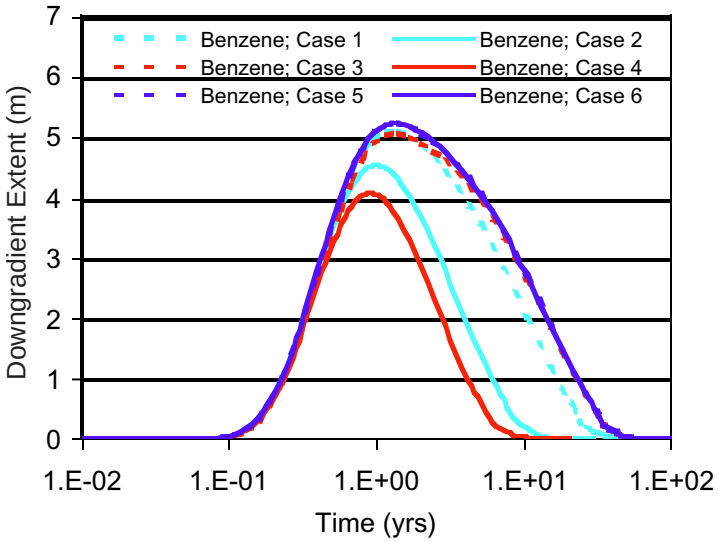

Figure 6-24b. Breakthrough curves for benzene 5 meters from the source for each soil and source.

6.3 PROBLEM #3: MTBE GASOLINE IN A MULTILAYER GEOLOGIC SETTING

This problem is more complex and incorporates the effects of a relatively low degradability compound (MTBE), coupled with aspects pertaining to heterogeneity and remediation by soil vapor extraction (SVE). The challenges in characterizing site conditions and the uncertainty in doing so will become evident in this example. This site, like many, has had very few of the critical parameters measured, and geologic interpretation is necessary to prescribe the evaluations. For tutorial purposes, not all the complexities of the actual site are presented here.

For this evaluation, we want to know how SVE has affected the LNAPL chemistry and conditions, and what the potential groundwater transport and residence time conditions may be for remaining impacts. For this site, the regulatory agencies and the responsible party must decide whether additional cleanup actions are needed based in part on this technical analysis.

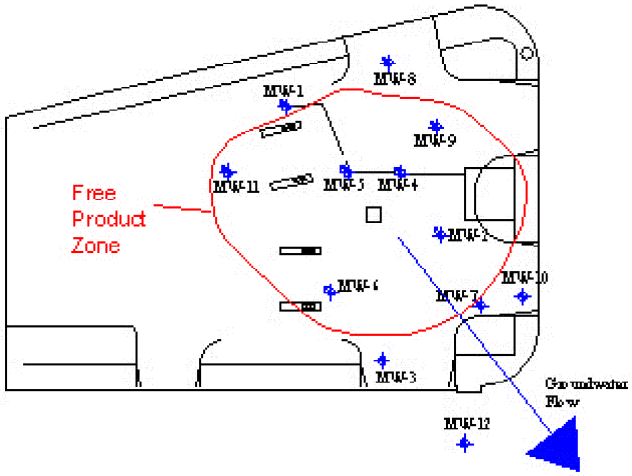

Figure 6-25. Site plan showing well locations and historic LNAPL distribution.

6.3.1 General Conditions

This site is a fuel service station in coastal Southern California that experienced a gasoline free product release, resulting in observable LNAPL accumulations in wells historically to as much as 7-ft (Figure 6-25, Site Plan & LNAPL Plume). The problem was identified in the early 1990s during station renovation. In response to the spill, soil vapor extraction (SVE) cleanup actions were performed. After approximately 6 years of cleanup operations, concentrations in recovered vapor (Figure 6-26) and groundwater (Figure 6-27) have decreased, and free product accumulations in wells are no longer present beyond trace levels (Figure 6-28). The initial hydrocarbon recovery rate of greater than 100 lbs/hr dropped to about 1 to 3 lbs/hr at the end of cleanup in early 1999 (Figure 6-26).

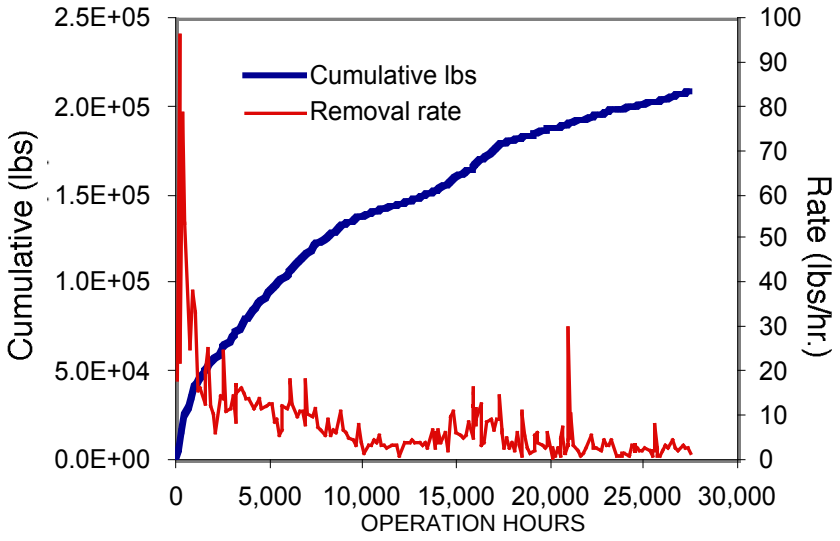

Figure 6-26. SVE recovery rate and cumulative total.

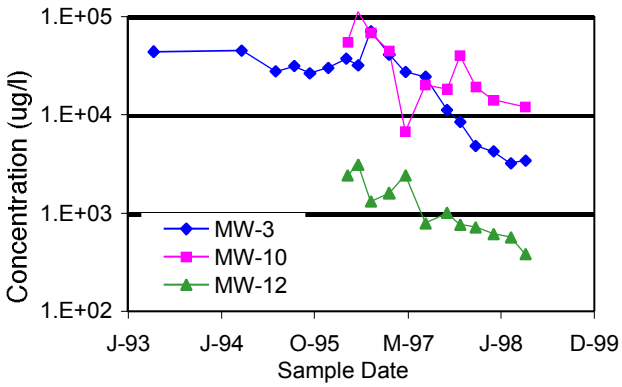

Figure 6-27a. TPH concentration in groundwater through time of SVE operations. MW-3 and MW-10 are near source zone, MW-12 is about 50-ft downgradient.

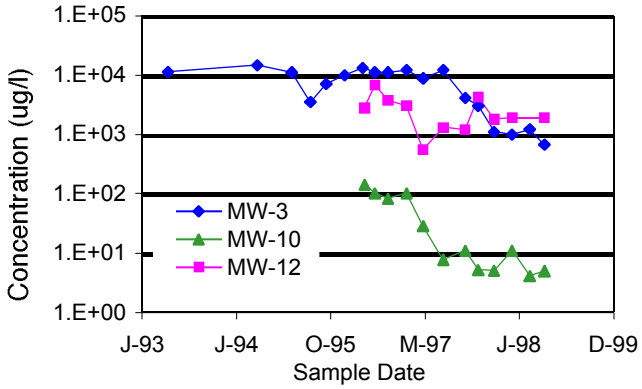

Figure 6-27b. Benzene concentration through time of SVE operations. MW-3 and MW-10 are near the source zone, MW-12 is about 50-ft downgradient.

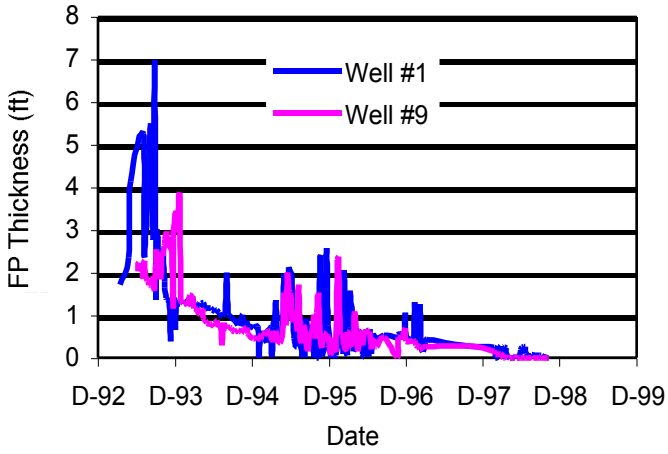

Figure 6-28. Observed free product thickness history over the period of SVE cleanup.

Approximately 200,000 lbs of hydrocarbon have been recovered through the SVE operation. Since about half of the compounds in gasoline account for 97% of the volatility, one can estimate that roughly a similar order of magnitude mass remains of lower volatility LNAPL compounds. More important, remaining dissolved-phase groundwater impacts, and the character those impacts, suggest some of the source zone remains untreated, as discussed below.

The geologic setting is an interbedded sequence of sand, silty sand, and clayey horizons of predominantly marine and bay sediments. Based on aquifer testing and boring log descriptions, the sands have a hydraulic conductivity (*K*) of about 6 m/day, the fine-grained layers have an average *K* of 0.1 m/day and the contact between beds is sharp. The water table is stable about 40-ft (12.2 m) below grade with a groundwater gradient of 0.005 m/m. The stratigraphic beds have a fair degree of lateral continuity with respect to the plume dimensions in the water table region (Figure 6-29, geologic cross-section).

6.3.2 Defining the Problem

The layered geology indicates we should consider both the low and high permeability zones in our evaluation, using the *Vertically Layered Conditions* option on the **Soil Properties** Tab. Based on geologic logs through the LNAPL impacted interval, a 2-layer condition is a reasonable starting point, with a sandy material overlying a finer-grained bed, each 1 m thick (Figure 6-29). Hydraulic

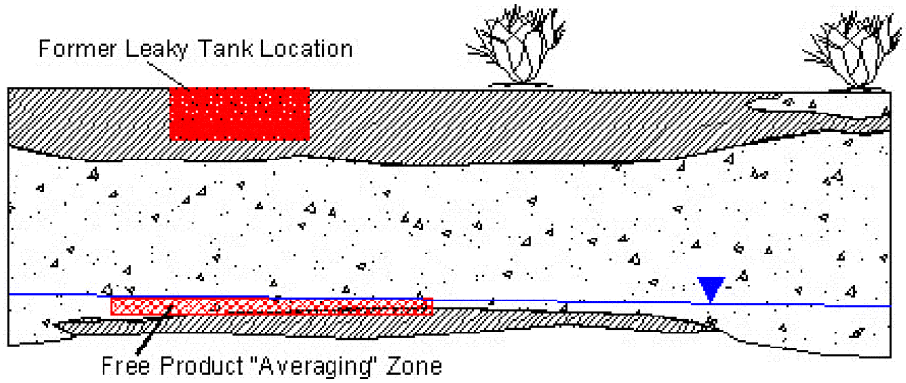

Figure 6-29. Geologic cross-section of beds in the near area of the LNAPL release from the underground storage tanks.

conductivities are known, as are capillary properties that have been measured for this formation at a nearby site (Table 6-2). The groundwater gradient is 0.005, and the remaining geologic and fluid parameters will be selected from the example parameters provided in the LNAST utility or through site related judgement.

TABLE 6-2
SOIL PARAMETERS FOR SAND AND SILTY BEDS

Soil Parameters	Soil Types	
	Sand	Silty Sand
Hydraulic Conductivity (m/d)	6.0	0.1
Porosity	0.4	0.5
Effective Porosity	0.34	0.365
VG alpha (m-1)	2.5	0.6
VG "n"	2.2	1.65
Residual water saturation	0.15	0.21
Specific Oil Retention	0.15	0.20

The primary challenge and focus of this problem lies in defining the LNAPL distribution and chemistry following the SVE cleanup. SVE cleanup of free product accumulations in the water table region has many complicating factors, such as multiphase interactions and associated multi-component chemical stripping efficiency. Efficient stripping generally depends on active vapor flow within or just above the zone containing the gasoline. The overall thickness of the LNAPL zone of interest is can be approximated to equal the maximum product thickness observed historically (~2 m). We can feel comfortable in this initial assumption because we know that some fraction of the initial LNAPL in place must remain, both because many of the compounds have relatively low volatility and would not be efficiently removed under ambient conditions, and also because groundwater impacts are still present and emanating from an LNAPL source. We will decide on an LNAPL source distribution for our problem after thinking about the chemical impacts discussed below.

Like many sites, no detailed chemical data were collected for the SVE system nor is there any characterization of the distributed subsurface cleanup response. The only related indicator we have to work with is the decrease in the dissolved-phase groundwater impacts. At this site, decreases in source zone groundwater impacts of 1- to 2-orders of magnitude have been observed (Figures 6-27a & b) and can be attributed to the SVE operations. One can easily verify that the concentration reductions are from SVE by running LNAST with an initial condition of 7-ft of free product at hydraulic equilibrium with initial "fresh" chemical mole fractions. The results would show that natural depletion alone would be several orders of magnitude longer than the short-term observed concentration decreases that must therefore must be primarily the result of the SVE cleanup operations.

Given the significant decrease in groundwater concentrations and large mass recovery, one might naturally think that the cleanup has been successful. However, while clearly successful in some ways, nuances in the groundwater chemical data suggest cleanup has had limited effect in some zones. These cleanup limitations are the control over the remaining impacts, both in terms of magnitude and longevity of the plume. This can be understood by looking at the chemical ratios of various compounds through time. In an ideal scenario, SVE would be expected to preferentially deplete the most volatile components in the gasoline, causing a change in the overall molar fractions in the LNAPL source are resulting groundwater concentrations through time. "Light" end compounds should be more depleted than "heavier" end compounds within the gasoline hydrocarbon range. Thus, one would expect to see the volatile/soluble compounds decrease faster than those less so. This expected "ideal" outcome is not evident in the site data. Instead, while the total dissolved-phase concentrations have fallen (Figure 6-27a & b), the ratio of benzene (more volatile/soluble) to xylenes (less volatile/soluble) and other components is unchanged (Figure 6-30a & b), as is MTBE.

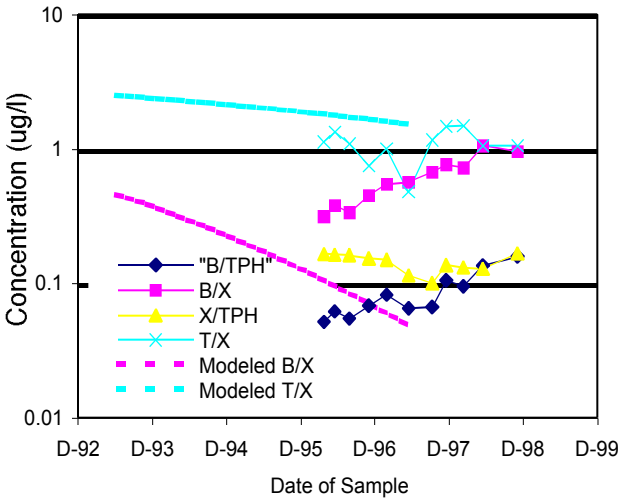

Figure 6-30a. Ratios of aromatic hydrocarbons in groundwater through time in MW-10. The dashed lines are the expected groundwater concentration trends under SVE stripping.

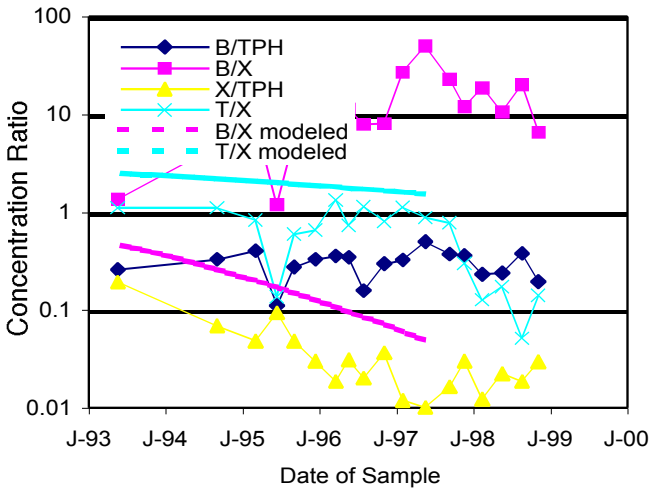

Figure 6-30b. Ratios of aromatic hydrocarbons in groundwater through time in MW-3, as in the prior figure.

This suggests that untreated LNAPL is still present in the system that is chemically similar to conditions before SVE began. But because total groundwater concentrations have fallen, something else must be happening. Because the site has varied lithologic beds, and because SVE would be expected to have limited effectiveness with depth into the aquifer because water limits vapor flow and partitioning, a working hypothesis is that groundwater dilution is now prevalent in the system. Essentially, some groundwater flow is now potentially through "clean" zones (with respect to benzene, etc.) that were formerly more impacted, and some smaller fraction of flow is through the remaining LNAPL impacted intervals containing the original chemistry. One can envision other scenarios that explain the observations, but for the sake of this tutorial, we will simply move forward with the given working hypothesis.

In prescribing the LNAPL source distribution and chemistry, we have 2 very different general approaches that produce similar but not identical results for the assumed conditions. We can use the "known" original thickness of the LNAPL zone (~ 2 m) and the "diluted" mole fractions (observed concentration/pure-phase solubility) of the compounds of concern to describe the LNAPL zone. In real terms, this would imply that the remaining high concentration zone has chemically re-equilibrated with the original LNAPL thickness interval. Or, our second choice is to assume that a discrete "layer" of LNAPL exists that is predominantly unchanged from initial conditions (using the same reasoning that created our working "model"), and we could then use a dilution factor to account for the differences in the model output and observed conditions. The dilution factor in this case is about 100 using xylenes (relatively low solubility/volatility) at MW-3 as the indicator and comparing initial concentrations to those seen after SVE remediation. This is no surprise, as this is equivalent to the approximate concentration decreases in the monitoring locations. You may also notice that the dilution factor is an approximation that does not fit all locations and compounds equally. Approximations are necessary to run screening calculations and one can make other assumptions to test against field conditions, as needed.

Of the 2 approaches to stipulating the chemistry and LNAPL distribution, the first is the simplest and is more conservative because groundwater dispersion losses are less important for a thicker LNAPL zone than for the thin discrete layer case. Also, we know that LNAPL is still present, though chemically changed, throughout the original zone of impact. Both scenarios have attributes that are representative, but neither condition represents the probable "real" conditions of heterogeneous LNAPL saturation and chemical distributions. Again, these reflect the fundamental constaints of screening evaluations. Since we do not have much in the way of constraining site data anyway, as is often the case, the point is somewhat academic. We need to move forward within the limitations of the observations and relationships we have. Because it is the simpler and more conservative approach, the LNAPL zone will be chemically and spatially constrained using the pre-remediation thickness and the current "apparent" mole fractions in groundwater leaving that zone. The current source zone

concentration of benzene and MTBE in MW-3 is about 1 mg/l for both compounds. The corresponding apparent mole fraction of benzene is then about 5.6×10^{-4}, and MTBE is about 2.1×10^{-5}. Recall that this is calculated simply from the observed concentration divided by the pure phase solubility (see Section 3). For this problem, we will not concern ourselves with the details of other gasoline compounds and will simply use LNAST default values for comparative purposes.

Dilution from variable saturations and concentration distributions in the LNAPL source zone, whether caused by remediation or natural processes, presents some interesting dilemmas. For instance, it might not be appropriate to consider dilution if the discrete zone of interest were in direct contact with a groundwater receptor, as opposed to a larger aquifer thickness. This also brings up questions regarding the point of measurement and compliance; is the target cleanup concentration applied in a spatially discrete sense, or is it applied across a vertical monitoring interval or across a receptor interval? Once again, judgement about conditions and potential ramifications of the spatial position of impacts relative to receptors or points of compliance is required. At this site, ongoing commercial fuel service station use and the lack of usable groundwater because of limited production potential and poor water quality suggests that consideration of dilution is appropriate in the calculations, as there are no discrete risks from zone specific transport in the aquifer.

In summary, we have an LNAPL zone that is about 2 m thick, but no longer able to accumulate in wells (residual saturation). The source zone has been depleted of soluble components, except for an undefined interval that apparently has a composition similar to the initial source now feeding a diluted groundwater plume. The source composition will be prescribed using the "diluted" mole fraction estimates provided above. The geologic conditions will be approximated by a 2-layer condition of a silty sand overlain by a clean sand. The remaining properties will be based on the example values given in the LNAST utility or through site specific interpretation.

6.3.3 Running the Problem

This problem is executed in the same sequence as the prior examples. The LNAST utility is opened, and the **Soil Properties** Tab selected first. Select the *Vertically Layered Conditions* option, 2-layers (Figure 6-31). Notice that a dialog box appears where you will highlight the soil layer of interest, with Layer 1 always being the lowermost. In our problem, Layer 1 is the silty sand material with the properties given in Table 6-2, and Layer 2 is the sand, both 1m in thickness.

The groundwater gradient was given at 0.005 (**Groundwater Conditions** Tab is not shown for this problem). The LNAPL **Source Area Parameters** are selected based on the geometry and LNAPL distribution observations discussed above (Figure 6-32). The LNAPL is assumed to be at residual saturation, as it no longer accumulates above trace levels in observation wells. The saturations could

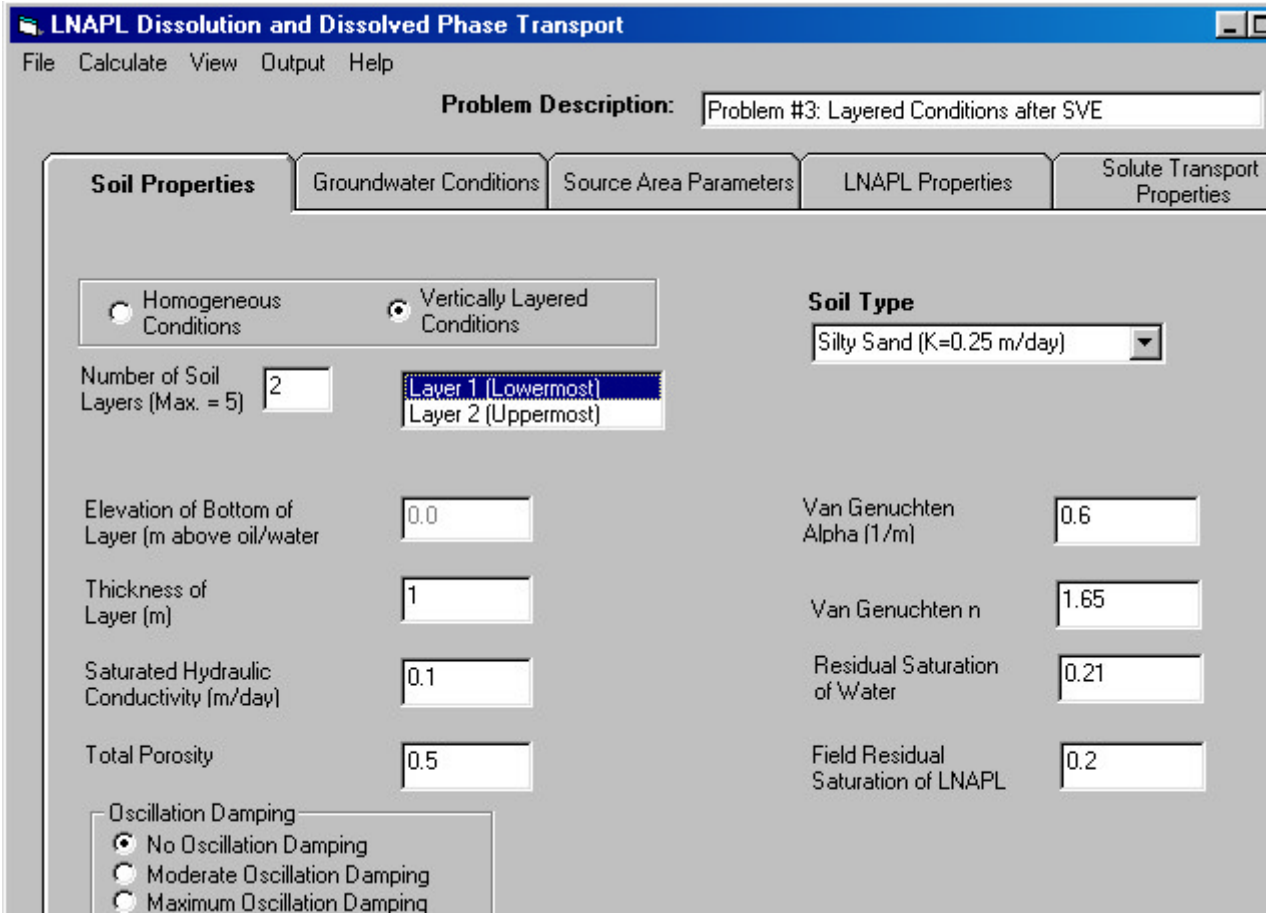

Figure 6-31. **Soil Properties** Tab for Problem #3, with Layer 1 shown (silty sand).

be lower than this, but we currently have no information from which to make that determination. Depending on the results of the analyses and the implications of the selected saturation values, one might choose to collect site specific data if it becomes important to know these values with more certainty.

The **LNAPL Properties** are specified next (Figure 6-33). The default example values for gasoline are used, except for the molar fractions of the compounds of interest. Recall that the apparent mole fractions of compounds in the LNAPL can be derived simply by dividing the observed concentrations in groundwater by the pure phase solubility for each compound. As discussed, this is an "apparent" mole fraction that includes the effects of dilution that are apparent in the site data. The degradation half-life for MTBE is left at 9000 days, essentially non-degraded, as a worst-case condition.

The **Solute Transport Properties** are modified with respect to dispersivity and volatilization efficiency, with other parameters left unchanged from initial default values. The longitudinal dispersivity is set to 25 m, which is about 10% of the expected field scale, the transverse dispersivity is 20% of this value (5 m), and the vertical dispersivity is 1% of the longitudinal (0.25 m). You may already recognize that the expected field scale of the plume is different for the various compounds,

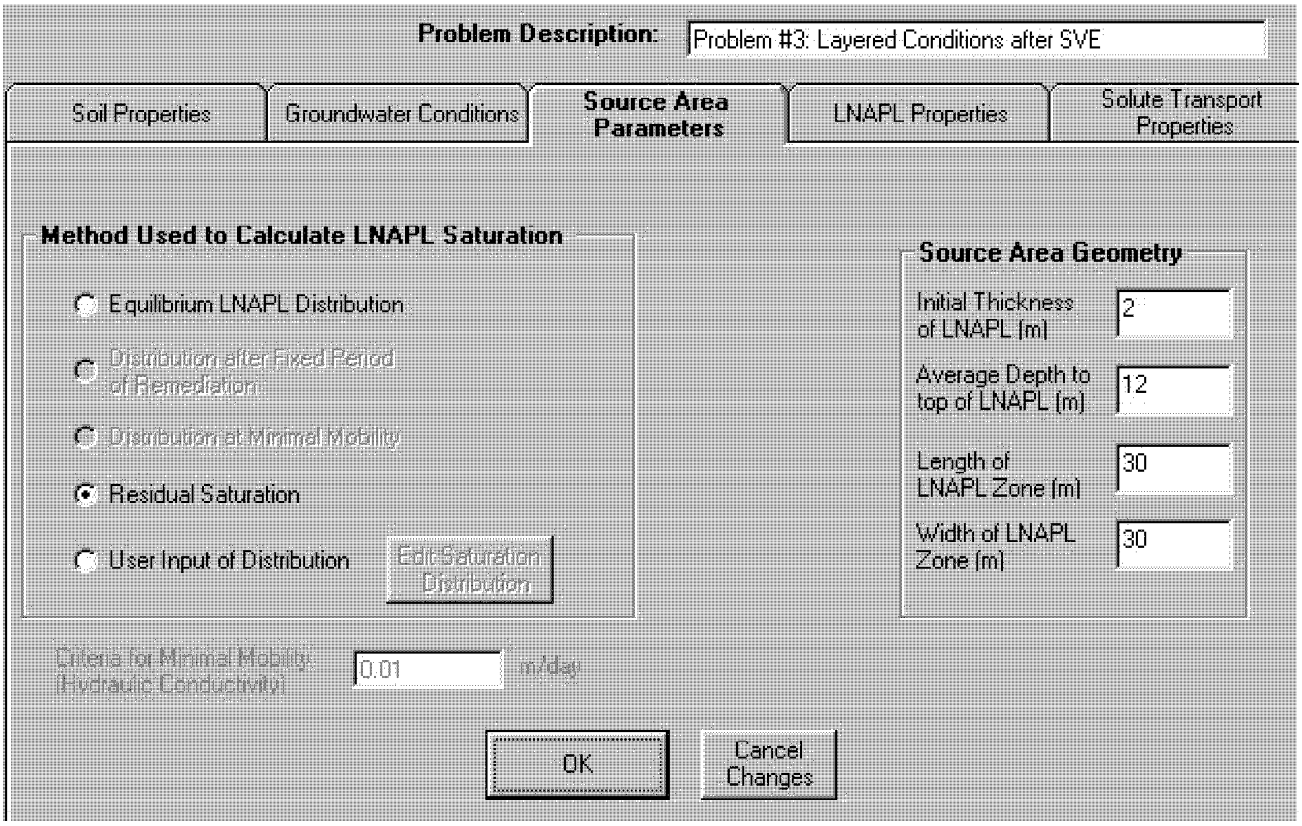

Figure 6-32. **Source Area Parameters** Tab and selections for Problem 3.

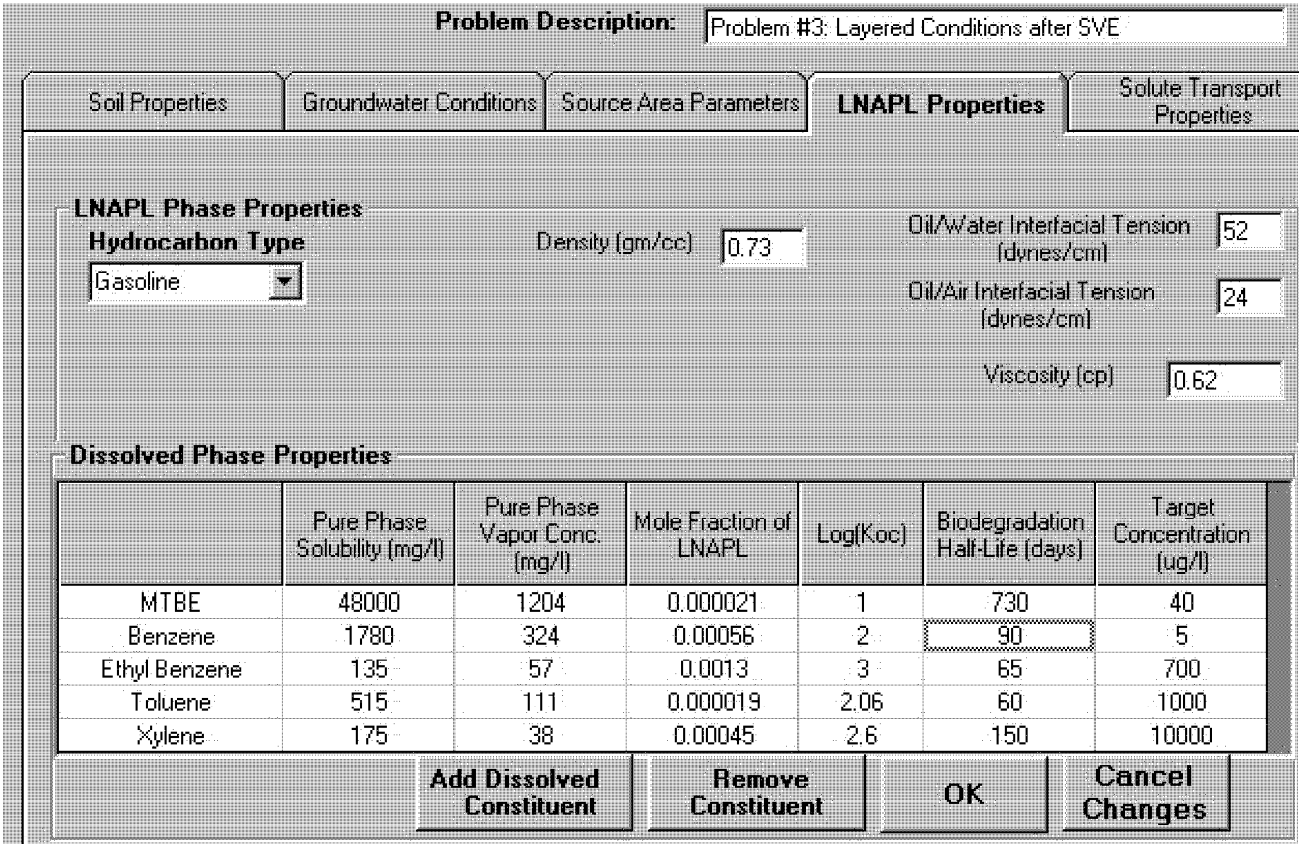

	Pure Phase Solubility (mg/l)	Pure Phase Vapor Conc. (mg/l)	Mole Fraction of LNAPL	Log(Koc)	Biodegradation Half-Life (days)	Target Concentration (ug/l)
MTBE	48000	1204	0.000021	1	730	40
Benzene	1780	324	0.00056	2	90	5
Ethyl Benzene	135	57	0.0013	3	65	700
Toluene	515	111	0.000019	2.06	60	1000
Xylene	175	38	0.00045	2.6	150	10000

Figure 6-33. The **LNAPL Properties** Tab for Problem 3. The only modified properties are the mole fractions of the compounds, which were derived by dividing the currently observed dissolved-phase concentrations by the pure phase solubility of each.

primarily as a function of the degradation term. One may therefore wish to run separate calculations of potentially low degradability compounds versus higher degradability chemical species; we will not do so in this tutorial. The vapor diffusion efficiency is set to 0.01 to account for the site concrete surface cover that is in good condition. This is a typical factor used in many vapor risk screening methods, though again, if it were to become critical to results, one would typically look closer at justifications for a site specific value.

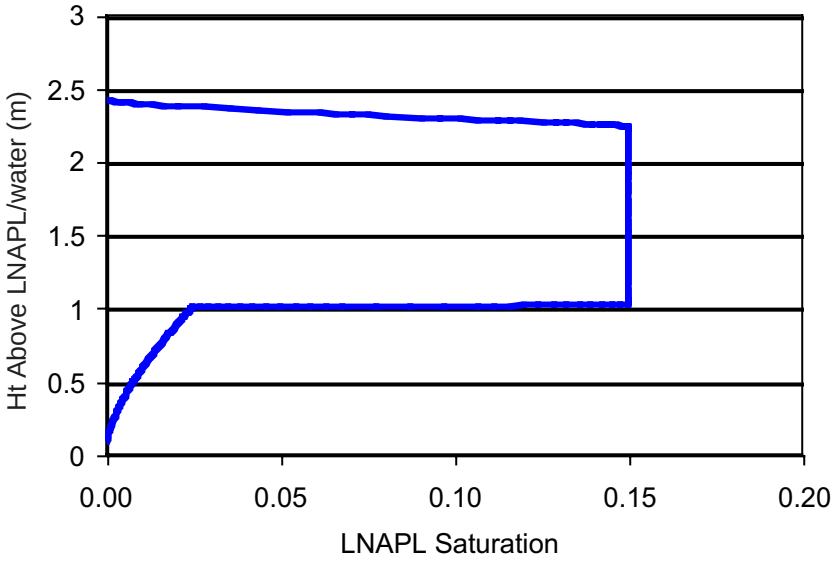

Figure 6-34. LNAPL saturation profile for the 2-layer soil condition, silty sand overlain by sand each bed 1 m thick. Notice that the saturation condition in the silty sand is less than the residual saturation for these particular conditions.

6.3.4 Results

We will again view results by first starting with the LNAPL saturation distribution and the associated groundwater flow through that zone, as this sets context for the chemical depletion and groundwater transport conditions. Recall that we specified residual saturation conditions for both geologic beds, the silty sand overlain by the sand. The associated LNAPL saturation profile shows that the calculated distribution in the silty material is less than the residual saturation for this particular problem, so the profile has a sharp predicted increase in LNAPL saturation at the contact between the two soil materials (1 m elevation above the oil/water interface; Figure 6-34). This presents an interesting condition, because while the hydraulic conductivity of the silty material is much smaller than the sand, the relative permeability to water is greater in the silty material because there is much less LNAPL. The result is that the contrast in groundwater flux through the 2 beds is not as great as one might have initially suspected, though a contrast of about 20 is present (Figure 6-35). The background contrast in groundwater flux through these units would be the ratio of the conductivities, or about a factor of 60. This is another example of the sometimes non-intuitive aspects of multiphase flow.

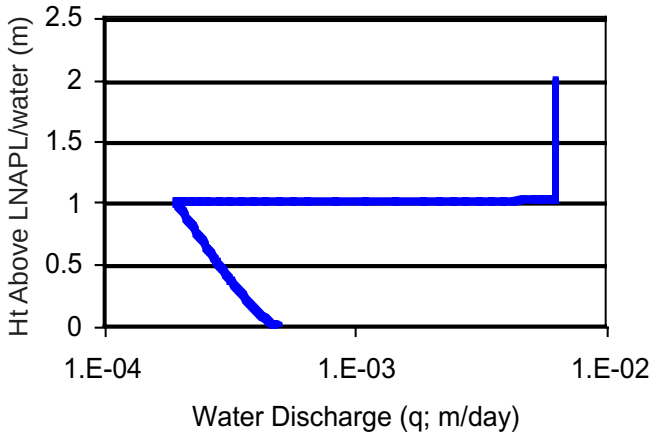

Figure 6-35. Groundwater discharge through the LNAPL zone.

The LNAPL source depletion estimates suggest depletion times of 100 years or more for the more soluble components (Figure 6-36). This is because the averaged "diluted" mole fraction is small, and therefore mass loss rates are also small. As mentioned previously, the result would be little different if a discrete zone at full mole fractions were specified in the silty material and dilution was factored into the output information. However, if on the other hand, the "stranded" LNAPL zone were in the sandy material and not treated by the SVE because of the intervening water saturation, then depletion would be much faster (Figure 6-37). This calculation is not detailed here, but briefly was derived from the User Input Distribution option in the LNAPL properties describing a thin zone of impacts, and adjusting the mole fractions back to "non-diluted" conditions. The expected groundwater transport under the assumed problem conditions, will in large part, dictate the need to better resolve the site conceptual model. Clearly if the second condition is more representative, one should see the gross-scale verification in less than 1 year in the field by significantly decreasing MTBE trends in source area groundwater.

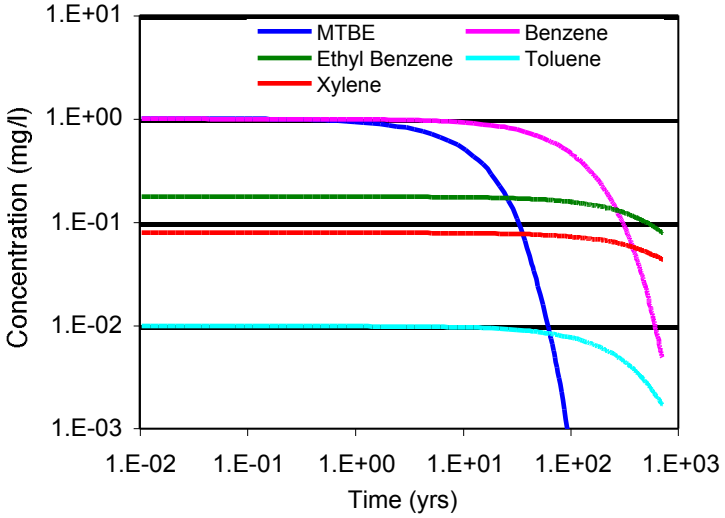

Figure 6-36. Estimated groundwater concentration versus time at the leading edge of the LNAPL source zone (depletion curves).

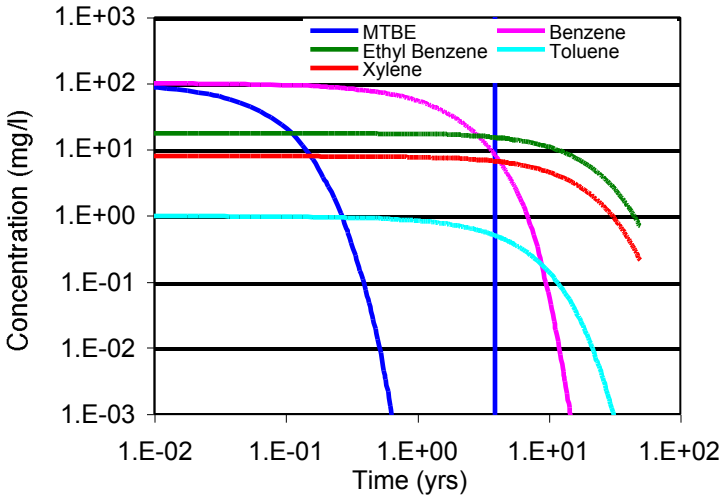

Figure 6-37. Hypothetical LNAPL zone depletion of soluble compound for conditions of a discrete LNAPL interval in only the sandy zone.

The estimated downgradient extents of the various compounds shows the importance of the degradation half-life selected for each and their target concentration (Figure 6-38). For this case, only benzene and MTBE are estimated to be present downgradient at concentrations exceeding the selected target levels. Again, this does not imply that the other components are not present, but simply that they are below the selected threshold. For the given case, MTBE is expected to reach a downgradient distance of about 100 m before the combined transport processes reduce the concentration to below the selected 40 ug/l target threshold. The estimated time to reach this distance for

the given conditions is about 10 years for MTBE, whereas benzene is expected to reach is maximum downstream distance of about 42 m after about 2.5 years. For the given scenario, one can also observe that the residence time of downstream impacts for benzene is more than 100 yrs before source zone depletion starts to reduce impacts for the given conditions.

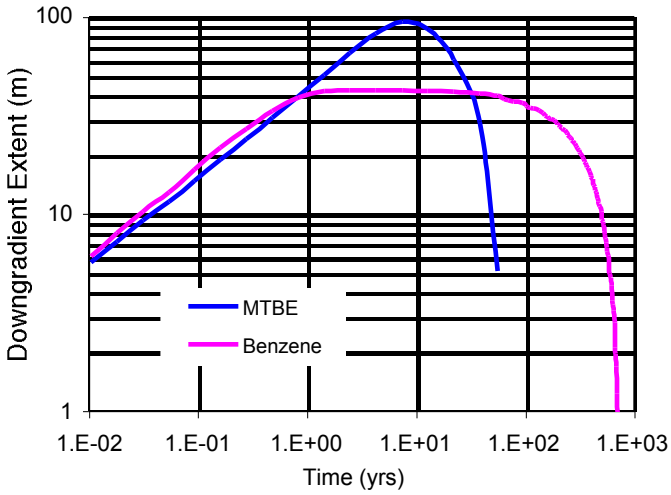

Figure 6-38. Estimated downgradient extents of MTBE and benzene. The other gasoline compounds of potential concern do not extend downgradient in relation to their target concentrations.

As is sometimes the case, where one goes from here depends on the specifics of the site, regulatory context, potential use conditions, and the environmental setting. From the prior discussion and evaluations, it is clear that a range of residual LNAPL impacts and chemical conditions are possible at the site following the SVE cleanup operations, none of which can be further discerned or constrained from the available information. At least now we have some conceptual models and ideas that can be tested in the field. Therefore the site context and need for further investigation rests on a few general technical considerations. First, within the zone of remaining LNAPL, vapor, and dissolved-phase impacts, it is important to consider whether those impacts pose any near-term potential threat. If not, then continued monitoring of groundwater conditions will assist in shedding light on which of the various possible scenarios is most consistent with the monitoring data. One would typically use the range of estimated chemical trends, including breakthrough curves, in this comparison (Figure 6-39). Second, if there is no near-term threat, but the potential for long-term impacts is a concern, then a determination must be made on how continued groundwater monitoring will fold into the constraining the site conceptual models and over what timeframe before other actions would be needed. Last, if potential near-term or other impacts are unacceptable as they stand or if other factors require better resolution of the problem, then one would typically collect in situ field data to constrain key assumptions in the various conceptual models. For this case, the key data

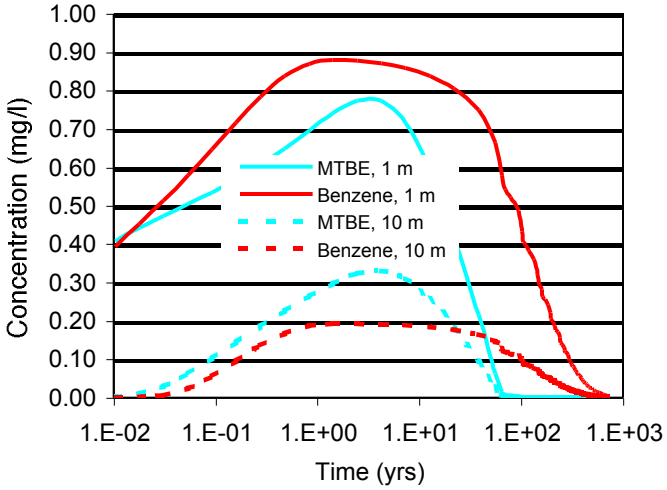

Figure 6-39. Predicted breakthrough curves for MTBE and benzene at 1 m and 10 m downgradient of LNAPL.

would be the remaining LNAPL saturation distribution and its chemistry. But as one is investigating subsurface conditions, other parameters could certainly also be obtained at the same time.

This example shows that real world problems often have no immediate answer. Often the best we can do is eliminate unrealistic assumptions and conditions to assist in focussing on the key concerns and the related potential data deficiencies to improve the certainty of the analysis. A reminder: while the processes are fairly well known, the challenge lies in describing spatial distributions of parameters controlling those processes on a site specific basis. Because the processes are pore- and molecular scale, it is easy to become mired in details that have bearing, but may not be critically important. That is the importance of setting clearly defined boundaries for site conceptual models so that only useful improvements are sought, as needed. For the given case, little would be gained by trying to better constrain the groundwater gradient, general geologic setting, or transport parameters. However, as discussed at the beginning of the problem, the conceptual questions of greatest importance were where the LNAPL resides and at what saturations and chemical state.

Section 7.0

CONCLUDING REMARKS

The body of this report has provided an overview understanding of the processes and factors affecting LNAPL, water, and vapor in and around the water table region. Key technical observations are provided in the Executive Summary, as well as in various report sections, and are not redeveloped here. The bibliography is a good starting point for those wishing to further investigate the details and complexities of multiphase and multicomponent processes.

It should be clear by now that most of the parameters necessary to constrain site conceptual models for multiphase conditions are generally unavailable on a site-specific basis. This should not stop you from building conceptual models around what you know and can infer about site-specific properties. As mentioned, most chemical and physical observations are linked to these underlying processes and controlling parameters. In many cases, all one will have to start with is a set of boring logs and some groundwater and LNAPL monitoring data. As sparse as this may appear, it is enough to bracket a range of parameters and conceptual conditions and inspect the associated outcomes for consistency with field information. In this bracketing and screening mode, one is looking for key factors of importance at a site. In this way, the site understanding can be attuned to the underlying LNAPL and chemical transport processes. Depending on the outcome of the screening evaluations, one may find no further work is needed, or that identification of key factors may be useful in constraining the potential risk and longevity of and LNAPL source, as well as the potential benefits of remediation actions.

We also have seen the many reasons why LNAPL recovery by hydraulic methods often does little, in the long run, toward mitigating risk magnitude and only slightly reduces risk longevity for most conditions. There are, however, many other reasons for applying hydraulic recovery strategies. One might wish to contain the LNAPL and the associated dissolved-phase plume for some period until changes in site use allow more aggressive cleanup actions. Hydraulic recovery strategies could also be used to assist in formation immobilization of the LNAPL, which while still largely present, would no longer constitute a risk with respect to direct migration of the product phase.

As mentioned and implied throughout the text, your ability to successfully use this methodology for evaluating LNAPL removal from source zones by natural or remediation processes depends on good judgement and consistency with whatever field observations are available. As a technical decision support tool, one must be critical of both the input information and the results. We have often found that LNAPL conditions in the field are not at all what has been reported in past investigations, so be cautious and proactive with the information and evaluation results.

We suggest you remember this overall advice as you go through the process: The screening tool calculates general and comparative outcomes that must be placed in site context by the user. Do not expect the screening model to calibrate precisely to site-specifics, but rather to represent general trends in time and space. Trends that are clearly inconsistent with field observations mean that one of the underlying inputs or assumptions have not been met. It is in the thinking about these data and processes that good interpretations can be generated.

Section 8.0
BIBLIOGRAPHY

Abriola, L.M., 1983. Mathematical modeling of the multiphase migration of organic compounds in a porous medium. Ph.D. Dissertation, Department of Civil Engineering, Princeton University, Princeton, N.J., pp. 187.

Abriola, L.M. and Pinder, G.F., 1985a. A multiphase approach to the modeling of porous media contamination by organic compounds, 1. Equation development. Water Resour. Res., Vol. 21, No. 1, pp. 11-18.

Abriola, L.M. and Pinder, G.F., 1985b. A multiphase approach to the modeling of porous media contamination by organic compounds, 2. Numerical simulation. Water Resour. Res., Vol. 21, No. 1, pp. 19-26.

Association for the Environmental Health of Soils (AEHS), 1999. Total Petroleum Hydrocarbon Criteria Working Group Series Volume 1: Analysis of Petroleum Hydrocarbons in Environmental Media, edited by Wade Weisman, Amherst Scientific Publishers, Amherst, MA.

AEHS, 1999. Total Petroleum Hydrocarbon Criteria Working Group Series Volume 2: Composition of Petroeum Mixtures, prepared by T.L. Potter and K.E. Simmons, Amherst Scientific Publishers, Amherst, MA.

AEHS, 1999. Total Petroleum Hydrocarbon Criteria Working Group Series Volume 3: Selection of Representative TPH Fractions Based on Fate and Transport Considerations, by J.B. Gustafson, J. Griffith Tell, and D. Orem, Amherst Scientific Publishers, Amherst, MA.

AEHS, 1999. Total Petroleum Hydrocarbon Criteria Working Group Series Volume 4: Development of Fraction Specific Reference Doses (RfDs) and Reference Concentrations (RfCs) for Total Petroleum Hydrocarbons (TPH), by Edwards, D.A., Andriot, M.D., Amoruso, M.A., Tummey, A.C., Bevan, C.J., Tveit, A., Hayes, L.A., Youngren, S.H., and Nakles, D.V., Amherst Scientific Publishers, Amherst, MA.

Ahlfeld, D., Dahmani, A, Hoag, G., Farrell, M., Ji, W., 1994. Field Measurements of Air Sparging in a Connecticut Site: Results and Comments. Proceedings of Petroleum Hydrocarbons and Organic Chemicals in Ground Water: Prevention, Detection and Restoration, Houston, Nov. 1994.

American Petroleum Institute, 1994. Transport and Fate of Non-BTEX Petroleum Chemicals in Soils and Groundwater, Health and Sciences Department, API Publication Number 4593, Washington, DC.

American Petroleum Institute, 1999. Assessing the Significance of Subsurface Contaminant Vapor Migration to Enclosed Spaces. API Publication 4674.

American Society for Testing and Materials (ASTM), 1995. Standard Guide for Risk-Based Corrective Action Applied at Petroleum Release Sites: ASTM E-1739-95, Philadelphia, PA.

Arya, L.M., and Paris, J.F., 1981. A physico-empirical model to predict soil moisture characteristics from particle-size distribution and bulk density data. Soil Science Soc. Am., # 45.

Ballestero, T.P., Fiedler, F.R., and Kinner, N.E., 1994. An investigation of the relationship between actual and apparent gasoline thickness in a uniform sand aquifer. Journal of Ground Water, Vol. 32, No. 5, pp. 708-718.

Beahr, A.L. and Corapcioglu, M.Y., 1987. A compositional multiphase model for groundwater contamination by petroleum products, 2. Numerical solution. Water Resour. Res., Vol 23, No. 1, pp. 201-214.

Baehr, A.L., 1987. Selective Transport of Hydrocarbon in the Unsaturated Zone Due to Aqueous and Vapor Phase Partitioning. Water Resources Research, Vol. 23, No. 10, pp. 1926-1938, October 1987.

Bear, J., 1972. Dynamics of Fluids in Porous Media. American Elsevier, New York, N.Y., pp. 764 (see especially pp. 444-449).

Beckett, G.D., Lundegard, P., 1997. Practically Impractical - The Limits Of LNAPL Recovery And Relationship To Risk. Proceedings of Petroleum Hydrocarbons and Organic Chemicals in Ground Water: Prevention, Detection and Restoration, Houston.

Beckett, G.D., Huntley, D., 1994. Characterization of Flow Parameters Controlling Soil Vapor Extraction. Journal of Ground Water, Vol. 32, No. 2, pp. 239-247.

Beckett, G.D., Huntley, D., Panday, S., 1995. Air Sparging: a Case Study in Characterization, Field Testing, and Modeling Design. Proceedings of the Petroleum Hydrocarbons and Organic Chemicals in Ground Water: Prevention, Detection and Restoration, Houston, Nov. 1995.

Beckett, G.D., and Huntley, D., 1998. Soil Properties and Design Factors Influencing Free-phase Hydrocarbon Cleanup. January 1998, Environmental Science and Technology.

Benson, D.A., Huntley, D., and Johnson, P.C.1993. Modeling Vapor Extraction and General Transport in the Presence of NAPL Mixtures and Nonideal Conditions. Journal of Groundwater v. 31, No. 3, pg 437-455

Blake, S.B. and Hall, R.A., 1984. Monitoring petroleum spills with wells: Some problems and solutions. Proc. 4th Natl. Symp. On Aquifer Restoration and Groundwater Monitoring Natl. Water Works Assoc., Columbus, Ohio, pp. 305-310.

Blake, S.B. and Lewis, R.W., 1983. Underground oil recovery. Ground Water Momt. Rev., Vol. 3, No. 2, pp. 40-46.

Bouwer, H., and Rice, R.C., 1976. A slug test for determining hydraulic conductivity of inconfined aquifers with completely or partially penetrating wells. Water Resources Res., v. 12, p. 423-428.

Bradley, H.B., 1987. Petroleum Engineering Handbook. Society of Petroleum Engineers, Richardson, TX., 1v. (various pagings).

Brooks, R.H. and Corey, A.T., 1964. Hydraulic properties of porous media. Colo. State Univ., Fort Collins, Colo., Hydrol. Pap. No. 3, pp. 27.

Brost, E., and Beckett, G.D., 2000. A multiphase screening method to determine fuel immobility in the unsaturated zone. AEHS Conference workshop, San Diego, California.

Buckley, S.E. and Leverett, M.C., 1942. Mechanism of Fluid Displacement in Sands, Trans., AIME, pp. 107-117.

Burdine, N.T., 1952. Relative permeability calculations from pore-size distribution data. Trans. AIME 198, pp. 35-42.

Carsel, R. F. and Parish, R. S., 1988. Developing Joint Probability Distributions of Soil Water Retention Characteristics, Water Resources Research, 24(5), pp. 755-769.

Charbeneau, Randall, 1997. Free Product Recovery of Petroleum Hydrocarbon Liquids, prepared for American Petroleum Institute.

Charbeneau, Randall, 1999. Free Product Recovery of Petroleum Hydrocarbon Liquids, prepared for the American Petroleum Institute.

Chatzis, I, Morrow, N. R., and Lim, H. T., 1983, Magnitude of detailed structure of residual oil saturation: SPE Journal, April 1983, p. 311-326.

Chatzis, I, Kuntamukkala, M. S., and Morrow, N. R., 1988, Effect of capillary number on the microstructure of residual oil in strongly water-wet sandstones: SPE Reservoir Engineering, August 1988, p. 902-912.

Chiang, C.Y., Nevin, J.P., and Charbeneau, R.J., 1990. Optimal free hydrocarbon recovery from a single pumping well. Proceedings of Petroleum Hydrocarbons and Organic Chemicals in Ground Water: Prevention, Detection, and Restoration Conference, Houston, TX. National Water Well Association., pp.161-178.

Cooley, R.L., 1983. Some New Procedures for Numerical Solution of Variably Saturated Flow Problems. Water Resour. Res., Vol. 19, No. 5, pp. 1271-1285.

Corey, A.T., 1986. Mechanics of Immiscible Fluids in Porous Media. Water Resources Publications, Littleton, Colo., pp. 259.

Corapcioglu, M.Y. and Beahr, A.L., 1987. A compositional multiphase model for groundwater contamination by petroleum products, 1. Theoretical considerations. Water Resour. Res., Vol. 23, No. 1, pp. 191-200.

Crichlow, H.B., 1977. Modern Reservoir Engineering - A Simulation Approach. Prentice Hall, Englewood Cliffs, N.J., pp. 354.

Delshad, M. and Pope, G.A., 1989. Comparison of the thee-phase oil relative permeability models. Transp. Porous Media, Vol. 4, No.1, pp. 59-83.

Domenico, P.A. 1987. An Analytical Model for Multidimensional Transport of a Decaying Contaminant Species. Journal of Hydrology, 91 (1987) 49-58.

Domenico, P.A. and F. W. Schwartz, 1990. Physical and Chemical Hydrogeology, Wiley, New York, NY.

Dragun, J., 1988. The Soil Chemistry of Hazardous Materials. Hazardous Materials Research Institute, Silver Spring, MD.

Dupont, R.R., Doucett, W.J., Hinchee, R.J., 1991. Assessment of in-situ bioremediation potential and the applicability of bio-venting at a fuel contaminated site. In: Hinchee, R.E. and Olfenbuttel, eds. In-Situ Bioremedation, Butterworth-Heinemann Pub., pp. 262-282.

Dupuit, J., 1863. Etudes theoriques et pratiques sur le mouvement des eaux dans les canaux decouverts et a travers les terrains permeables. Dunod, Paris.

Ehrlich, G.G., Schroeder, R.A. and Martin, P., 1985. Microbial populations in a jet-fuel contaminated shallow aquifer at Tustin, California. U.S. Geol. Surv. Open File Rep., pp. 85-335.

Environmental Protection Agency (EPA), 1995. Risk Assessment Guidance for Superfund, Office of Emergency and Remedial Response, EPA Publication EPA/540/R-95/132, Washington, DC.

Falta, R.W., Javandel, I., Pruess, K. and Witherspoon, P.A., 1989. Density-driven flow of gas in the unsaturated zone due to evaporation of volatile organic chemicals. Water Resour. Res., Vol. 25, No. 10, pp. 2159-2169.

Farr, A.M., Houghtalen, R.J. and McWhorter, D.B., 1990. Volume estimates of light nonaqueous phase liquids in porous media. Ground Water, Vol. 28, No.1, pp. 48-56.

Faust, C.R., 1885. Transport of immiscible fluids within and below the unsaturated zone: A numerical model. Water Resour. Res., Vol. 21, No. 4, pp. 587-596.

Ferrand, L.A., Milly, P.C.D. and Pinder, G.F., 1989. Experimental determination of three-fluid saturation profiles in porous media. J. Contam. Hydrol., Vol. 4, No. 4, pp. 373-395.

Forsyth, P.A., 1990. A Finite Volume Approach to NAPL Groundwater Contamination, Research Report, CS-89-46, University of Waterloo, Waterloo, Ontario, Canada.

Frank, R.J. and Huntley, D., 1997. Processes affecting free-phase hydrocarbon removal by vapor extraction. Proceedings of the 1997 Petroleum Hydrocarbons and Organic Chemicals in Ground Water: Prevention, Detection, and Remediation. National Ground Water Association. Houston, TX, pp. 722-734.

Freeze, R.A., and Cherry, J.A., 1979. Groundwater. Prentice-Hall, Inc., Englewood Cliffs, NJ.

Gardner, W.R., 1956a. Calculation of capillary conductivity from pressure plate outflow data. Soil Sci. Soc. Am. Proc. 20, pp. 317-320.

Gardner, W.R., 1956b. Representation of soil aggregate-size distribution by a logarithmic-normal distribution. Soil Sci. Soc. Am. Proc. 20, pp. 151-153.

Gillham, R.W., Klute, A. and Heermann, D.F., 1979. Measurement and Numerical Simulation of Hysteretic Flow in a Heterogeneous Porous Media, Soil Sci. Soc. J., Vol. 43, pp. 1061-1067.

Hall, R.A., Blake, S.B. and Champlin, Jr., S.C., 1984. Determination of hydrocarbon thickness in sediments using borehole data. In: Proceedings of the 4th National Symposium on Aquifer Restoration and Groundwater Monitoring. Natl Water Well Assoc., Columbus, Ohio, pp. 300-304.

Heath, R.C., 1989. Basic Ground-Water Hydrology. United States Geological Survey Water-Supply Paper 2220, United States Government Printing Office.

Hillel, D., 1982. Introduction to Soil Physics. Academic Press, New York, 364 p.

Hinchee, R.E., Olfenbuttel, R.F., 1991. In-Situ Bioremediation. Butterworth-Heinemann Pub.

Hoag, G.E., and Marley, M.C., 1986. Gasoline residual saturation in unsaturation uniform aquifer materials. Journal of Environmental Engineering, Proceedings of the American Society of Civil Engineering,Vol. 112, No. 13, pp. 586-604.

Honapour, M. and Mahmood, S.M., 1988. Relative-permeability measurements: An overview. J. Pet. Technol., Vol. 40, No. 8, pp. 963-966.

Honapour, M., Koederitz, L. and Harvey, A.H., 1986. Relative Permeability of Petroleum Reservoirs, CRC Press, Inc., Boca Raton, Florida.

Howard, P.H., Boethling, R.S., Jarvis, W.F., Meylan, W.M., and Michalenko, E.M., 1991. Handbook of Environmental Degradation Rates. CRC Press, Inc., Boca Raton, Florida.

Hunt, J.R., Sitar, N. And Udell, K.S., 1988a. Nonaqueous phase liquid transport and cleanup, 1. Analysis of mechanisms. Water Resour. Res., Vol. 24, No. 8, pp. 1247-1258.

Hunt, J.R., Sitar, N. And Udell, K.S., 1988b. Nonaqueous phase liquid transport and cleanup, 2. Experimental studies. Water Resour. Res., Vol. 24, No. 8, pp. 1259-1269.

Huntley, D., 1997. Analytic Determination of Hydrocarbon Transmissibility from Baildown Tests. Conference Proceedings of the 1997 Petroleum Hydrocarbons & Organic Chemicals in Ground Water. Houston, Texas, sponsored by the National Ground Water Association & American Petroleum Institute.

Huntley, D., Hawk, R.N., and Corley, H.P., 1994, Non-aqueous phase hydrocarbon in a fine-grained sandstone, (1) Comparison between measured and predicted saturations and mobility: Journal of Ground Water, v. 32, n. 4.

Huntley, D., Hawk, R., and Wallace, J., 1991, An analysis of the history, distribution, and movement of the blob, a hydrocarbon pool underlying downtown San Diego; in, Abbott, P. (ed), Environmental Perils: San Diego Association of Geologists.

Huyakorn, P.S., Panday, S., and Wu, Y.S., 1994. A three-dimensional multiphase flow model for assessing NAPL contamination in porous and fractured media: I. Formulation. Journal of Contaminant Hydrology (in press).

Huyakorn, P.S., Wu, Y.S. and Park N.S., 1994. An improved sharp-interface model for assessing NAPL contamination and remediation of groundwater systems. Journal of Contaminant Hydrology, Vol. 16, pp. 203-234.

Jacob, C.E., and Lohman, S.W., 1952. Nonsteady flow to a well of a constant drawdown in an extensive aquifer. Transactions, American Geophysical Union, Vol. 33, No. 4, pp. 559-569.

Jennings, J.B., 1987. Capillary Pressure Techniques: Application to Exploration and Development Geology, The American Association of Petroleum Geologists, pp. 67-80.

Ji, W., Dahmani, A., Ahlfeld, D., Lin, J., and Hill, E., 1993. Laboratory study of air sparging: Air flow visualization. Ground Water Monitoring and Remediation, Vol. 13, No. 4, Fall 1993, p. 115.

Johnson, P.C., Stanley, C. C., Kemblowski, M.W., Byers, D.L, Colthart, J.D. 1990. A Practical Approach to the Design, Operation, and Monitoring of In Situ Soil Venting Systems. Ground Water Monitoring Review, Vol. 10, No. 2, Spring 1990.

Johnson, P.C., Kemblowski, M.W. and Colthart, J.D., 1988. Practical screening models for soil venting applications. Proceedings of Petroleum Hydrocarbons and Organic Chemicals in Ground Water: Prevention, Detection and Restoration. Natl. Water Well Assoc., Houston, Texas, pp. 521-546.

Johnson, R. L., and Pankow, J. F., 1992, Dissolution of dense chlorinated solvents in groundwater. 2. Source functions for pools of solvent: Environ. Sci. Technol., v. 26, n. 5, p. 896-901.

Johnson, R.L., Johnson, P.C., McWhorter, D.B., Hinchee, R.E., and Goodman, I., 1993. An overview of in situ air sparging. Groundwater Monitoring and Remediation, v. XIII, No. 4, pp.127-135.

Kaplan, E., Banerjee, S., Ronen, D., Magaritz, M., Machlin, A., Sosnow, M., and Koglin, E., 1991. Multilayer sampling in the water table region of a sandy aquifer. Groundwater, 29, pp. 191-198.

Karickhoff, S.W. and D.S. Brown, 1979. Determination of Octanol/Water Distribution Coefficients, Water Solubilities, and Sediment/Water Partition Coefficients for Hydrophobic Organic Pollutants. Series Title: Research Reporting Series 4, Environmental Monitoring ; EPA-600/4-79-032. Environmental Research Laboratory, Office of Research and Development, Athens, GA. U.S. Environmental Protection Agency, Springfield, VA. pp. 17.

Kearl, P.M., Korte, N.E., Stites, M., and Baker, J., 1994. Field comparison of micropurging vs. traditional groundwater sampling. Ground Water Monitoring and Remediation, Fall, pp. 183-190.
Kemblowski, M.W., and Chiang, C.Y., 1990. Hydrocarbon thickness fluctuations in monitoring wells. Ground Water, Vol. 28, No. 2, p. 244-252.

Lake, L.W., Enhanced Oil Recovery, Prentice Hall, Englewood Cliffs, N.J., 1989.

Lenhard, R. J. and Parker, J. C., Measurement and Prediction of Saturation-Pressure Relationships in Three-Phase Porous Media Systems, Journal of Contaminant Hydrology, v.1, pp. 407-424, 1987.

Lenhard, R. J. and Parker, J. C., Estimation of Free Hydrocarbon Volume from Fluid Levels in Monitoring Wells, Ground Water, 28(1), 57-67, 1990.

Lenhard, R.J., and Parker, J.C., 1990. Estimation of free hydrocarbon volume from fluid levels in monitoring wells. Ground Water, v. 28, No.1, pp.57-67.

Lenhard, R.J. and Parker, J.C., 1988. Experimental validation of the theory of extending two-phase saturation - pressure relations to three-fluid phase systems for monotonic drainage paths. Water Resour. Red., Vol. 24, No. 3, pp. 373-380.

Leverett, M.C., 1941. Capillary behavior in porous solids. Trans. Soc. Pet. Eng., AIME. v. 142, pp.152-169.

Mace, R.E., Fisher, R.S., Welch, D.M., and Parra, S.P., 1997. Extent, Mass, and Duration of Hydrocarbon Plumes from Leaking Petroleum Storage Tank Sites in Texas. Bureau of Economic Geology, The University of Texas, Austin, TX, Geologic Circular 97-1.

Mackay, D. and Shiu, W.Y., 1981. A critical review of Henry's law constant for chemicals of environmental interest. Journal of Physical Chemistry Reference Data, Vol. 10, No. 4.

MAGNAS3, 1992. Multiphase analysis of groundwater, non-aqueous phase liquid and soluble component in 3 dimensions. Documentation and user's guide, HydroGeoLogic, Inc., Herndon, Virginia.

McCaffery, F.G. and Batycky, J.P., 1983. Flow of immiscible liquids through porous media. In: N.P. Cheremisinoff and R. Gupta (Editors). Handbook of Fluids in Motion. Ann Arbor Science Publishers, Ann Arbor, Mich., pp. 1027-1048.

Melrose, J.C. and Brandner, C.F., 1974. Role of capillary forces in determination of microscopic displacement efficiency for oil recovery by water flooding. Journal of Canadian Petroleum Technology, Vol. 13, No. 4, pp. 54-62.

Mendoza, C.A. and Frind, E.O., 1990. Advective-dispersive transport of dense organic vapours in the unsaturated zone, 2. Sensitivity analysis. Water Resour. Res., Vol. 26, No. 3, pp. 388-398.

Mercer, J.W., and Cohen, R.M., 1990. A review of immiscible fluids in the subsurface: Properties, models, characterization and remediation. Journal of Contaminant Hydrology, Vol. 6, pp. 107-163.

Mercer, J.W., Faust, C.R., Cohen, R.M., Andersen, P.F. and Huyakorn, P.S., 1985. Remedial action assessment for hazardous waste sites via numerical simulation. Water Manage. Res., 3, pp. 377-387.

Millington, R.J. and Quirk, J.P., 1959. Permeability of porous media. Nature (London) 183, 387-388.

Mishra, S., Parker, J.C., and Singhal, N., 1989. Estimation of soil hydraulic properties and their uncertainty from particle size distribution data. Journal of Hydrology, 108, pp. 1-18.

Morrow, N.R., Chatzis, I. and Taber, J.J., 1988. Entrapment and mobilization of residual oil in bead packs. Soc. Pet. Eng. Reserv. Eng., Aug. 1988, pp. 927-934.

Mualem, Y., 1976. A Catalogue of the Hydraulic Properties of Unsaturated Soils. Development of Methods, Tools and Solutions for Unsaturated Flow with Application to Watershed Hydrology and Other Fields. Israel Institute of Technology.

Mualem, Y., 1976. A New Model for Predicting the Hydraulic Conductivity of Unsaturated Porous Media. Water Resources Research. Volume 12, pp. 513-522.

Nilkuha, K. and Huyakorn, P., 1989. Numerical Solution of Two-Phase Flow Through Porous Media, Dept. Of Geoscience, New Mexico Inst. Of Mining and Technology.

Ostendorf, D.W., 1990. Long term fate and transport of immiscible aviation gasoline in the subsurface environment. Water Science and Technology, Vol. 22, pp. 37-44.

Panday, S., Forsyth, P.A., Falta, R.W., Wu, Y.S. and Huyakorn, P.S., 1995. Considerations for robust compositional simulations of subsurface nonaqueous phase liquid contamination and remediation. WRR, Vol. 31, No. 5, pp. 1273-1289.

Panday, S., Wu, Y.S., Huyakorn, P.S., and Springer, E.P., 1994. A three-dimensional multiphase flow model for assessing NAPL contamination in porous and fractured media: II. Porous Medium Simulation Examples. Journal of Contaminant Hydrology (in press).

Pankow, J.F., and Cherry, J.A., 1996. Dense Chlorinated Solvents and Other DNAPLs in Groundwater: History, Behavior, and Remediation. Waterloo Press, 522 p.

Parker, J.C., Lenhard, R.J., and Kuppusamy, T., 1987. A parametric model for constitutive properties governing multiphase flow in porous media. Water Resour. Res. v. 23, pp. 618-624.

Parker, J.C., 1989. Multiphase flow and transport in porous media. Review of Geophysics, vol. 27, No. 3.

Parker, J.C., and Kayal, A., 1990. Technical documentation for the numerical modeling code, ARMOS. Environmental Science and Technology, Blacksburg, Virginia.

Peaceman, D.W., 1977. Fundamentals of Numerical Reservoir Simulation. Elsevier, Amsterdam, pp. 176.

Pickens, J.F., and Grisak, G.E., 1981. Scale-dependent dispersion in a stratified granular aquifer. Journal of Water Resources Research, Vol. 17, No. 4, pp. 905-908.

Pinder, G.F. and Abriola, L.M., 1986. On the simulation of nonaqueous phase organic compounds in the subsurface. Water Reserv. Res., Vol. 22, No. 9, pp. 109S-119S.

Powell, R.W., and Puls, R.W., 1993. Passive sampling of groundwater monitoring wells without purging: Multilevel well chemistry and tracer disappearance. Journal of Contaminant Hydrology, 12, pp. 51-77.

Puls, R.W., Paul, C.J., 1995. Low-flow purging and sampling of ground water monitoring wells with dedicated systems. Groundwater Monitoring & Remediation, Winter 1995.

Puls, R.W. and Barcelona, M.J., 1996. Ground water issue : low-flow (minimal drawdown) groundwater sampling. Ada, Okla. : National Risk Management Research Laboratory, Subsurface Protection and Remediation Division, Robert S. Kerr Environmental Research Center, 1996. EPA/540/S-95/504

Rathmell, J.J., Braun, P.H., and Perkins, T.K., 1973. Reservoir waterflood residual oil saturation from laboratory tests. Journal of Petroleum Technology, p. 175-185.

Reid, R.C., Prausnitz, J.M., and Poling, B.E., 1987. The Properties of Gases and Liquids. McGraw - Hill, Inc.

Rice, D.W., Grose, R.D., Michaelsen, J.C., Dooher, B.P., MacQueen, D.H., Cullen, S.J., Kastenberg, W.E., Everette, L.G., and Marino, M.A., 1995. “California Underground Leaking Fuel Tank (LUFT) Historical Case Analyses”. Submitted to the California State Water Resources Control Board and the Senate Bill 1764 Advisory Committee, Nov. 16, 1995.

Ririe, G.T., Sweeney, R.E., Daugherty, S.J., and Peuron, P.M., 1998. A vapor transport model that is consistent with field and laboratory data. Proceedings of the 1998 Petroleum Hydrocarbons and Organic Chemicals in Ground Water: Prevention, Detection, and Remediation. National Ground Water Association. Houston, TX, pp. 299-308.

Rixey, W.G., Garg, S., and Nie, Y., 1997. Dissolution of BTEX and naphthalene from residually trapped hydrocarbons in soils and oily wastes.Proceedings of the 1998 Petroleum Hydrocarbons and Organic Chemicals in Ground Water: Prevention, Detection, and Remediation. National Ground Water Association. Houston, TX, pp. 461-476.

Rouleau, A., 1988. A numerical simulator for flow and transport in stochastic discrete fracture networks. Inland Waters Directorate, National Hydrology Research Institute, National Hydrology Research Centre, 1988. vii, 204 p.

Salinitro, J.P., Diaz, L.A., Williams, M.P., and Wisniewski, H.L., 1994. Isolation of a bacterial culture that degrades methyl-t-butyl ether. Appl. Environ. Microbiol. 60:2593-2596.

Salinitro, J.P., Spinnler, G.E., Neaville, C.C., Maner, P.M., Stearns, S.M., Johnson, P.C., and Bruce, C., 1999. Demonstration of the enhanced MTBE bioremediation (EMB) in situ process. In: Proceedings of the Batelle Fifth International Symposium on In Situ and On-Site Bioremediation, San Diego, CA, April, 1999.

Sauty, Jean-Pierre, 1980. An analysis of hydrodispersive transfer in aquifers. Water Resources Research, Vol. 16, No. 1, pp.145-158.

Schiegg, H.O., 1985. Considerations on water, oil, and air in porous media. Water Science Technol., Vol. 23, No. 4 & 5, pp. 467-476.

Schwille, F., 1984. Migration of organic fluids immiscible in water in the unsaturated zone. In: Yaron, B., Dagon, G., and Goldshmid J. (eds.), Pollutants in Porous Media: The Unsaturated Zone Between Soil Surface and Groundwater. Springer-Verlag, New York, p. 27.

Sleep, B.E. and Sykes, J.F., 1989. Modeling the transport of volatile organics in variable saturated media. Water Resour. Res., Vol. 25, No. 1, pp. 81-92.

Stephens, D.B., 1996. Vadose Zone Hydrology. CRC Press, Inc., Boca Raton, Florida, 347 p.

Stone, H.L., 1973. Estimation of three-phase relative permeability and residual oil data. Can. Pet. Technol., Vol. 12, No. 4, pp. 53-61.

Sudicky, E.A., 1986. A natural gradient experiment on solute transport in a sand aquifer: Spatial variability of hydraulic conductivity and its role with the dispersion process. Water Resources Research, 22(13), pp. 2069-2082.

Sweeney, R.E., Ririe, G.T., Chapman, B.H., and Lewis, E.T., 1998. 3-D approach to RNA groundwater investigations.Proceedings of the 1998 Petroleum Hydrocarbons and Organic Chemicals in Ground Water: Prevention, Detection, and Remediation. National Ground Water Association. Houston, TX, pp. 447-455.

Thiem, G., 1906. Hydrologische methoden. Leipzig, 56 p.

Tyler, N., and Finley, R. J., 1991, Architectural controls on the recovery of hydrocarbons from sandstone reservoirs: In Miall, A. D., and Tyler, N. (eds.), The three-dimensional facies architecture of terrigenous clastic sediments and its implications for hydrocarbon discovery and recovery: Society of Economic Paleontologists and Mineralogists, Tulsa, Oklahoma, Concepts in Sedimentology and Paleontology, volume 3, p. 1-5.

van Genuchten, M.Th., 1980. A closed form equation for predicting the hydraulic conductivity of unsaturated soils. Soil Sci. Soc. Am. J. 44, pp.892-898.

White, H., Faust, C., Montroy, M., 1996. How To Effectively Recover Free Product At Leaking Underground Storage Tank Sites; A Guide For State Regulators. EPA Bulletin 510-R-96-001.

Wiedemeier, T., 1995. Technical Protocol for Implementing Intrinsic Remediation with long-Term Monitoring for Natural Attenuation of Fuel Contamination Dissolved in Groundwater. Air Force Center for Environmental Excellence, Technology Transfer Division, Brooks AFB, San Antonio, TX.

Wilson, J.T., Kampbell, D.H., and Armstrong, J., 1993. Natural bioreclamation of alkylbenzenes (BTEX) from a gasoline spill in methanogenic groundwater. Proc II Int Symp on in situ bioremediation, San Diego, CA, April 5-8.

Wise, W.R., Chang, C.C., Klopp, R.A. and Bedient, P.B., 1991. Impact of Recharge Through Residual Oil Upon Sampling of Underlying Ground Water. GWMR, pp. 93-99.

Wu, Y.S., Huyakorn, P.S. and Park, N.S., 1994. A vertical equilibrium model for assessing nonaqueous phase liquid contamination and remediation of groundwater systems. WRR, Vol. 30, No. 4, pp. 903-912.

Xu, M., and Eckstein, Y., 1995. Use of weighted least-squares method in evaluation of the relationship between dispersivity and field scale. Ground Water, Vol. 33, No. 6, pp. 905-908.

Appendix A

EQUATIONS NECESSARY FOR DESCRIPTION OF LNAPL SOURCE AND TRANSPORT

A.1 DEFINITIONS OF HEAD AND PRESSURE RELATED TO CAPILLARY BATH AND SOIL PORE ANALOGY:

$$H = Z + \frac{P}{\rho g} \quad (1) \qquad P_c = P_n - P_w \quad (2) \qquad h_c = \frac{P_c}{\rho g} \quad (3) \qquad P_c = \frac{2\sigma}{r_c} \quad (4)$$

Where H = total head, Z = elevation, P = pressure, P_c = capillary pressure, P_n = pressure in nonwetting phase, P_w = pressure in wetting phase, σ = the interfacial tension between the fluid pairs, r_c is the radius of curvature of the pore throat, h_c = capillary pressure head, ρ = fluid density 1.0 g/cc when referenced to the water phase as all couplets are for convenience and consistency.

And noting that the capillary rise between each capillary couplet is dependent on the interfacial tension (IFT), we can develop the following scaling relationships between couplets referenced to the water system by equation 4 above.

$$P_c^{aw} = \frac{2\sigma_{ow}}{r} \quad (5) \qquad P_c^{ow} = \frac{2\sigma_{ow}}{r} \quad (6) \qquad P_c^{ao} = \frac{2\sigma_{ao}}{r} \quad (7)$$

Since the pore radius of curvature is equal for each of these relationships, we can rewrite to scale the capillary rise of one system (we will assume air/water) to any of the other systems. Recall the definition of capillary head above (Equation 3), with each couplet referenced to the air/water system.

$$h_c^{ij} = \frac{2\sigma_{ij}}{\rho_w g r} \quad (8) \qquad h_c^{ao} = h_c^{aw}\frac{\sigma_{ao}}{\sigma_{aw}} \quad (9) \qquad h_c^{ow} = h_c^{aw}\frac{\sigma_{ow}}{\sigma_{aw}} \quad (10)$$

This scaling relationship can be used to take the air/water capillary data measured in a lab and scale it to the oil/water or air/oil fluid systems. The new curves are then refit by a capillary function to define the capillary parameters for that new couplet (e.g., equations 12 & 13 below, van Genuchten [VG] and Brooks Corey [BC] functions). Alternatively, a simpler approach is to note that the pore radius is the key factor for this conversion and, therefore, one should be able to scale the capillary rise or bubbling pressure parameter accordingly (Farr et al., 1990); these are the parameters "α" for the VG equation, and "Ψ_b" for the BC equation that are discussed below.

A.2 DEFINITIONS OF SATURATION, VOLUMETRIC FLUID CONTENT, AND HEAD IN SOIL:

$$S_e = \frac{\theta - \theta_r}{\theta_m - \theta_r} \quad (11) \qquad S_e = \left[1+\left(\alpha_{ij} H_{c_{ij}}\right)^N\right]^{-m} \quad (12) \qquad S_e = \left[\frac{\Psi_{bij}}{\Psi_{c_{ij}}}\right]^{\lambda} \text{ for } \Psi_c > \Psi_b, \text{ else } S_e = 1.0 \quad (13)$$

$$h_{ow} = (1-\rho_{ro})\, Z_{ow} \quad (14) \qquad h_{ao} = (\rho_{ro})\, Z_{ao} \quad (15)$$

*Where $\mathbf{S_e}$ is the effective water saturation below the oil/air table and the total liquid saturation above the oil/air table; **i** & **j** denote the couplet of interest; Ψ_b is the Brooks-Corey bubbling pressure; λ is the BC pore size index; θ is the volumetric fluid content, with **r** & **m** subscripts indicating residual and maximum endpoints; α is a capillary parameter inversely related to the soil capillary rise; **N** is a capillary parameter related to the uniformity of pore throat distribution; m = 1-1/N; ρ_{ro} is the relative oil density scaled against water (specific gravity); $\mathbf{h_{ow}}$ and $\mathbf{h_{ao}}$ are the oil/water and air/oil capillary heads.*

Between the oil/water and oil/air interfaces, we have a two-phase system of oil and water controlled by the oil-water capillary parameters. Above the oil/air interface, we have a 3-phase system controlled by the air/oil and oil/water water parameters. And above the oil capillary fringe, we revert back to an air-water capillary system.

$$Vo = \Theta_e \int_0^{surf} S_o\, dz \quad (16)$$

The oil saturation profile corresponding to some observed oil thickness, is calculated using the capillary relationships above. The total oil volume (V_o - Equation 16) per unit area is simply the vertical integral of the oil saturation profile multiplied by the effective porosity ($\Theta_e = \Theta_t - \Theta_r$). It is also possible to rewrite the VG and BC equations above to explicitly account for the residual water saturation, in which case the total porosity would be used for the volume/area integration. The calculations in the toolkit account for this factor in calculating the total LNAPL and component mass used for the transport calculations. Whether using the VEQ approximation, or some other oil distribution defined by the user or approximated by a recovery calculation (see Appendix B), the evaluation method integrates the volume per area over the area of the plume as defined by the user input.

A.3 DEFINITIONS OF CONDUCTIVITY, RELATIVE PERMEABILITY, EFFECTIVE CONDUCTIVITY AND TRANSMISSIVITY

$$K = k_i \frac{\rho g}{\mu} \quad (17) \qquad K_{eff} = k_r\, k_i \frac{\rho g}{\mu} \quad (18) \qquad T_{eff} = \frac{k_i\, \rho_o\, g}{\mu_o} \int_0^{Z_o} k_{ro}\, z \quad (19)$$

$$k_{ro} = \left(S_o\right)^{0.5} \left[\left(1 - S_w^{1/m}\right)^m - \left(1 - S_t^{1/m}\right)^m\right]^2 \quad (20) \qquad k_{rw} = S_w^{1/2} \left[1 - \left(1 - S_w^{1/m}\right)^m\right]^2 \quad (21)$$

$$k_{ra} = \left(1 - S_t\right)^{1/2} \left(1 - S_t^{1/m}\right)^{2m} \quad (22)$$

*Where kr = is relative permeability with respect to w - water, o -oil (LNAPL), a -air phases (Mualem, 1976; Parker, 1989), S = phase saturation (t - total, w - water, o - oil), m = 1-1/N where **N** is a capillary parameter, as defined above.*

$$q_p = -K_{eff_p} i_p \quad (23) \qquad q_{pi} = -\frac{k_{rp} k_{ij}}{\mu_p}\left[\frac{\partial P_p}{\partial x_j} + \rho_p g \frac{\partial z}{\partial x_j}\right] \quad (24)$$

*Darcy's Law may be written in 2 forms: where **i** and **j** are direction indices with repeated values indicating tensor notation, **p** is an index indicating fluid phase, $\mathbf{q_{pi}}$ is the Darcy velocity, $\mathbf{k_{rp}}$ is the relative permeability scalar, $\mathbf{k_{ij}}$ is the intrinsic permeability tensor of the soil, μ_p is viscosity, P_p is the pressure, ρ_p is the density, **g** is gravitational acceleration, **z** is elevation.*

The mass conservation equation is necessary to account for changes in fluid movement in any phase and any direction [eq. A-2]. The equation mathematically states that a change in flux in any given direction must be equaled by a change in fluid storage in the corresponding elemental pore space.

$$\frac{\delta q_{pi}}{\delta x_j} = \frac{\delta}{\delta t}\left(\theta_e \rho_p S_p\right) - M_p \quad (25)$$

*Where **t** is time, θ_p is effective porosity, ρ is density, **S** is phase saturation, and $\mathbf{M_p}$ is a source/sink term with respect to phase **p** accounting for pumping, injection, or other boundary functions, and **x** indicates the Cartesian direction of the differential equation.*

Groundwater Flux

The volumetric groundwater flux (q) below and within the LNAPL pool varies as a function of the background or regional specific discharge (q_{max}) and the water saturation. Below the LNAPL/water interface, the groundwater flux is equal to the regional specific discharge. Above the groundwater piezometric surface, or corrected water table (defined as elevation where the groundwater pressure is equal to zero), there is no horizontal groundwater flux. Between the LNAPL/water interface and the groundwater piezometric surface, the groundwater specific discharge is given by:

$$q = k_{rw} k_i \frac{\rho_w g}{\mu} i \quad (26)$$

*where $\mathbf{k_{rw}}$ is the relative permeability of the wetting phase (water), $\mathbf{k_i}$ is the intrinsic permeability of the soil, ρ_w is the density of water, μ is the viscosity of water, and **i** is the hydraulic gradient.*

Recognizing that the background or regional specific discharge (q_{max}) is given by:

$$q_{max} = k_i \frac{\rho_w g}{\mu} i \quad (27)$$

equation (26) can be rewritten as $q = k_{rw}\, q_{max}$, or $\frac{q}{q_{max}} = k_{rw}$, where the relative permeability, k_{rw} was given above. In a multilayer case, q_{max} through each zone is defined by the permeability or conductivity of that horizon. The water fluxes from each layer are summed to give the total flux across the zone. The above equations can be used to calculate the ratio of groundwater flux through the LNAPL zone (q) to the regional flow q_{max}.

Constituent Concentrations

Above the LNAPL/water interface, groundwater flowing through the soil is in direct contact with LNAPL, so the equilibrium concentration of a soluble constituent in a multicomponent LNAPL is simply given by an analogy to Raoult's Law:

$$C_{eff\,m} = x_m\, C_{sol\,m} \quad (28)$$

where $\mathbf{C_{eff_m}}$ *is the effective solubility of the* **m**, *compound,* $\mathbf{x_m}$ *is the mole fraction and* $\mathbf{C_{sol_m}}$ *is the pure phase solubility of compound* **m**.

The mole fraction x_m is also applied, at the user's option, to calculate the vapor phase concentration and loss from the system for volatile components. Similar to the water phase, Raoult's Law for the gas phase may be written:

$$C_{veff} = \frac{x_m\, VP_m\, MW_m}{R\,T} \quad (29)$$

where $\mathbf{C_{veff}}$ *is the effective vapor concentration (mg/l),* $\mathbf{VP_m}$ *is the pure phase vapor pressure,* $\mathbf{MW_m}$ *is the molecular weight of the pure component,* **R** *is the ideal gas constant (0.0821 mol-l/atm) and* **T** *is temperature (**K**).*

Below the LNAPL/water interface, the concentration is controlled by vertical downward diffusion of the soluble constituent. This process is discussed extensively by Johnson and Pankow (1992), which, in turn, is based on the work of Hunt et al., (1988). These authors show that the concentration (C) above a DNAPL pool (or analogously below an LNAPL pool) is given by:

$$\frac{C}{C_{eff}} = erfc\left[\frac{z}{2\left(\frac{D_v L_p}{\bar{v}}\right)^{1/2}}\right] \quad (30)$$

where $\mathbf{z}$ *is the distance below the LNAPL/water interface,* $\mathbf{L_p}$ *is the length of the pool along the groundwater flow direction,* $\bar{v}$ *is the groundwater flow velocity (=* q/ϕ*), and* $\mathbf{D_v}$ *is the vertical dispersion coefficient, given by* $D_v = D_e + \bar{v}\alpha_v$*, where* $\mathbf{D_e}$ *is the effective aqueous molecular diffusion coefficient, and* α_v *is the vertical dispersivity.* For a layered condition, this same chemical dispersion is allowed between adjacent soil zones.

Mass Flux

There are three potential components to mass flux, as suggested from the equations above: 1) Solubilization and transport within the LNAPL zone later rejoining the regional flow field; 2) Diffusion below the LNAPL lens and transport at the regional flow rate; 3) Volatilization of components through the vadose zone.

Beginning with the soluble phases, the above calculations of aqueous concentration distribution can be combined with the calculated groundwater flux, resulting in the mass flux distribution, by noting that the mass flux (j) is given by (31):

$$j = q\,C \quad (31)$$

This soluble mass flux can be normalized to the maximum mass flux, which is simply the product of the regional specific discharge (q_{max}) multiplied by the effective solubility of the constituent of concern (C_{eff}). The total mass flux depleting the LNAPL source is simply the vertical integral of eq. (31) across the LNAPL zone multiplied by a unit width of the pool, including zones of layering where q varies because of soil properties. Above the LNAPL/water interface, the concentration of the soluble phase is constant with height, so the total mass flux (J_1) per unit width of LNAPL pool is given as:

$$J_1 = C_{eff} \int_0^{z_{wt}} q(z)\,dz \quad (32)$$

where $\mathbf{z_{wt}}$ *is the elevation of the groundwater piezometric surface (or corrected water table).*

Because the water saturation profile, and therefore the relative permeability profile and flux, cannot be integrated analytically, equation (32) must be numerically evaluated by piecewise summation. Below the LNAPL/water interface, as noted above, the groundwater flux (q) remains constant while the concentration varies. Thus, the total mass flux below the interface (J_2) is given as:

$$J_2 = q \int_{-\infty}^{0} C(z)\, dz \quad (33)$$

The distribution of concentration as a function of depth below the LNAPL/water interface is given by equation (30) and can be integrated analytically, resulting in;

$$J_2 = C_{eff} \sqrt{4 D_v\, q\, \phi\, L_p / \pi} \quad (34)$$

The total mass flux in the water phase from both factors is simply $J_1 + J_2$. This distributed flux is used to track losses from the LNAPL phase. The zones through and below the LNAPL are discretized into 100-layer wise pieces. For as long as there is flux and chemical mass within a layer, the corresponding effective concentration of a compound of concern in that zone is used as input to the Domenico 2-dimensional groundwater transport equation (Domenico & Schwartz, 1990). As mass is depleted in a zone, only the diffusive portion of concentration is used as input.

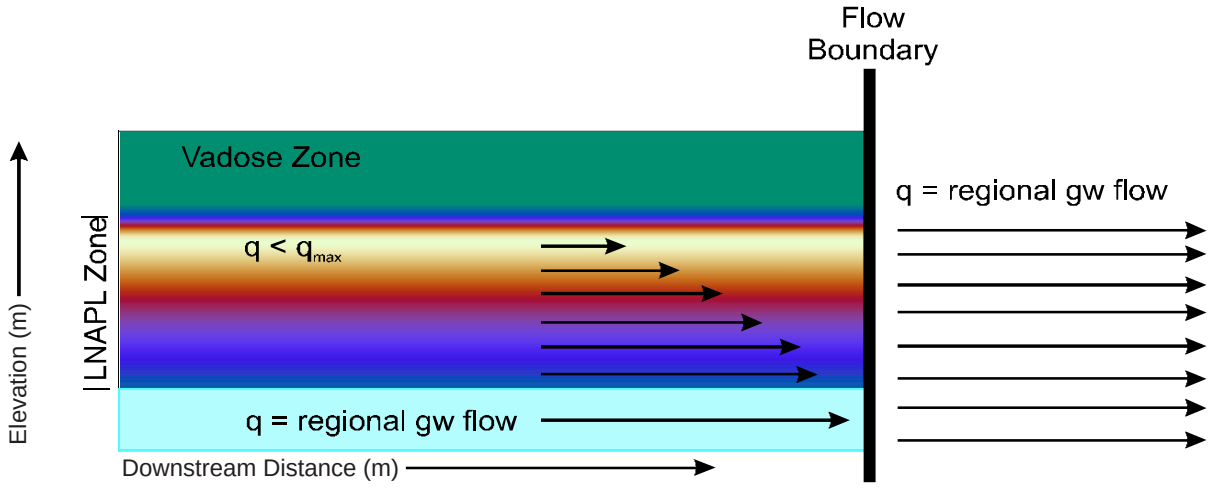

Figure A-1. Cross-section view of groundwater flow through & below the LNAPL interval and the boundary that results for the transport condition.

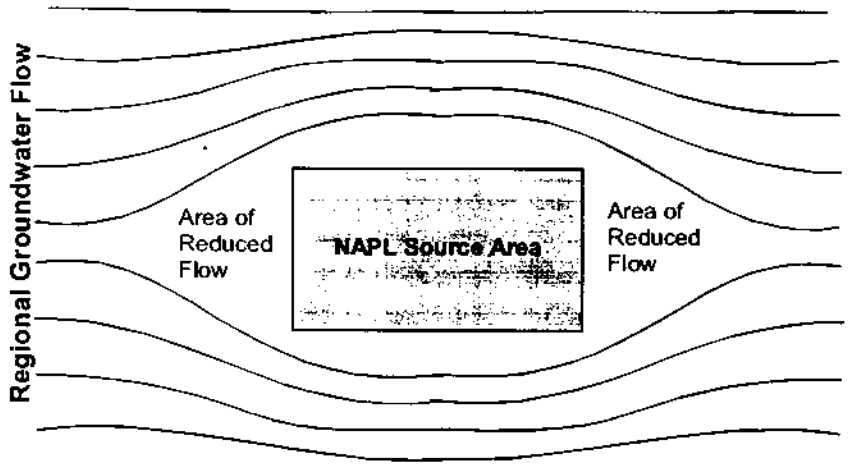

Figure A-2. Plan view of groundwater flow lines that will diverge and then converge around an LNAPL source area, that is in effect, a zone of overall lower hydraulic conductivity toward water.

Invoking analytic assumptions results in a numerical discontinuity at the front of the LNAPL source zone. At this boundary, the regional groundwater flux changes from a slowed condition in the LNAPL interval to regional conditions assumed for the transport algorithm (see figures A-1 and A-2). As concentration is the input to the transport solution, this means that there is a flux discontinuity at this boundary that results in somewhat greater predicted concentrations that may be evident under field conditions. The flux is tracked through the LNAPL zone, so the discontinuity becomes less important through time as mass is depleted from the system. Since the discontinuity results in an overestimate of concentrations in groundwater immediately ahead of the source zone, the analytic boundary condition is conservative (i.e., worst-case).

Turning to the vapor phase, the flux is assumed to occur under ambient (non-flowing) conditions and is therefore diffusion gradient driven. This flux modifies the remaining mass in the LNAPL source of any particular component through time, in turn modifying the source concentration term for groundwater. It is assumed that the ground surface is a zero concentration boundary, and at steady-state, one may calculate the concentration flux using Fick's Law:

$$J_3 = E_v D_e \frac{dC}{dZ} \quad (35) \qquad\qquad D_e = D_a \frac{\theta_a^{3.33}}{\theta_t^2} \quad (36)$$

where $\boldsymbol{J_3}$ is the flux loss from volatilization, $\boldsymbol{E_v}$ is a volatilization efficiency (see below); $\boldsymbol{D_e}$ is the effective air diffusion coefficient (36), $\boldsymbol{Z}$ is depth, $\boldsymbol{D_a}$ is the free-air diffusion coefficient, θ_a is the air-filled porosity, and θ_t is the total porosity (Millington-Quirk, 1959).

The change in vapor concentration is simply the range between the Raoult's derived concentration above the source LNAPL at any particular time in the volatilization and zero at ground surface. Notice that because of capillarity, the θ_a is not constant, but varies with vertical position in accordance with the change in liquid content. For the calculations here, the effective diffusion coefficient

is calculated across the interval of diffusion as a weighted series (37):

$$D_e^* = \frac{Z_t}{\sum_{i=1}^{n=100} Z_i / D_e} \quad (37)$$

The user also has the option of providing a volatilization efficiency factor (E_v) that varies from 0 to 1.0, with zero being no diffusive losses and 1.0 being maximum losses. The factor is included so that real world conditions limiting vapor flux can be considered, as appropriate. Such conditions may include asphalt and concrete covers, zones of high relative wetness, and/or zones of geologic contrast.

The total mass loss of any compound from the LNAPL zone is simply the time integral of the sum of the fluxes subtracted from the initial mass in the LNAPL zone at the start of the calculation:

$$Mass_t = Mass_{init} - \left[\int_0^t J_1 dt + \int_0^t J_2 dt + \int_0^t J_3 dt \right] \quad (38)$$

where ***Mass***$_t$ *is the mass of any compound in the LNAPL at any time* ***t****.*

As the component specific mass is depleted, its mole fraction in the remaining product is reduced, as is its effective solubility and volatility by equations (28 & 29). This ever diminishing flux controls the longevity and strength of the LNAPL source and by implication, the risk. In the calculation utility provided in the toolkit, the change in mass through time (source depletion) is calculated and updated at each timestep to define the concentration input into the Domenico transport equation.

Appendix B

DERIVATION OF LNAPL RECOVERY EQUATIONS

Charbeneau et al., 1999
API Publication 4682

This appendix presents the derivation of recovery equations for oil recovery under a variety of conditions. The equations are modified after Charbeneau (1999), which the reader is encouraged to review for clarification of principles and assumptions. The key assumptions needed to develop these equations are as follows:

1) VEQ conditions are approximated at all times;
2) The spatial variability of recovery is not significant within the phase radius of influence;
3) Pumping recovery can be approximated by steady-state conditions;
4) Multiple recovery wells are simply additive;
5) The oil saturation profile diminishes through time, but is distributed uniformly throughout the ROI at any given time;
6) Volumetric recovery is proportional to change in saturation and LNAPL thickness;
7) The effective transmissivity toward LNAPL is dependent on the vertical integral of the relative permeability function, which depends on the saturation distribution at any time during recovery (see Appendix A);
8) The maximum endpoint to recovery is the field oil capacity (residual oil);
9) There is no recovery at equivalent oil thicknesses less than the bubbling pressure for the oil/water system.

Equation Development

We will use a simple radial recovery system as our basis for developing the recovery approximation method. The principles will then be extended to trench recovery as an alternate geometry, and to vacuum enhanced recovery as a gradient improvement without chemical stripping. Figure B-1 illustrates a skimming or dual-pump recovery well where both LNAPL and water are coned down from their initial thicknesses b_{oi} and b_{wi}. The air phase is assumed to be static and flow of LNAPL and water is steady. The thickness of the LNAPL and water layers is equal to b_{oi} and b_{wi}, respectively, at a distance R from the well. The distance R, therefore, is the well's hydraulic radius of influence. The wellbore has a radius of r_w.

Under these assumed conditions, the Thiem equation (1906) and Dupuit assumptions (1863) can be used to describe the recovery of fluids (water and oil) under steady radial pumping.

$$(H_i^2 - H_w^2) = \frac{Q}{\pi K} ln \frac{r_i}{r_w} \qquad\qquad Q = \frac{\pi K(H_i^2 - H_w^2)}{\ln \frac{r_i}{r_w}}$$

*Where **Q** is the volumetric flow rate, **K** is the conductivity, $\mathbf{r}_1$ is the radius of influence, $\mathbf{r}_w$ is the well radius, and **H** is the head. This form of the Thiem equation can be re-written in terms of flow.*

Focusing for now on oil flow, we know that for a multiphase system the average effective oil conductivity depends on the oil saturation profile and resultant relative permeability (Appendix A). As oil is incrementally recovered, that volume can be subtracted from the volume in place to result in a new average saturation and conductivity profile (Figure B-1, showing initial and changing saturation profiles during recovery, with Tr = relative transmissivity to show change in bulk mobility).

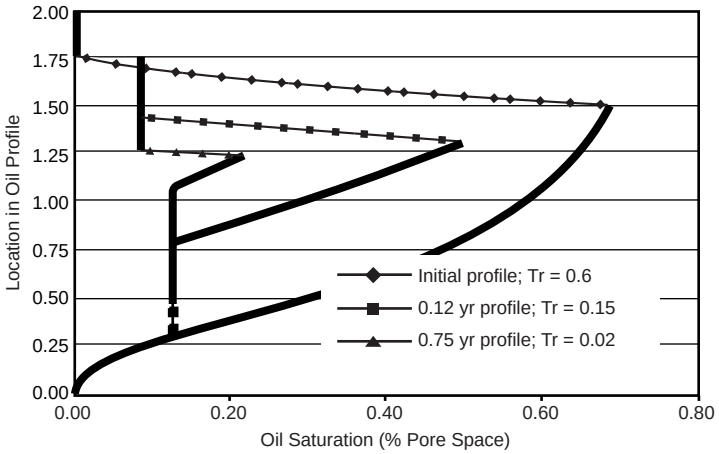

Figure B-1. Changes in LNAPL saturation profiles in response to continuing hydraulic recovery.

This principle can now be used to calculate the diminishing oil recovery through time. Each increment of recovery reduces the average conductivity, in turn diminishing the next increment of recovery. Note that the hydraulic conductivity toward water is scaled to the oil system by appropriate fluid properties.

I. Trench System

$$Q_o = W\, b_o\, \overline{k_{ro}}\, K_w\, \frac{r_{ro}}{\pi_{ro}}\, i$$

W = Width of trench (up to width of LNAPL source).
b_o = Thickness of LNAPL.
$\overline{k_{ro}}$ = Average relative permeability of LNAPL.
K_w = Water-saturated hydraulic conductivity of soil.

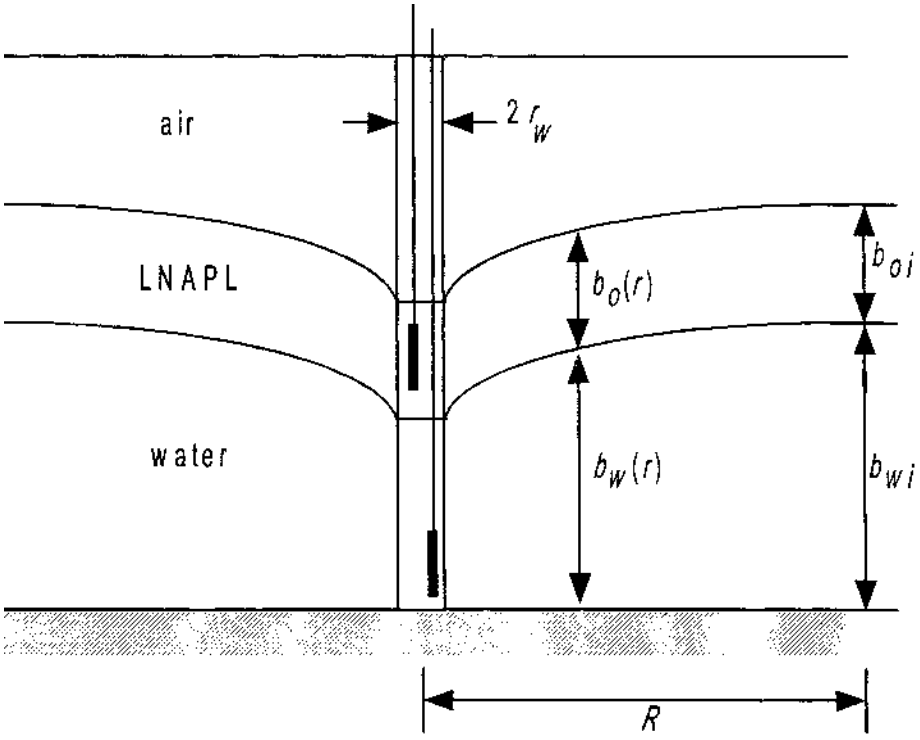

Figure B-2. Steady Incompressible Radial Flow of LNAPL and water to a Dual-Pumping Well in a Homogeneous Medium (after Charbeneau, 1999)

ρ_{ro} = Relative density of LNAPL.

μ_{ro} = Relative viscosity of LNAPL.

i = Gradient of LNAPL (assumed to be same as groundwater gradient).

The trench system assumes that lateral boundary effects can be ignored, and that flow is effectively 1-D for calculation purposes. All upgradient product will flow directly toward the recovery trench.

II. Skimmer well

$$Q_o = \frac{2\pi(1-\rho_{ro})\rho_{ro} b_o^2 K_w \overline{k_{ro}}}{\mu_{ro} \ln(r_i / r_w)}$$

r_i = Radius of influence of well.

r_w = Radius of well.

The skimmer well assumes that product drawdown is to the water piezometric surface. That is, all product from the well is removed to a "sheen", and the gradient is then this drawdown propagated across the radius of influence as defined by the Thiem equation.

III. Dual Pump/Total Fluids Recovery Well

$$Q_o = \frac{2\rho_{ro} b_o \overline{k_{ro}} Q_w}{\mu_{ro} b_w \left(1 + \sqrt{1 - \frac{Q_w}{\pi K_w b_w^2} ln \frac{r_i}{r_w}}\right)}$$

$$Q_w = \frac{(b_w^2 - h_{ow}^2)\pi K_w}{ln\left(R_w / r_w\right)}$$

Where $\mathbf{Q_o}$ *is oil production and* $\mathbf{Q_w}$ *is water.*

b_w = Distance from bottom of well screen to piezometric surface.
h_{ow} = Distance from bottom of well screen to oil-water interface.

IV. Vacuum Enhanced Skimmer Well

$$Q_o = \frac{2\pi(1-\rho_{ro})\rho_{ro} b_o^2 K_w \overline{k_{ro}}}{\mu_{ro} ln(r_i / r_w)} + \frac{\mu_a \rho_{ro} Q_a b_o \overline{k_{ro}}}{\mu_o k_{ra} L_a}$$

$$Q_a = \frac{s_a 2\pi L_a K_w k_{ra}}{\mu_{ra} ln\left(r_i / r_w\right)}$$

Where $\mathbf{Q_o}$ *is oil production, the first component equivalent to the skimmer well above, and the second component a gradient factor from the air flow component* $\boldsymbol{Q_a}$.

μ_{ra} = Relative viscosity of air.
L_a = Length of vacuum screen.
k_{ra} = Relative permeability of air phase.
s_a = Air drawdown (applied vacuum).

Lastly, for all the calculations above, an approximation derived by Charbeneau (1999) is used to simplify calculation of the relative permeability function.

$$\overline{k_{ro}} = \left(\overline{S_o}\right)^2 \qquad \left(\overline{S_o}\right) = \frac{V_o}{nb_o}$$

Where $\mathbf{S_o}$ is the average oil saturation calculated by the area volume ($\mathbf{V_o}$) divided by the porosity ($\mathbf{n}$) and oil thickness interval ($\mathbf{b_o}$)

IMPLEMENTATION

The equations above are implemented to act upon a user selected VEQ distribution of LNAPL. The time increments of calculation are selected such that no more than 25% of the oil in place is recovered during any single timestep. The recovered oil causes the saturation profile to move upward, leaving behind residual oil along the way (Figure B-1). Therefore, of the initial oil in place, some fraction (the area and vertical integral of the user selected residual oil) will be permanently unrecoverable. The time to reach asymptotic or residual state depends on the hydraulic conductivity of the soil, the gradient applied, and the average saturation of oil in place.

Given this and the simple form of the approximation, it is not surprising that all cleanup methods reach the same endpoint, residual saturation. The only difference between remediation techniques or the specifics of the setting is the time required to reach that endpoint. In practicality, complications of well field mechanics, interference, well operations, and hydraulic variability will result in slower cleanup times and greater variability in effectiveness than estimated by this method. These calculations are best-case and for screening purposes only.

Appendix C

SOIL, FLUID, AND CHEMICAL PROPERTIES FROM VARIOUS SOURCES

SOIL PROPERTIES

Source:

Charbeneau, Randall (1999). Free Product Recovery of Petroleum Hydrocarbon Liquids, prepared for American Petroleum Institute.

Table C-1. Typical Value of Hydraulic Conductivity (after Marsily, 1986).

Medium	***K* (cm/s)**
Unconsolidated Material	
Coarse gravel	10^{1} - 10^{0}
Sands and gravel	10^{0} - 10^{-3}
Fine sand, silt, and loess	10^{-3} - 10^{-7}
Clay, shale,and glacial till	10^{-7} - 10^{-11}
Unfractured Rock	
Dolomitic limestone	10^{-1} - 10^{-3}
Weathered chalk	10^{-1} - 10^{-3}
Unweathered chalk	10^{-4} - 10^{-7}
Limestone	10^{-3} - 10^{-7}
Sandstone	10^{-2} - 10^{-8}
Granite, gneiss, and basalt	10^{-7} - 10^{-11}

Table C-2. Hydraulic Conductivity of Different Soil Texture Classes from the Data Set of Carsel and Parish (1988).

mean (standard deviation)

	K_w	K_w
Soil Type	(cm/s)	(m/day)
Clay	5.56E-05	0.0048 (0.10)
Clay Loam	7.22E-05	0.062 (0.17)
Loam	2.89E-04	0.25 (0.44)
Loamy Sand	4.05E-03	3.5 (2.7)
Silt	6.94E-05	0.060 (0.079)
Silt Loam	1.25E-04	0.11 (0.30)
Silty Clay	5.56E-06	0.0048 (0.026)
Silty Clay Loam	1.94E-05	0.017 (0.046)
Sand	8.25E-03	7.1 (3.7)
Sandy Clay	3.33E-05	0.029 (0.067)
Sandy Clay Loam	3.64E-04	0.31 (0.66)
Sandy Loam	1.23E-03	1.1 (1.4)

Table C-3. Total Porosity of Natural Porous Media.

(Bear, 1972)			(Freeze and Cherry, 1978)	
Sedimentary Materials/ Soil Type	Porosity Value in %		Unconsolidated Deposits	Porosity Value in %
Peat Soils	60-80		Gravel	25-40
Soils	50-60		Sand	25-50
Clay	45-55		Silt	35-50
Silt	40-50		Clay	40-70
Medium to Coarse Mixed Sands	35-40		Rocks	
Uniform Sand	30-40		Fractured Basalt	5-50
Fine to Medium Mixed Sands	30-35		Karst Limestone	5-50
Gravel	30-40		Sandstone	5-30
Gravel and Sand	30-35		Limestone Dolomite	0-20
Sandstone	10-20		Shale	0-10
Shale	1-10		Fractured Crystalline Rock	0-10
Limestone	1-10		Dense Crystalline Rock	0-5

Table C-4. Average Porosity (Standard Deviation) Values Based on Soil Texture.

	Porosity
Soil Type	(*n*)
Clay	0.38 (0.09)
Clay Loam	0.41 (0.09)
Loam	0.43 (0.10)
Loamy Sand	0.41 (0.09)
Silt	0.46 (0.11)
Silt Loam	0.45 (0.08)
Silty Clay	0.36 (0.07)
Silty Clay Loam	0.43 (0.07)
Sand	0.43 (0.06)
Sandy Clay	0.38 (0.05)
Sandy Clay Loam	0.39 (0.07)
Sandy Loam	0.41 (0.09)

Table C-5. Descriptive Statistics from Carsel & Parrish (1988) Data Set Tabulated Values: Mean (Standard Deviation).

Soil Type	Residual Saturation, S_{wr}	Bubbling Pressure Head, Ψ_b	Pore Size Distribution Index, λ
Clay	0.18 (0.089)	1.25 (1.88)	0.09 (0.09)
Clay Loam	0.23 (0.024)	0.53 (0.42)	0.31 (0.09)
Loam	0.18 (0.030)	0.28 (0.16)	0.56 (0.11)
Loamy Sand	0.14 (0.037)	0.081 (0.028)	1.28 (0.27)
Silt	0.074 (0.022)	0.62 (0.27)	0.37 (0.05)
Silty Loam	0.15 (0.033)	0.50 (0.30)	0.41 (0.12)
Silty Clay	0.19 (0.064)	2.0 (2.0)	0.09 (0.06)
Silty Clay Loam	0.21 (0.021)	1.0 (0.6)	0.23 (0.06)
Sand	0.10 (0.023)	0.069 (0.014)	1.68 (0.29)
Sandy Clay	0.26 (0.034)	0.37 (0.23)	0.23 (0.19)
Sandy Clay Loam	0.26 (0.015)	0.17 (0.11)	0.48 (0.13)
Sandy Loam	0.16 (0.041)	0.13 (0.066)	0.89 (0.17)

* Carsel and Parrish (1998) report mean and standard deviation of van Genuchten's 'α' parameter. Using Eq. (3.4.6) and a first-order expansion, the standard deviation of Ψ_b is approximated by.

$$\sigma \Psi_b \cong \frac{\sigma_\alpha}{\alpha^{-2}}$$

Table C-6. Brooks and Corey Soil Parameters from Carsel and Parrish (1988)
Example Values Converted to van Genuchten Capillary Parameters in LNAST Utility.

Soil Texture	Porosity n	Irreducible Water Saturation, S_{wr}	Displacement Pressure Head (m) Ψ_{baw}	Pore Size Distribution Index λ
Sand	0.43	0.105	0.045	1.13
Loamy Sand	0.41	0.139	0.051	0.908
Sandy Loam	0.41	0.159	0.083	0.685
Sandy Clay Loam	0.39	0.256	0.114	0.423
Loam	0.43	0.181	0.181	0.479
Sandy Clay	0.38	0.263	0.317	0.224
Silt Loam	0.45	0.149	0.353	0.372
Clay Loam	0.41	0.232	0.407	0.293
Silt	0.46	0.074	0.455	0.341
Silty Clay Loam	0.43	0.207	0.855	0.225
Clay	0.38	0.179	1.244	0.09
Silty Clay	0.36	0.194	1.990	0.09

LNAPL PHYSICAL PROPERTIES

Source:

Charbeneau, Randall (1997). Free Product Recovery of Petroleum Hydrocarbon Liquids, prepared for American Petroleum Institute.

Table C-7. Representative LNAPL Density Values (gm/cm^3).

Fluid Type	Temp. 0ºC	Source	Temp. 15ºC	Source	Temp. 20ºC	Source	Temp. 25ºC	Source
Water	1.000	C	0.998	C	0.998	C	0.996	C
Automotive Gasoline	0.746	A	0.729	A				
Automotive Diesel	0.838	A	0.827	A				
Kerosene	0.842	A	0.839	A			0.835	A
Jet Fuel (JP-3)			0.844	A	0.800	B		
Jet Fuel (JP-5)					0.820	B		
Fuel Oil #2	0.874	A	0.866	A	0.840	A		
Fuel Oil #4	0.914	A	0.904	A	0.900	B	0.898	A
Fuel Oil #5	0.932	A	0.923	A			0.917	A
Fuel Oil #6 or Bunker C	0.986	A	0.974	A			0.964	A
Electrical Lubricating Oil	0.882	A	0.974	A				
Electrical Lubricating Oil-used	0.883	A	0.874	A				
Electrical Insulating Oil	0.892	A	0.882	A				
Electrical Insulating Oil-used	0.878	A	0.867	A				
Norman Wells Crude	0.845	A	0.832	A			0.829	A
Avalon Crude	0.846	A	0.839	A			0.834	A
Alberta Crude	0.850	A	0.840	A			0.832	A
Transmountain Blend Crude	0.865	A	0.855	A				
Bow River Blend Crude	0.900	A	0.893	A			0.885	A
Prudhoe Bay Crude	0.915	A	0.905	A			0.900	A
Atkinson Crude	0.922	A	0.911	A			0.905	A
La Rosa Crude	0.923	A	0.914	A			0.908	A

Source: A-API, 1996; B-Mercer and Cohen, 1990; C-Vennard and Street, 1982.

Table C-8. Interfacial and Surface Tension (dynes/cm) at 20°C.

Chemical Name	Interfacial Tension	Surface Tension
Benzene	35	28.9
Ethylbenzene	35.5	29.3
Toulene	36.1	28.5
o-Xylene	36.1	30.3
Crude Oil	no data	24-38
Diesel Fuel	50	25
Gasoline	50	21
Naptha (BTX mixture)	45	20
Fuel Oil No. 1	48	27
Jet Fuel JP-4/5	50	25
Petroleum Distillates	50	21

Source: Mercer and Cohen (1990)

Note: Field experience strongly suggests that the oil/water interfacial tension is often much smaller than the laboratory based values in the table. Lower oil/water IFT implies a greater LNAPL saturation for the same capillary head condition. Since the IFT is used to scale exponential capillary parameters, it is suggested that literature values be used with caution. Measurements based on field samples is always preferred.

Table C-9. Representative Dynamic Viscosity Values (centipoise).

Fluid Type	Temp. 0 °C	Source	Temp. 15 °C	Source	Temp. 20 °C	Source	Temp. 25°C	Source
Water	1.79	B	1.14	B	1.00	B	0.89	B
Automotive Gasoline	0.75	A	0.62	A				
Automotive Diesel	3.90	A	2.70	A				
Kerosene	3.40	A	2.30	A			2.20	A
Jet Fuel (JP-3)								
Jet Fuel (JP-5)								
Fuel Oil #2	7.74	A			4.04	A		
Fuel Oil #4			47.2	A	22.7	A		
Fuel Oil #5			215	A			122	A
Fuel Oil #6 or Bunker C	7.0E+07	A					3180	A
Electrical Lubricating Oil	350	A	144	A				
Electrical Insulating Oil	37.8	A	18.8	A				
Norman Wells Crude	8.76	A	5.05	A			3.93	A
Avalon Crude	575	A	11.4	A			25.6	A
Alberta Crude	17.6	A	6.43	A			4.22	A
Transmountain Blend Crude	650	A	10.5	A				
Bow River Blend Crude	88.4	A	33.7	A			23.7	A
Prudhoe Bay Crude	577	A	68.4	A			35.3	A
Atkinson Crude	136	A	57.3	A			35	A
La Rosa Crude	640	A	180	A			104	A

Source: A-API, 1996; B-Vennard and Street, 1982.

LNAPL CHEMICAL PROPERTIES

Source:

American Petroleum Institute (1994). *Transport and Fate of Non-BTEX Petroleum Chemicals in Soils and Groundwater*, Health and Sciences Department, API Publication Number 4593, Washington, DC.

Table C-10. Concentrations of normal, branched, and cyclic alkanes in U.S. crude oils. Concentrations are in mg/l. From Speight (1991) (Page 1 of 2).

Compound	Ponca	n-Alkane Isoalkane	Santa Barbara	n-Alkane Isoalkane
Hexanes		2.2		0.76
n-hexane	18,000		7,230	
2-methylpentane	4,000		3,470	
3-methylpentane	3,000		4,180	
2,2-dimethylbutane	400		430	
2,3-dimethylbutane	800		1,400	
Heptanes		1.7		1.01
n-heptane	23,000		8,460	
3-methylhexane	5,000		1,880	
3-ethylpentane	500		--	
2-methylhexane	7,000		--	
2,3-dimethylpentane	1,000		6,010	
2,4-dimethylpentane	--		490	
Octanes		6.9		2.5
n-Octane	19,000		9,230	
2-methylheptane	--		--	
2,2-dimethylhexane	100		1,180	
2,3-dimethylhexane	600		1,630	
2,4-simethylhexane	600		--	
2,5-dimethylhexane	600		950	
3,3-dimethylhexane	300		--	
2-methyl-3-ethylpentane	400		--	
2,2,3-trimethylpentane	40		--	
2,3,3-trimethylpentane	60		--	
2,3,4-trimethylpentane	50		--	
Nonanes		2.6		0.87
n-nonane	18,000		5,800	
2-methyloctane	4,000		--	
3-methyloctane	1,000		4,200	
4-methyloctane	1,000		--	
2,3-dimethylheptane	500		--	

Table C-10. Concentrations of normal, branched, and cyclic alkanes in U.S. crude oils. Concentrations are in mg/l. From Speight (1991). (Page 2 of 2).

Compound	Ponca	Santa Barbara
Higher n-paraffins		
n-decane	18,000	--
n-undecane	17,000	--
n-dodecane	17,000	--
Cycloparaffins		
cyclopentane	500	460
methylcyclopentane	9,000	3,030
cyclohexane	7,000	--
ethylcyclopentane	2,000	1,860
1,1-dimethylcyclopentane	2,000	630
1-t-2-dimethylcyclopentane	5,000	1,540
1-c-3-dimethylcyclopentane	2,000	--
1-t-3-dimethylcyclopentane	9,000	2,380
propylcyclopentane	--	--
ethylcyclohexane	2,000	--
1-t-2-dimethylcyclohexane	--	2,640
1-c-3-dimethylcyclohexane	--	--
1,1,3-trimethylcyclopentane	3,000	--
1-t-2-c-trimethylcyclopentane	3,000	3,600
1-t-2-c-4-trimethylcyclopentane	2,000	--
1,1,2-trimethylcyclopentane	600	--
1,1,3-trimethylcyclopentane	2,000	--
1-t-2-t-4-trimethylcyclohexane	2,000	--

Table C-11. Concentrations of benzenes and naphthalenes in U.S. crude oils. Concentrations are in mg/kg. From Speight (1991).

Compound	Ponca	Santa Barbara	East Texas	Bradford	Greendale	Winkler	Midway	Conroe
benzene	2,000	2,210	700	600	2,100	400	700	4,100
toluene	5,000	7,780	5,800	5,100	5,900	900	4,300	24,600
ethylbenzene	2,000	2,090	2,200	900	1,200	800	2,200	3,100
o-xylene	3,000	2,900	3,000	2,100	1,700	300	3,100	6,800
m-xylene	5,000	--	6,400	6,100	4,000	800	3,600	20,300
p-xylene	1,000	6,800	1,700	1,700	900	1,200	1,500	5,900
n-propylbenzene	900	2,600	800	500	300	200	400	1,200
isopropylbenzene	700	600	400	300	300	300	300	900
1-methyl-2-ethylbenzene	900	--	700	300	400	100	300	900
1-methyl-3-ethylbenzene	1,700	--	1,600	1,300	800	100	400	4,000
1-methyl-4-ethylbenzene	600	--	700	500	300	500	300	1,300
1,2,3-trimethylbenzene	1,000	--	--	--	--	--	--	--
1,2,4-trimethylbenzene	5,100	--	3,400	3,300	1,500	1,300	1,300	6,900
1,3,5-trimethylbenzene	1,200	1,800	900	1,700	500	500	500	3,600
t-butylbenzene	100	--	100	20	30	20	0	100
1,2,3,4-tetramethylbenzene	2,000							
tetrahydronaphthalene	300							
naphthalene	600							
1-methylnaphthalene	1,000							
2-methylnaphthalene	2,000							
5-methyltetrahydronaphthalene	800							
6-methyltetrahydronaphthalene	900							

Table C-12. Concentrations of aromatic hydrocarbons in crude oils. Concentrations are in mg/kg. (Page 1 of 2).

Compound	S.Louisiana[1]	Kuwait[1]	Prudhoe Bay[2]	North Slope[3]	VMI Crude[4]	Wyoming Crude[5]
C_3-C_6 benzenes						8,100
tetralins						2,400
toluene			820			
ethylbenzene			560			
xylenes			2,840			
trimethylbenzenes			2,140			
indane			670			nd
C_2-C_4 indanes						800
tetramethylbenzenes			1,400			
naphthalene			920	210	326	900
C_1-C_3 naphthalenes						17,500
methylnaphthalenes			4,300	770	1,663	
dimethlynaphthalenes			3,980	1,400	3,142	
trimethylnaphthalenes			510	870	1,899	
tetramethylnaphthalenes				500	994	
biphenyl				63		400
C_1-C_3 biphenyls						2,200
fluorene				30	72	600
C_1-C_2 fluorenes						1,000
methylfluorenes				110	264	
dimethylfluorenes				160	435	
trimethylfluorenes				190	389	
phenanthrene	70	26	380	91	189	500
C_1-C_2 phenanthrenes						700
methylphenanthrenes	255	89	540	460	635	
dimethylphenanthrenes			110	790	825	
trimethylphenanthrenes				540	631	
tetramethylphenanthrenes				280	217	
dibenzothiophene				80	271	
methyldibenzothiophenes				150	849	
dimethyldibenzothiophenes				220	732	
trimethyldibenzothiophenes				190	888	
tetramethyldibenzothiophenes					309	
fluoranthene	5.0	2.9		nd	3.0	
pyrene	3.5	4.5		3.4	4.0	
methylfluoranthenes/ pyrenes				46	35	
benz(a)anthracene	1.7	2.3		nd	2.0	

Table C-12. Concentrations of aromatic hydrocarbons in crude oils. Concentrations are in mg/kg. (Page 2 of 2).

Compound	S.Louisiana[1]	Kuwait[1]	Prudhoe Bay[2]	North Slope[3]	VMI Crude[4]	Wyoming Crude[5]
methyl/dimethyl-benzanthracene					nd	
chrysene	18	6.9		16	14	
methylchrysenes				23	26	
dimethylchrysenes				32	47	
trimethylchrysenes				30		
triphenylene	10	2.8				
benzofluoranthenes	1.0	<1.0		2.0		
benzo(a)pyrene	0.75	2.8		nd		
benzo(e)pyrene	2.5	0.5		4.9		
perylene	34.8	<0.1		nd		
benzo(ghi)perylene	1.6	<1.0		nd		

(1) Pancirov and Brown, 1975
(2) Riley et al., 1981
(3) A.D. Little, 1991
(4) Burns et al., 1991
(5) Woodward et al., 1981

Table C-13. Concentrations of alkylbenzenes, selected polycyclic aromatic hydrocarbons, and dibenzothiophenes in crude oils. Concentrations are in mg/kg.

Compound	Alberta Sweet[1]	Mega Borg[2]	Handil Crudes[3]
alkylbenzenes		600	
naphthalene	382		
methylnaphthalenes		1092	4860
ethylnaphthalenes			960
dimethylnaphthalenes		1428	9480
trimethylnaphthalenes		924	5100
tetramethylnaphthalenes	336		
acenaphthylene	13		
acenaphthene	57		
fluorene	59	66	
methylfluorenes	150	150	
dimethylfluorenes		228	
trimethylfluorenes		156	
phenanthrene	150	252	258
methylphenanthrenes	370	420	578
dimethylphenanthrenes	500	304	372
trimethylphenanthrenes		63	
dibenzothiophene		63	
methyldibenzothiophenes	143		
dimethyldibenzothiophenes		155	
trimethyldibenzothiophenes		63	
anthracene	11		
fluoranthene	6.0		
pyrene	17		
methylpyrene	39		
chrysene	30		
benzo(b)fluoranthene	4.0		
benzo(e)pyrene	5.0		
benzo(a)pyrene	nd		
methylcholanthrene	3.0		

(1) Benner et al., 1990
(2) Fawn and Barker, 1991
(3) Radke et al., 1990

Table C-14. Concentrations of PAH and heterocyclic compounds in a sample of Qatar crude oil. Concentrations are mg/kg. Numbers in parentheses are number of isomers quantified. From Grimmer et al. (1983).

Aromatics		Heterocyclics	
Compound	**Concentration**	**Compound**	**Concentration**
phenanthrene	>128.7	dibenzothiophene	>336.5
3-methylphenanthrene	>17.2	4-methyldibenzothiophene	>6.7
2-methylphenanthrene	>12.7	2-methyldibenzotheophene	>21.4
9-methylphenanthrene	>33.4	3-methyldibenzothiophene	>0.2
1-methylphenanthrene	>20.9	1-methyldibenzothiophene	>0.6
1-phenylnaphthalene	>0.1	C_2-carbazoles (6)	>2.7
fluoranthene	1.7	dimethdibenzotheophene	>3.5
pyrene	10.7	dimethylxanthene	>0.4
benzo(a)fluorene	10.8	C_3-carbazoles (8)	36.5
benzo(b&c)fluorenes	6.2	C_4-carbazoles (8)	56.5
4-methylpyrene	11.6	C_5-carbazoles (9)	49.8
1-methylpyrene	22.9	methylphenanthrothiophene	2.2
benzo(c)phenanthrene	0.4	C_6-carbazoles (9)	45.3
benz(a)anthracene	6.7	benzonaphthothiophene	122.3
chrysene/triphenyline	43.5	methylbenzonaphthothiophenes	200.4
3-methylchrysene	43.9	dimethylbenzonaphthothiophenes	9.8
2-methylchrysene	24.5	methylfuran derivatives (3)	13.6
4-/6-methylchrysene	15.6	thiophene derivative	39.2
other methylchrysenes (3)	27.6	triphenylene (4,4a,4b,5-bcd)-thiophene	6.2
dimethylchrysenes (8)	82.9	methylthiophene derivatives (9)	107.7
benzo(b&j)fluoranthenes	7.4	thiophene derivative	11.0
benzo(k)fluoranthene	15.9	methylfuran derivative	1.2
benzo(e)pyrene	28.9	methylthiophene derivatives (10)	30.7
benzo(a)pyrene	3.6	dithiophene derivatives (9)	13.7
methylbenzofluoranthenes (7)	58.0	sulfur-substituted PAHs (2)	6.3
dimethylbenzofluoranthenes (12)	27.2	methylfuran derivative	11.9
indeno(1,2,3-cd)pyrene	7.4	methylated sulfur-substituted PAHs (4)	13.7
benzo(ghi)perylene	5.0		
methylpicines (2)	6.4		
methylindeno(1,2,3-cd) pyrenes (2)	4.5		
coronene	0.3		

Table C-15. Concentrations of sulfur-substituted alkanes in Wasson, Texas crude oil. Concentrations are in mg/l. From Speight (1991).

Compound	Wasson Crude
methanethiol	24
ethanethiol	53
2-thiapropane	8.8
2-propanethiol	19.9
2-methyl-2-propanethiol	5.5
2-thiabutane	22.2
1-propanethiol	4.1
3-methyl-2-thiabutane	6.4
2-butanethiol	38.6
2-methyl-1-propanethiol	0.3
3-thiapentane	7.5
2-thaipentane	3.0
1-butanethiol	trace
2-methyl-2-butanethiol	6.4
2-pentanethiol	14.0
3-pentanethiol	5.7
3-thiahexane	1.2
2,4-dimethyl-3-thiapentane	5.3
2,2-dimethyl-3-thiapentane	0.58
thiacyclopentane	0.77
2-thiahexane	0.77
2-methyl-3-thiahexane	0.78
2-methylthiacyclopentane	23
4-methyl-3-thiahexane	5.0
3-methyltiacyclopentane	4.6
2-hexanethiol	28
thiacyclohexane	3.2
t-2,2-dimethylthiacyclopentane	25
c-2,5-dimethylthiacyclopentane	24
3-thiapentane	0.78
2-methylthiacyclohexane	29
3-methylthiacyclohexane	0.24
4-methylthiacyclohexane	0.48
cyclohexanethiol	12

Table C-16. Variability in the concentrations of major aromatic components of 31 samples of leaded and unleaded gasoline from north and central Florida. From Cline et al. (1991).

Compound	Concentration (wt%)			
	Mean	Minimum	Maximum	Standard Deviation
benzene	1.73	0.7	3.8	0.68
toluene	9.51	4.5	21.0	3.59
ethylbenzene	1.61	0.7	2.8	0.48
m-,p-xylenes	5.95	3.7	14.5	2.07
o-xylene	2.33	1.1	3.7	0.72
n-propylbenzene	0.57	0.13	0.85	0.14
3,4-ethyltoluene	2.20	1.5	3.2	0.40
1,2,3-trimethylbenzene	0.8	0.6	1.1	0.12

Table C-17. Concentrations of alkanes, olefins, aromatic hydrocarbons, and additives in gasolines. Concentrations in volume or weight percent, except as indicated. (Page 1 of 3).

Compound	PS-6[1]	Unleaded[2]	Leaded[2]	1974 Gasoline[3]	IARC[4]	36-117 US Cut[5]
n-alkanes						
butane	3.83	4-5	4-5		3-12	
pentane	3.11	2.6-2.7	2.6-2.7		1-9	
hexane	1.58				<1-6	
C_7-C_{10}-n-alkanes	1.21				<1-5	
Isoalkanes						
isobutane	1.14					
isopentane	8.72	9-11	9-11		5-10	
methhylpentanes	6.29				4-19	
2,3-dimethylbutane	1.66				<1-2	
C_6-isoalkanes	0.18					
dimethylpentane					<1-7	
methylhexanes	2.38					
dimethylhexanes	2.16					
C_7-isoalkanes	0.23					
trimethylpentanes	11.74				<1-14	
C_8-isoalkanes	4.98					
methyloctanes	1.51					
C_9-isoalkanes	0.50					
C_{10}-C_{13}-isoalkanes	2.65					
Cycloalkanes						
cyclopentane	0.15					1.13
methylcyclopentane	0.97				<1-3	7.27
ethylcyclopentane						2.92
trimethylcyclopentane						5.31
cyclohexane	0.08				<1-3	8.39
dimethylcyclopentane	0.77					
methylcyclohexane					<1-7	18.2
C_7-cycloalkanes	0.32					
C_8-cycloalkanes	0.74					
C_9-cycloalkanes	1.03					
C_{10}-C_{13}-cycloalkanes	0.62					

Table C-18. Concentrations of alkanes, olefins, aromatic hydrocarbons, and additives in gasolines. Concentrations in volume or weight percent, except as indicated. (Page 2 of 3).

Compound	PS-6[1]	Unleaded[2]	Leaded[2]	1974 Gasoline[3]	IARC[4]	36-117 US Cut[5]
Mono-olefins		5	10			
propylene	0.03					
butene	0.75					
C_4-alkenes	0.15					
methylbutenes					<1-4	
pentenes	1.22				<1-2	
C_5-alkenes	0.07					
C_6-alkenes	0.14					
methylpentenes	1.26					
C_7-C_{12}-alkenes	5.34					
Aromatics						
benzene	1.94	0.7-3.8	2-5		<1-4	3.03
toluene	4.73	4.5-21	6-7		5-22	12.05
ethylbenzene	2.00	0.7-2.8	5		<1-2	
o-xylene	2.27	1.1-3.7			1-10	
m-xylene	5.66	3.7-14.5				
p-xylene	1.72	"				
n-propylbenzene		0.13-0.85				
methylethylbenzenes	3.10	1.5-3.2			<1-2	
trimethylbenzene	3.26	0.6-1.1				
C_9-alkylbenzenes	2.51					
C_{10}-alkylbenzenes	2.21					
C_{11}-alkylbenzenes	0.57					
C_{12}-alkylbenzenes	0.21					
C_9-C_{13}-indans/ tetralins	1.59					
naphthalene		0.2-0.5	0.2-0.5			
C_{10}-C_{12}-naphthalenes	0.74					
anthracene		1.8 mg/l	1.8 mg/l			
fluoranthene				6.5 mg/l		
pyrene				4.4 mg/l		
benz(a)anthracene				4.3 mg/l		
chrysene				2.0 mg/l		
benzo(b)fluoranthene		3.9 mg/l	3.9 mg/l			
benzo(e)pyrene			0.8 mg/l			

Table C-18. Concentrations of alkanes, olefins, aromatic hydrocarbons, and additives in gasolines. Concentrations in volume or weight percent, except as indicated. (Page 3 of 3).

Compound	PS-6[1]	Unleaded[2]	Leaded[2]	1974 Gasoline[3]	IARC[4]	36-117 US Cut[5]
Aromatics (continued)						
benzo(a)pyrene				1.8 mg/l		
benzo(ghi)perylene				2.2 mg/l		
coronene				1.1 mg/l		
Nonhydrocarbons						
tetraethyllead			600 mg/l			
tetramethyllead		5 mg/l				
dichloroethane		210 mg/l				
dibromomethane			190 mg/l			
methyl *tert*butyl ether		to 15%			<1-4	

(1) Barker et al., 1991
(2) Cline et al., 1991
(3) Guerin, 1977
(4) IARC, 1989
(5) Nyer and Skladany, 1989

Table C-19. Variability in composition of gasolines from Houston, TX area in 1984. Concentrations are weight percent. From Diakun (1984). (Page 1 of 2).

Compound	Regular Blend	Lead-Free Blend	Super Unleaded	API Generic
Alkanes				
propane	0.10	0.04	0.04	0.07
iso-butane	0.59	0.77	0.90	0.75
n-butane	4.31	4.41	3.42	4.50
iso-pentane	7.77	10.13	8.02	9.25
n-pentane	5.05	5.09	1.94	4.91
2,2-dimethylbutane	0.61	0.41	0.10	0.48
cyclopentane	0.87	0.52	0.18	0.66
2,3-dimethylbutane	1.18	1.04	0.92	1.14
MTBE*	0.12	0.25	2.02	0.42
2-methylpentane	5.44	3.97	2.01	4.59
3-methylpentane	3.52	2.44	1.22	2.90
n-heptane	3.91	1.92	0.72	2.79
methylcyclopentane	2.10	1.48	0.82	1.74
2,2-dimethylpentane	0.52	0.56	0.72	0.59
cyclohexane	0.44	0.17	0.07	0.29
2-methylhexane	2.59	2.12	1.58	2.34
2,3-dimethylpentane	0.06	0.04	0.06	0.05
3-methylhexane	2.07	1.57	0.94	1.77
1-cis-3-dimethylcyclopentane	0.39	0.34	0.21	0.36
1-trans-3-dimethylcyclopentane	0.34	0.30	0.18	0.32
3-ethylpentane	0.54	0.40	0.25	0.46
2,2,4-trimethylpentane	1.21	2.43	5.02	2.26
n-heptane	1.42	0.91	0.51	1.12
methylcyclohexane	0.91	0.70	0.43	0.77
ethylcyclopentane	0.22	0.20	0.12	0.21
2,5-dimethylhexane	0.43	0.60	0.98	0.58
2,4-dimethylhexane	0.37	0.45	0.64	0.45
3,3-dimethylhexane	0.57	1.08	1.98	1.06
2,3-dimethylhexane	0.34	0.35	0.53	0.36
2-methylheptane	0.67	0.57	0.45	0.60
3-methylheptane	0.74	0.66	0.49	0.67
2,2,5-trimethylhexane	0.28	0.37	0.67	0.37
n-octane	0.62	0.49	0.41	0.54
n-nonane	0.36	0.22	0.17	0.28
n-decane	0.24	0.14	0.09	0.17
n-undecane	0.34	0.32	0.30	0.32
n-dodecane	0.19	0.12	0.07	0.13
C_{11}-C_{12}	3.21	2.38	1.97	2.13
C_{12} plus	1.21	2.12	1.37	0.92

Table C-19. Variability in composition of gasolines from Houston, TX area in 1984. Concentrations are weight percent. From Diakun (1984). (Page 2 of 2).

Compound	Regular Blend	Lead-Free Blend	Super Unleaded	API Generic
Olefins				
propylene	0.01	0.01	0.02	0.01
isobutylene	0.10	0.10	0.11	0.11
1-butene	0.14	0.20	0.27	0.19
trans-2-butene	0.28	0.38	0.45	0.37
cis-2-butene	0.28	0.35	0.39	0.34
3-methyl-1-butene	0.11	0.13	0.10	0.12
1-pentene	0.40	0.44	0.33	0.43
2-methyl-1-butene	0.63	0.75	0.58	0.71
isoprene	0.03	0.03	0.03	0.03
trans-2-pentene	0.98	1.05	0.90	1.05
cis-2-pentene	0.50	0.52	0.44	0.52
2-methyl-2-butene	1.14	1.19	1.06	1.21
trans-1,3-pentadiene	0.04	0.04	0.03	0.04
cyctopentadiene	0.02	0.02	0.03	0.02
cis-1,3-pentadiene	0.02	0.02	0.01	0.02
cyclopentene	0.21	0.21	0.24	0.22
3-methyl-1-pentene	0.12	0.12	0.09	0.12
4-methyl-2-pentene	0.13	0.12	0.10	0.13
2-methyl-1-pentene	0.23	0.21	0.17	0.22
1-hexene	0.16	0.15	0.11	0.15
C_6-olefins	1.85	1.67	1.68	1.84
1-methylcyclopentene	0.14	0.09	0.05	0.11
1-octene	0.14	0.12	0.08	0.12
1-nonene	0.04	0.09	0.01	0.10
1-decene	0.03	--	0.01	0.01
1-undecene	--	0.02	0.01	--
1-dodecene	0.22	0.13	0.10	0.14
Aromatics				
benzene	1.80	1.92	1.42	1.79
toluene	5.46	7.77	15.87	7.92
ethylbenzene	1.52	1.96	2.45	1.83
p- and m-xylenes	4.45	5.82	7.18	5.38
o-xylene	1.68	2.23	2.82	2.06
isopropylbenzene	0.16	0.18	0.27	0.17
n-propylbenzene	0.51	0.64	0.75	0.61
1-methyl-3-ethylbenzene	1.93	2.19	2.36	2.05

Table C-20. Typical hydrocarbon composition of three grades of jet fuel. Concentrations are in weight percent. From Smith et al., (1981). (Page 1 of 3).

Compound	JP-4	JP-5	JP-8
n-alkanes			
butane	0.12	--	--
pentane	1.06	--	--
hexane	2.21	--	--
heptane	3.67	--	0.03
octane	3.80	0.12	0.09
nonane	2.25	0.38	0.31
decane	2.16	1.79	1.31
undecane	2.32	3.95	4.13
dodecane	2.00	3.94	4.72
tridecane	1.52	3.45	4.43
tetradecane	0.73	2.72	2.99
pentadecane	--	1.67	1.61
hexadecane	--	1.07	0.45
heptadecane	--	0.12	0.08
octadecane	--	--	0.02
isoalkanes			
isobutane	0.66	--	--
2,2-dimethylbutane	0.10	--	--
2-methylpentane	1.28	--	--
3-methylpentane	0.89	--	--
2,2-dimethylpentane	0.25	--	--
2-methylhexane	2.35	--	--
3-methylhexane	1.97	--	--
2,2,3,3-tetramethylbutane	0.24	--	--
2,5-dimethylhexane	0.37	--	--
2,4-dimethylhexane	0.58	--	--
3,3-dimethylhexane	0.26	--	--
2,2-dimethylhexane	0.71	--	--
2-methylheptane	2.70	--	--
4-methylheptane	0.92	--	--
3-methylheptane	3.04	--	--
2,5-dimethylheptane	0.52	--	--
2,4-dimethylheptane	0.43	--	--
4-ethylheptane	0.18	--	--
4-methyloctane	0.86	--	--
2-methyloctane	0.88	--	--

Table C-20. Typical hydrocarbon composition of three grades of jet fuel. Concentrations are in weight percent. From Smith et al., (1981). (Page 2 of 3).

Compound	JP-4	JP-5	JP-8
isoalkanes, continued			
3-methyloctane	0.79	0.07	0.04
2-methylundecane	0.64	--	--
2,6-dimethylundecane	0.71	--	--
2,4,6-trimethylheptane	--	0.07	0.07
4-methyldecane	--	0.78	--
2-methyldecane	--	0.61	0.41
2,6-dimethyldecane	--	0.72	0.66
2-methylundecane	--	1.39	1.16
2,6-dimethylundecane	--	2.00	2.06
cycloparaffins			
methylcyclopentane	1.16	--	--
cyclohexane	1.24	--	--
t-1,3-dimethylcyclopentane	0.36	--	--
c-1,3-dimethylcyclopentane	0.34	--	--
c-1,2-dimethylcyclopentane	0.54	--	--
methylcyclohexane	2.27	--	--
ethylcyclopentane	0.26	--	--
1,2,4-trimethylcyclopentane	0.25	--	--
1,2,3-trimethylcyclopentane	0.25	--	--
c-1,3-dimethylcyclohexane	0.42	--	--
1-methyl-3-ethylcyclohexane	0.17	--	--
1-methyl-2-ethylcyclohexane	0.39	--	--
dimethylcyclohexane	0.43	--	--
1,3,5-trimethylcyclohexane	0.99	0.09	0.06
1,1,3-trimethylcyclohexane	0.48	0.05	0.06
1-methyl-4-ethylcyclohexane	0.48	--	0.10
n-butylcyclohexane	0.70	0.90	0.74
propylcyclohexane	--	--	0.14
hexylcyclohexane	--	--	0.93
heptylcyclohexane	--	0.99	1.00
aromatic hydrocarbons			
benzene	0.50	--	--
toluene	1.33	--	--
ethylbenzene	0.37	--	--

Table C-20. Typical hydrocarbon composition of three grades of jet fuel. Concentrations are in weight percent. From Smith et al., (1981). (Page 3 of 3).

Compound	JP-4	JP-5	JP-8
aromatic hydrocarbons, continued			
m-xylene	0.96	0.13	0.06
p-xylene	0.35	--	--
o-xylene	1.01	0.09	0.06
isopropylbenzene	0.30	--	--
n-propylbenzene	0.71	--	--
1-methyl-3-ethylbenzene	0.49	--	--
1-methyl-4-ethylbenzene	0.43	--	--
1,3,5-trimethylbenzene	0.42	--	--
1-methyl-2-ethylbenzene	0.23	--	--
1,2,4-trimethylbenzene	1.01	0.37	0.27
1,3-diethylbenzene	0.46	0.61	--
1,4-diethylbenzene	--	0.77	--
1-methyl-4-propylbenzene	0.40	--	--
1,3-dimethyl-5-ethylbenzene	0.61	--	0.62
1-methyl-2-isopropylbenzene	0.29	--	0.56
1,4-dimethyl-2-ethylbenzene	0.70	--	--
1,2-dimethyl-4-ethylbenzene	0.77	--	--
1,2,3,4-titramethylbenzene	0.75	1.48	1.12
1-ethylpropylbenzene	--	1.16	0.99
1,2,4-triethylbenzene	--	0.72	0.99
1,3,5-triethylbenzene	--	--	0.60
phenylcyclohexane	--	0.82	0.87
1-t-butyl-3,4,5-trimethylbenzene	--	0.24	--
n-heptylbenzene	--	0.27	0.25
naphthalene	0.50	0.57	1.14
2-methylnaphthalene	0.56	1.38	1.46
1-methylnaphthalene	0.78	1.44	1.84
2,6-dimethylnaphthalene	0.25	1.12	1.34
biphenyl	--	0.70	0.63
1-ethylnaphthalene	--	0.32	0.33
2,3-dimethylnaphthalene	--	0.46	0.36
n-octylbenzene	--	0.78	0.61
olefins			
tridecene	--	0.45	0.73

Table C-21. Hydrocarbon composition of two samples of kerosene. From Goodman and Harbison (198?). (Page 1 of 2).

Compound/Class	Sample A	Sample B
hydrocarbon type (vol %)		
paraffins	50.5	42.7
monocycloparaffins & olefins	25.3	19.3
dicycloparaffins	5.6	8.9
alkylbenzenes	12.7	14.7
indans/tetralins	2.9	7.5
naphthalene & alkylnaphthalenes	3.0	6.9
n-paraffins (wt %)		
heptane	0.1	0.1
octane	0.2	0.3
nonane	0.4	0.8
decane	1.5	1.7
undecane	3.5	6.1
dodecane	2.8	5.7
tridecane	3.1	5.2
tetradecane	2.3	4.7
pentadecane	0.6	2.3
hexadecane	0.1	0.7
heptadecane	--	0.4
octadecane	--	0.3
nonadecane	--	0.2
eicosane	--	0.1
heneicosane	--	0.1
aromatic hydrocarbons (ppm, wt/vol)		
indene	<50	2.2
naphthalene	2,000	1,286
1-methylnaphthalene	2,200	2,160
2-methylnaphthalene	2,100	2,860
acenaphthene	51	40
acenaphthalene	25	38
fluorene	<2.0	36
1,4-dimethylnaphthalene	1,200	1,580
phenanthrene	1.9	493

Table C-21. Hydrocarbon composition of two samples of kerosene. From Goodman and Harbison (198?). (Page 2 of 2).

Compound/Class	Sample A	Sample B
anthracene	<2.0	7.3
fluoranthene	<4.0	1.0
pyrene	<2.0	2.0
benz(a)anthracene	<0.75	<0.09
chrysene	<2.0	<0.11
benzo(b)fluoranthene	<0.75	<0.20
benzo(k)fluoranthene	<0.50	<0.04
benzo(a)pyrene	<0.50	<0.30
benzo(g,h,i)perylene	<2.0	<0.30
indeno(1,2,3-c,d)pyrene	<2.0	<0.30
perylene	<3.0	<0.90
dibenz(a,h)anthracene	<0.75	<0.50
dibenzo(def,p)chrysene	<0.30	<0.15
9,10-dimethylanthracene	<4.0	6.0
2-methylanthracene	<4.0	3.9
benzo(b)fluorene	<4.0	1.0
benzo(a)fluorene	<4.0	0.78
7,12-dimethylbenz(a)anthracene	--	17.0
dibenzo(a,e)pyrene	<0.45	<0.30
benzo(b)chrysene	<0.45	<0.30
picene	<1.5	<1.4
p-quarterphenyl	<0.5	<0.50
coronene	<0.45	<0.30
dibenz(a,h)acridine	<0.2	<0.13
dibenzo(a,h)pyrene	<1.0	<0.70
3-methylcholanthrene	<0.1	<0.08
benzo(g,h,i)fluoranthene	<1.0	<0.04
naphtho(1,2,3,4,def)chrysene	<0.15	<0.10

Table C-22. Hydrocarbon composition of typical home heating oils. Concentrations are volume percent. From IARC (1989).

Hydrogen Type	Straight-run No. 1 Furnace Oils 1	Straight-run No. 1 Furnace Oils 2	Hydrotreated No. 1 Furnace Oil	Straight-run No. 2 Furnace Oil	No. 2 Furnace Oil 10% Calalytic	No. 2 Furnace Oil 50% Calalytic
n/iso-paraffins	50.5	54.3	42.6	41.3	61.2	57.2
monocycloparaffins	25.3	18.4	19.3	22.1	8.5	6.0
bicycloparaffins	5.6	4.5	8.9	9.6	8.3	5.0
tricycloparaffins	--	0.8	--	2.3	1.4	0.7
total alkanes	81.4	78	70.9	75.3	79.4	68.9
olefins	--	--	--	--	2.0	7.5
alkylbenzenes	12.7	14.3	14.7	5.9	5.3	8.0
indans/tetralins	2.9	3.8	7.5	4.1	4.3	5.4
dinaphthenobenzenes/indenes	--	0.9	--	1.8	1.3	1.0
naphthalenes	3.0	2.6	6.9	8.2	5.8	6.8
biphenyls/acenaphthanes	--	0.4	--	2.6	1.1	1.6
fluorenes/acenaphthylenes	--	--	--	1.4	0.6	0.3
phenanthrenes	--	--	--	0.7	0.2	0.5
total aromatic hydrocarbons	18.6	29.1	22.0	24.7	18.6	23.6

Table C-23. Concentrations of benzenes and PAH in middle distillate fuels. Concentrations are in mg/kg.

Compound	No. 2 Fuel Oil[1]	Artic Diesel[2]	Refined Spilled[3]	Diesel Fuel[4]	No. 2 Heating[4]
benzene	222,000[a]	<10			
toluene		2,549			
ethylbenzene		991			
xylenes	5,211				
naphthalene	4,000	4,086[a]	2,468		
methylnaphthalenes	27,100		23,312		
ethylnaphthalenes			5,576		
dimethylnaphthalenes	31,100		26,214		
trimethyl-naphthalenes	18,400				
fluorene	3,600	302[a]			
anthracene				2.9	3.6
phenanthrene	429	171[a]			
methylanthracenes				9.3	15.7
methylphenanthrenes	7,850				
fluoranthene	37			0.57	2.4
pyrene	41			0.37	1.3
benz(a)anthracene	1.2			0.13	0.04
chrysene	2.2	<10[a]		0.45	0.54
triphenylene	1.4			3.3	0.73
benzo(a)pyrene	0.6			0.07	0.03
benzo(e)pyrene	0.1			0.18	0.02
benzo(g,h,i)perylene				0.03	0.03

(1) Pancirov and Brown, 1975
(2) Kennicutt et al., 1991
(3) Woodward et al., 1983
(4) Norris and Hill, 1974
(a) includes alkyl homologues

Table C-24. Concentrations of benzenes and PAH in No. 2 diesel fuels. Concentrations are in mg/l or mg/kg.

Compound	No. 2 Fuel Oil[1]	No. 2 Fuel Oil[2]	High S Diesel Fuel[2]	Low S Diesel Fuel[2]
toluene			8,300	nd
xylenes			200	2,700
trimethylbenzenes			27,000	17,000
C_4-benzenes			31,000	23,000
C_5-benzenes			13,000	11,000
C_6-benzenes			1,900	4,600
naphthalene	500	76	25,000	2,200
methylnaphthalenes	1,000	560	30,000	7,100
dimethylnaphthalenes	1,300	1,500	43,000	10,000
trimethylnaphthalenes	950	1,000	34,000	7,200
tetramethylnaphthalenes	550	520	1,200	900
biphenyl	75	52		
fluorene	38	40		
methylfluorenes	135	130		
dimethylfluorenes	305	240		
trimethylfluorenes	315	170		
phenanthrene	80	88	2,100	400
methylphenanthrenes	500	370	5,300	400
dimethylphenanthrenes	950	470	4,300	200
trimethylphenanthrenes	700	190	1,500	nd
tetramethylphenenthrenes	285	76		
dibenzothiophene	nd	150		
methyldibenzothiophenes	22	65		
dimethyldibenzothiophenes	80	84		
trimethyldibenzothiophenes	90	62		
fluoranthene	2.8	1.2		
pyrene	20	7.0		
methylfluoranthenes/pyrenes	80	15		
benz(a)anthracene	0.8	0.12		
chrysene	3.4	0.5		
methylchrysenes	6.0	0.8		
diemthylchrysenes	3.7	0.4		
trimethylchrysenes	1.6	0.08		
benzo(a)pyrene	nd	0.13		
benzo(e)pyrene	nd	nd		
benzo(g,h,i)perylene	nd	0.05		

(1) Page et al., 1994

(2) Boehm et al., 1989

Table C-25. Concentrations of benzenes and PAH in residual petroleum products. Concentrations are in mg/l or mg/kg.

Compound	Bunker C No. 6 Oil[1]	Bunker C[2]	Asphalts[3]	Paving Asphalts[4]
benzenes	60,000[a]			
naphthalene	1,000			
methylnaphthalenes	7,500	1,700		
dimethylnaphthalenes	12,300	6,100		
trimethylnaphthalenes	8,800			
biphenyls	<100			
fluorenes	2,400			3.0
phenanthrene	482	1,700	0.4-3.5	9.6
methylphenenthrenes	871	3,300		
dimethylphenanthrenes		3,500		
fluoranthene	240		nd-5	
pyrene	23		0.08-38	
benz(a)anthracene	90		nd-35	90
chrysene	196		0.04-34	80
triphenylene	31		0.25-7.6	
dimethylbenzanthracenes				4.3
benzo(k)fluoranthene				1.8
benzo(a)pyrene	44		nd-27	1.3
benzo(e)pyrene	10		0.03-52	
perylene	22		nd-39	1.5
benzo(g,h,i)perylene			tr-15	1.2
dibenz(a,h)anthracene				4.6

(1) Pancirov and Brown, 1975
(2) Petersen, 1978
(3) Wallcave et al., 1971
(4) Malaiyandi et al., 1982

Table C-26. Concentrations of PAH in new engine oils and lube oil. Concentrations are in mg/kg.

Compound	Engine Oil (new)[1]	Average[1]	Maximum	Rerefined[1]	Lube Oil[2]
dibenzo(b,d)thiophene	5				
fluorene					11.7
phenanthrene	7				46.5
anthracene	0.1				9.5
methyldibenzothiophenes	1				
methylphenanthrenes	8				
fluoranthene	0.7	0.3	3	69 2.0	
phenanthrothiophene	0.4				
pyrene	2	0.7	7	12 2.5	
benzonaphthofurans	1				
methylpyrenes/ fluoranthenes	1				
benzofluorenes	4				
methylbenzonaphthofurans	0.3				
methylpyrenes	3				
dimethylpyrenes/ fluoranthenes	1				
benzonaphthothiophenes	5	1	9	5	
benz(a)anthracene	0.30.2	2			0.68
triphenylene	3				
chrysene	1	1	12	30	3.2
methylbenzonaphtho-thiophenes	7				
methylchrysenes	1				
dimethylchrysenes	1				
benzofluoranthenes	0.4	0.1	0.2	8 0.62	
triphenylenethiophene	0.1				
benzo(e)pyrene	0.25	0.2	0.4	4	
benzo(a)pyrene	0.03	0.06	0.3	1	0.23
methyltriphenylene/ thiophene	0.3				
methylbenzo(e)pyrenes	0.2				
methylbenzo(a)pyrenes	0.1				
dimethylbenzopyrenes	0.5				
indeno(1,2,3-c,d)pyrene	0.02	0.006	0.02	0.7	
dibenz(a)anthracene	0.1				
benzo(g,h,i)perylene	0.1	0.05	0.1	1	0.85
anthranthrene	0.01	0.03			
coronene		0.007	0.02	0.6	

(1) Grimmer et al., 1981a
(2) Eisenberg et al., 1988

Table C-27. Concentrations of alkylbenzenes and PAH in used engine oils from North America. Concentrations are in mg/l or mg/kg. (Page 1 of 2).

Compound	Winter Gas Engine Calgary[1]	Gas Engine 3928 mi[2]	Gas Engine 5817 mi	Waste Crankcase Oil (MD)[3]
Σ alkylbenzenes	>900			
tetralin				24
naphthalene	2,350	2,520	368	
methylnaphthalenes		6,350	4,150	57
dimethylnaphthalenes		4,470	3,000	114
trimethylnaphthalenes				37
Σ alkylnaphthalenes	440			
biphenyl		82.8	45.8	
methylbiphenyls	2.05			6
fluorene	1.47	98.3	109	6
methylfluorenes	2.45			
dimethylfluorenes	1.29			
trimethylfluorenes	1.10			
phenanthrene	7.80	186	193	33
anthracene	0.33	30.1	47.0	
phenylnaphthalene	0.90			
methylphenanthrenes	11.67	648	668	
dimethylphenanthrenes	10.59			
trimethylphenanthrenes	6.13			
diethylphenanthrenes	1.19			
ethylcyclopentaphenanthrene	1.42			
methylanthracenes	0.58			
dimethyanthracenes	0.26			
trimethylanthracenes	0.51			
dibenzothiophene	0.79			
methyldibenzothiophenes	2.26			
dimethyldibenzothiophenes	3.86			
trimethyldibenzothiophenes	1.94			
benzonaphthiophene	0.34			
methylbenzonaphthothiophene	0.54			
terphenyl	0.12			
fluoranthene	4.36	69.8	91.2	
pyrene	6.69	88.4	95.6	
methylpyrenes	4.25			
dimethylpyrenes	1.71			
ethylmethylpyrenes	0.14			
benzofluorenes	2.75			

Table C-27. Concentrations of alkylbenzenes and PAH in used engine oils from North America. Concentrations are in mg/l or mg/kg. (Page 2 of 2).

Compound	Winter Gas Engine Calgary[1]	Gas Engine 3928 mi[2]	Gas Engine 5817 mi	Waste Crankcase Oil (MD)[3]
benzo(c)phenanthrene	0.12			
benz(a)anthracene	0.87	32	47.4	
methylbenz(a)anthracene	2.45			
ethylbenz(a)anthracene	0.65			
chrysene/triphenylene	2.48	50	84.7	
cyclopenta(cd)pyrene	0.78			
benzo(b)fluoranthene	1.44			
methylbenzofluoranthenes	0.43			
benzo(e)pyrene	1.74	nd	27.1	
benzo(a)pyrene	0.36	nd	22.3	
methylbenzopyrenes	0.41			
perylene	0.13			
benzo(ghi)perylene	1.67			

(1) Peake and Parker, 1980
(2) Pruell and Quinn, 1988
(3) Hoffman et al., 1982

Table C-28. Concentrations of PAH in used engine oils (crankcase oils). Concentrations are in mg/kg. From Grimmer et al., (1981b).

Compound	Length of Use and Engine Type				
	610K km Gasoline	1-6K km Gasoline	0.5-6K km Diesel	3-30K km Diesel	9-31K Diesel
phenanthrene	158				
anthracene	46				
methylphenanthrenes	381				
2-phenylnaphthalene	44				
dimethylphenanthrenes (includes O-PAC)	56				
fluoranthene	178	109	59	3	3
pyrene	430	326	78	6	5
methylfluoranthenes /methylpyrenes	883				
dimethylfluoranthenes	263				
benz(a)anthracene	245				
benzo(b)naphtho-(2,1-d)thiophene			4	6	5
chrysene+triphenylene	223	74	43	6	8
methylchrysenes/ benz(a)anthracenes	485				
dimethylbenz(a)anthracene	21				
benzo(b+j)fluoranthenes	134	44	17	1	1
benzo(k)fluoranthene	37				
benzo(a)fluoranthene	19				
benzo(e)pyrene	278	49	11	1	1
benzo(a)pyrene	217	35	12	0.6	0.6
perylene	51	10	3	0.4	0.3
methylperylenes/ benzopyrenes/benzo-fluoranthenes	540				
dimethylperylenes/ benzopyrenes/benzo-fluoranthenes	62				
dibenz(a,j)anthracene	23				
indeno(1,2,3-cd)pyrene	89	12	9	0.3	0.2
dibenz(a,h)anthracene	14				
dibenz(a,c)anthracene	3				
benzo(ghi)perylene	334	85	16	0.8	0.6
anthranthrene	15	11	4	0.1	0.2
methyldibenzanthracenes	203				
dibenzo(b,k)fluoranthene	10				
coronene	60	29	6	0.1	0.1
dibenz(gf,op)naphthacene	41.32				
benzo(rst)pentaphene	7.51				

FUEL RANGES

Source:

Potter, T.L. and K. Simmons (1998). *Total Petroleum Hydrocarbon Criteria Working Group Volume 2: Composition of Petroleum Mixtures.* Amherst Scientific Press, Amherst, MA.

Table C-29
Individual Sample Fuel Mixture Composition Data

Fuel mixture: Crude Oil

Sample #: 14/Prudhoe

From: Riley, R.G., B.L. Thomas, J.W. Anderson, and R.M. Bean, Marine Environmentalist

Compound Class	Carbon #	Compound	Weight Percent	Number of Data Points	Flag (s)
Alkyl-Monoaromatics	7	Toluene	8.2E-02%	1	5
	8	1,2-Diethylbenzene	2.4E-02	1	5
	8	Ethylbenzene	5.6E-02	1	5
	8	m+p-Xylenes	2.0E-01	1	5
	8	o-Xylene	7.9E-02	1	5
	9	1,2,4-Trimethylbenzene	1.1E-01	1	5
	9	1,3,5-Trimethylbenzene	4.1E-02	1	5
	9	Isopropylbenzene	1.6E-02	1	5
	10	1,2,3,5-Tetramethylbenzene	2.7E-02	1	5
	10	1,2,4,5-Tetramethylbenzene	3.8E-02	1	5
	10	1,2-Dimethyl-4-ethylbenzene	2.4E-02	1	5
	10	1,3-Dimethyl-5-ethylbenzene	2.7E-02	1	5
	10	1-Methyl-4-isopropylbenzene	1.2E-02	1	5
	10	Indane	6.7E-02	1	5
	10	sec-Butylbenzene	1.4E-02	1	5
Branched Alkanes	19	Pristane	2.1E-01	1	5
	20	Phytane	1.0E-01	1	5
n-Alkanes	8	n-Octane	4.2E-01	1	5
	9	n-Nonane	4.4E-01	1	5
	10	n-Decane	4.4E-01	1	5
	11	n-Undecane	4.7E-01	1	5
	12	n-Dodecane	4.6E-01	1	5
	13	n-Tridecane	4.5E-01	1	5
	14	n-Tetradecane	4.2E-01	1	5
	15	n-Pentadecane	4.0E-01	1	5
	16	n-Hexadecane	3.7E-01	1	5
	17	n-Heptadecane	3.4E-01	1	5
	18	n-Octadecane	2.5E-01	1	5

Table C-29 (continued)
Individual Sample Fuel Mixture Composition Data

Fuel mixture: Crude Oil

Sample #: 14/Prudhoe

From: Riley, R.G., B.L. Thomas, J.W. Anderson, and R.M. Bean, Marine Environmentalist

Compound Class	Carbon #	Compound	Weight Percent	Number of Data Points	Flag (s)
n-Alkanes	19	n-Nonadecane	3.0E-01	1	5
	20	n-Eicosane	1.9E-01	1	5
	21	n-Heneicosane	1.6E-01	1	5
	22	n-Docosane	1.9E-01	1	5
	23	n-Tricosane	1.7E-01	1	5
	24	n-Tetracosane	1.3E-01	1	5
	25	n-Pentacosane	1.0E-01	1	5
	26	n-Hexacosane	7.6E-02	1	5
Naphthalenes	10	Naphthalene	9.2E-02	1	5
	11	1-Methylnaphthalene	1.3E-01	1	5
	11	2-Methylnaphthalene	1.6E-01	1	5
	12	1,2-Dimethylnaphthalene	4.0E-02	1	5
	12	1,3- & 1,6-Dimethylnaphthalene	8.0E-02	1	5
	12	1,4- & 2,3- & 1,5-Dimethylnaphthalene	8.0E-02	1	5
	12	1,7-Dimethylnaphthalene	1.1E-01	1	5
	12	1- & 2-Ethylnaphthalene	4.8E-02	1	5
	12	2,6- & 2,7-Dimethylnaphthalene	6.9E-02	1	5
	13	2,3,6-Trimethylnaphthalene	5.1E-02	1	5
Polynuclear Aromatics	14	Phenanthrene	3.8E-02	1	5
	15	1-Methylphenanthrene	3.3E-02	1	5
	15	2-Methylphenanthrene	2.1E-02	1	5
	16	3,6-Dimethylphenanthrene	1.1E-02	1	5

Flag(s)

5 Data was converted using formula WT%=mg/kg*10-4.

Table C-30
Individual Sample Fuel Mixture Composition Data

Fuel mixture: Crude Oil

Sample #: 41/Ponca

From: Speight, J.K., 2nd edition, Marcel Dekker, Inc, NYC, NY, 1991

Compound Class	Carbon #	Compound	Weight Percent	Number of Data Points	Flag (s)
Alkyl-Monoaromatics	6	Benzene	2.0E-01	1	1 5
	7	Toluene	5.0E-01	1	1 5
	8	Ethylbenzene	2.0E-01	1	1 5
	8	m+p-Xylenes	8.0E-01	1	1 5
	8	m-Xylene	5.0E-01	1	1 5
	8	o-Xylene	3.0E-01	1	1 5
	8	p-Xylene	1.0E-01	1	1 5
	9	1,2,3-Trimethylbenzene	1.0E-01	1	1 5
	9	1,2,4-Trimethylbenzene	5.1E-01	1	1 5
	9	1,3,5-Trimethylbenzene	1.2E-01	1	1 5
	9	1-Methyl-2-ethylbenzene	9.0E-02	1	1 5
	9	1-Methyl-3-ethylbenzene	1.7E-01	1	1 5
	9	1-Methyl-4-ethylbenzene	6.0E-02	1	1 5
	9	Isopropylbenzene	7.0E-02	1	1 5
	9	n-Propylbenzene	9.0E-02	1	1 5
	10	tert-Butylbenzene	1.0E-02	1	1 5
Branched Alkanes	6	2,2-Dimethylbutane	4.0E-02	1	1 5
	6	2,3-Dimethylbutane	8.0E-02	1	1 5
	6	2-Methylpentane	4.0E-01	1	1 5
	6	3-Methylpentane	3.0E-01	1	1 5
	7	2,3-Dimethylpentane	1.0E-01	1	1 5
	7	3-Ethylpentane	4.0E-03	1	1 5
	7	3-Methylhexane	1.0E-02	1	1 5
	8	2,2,3-Trimethylpentane	6.0E-03	1	1 5
	8	2,2-Dimethylhexane	5.0E-03	1	1 5
	8	2,3,3-Trimethylpentane	6.0E-02	1	1 5
	8	2,3,4-Trimethylpentane	6.0E-02	1	1 5
	8	2,3-Dimethylhexane	6.0E-02	1	1 5

Table C-30 (continued)
Individual Sample Fuel Mixture Composition Data

Fuel mixture: Crude Oil

Sample #: 41/Ponca

From: Speight, J.K., 2nd edition, Marcel Dekker, Inc, NYC, NY, 1991

Compound Class	Carbon #	Compound	Weight Percent	Number of Data Points	Flag (s)
Branched Alkanes	8	2,4 Dimethylhexane	6.0E-02	1	15
	8	2,5 Dimethylhexane	6.0E-02	1	15
	8	2-Methyl-3-heptane	4.0E-02	1	15
	8	3,3-Dimethylhexane	3.0E-02	1	15
	8	Ethylcyclohexane	2.0E-02	1	15
	9	2,3-Dimethylheptane	5.0E-02	1	15
	9	2,6-Dimethylheptane	5.0E-02	1	15
	9	2-Methyloctane	4.0E-02	1	15
	9	3-Methyloctane	1.0E-02	1	15
	9	4-Methyloctane	1.0E-02	1	15
Cycloalkanes	5	Cyclopentane	5.0E-02	1	1 5
	6	Cyclohexane	7.0E-01	1	1 5
Cycloalkanes	6	Methylcyclopentane	9.0E-01	1	1 5
	7	1,1-Dimethylcyclopentane	2.0E-01	1	1 5
	7	cis-1,3-Dimethylcyclopentane	2.0E-01	1	1 5
	7	Ethylcyclopentane	2.0E-01	1	1 5
	7	trans-1,2-Dimethylcyclopentane	5.0E-01	1	1 5
	7	trans-1,3-Dimethylcyclopentane	9.0E-01	1	1 5
	8	1,1,2-Trimethylcyclopentane	6.0E-02	1	1 5
	8	1,1,3-Trimethylcyclopentane	2.0E-01	1	1 5
	8	1,1,3-Trimethylcyclopentane	3.0E-01	1	1 5
	8	trans-1,2-cis-4-Trimethylcyclopentane	3.0E-01	1	1 5
	9	trans-1,2,4-Trimethylcyclohexane	2.0E-01	1	1 5
	9	trans-1,2,4-Trimethylcyclohexane	2.0E-01	1	1 5
n-Alkanes	6	n-Hexane	1.8E+00	1	1 5
	7	n-Heptane	2.3E+00	1	1 5
	8	n-Octane	1.9E+00	1	1 5
	9	n-Nonane	1.8E+00	1	1 5

Table C-30 (continued)
Individual Sample Fuel Mixture Composition Data

Fuel mixture: Crude Oil

Sample #: 41/Ponca

From: Speight, J.K., 2nd edition, Marcel Dekker, Inc, NYC, NY, 1991

Compound Class	Carbon #	Compound	Weight Percent	Number of Data Points	Flag (s)
n-Alkanes	10	n-Decane	1.8E+00	1	1 5
	11	n-Undecane	1.7E+00	1	1 5
	12	n-Dodecane	1.7E+00	1	1 5
Naphthalenes	10	Naphthalene	6.0E-02	1	1 5
	11	1-Methylnaphthalene	1.0E-01	1	1 5
	11	2-Methylnaphthalene	2.0E-01	1	1 5
	11	5-Methyltetralin	8.0E-02	1	1 5
	11	6-Methyltetralin	9.0E-02	1	1 5

Flag(s)

1 Data source was unavailable and data was not reviewed
5 Data was converted using formula WT%=mg/kg*10-4.

Table C-31
Individual Sample Fuel Mixture Composition Data

Fuel mixture: Diesel (#2) Fuel Oil

Sample #: 19/Sample 1910

From: Griest, W. H., E. E. Higgens, and M. R. Guerin, Oak Ridge National Laboratory, Oak Ridge, TN Conf. 851027--5, 1985

Compound Class	Carbon #	Compound	Weight Percent	Number of Data Points	Flag (s)
Alkyl-Monoaromatics	6	Benzene	2.6E-03	1	9
	7	Toluene	2.7E-02	1	9
	8	Ethylbenzene	1.7E-02	1	9
	8	m+p-Xylenes	1.3E-01	1	9
	8	o-Xylene	4.2E-02	1	9
	9	1,3,5-Trimethylbenzene	2.0E-01	1	9
	9	n-Propylbenzene	3.0E-02	1	9
	10	1-Methyl-4-isopropylbenzene	2.6E-02	1	9
	10	n-Butylbenzene	3.1E-02	1	9
	12	3-Methylundecane	1.7E-01	1	9
	13	2-Methyldodecane	2.8E-01	1	9
	14	3-Methyltridecane	2.0E-01	1	9
	15	2-Methyltetradecane	5.5E-01	1	9
	19	Pristane	8.1E-01	1	9
	20	Phytane	5.9E-01	1	9
	13	Fluorene	1.3E-01	1	9
	9	n-Nonane	4.9E-01	1	9
	10	n-Decane	1.0E+00	1	9
	11	n-Undecane	1.7E+00	1	9
	12	n-Dodecane	1.9E+00	1	9
	13	n-Tridecane	2.3E+00	1	9
	14	n-Tetradecane	2.5E+00	1	9
	15	n-Pentadecane	3.1E+00	1	9
	16	n-Hexadecane	2.8E+00	1	9
	17	n-Heptadecane	2.5E+00	1	9
	18	n-Octadecane	2.0E+00	1	9
	19	n-Nonadecane	1.2E+00	1	9
	20	n-Eicosane	5.4E-01	1	9

Table C-31 (continued)
Individual Sample Fuel Mixture Composition Data

Fuel mixture: Diesel (#2) Fuel Oil

Sample #: 19/Sample 1910

From: Griest, W. H., E. E. Higgens, and M. R. Guerin, Oak Ridge National Laboratory, Oak Ridge, TN Conf. 851027--5, 1985

Compound Class	Carbon #	Compound	Weight Percent	Number of Data Points	Flag (s)
Alkyl-Monoaromatics	21	n-Heneicosane	2.3E-01	1	9
Naphthalenes	10	Naphthalene	1.3E-01	1	9
	11	1-Methylnaphthalene	8.1E-01	1	9
	11	2-Methylnaphthalene	1.5E+00	1	9
	12	1,3-Dimethylnaphthalene	1.3E+00	1	9
	12	1,4-Dimethylnaphthalene	2.2E-01	1	9
	12	1,5-Dimethylnaphthalene	3.6E-01	1	9
Polynuclear Aromatics	14	Phenanthrene	2.4E-01	1	9
	15	2-Methylphenanthrene	1.4E-01	1	9
	20	Benzo(a)pyrene	5.0E-06	1	3.4

Flag(s)

3 Data was cited from a secondary source. Original data was not reviewed.
5 Data was converted using formula WT%=ug/g*10-4.
9 Data was converted using formula WT%=mg/g*0.10.

Table C-32
Individual Sample Fuel Mixture Composition Data

Fuel mixture: Diesel (#2) Fuel Oil

Sample #: 19/Sample 1914

From: Griest, W. H., E. E. Higgens, and M. R. Guerin, Oak Ridge National Laboratory, Oak Ridge, TN Conf. 851027--5, 1985

Compound Class	Carbon #	Compound	Weight Percent	Number of Data Points	Flag (s)
Alkyl-Monoaromatics	6	Benzene	8.2E-03	1	9
	7	Toluene	8.3E-02	1	9
	8	Ethylbenzene	4.3E-02	1	9
	8	m+p-Xylenes	2.0E-01	1	9
	8	o-Xylene	7.8E-02	1	9
	9	1,3,5-Trimethylbenzene	9.0E-02	1	9
	9	n-Propylbenzene	4.0E-02	1	9
	10	1-Methyl-4-isopropylbenzene	3.0E-03	1	9
	10	n-Butylbenzene	4.6E-02	1	9
Branched Alkanes	12	3-Methylundecane	9.0E-02	1	9
	13	2-Methyldodecane	2.5E-01	1	9
	14	3-Methyltridecane	2.2E-01	1	9
	15	2-Methyltetradecane	5.8E-01	1	9
	19	Pristane	6.0E-01	1	9
	20	Phytane	5.3E-01	1	9
Diaromatics (Except Naphthalenes)	12	Biphenyl	1.2E-01	1	9
	13	Fluorene	1.2E-01	1	9
n-Alkanes	9	n-Nonane	2.1E-01	1	9
	10	n-Decane	2.8E-01	1	9
	11	n-Undecane	5.7E-01	1	9
	12	n-Dodecane	1.0E+00	1	9
	13	n-Tridecane	2.0E+00	1	9
	14	n-Tetradecane	2.5E+00	1	9
	15	n-Pentadecane	2.5E+00	1	9
	16	n-Hexadecane	2.0E+00	1	9
	17	n-Heptadecane	2.9E+00	1	9
	18	n-Octadecane	1.2E+00	1	9
	19	n-Nonadecane	7.3E-01	1	9

Table C-32 (continued)
Individual Sample Fuel Mixture Composition Data

Fuel mixture: Diesel (#2) Fuel Oil

Sample #: 19/Sample 1914

From: Griest, W. H., E. E. Higgens, and M. R. Guerin, Oak Ridge National Laboratory, Oak Ridge, TN Conf. 851027--5, 1985

Compound Class	Carbon #	Compound	Weight Percent	Number of Data Points	Flag (s)
	20	n-Eicosane	4.0E-01	1	9
	21	n-Heneicosane	2.4E-01	1	9
	10	Naphthalene	2.5E-01	1	9
	11	1-Methylnaphthalene	8.1E-01	1	9
	11	2-Methylnaphthalene	1.4E+00	1	9
	12	1,3-Dimethylnaphthalene	1.2E+00	1	9
	12	1,4-Dimethylnaphthalene	2.3E-01	1	9
	12	1,5-Dimethylnaphthalene	3.6E-01	1	9
	14	Phenanthrene	1.9E-01	1	9
	15	2-Methylphenanthrene	1.7E-01	1	9
	20	Benzo(a)pyrene	1.9E-04	1	3 4

Flag(s)

3 Data was cited from a secondary source. Original data was not reviewed.
4 Data was converted using formula WT%=ug/g*10-4.
9 Data was converted using formula WT%=mg/g*0.10.

Table C-33
Individual Sample Fuel Mixture Composition Data

Fuel mixture: JP-4 Fuel Oil

Sample #: 42/JP-4 Fuel

From: Harper,C.C., O.Faroon and M.A.Melman, Hydrocarbon Contaminated Soils, vol III, E.Calabrese and P.Kostecki, eds., pp 215-241, 1993

Compound Class	Carbon #	Compound	Weight Percent	Number of Data Points	Flag (s)
Alkyl-Monoaromatics	6	Benzene	5.0E-01	1	21
	7	Toluene	1.3E+00	1	21
	8	Ethylbenzene	3.7E-01	1	21
	8	m-Xylene	9.6E-01	1	21
	8	o-Xylene	1.0E+00	1	21
	8	p-Xylene	3.5E-01	1	21
	9	1,2,4-Trimethylbenzene	1.0E+00	1	21
	9	1,3,5-Trimethylbenzene	4.2E-01	1	21
	9	1-Methyl-2-ethylbenzene	2.3E-01	1	21
	9	1-Methyl-3-ethylbenzene	4.9E-01	1	21
	9	1-Methyl-4-ethylbenzene	4.3E-01	1	21
	9	Isopropylbenzene	3.0E-01	1	21
	9	n-Propylbenzene	7.1E-01	1	21
	10	1,2,3,4-Tetramethylbenzene	7.5E-01	1	21
	10	1,2-Dimethyl-4-ethylbenzene	7.7E-01	1	21
	10	1,3-Diethylbenzene	4.6E-01	1	21
	10	1,3-Dimethyl-5-ethylbenzene	6.1E-01	1	21
	10	1,4-Dimethyl-2-ethylbenzene	7.0E-01	1	21
	10	1-Methyl-2-isopropylbenzene	2.9E-01	1	21
	10	1-Methyl-4-propylbenzene	4.0E-01	1	21
Branched Alkanes	4	Isobutane	6.6E-01	1	21
	6	2,2-Dimethylbutane	1.0E-01	1	21
	6	2-Methylpentane	1.3E+00	1	21
	6	3-Methylpentane	8.9E-01	1	21
	7	2,2-Dimethylpentane	2.5E-01	1	21
	7	2-Methylhexane	2.3E+00	1	21
	7	3-Methylhexane	2.0E+00	1	21
	8	2,2,3,3-Tetramethylbutane	2.4E-01	1	21

Table C-33 (continued)
Individual Sample Fuel Mixture Composition Data

Fuel mixture: JP-4 Fuel Oil

Sample #: 42/JP-4 Fuel

From: Harper,C.C., O.Faroon and M.A.Melman, Hydrocarbon Contaminated Soils, vol III, E.Calabrese and P.Kostecki, eds., pp 215-241, 1993

Compound Class	Carbon #	Compound	Weight Percent	Number of Data Points	Flag (s)
Branched Alkanes	8	2,2-Dimethylhexane	7.1E-01	1	21
	8	2,4-Dimethylhexane	5.8E-01	1	21
	8	2,5-Dimethylhexane	3.7E-01	1	21
	8	2-Methylheptane	2.7E+00	1	21
	8	3,3-Dimethylhexane	2.6E-01	1	21
	8	3-Methylheptane	3.0E+00	1	21
	8	4-Methylheptane	9.2E-01	1	21
	9	2,5-Dimethylheptane	5.2E-01	1	21
	9	2-Methyloctane	8.8E-01	1	21
	9	3,4-Dimethylheptane	4.3E-01	1	21
	9	3-Methyloctane	7.9E-01	1	21
	9	4-Ethylheptane	1.8E-01	1	21
	9	4-Methyloctane	8.6E-01	1	21
	12	2-Methylundecane	6.4E-01	1	21
	13	2,6-Dimethylundecane	7.1E-01	1	21
Cycloalkanes	6	Cyclohexane	1.2E+00	1	21
	6	Methylcyclopentane	1.2E+00	1	21
	7	cis-1,2-Dimethylcyclopentane	5.4E-01	1	21
	7	cis-1,3-Dimethylcyclopentane	3.4E-01	1	21
	7	Ethylcyclopentane	2.6E-01	1	21
	7	Methylcyclohexane	2.3E+00	1	21
	7	trans-2,3-Dimethylcyclopentane	3.6E-01	1	21
	8	1,2,3-Trimethylcyclopentane	2.5E-01	1	21
	8	1,2,4-Trimethylcyclopentane	2.5E-01	1	21
	8	cis-1,3-Dimethylcyclohexane	4.2E-01	1	21
	8	Dimethylcyclohexane	4.3E-01	1	21
	9	1,1,3-Trimethylcyclohexane	4.8E-01	1	21
	9	1,3,5-Trimethylcyclohexane	9.9E-01	1	21

Table C-33 (continued)
Individual Sample Fuel Mixture Composition Data

Fuel mixture: JP-4 Fuel Oil

Sample #: 42/JP-4 Fuel

From: Harper,C.C., O.Faroon and M.A.Melman, Hydrocarbon Contaminated Soils, vol III, E.Calabrese and P. Kostecki, eds., pp 215-241, 1993

Compound Class	Carbon #	Compound	Weight Percent	Number of Data Points	Flag (s)
Branched Alkanes	9	1-Methyl-2-ethylcyclohexane	3.9E-01	1	21
	9	1-Methyl-3-ethylcyclohexane	1.7E-01	1	21
	9	1-Methyl-4-ethylcyclohexane	4.8E-01	1	21
n-Alkanes	4	n-Butane	1.2E-01	1	21
	5	n-Pentane	1.1E+00	1	21
	6	n-Hexane	2.2E+00	1	21
	7	n-Heptane	3.7E+00	1	21
	8	n-Octane	3.8E+00	1	21
	9	n-Nonane	2.3E+00	1	21
	10	n-Decane	2.2E+00	1	21
	11	n-Undecane	2.3E+00	1	21
	12	n-Dodecane	2.0E+00	1	21
	13	n-Tridecane	1.5E+00	1	21
	14	n-Tetradecane	7.3E-01	1	21
Naphthalenes	10	Naphthalene	5.0E-01	1	21
	11	1-Methylnaphthalene	7.8E-01	1	21
	11	2-Methylnaphthalene	5.6E-01	1	21
	12	2,6-Dimethylnaphthalene	2.5E-01	1	21

Flags(s) 1 Data source was unavailable and data was not reviewed

Table C-34
Individual Sample Fuel Mixture Composition Data

Fuel mixture: JP-8 Fuel Oil

Sample #: 43/JP-8 Fuel

From: Smith, J.H. et. al., Department of the Air Force, Final Report 54; pp. 1–50; National Technical Information Services, Springfield,VA, A115949/LP, 1981

Compound Class	Carbon #	Compound	Weight Percent	Number of Data Points	Flag (s)
Alkenes	13	Tridecene	7.3E-01	1	21
Alkyl-Monoaromatics	8	m-Xylene	6.0E-02	1	21
	8	o-Xylene	6.0E-02	1	21
	9	1,2,3-Trimethylbenzene	2.7E-01	1	21
	10	1,2,3,4-Tetramethylbenzene	1.1E+00	1	21
	10	1,3-Dimethyl-5-ethylbenzene	6.2E-01	1	21
	10	1-Methyl-2-isopropylbenzene	5.6E-01	1	21
	12	1,2,4-Triethylbenzene	9.9E-01	1	21
	12	1,3,5-Triethylbenzene	6.0E-01	1	21
	13	n-Heptylbenzene	2.5E-01	1	21
	14	n-Octylbenzene	6.1E-01	1	21
	15	1-Ethylpropylbenzene	9.9E-01	1	21
Branched Alkanes	9	3-Methyloctane	4.0E-02	1	21
	10	2,4,6-Trimethylheptane	7.0E-02	1	21
	11	2-Methyldecane	4.1E-01	1	21
	12	2,6-Dimethyldecane	6.6E-01	1	21
	12	2-Methylundecane	1.2E+00	1	21
	13	2,6-Dimethylundecane	2.1E+00	1	21
Cycloalkanes	9	1,1,3-Trimethylcyclohexane	6.0E-02	1	21
	9	1,3,5-Trimethylcyclohexane	6.0E-02	1	21
	9	1-Methyl-4-ethylcyclohexane	1.0E-01	1	21
	9	Propylcyclohexane	1.4E-01	1	21
	10	n-Butylcyclohexane	7.4E-01	1	21
	12	Hexylcyclohexane	9.3E-01	1	21
	12	Phenylcyclohexane	8.7E-01	1	21
	13	Heptylcyclohexane	1.0E+00	1	21
Diaromatics (Except Naphthalenes)	12	Biphenyl	6.3E-01	1	21

Table C-34 (continued)
Individual Sample Fuel Mixture Composition Data

Fuel mixture: JP-8 Fuel Oil

Sample #: 43/JP-8 Fuel

From: Smith, J.H. et. al., Department of the Air Force, Final Report 54; pp. 1–50; National Technical Information Services, Springfield,VA, A115949/LP, 1981

Compound Class	Carbon #	Compound	Weight Percent	Number of Data Points	Flag (s)
n-Alkanes	7	n-Heptane	3.0E-02	1	21
	8	n-Octane	9.0E-02	1	21
	9	n-Nonane	3.1E-01	1	21
	10	n-Decane	1.3E+00	1	21
	11	n-Undecane	4.1E+00	1	21
	12	n-Dodecane	4.7E+00	1	21
	13	n-Tridecane	4.4E+00	1	21
	14	n-Tetradecane	3.0E+00	1	21
	15	n-Pentadecane	1.6E+00	1	21
	16	n-Hexadecane	4.5E-01	1	21
	17	n-Heptadecane	8.0E-02	1	21
	18	n-Octadecane	2.0E-02	1	21

Flag(s)

21 no flag

Table C-35
Individual Sample Fuel Mixture Composition Data

Fuel mixture: Lubricating and Motor Oils

Sample #: 28/Engine Oil/New

From: Grimmer G, J. Jacob, K.-W. Naujack, Fresenius Zeitschrift fur Analytical Chemistry, Vol. 306, pp. 347-355, 1981

Compound Class	Carbon #	Compound	Weight Percent	Number of Data Points	Flag (s)
Other	16	Benzo(b)naptho(2,1-d)thiophene	3.9E-04	1	4
	16	Other Benzonaphthothiophenes	1.4E-04	1	4
	16	Phenanthro(4,4a,4b,5-bcd)thiophene	4.1E-05	1	4
	16	Total Benzonaphthofurans	5.1E-05	1	4
	22	Triphenylene(4,4a,4b,5-bcd)thiophene	1.2E-05	1	4
Polynuclear Aromatics	16	Fluoranthene	7.0E-05	1	4
	16	Pyrene	1.8E-04	1	4
	17	1-Methylpyrene	1.3E-04	1	4
	17	4-Methylpyrene	1.9E-04	1	4
	17	Benzo(a)fluorene	2.7E-04	1	4
	17	Total Benzofluorenes	3.8E-04	1	4
	18	Benz(a)anthracene	3.4E-05	1	4
	18	Chrysene	1.3E-04	1	4
	18	Triphenylene	2.5E-04	1	4
	20	Benzo(a)pyrene	3.0E-06	1	4
	20	Benzo(b)fluoranthene	3.7E-05	1	4
	20	Benzo(e)pyrene	2.5E-05	1	4
	20	Benzo(k)fluoranthene	4.0E-06	1	4
	21	Total Methylbenzo(e)pyrenes	2.6E-05	1	4
	22	Benzo(g,h,i)perylene	7.0E-06	1	4
	22	Dibenz(a,c)anthracene	8.0E-06	1	4
	22	Indeno(1,2,3-cd)pyrene	2.0E-06	1	4

Flag(s)

4 Data was converted using formula WT%=ug/g*10-4.

Table C-36
Individual Sample Fuel Mixture Composition Data

Fuel mixture: Lubricating and Motor Oils

Sample #: 33/Crankcase oil C

From: Peake, E. and K. Parker, Polynuclear Aromatic Hydrocarbons: Chemistry and Biological Effects, pp. 1025–1039, 1980.

Compound Class	Carbon #	Compound	Weight Percent	Number of Data Points	Flag (s)
Alkyl-Monoaromatics		Total Alkyl-Monoaromatics	1.0E-01	1	2 6
Diaromatics (Except Naphthalenes)		Total Fluorenes	3.4E-03	1	2 6
	13	Fluorene	1.7E-04	1	2 6
	13	Total Methylbiphenyls	2.3E-04	1	2 6
	14	Total Methylfluorenes	2.8E-04	1	2 6
	15	Total Dimethylfluorenes	1.4E-04	1	2 6
	16	Total Trimethylfluorenes	1.3E-04	1	2 6
Naphthalenes		Total Naphthalenes	5.0E-02	1	2 6
Other		Total Sulfur Containing Heterocyclics	2.3E-03	1	2 6
	12	Dibenzothiophene	9.0E-05	1	2 6
	13	Total Methyldibenzothiophenes	2.6E-04	1	2 6
	14	Total Dimethyldibenzothiophenes	4.4E-04	1	2 6
	15	Total Trimethyldibenzothiophenes	2.2E-04	1	2 6
	16	Benzonaphthothiophene	3.9E-05	1	2 6
	17	Total Methylbenzonaphthothiophenes	6.2E-05	1	2 6
Polynuclear Aromatics		Terphenyl	1.4E-05	1	2 6
		Total Benzanthracenes/ Chrysenes/Triphenylenes	3.4E-03	1	2 6
		Total Fluoranthenes	6.8E-03	1	2 6
		Total Phenanthrenes	2.5E-02	1	2 6
	14	Anthracene	3.8E-05	1	2 6
	14	Phenanthrene	8.9E-04	1	2 6
	15	Total Methylanthracenes	6.6E-05	1	2 6
	15	Total Methylphenanthrenes	1.3E-03	1	2 6

Table C-36 (continued)
Individual Sample Fuel Mixture Composition Data

Fuel mixture: Lubricating and Motor Oils

Sample #: 33/Crankcase oil C

From: Peake, E. and K. Parker, Polynuclear Aromatic Hydrocarbons: Chemistry and Biological Effects, pp. 1025–1039, 1980.

Compound Class	Carbon #	Compound	Weight Percent	Number of Data Points	Flag (s)
Aromatics	16	Fluoranthene	5.0E-04	1	2 6
	16	Phenylnaphthalene	1.0E-04	1	2 6
	16	Pyrene	7.6E-04	1	2 6
	16	Total Dimethylanthracenes	3.0E-05	1	2 6
	16	Total Dimethylphenanthrenes	1.2E-03	1	2 6
	17	Benzo(a)fluorene	1.1E-04	1	2 6
	17	Benzo(b)fluorene	1.6E-04	1	2 6
	17	Benzo(c)fluorene	5.0E-05	1	2 6
	17	Total Dihydromethylpyrenes	5.1E-05	1	2 6
	17	Total Methylpyrenes	4.8E-04	1	2 6
	17	Total Trimethylanthracenes	5.8E-05	1	2 6
	17	Total Trimethylphenanthrenes	6.9E-04	1	2 6
	18	Benz(a)anthracene	9.9E-05	1	2 6
	18	Benzo(c)phenanthrene	1.4E-05	1	2 6
	18	Total Chrysenes and Triphenylenes	2.8E-04	1	2 6
	18	Total Diethylphenanthrenes	1.4E-04	1	2 6
	18	Total Dimethylpyrenes	1.9E-04	1	2 6
	19	Total Ethylmethylpyrenes	1.6E-05	1	2 6
Polynuclear Aromatics	19	Total Methylbenzo(a)anthracenes	2.8E-0	1	2 6
	20	Benzo(a)pyrene	4.1E-05	1	2 6
	20	Benzo(e)pyrene	2.0E-04	1	2 6
	20	Benzo(k)fluoranthene	1.6E-04	1	2 6
	20	Ethylbenz(a)anthracene	7.4E-05	1	2 6

Table C-36 (continued)
Individual Sample Fuel Mixture Composition Data

Fuel mixture: Lubricating and Motor Oils

Sample #: 33/Crankcase oil C

From: Peake, E. and K. Parker, Polynuclear Aromatic Hydrocarbons: Chemistry and Biological Effects, pp. 1025–1039, 1980.

Compound Class	Carbon #	Compound	Weight Percent	Number of Data Points	Flag (s)
	20	Perylene	1.5E-05	1	2 6
	20	Total Benzpyrenes and Benzfluoranthenes	2.5E-03	1	2 6
	21	Cyclopenta(cd)pyrene	8.9E-05	1	2 6
	21	Methylbenzo(mno)fluoranthene	3.4E-05	1	2 6
	21	Total Ethylcyclopenta(def) phenanthrenes	1.6E-04	1	2 6
	21	Total Methylbenzofluoranthenes	2.1E-05	1	2 6
	21	Total Methylbenzopyrenes	4.7E-05	1	2 6
	22	Benzo(g,h,i)perylene	1.9E-04	1	2 6
	24	Total Benzperylenes	2.7E-03	1	2 6
Total Aromatics		Total Aromatics	2.0E-01	1	2 6

Flag(s)

2 Product has been used in an engine and may have a different composition than a new oil.

6 Data was converted using formula WT%=mg/l*(1/0.8762)*10-4.

Table C-37
Individual Sample Fuel Mixture Composition Data

Fuel mixture: Kerosene Fuel Oil

Sample #: 45/Kjaw&Al-Zaid 1977

From: Goodman, D.R., R.D.Harbison, Division of Interdisciplinary Toxicology, University of Arkansas for Medical Sciences, Little Rock, AK.

Compound Class	Carbon #	Compound	Weight Percent	Number of Data Points	Flag (s)
Alkyl-Monoaromatics	10	1,2,3,4-Tetramethylbenzene	1.1E+00	1	3
Branched Alkanes	10	Isodecane	1.3E+00	1	3
	11	Isoundecane	1.2E+00	1	3
	12	Isododecane	1.2E+00	1	3
	13	Isotridecane	9.0E-01	1	3
	14	Isotetradecane	6.0E-01	1	3
Monoaromatics	10	Tetralin	2.7E-01	1	3
	11	1-Methyltetralin	6.5E-01	1	3
	11	2-Methyltetralin	6.8E-01	1	3
n-Alkanes	8	n-Octane	3.1E+00	1	3
	9	n-Nonane	5.6E+00	1	3
	10	n-Decane	5.6E+00	1	3
	11	n-Undecane	5.6E+00	1	3
	12	n-Dodecane	5.5E+00	1	3
	13	n-Tridecane	2.5E+00	1	3
Naphtalenes	10	Naphthalene	4.6E-01	1	3
	11	1-Methylnaphthalene	8.4E-01	1	3
	11	2-Methylnaphthalene	1.8E+00	1	3

Flag(s)

3 Data was cited from a secondary source. Original data was not reviewed.

Table C-38
Individual Sample Fuel Mixture Composition Data

Fuel mixture: Kerosene Fuel Oil

Sample #: 45/Stucky 1972

From: Goodman, D.R., R.D.Harbison, Division of Interdisciplinary Toxicology, University of Arkansas for Medical Sciences, Little Rock, AK.

Compound Class	Carbon #	Compound	Weight Percent	Number of Data Points	Flag (s)
n-Alkanes	7	n-Heptane	1.4E+00	1	3
	8	n-Octane	1.5E+00	1	3
	9	n-Nonane	4.8E-01	1	3
	10	n-Decane	2.3E+00	1	3
	11	n-Undecane	4.0E+00	1	3
	12	n-Dodecane	2.4E+00	1	3
	13	n-Tridecane	2.1E+00	1	3
	14	n-Tetradecane	2.0E+00	1	3
	15	n-Pentadecane	2.2E+00	1	3

Flag(s)

3 Data was cited from a secondary source. Original data was not reviewed.

Appendix D
LNAPL DATA EVALUATIONS AND CROSS CORRELATIONS

LNAPL DATA EVALUATIONS & CROSS CORRELATIONS

As discussed in the main body of the report, there are many linked relationships between the various principles describing the distribution of LNAPL and other fluids in the pore space and the transport of chemicals away from the LNAPL in the water and vapor phases. This appendix provides some analysis methods to cross-check inputs and assumptions used in calculating LNAPL distribution, mobility, and chemical transport away from the source. This is not intended to be a comprehensive tome, but touches on some key aspects as both an immediate test of assumptions and a starting point for further site specific investigations, as warranted. The appendix is broken up into two broad sections, hydraulics and chemistry, and will focus on use of field information to test key assumptions in the calculation methods. The appendix is presented in no particular priority, as site specific needs will dictate which evaluations may be of use.

SOME PRINCIPLES IN PRACTICE

Following are some bullet points about what the theory and reality suggest you should see in the field under most conditions. If you do not see these things, in general, you would begin to suspect that your site conceptual model requires revision or rethinking.

LNAPL Hydraulics

1. LNAPL plumes will be fully contained and immobilized in a formation volume less than the residual capacity soil volume. Ongoing LNAPL mobility requires an ongoing source or specific geologic conditions such as fractures or zones with high effective LNAPL conductivity.

2. Related to above, LNAPL recovery in the liquid phase is expected to be strongly asymptotic, because as mass is recovered, saturation and effective LNAPL conductivity are decreased. If one does not see this asymptotic decline, it may mean that a large source is in place, or there is a continuing source of product.

3. When LNAPL is observed in monitoring wells, it is present in the formation at concentrations above residual saturation, except possibly under conditions of first lateral entry of LNAPL into water saturated materials. Therefore under most conditions, if geologic sampling suggests relatively small concentrations of LNAPL (e.g., < 5,000 mg/kg for most conditions), you should suspect that sampling did not encounter the intervals in which significant LNAPL resides. Many cases have been observed where changes in groundwater basin management have resulted in “stranding” of LNAPL many tens of feet below current

water table levels. Note that local scale LNAPL mobility does not imply LNAPL plume mobility as a whole.

4. During transient LNAPL pool migration, observed thickness in monitoring wells is expected to show a tailed bell shape through time; thicken quickly during initial release conditions, then diminishing slowly with time and lateral spreading. The timing should also slow significantly with distance away from the release area. Water table variability will skew and overprint these expectations.

5. During transient LNAPL pool migration, a semi-radial gradient mound is expected that may be skewed in the general direction of groundwater flow. It is unusual for free product to closely follow the groundwater gradient in a uniform direction. The magnitude of the LNAPL gradient is expected to slowly diminish through time toward field equilibrium.

6. Multiphase hysteresis, entrapment, and differences between the effective LNAPL conductivity in 2-phase versus 3-phase systems suggest that observed free product thicknesses will be greatest during low water table stands, and vice versa. This condition may or may not manifest itself when the mobility of the free phase is so small that there is effectively permanent disequilibrium in the system. This is expected for fine-grained materials and/or when product saturations in the formation are small.

Dissolved-Phase LNAPL Relationships

1. Dissolved concentrations should decrease upstream to downstream in the source area versus time. Weathering of the fuel is expected to occur most significantly on the upstream side of the source area, and from the top and bottom of the smear zone toward the middle.

2. A dissolved-phase plume in purely high conductivity formations should generally show chromatographic shifts through time with respect to dissolved-phase impacts when the source mass is relatively small. That is, components such as MTBE and benzene should show molar and mass depletion ahead of compounds like xylenes and other, heavier weight molecular compounds.

3. Plumes in interbedded geologic materials may show concentration decreases over time as mass is depleted from permeable zones, but molar shifts in chemistry are likely to be significantly slower because of the slow diffusion of compounds from the fine-grained zones into the coarse-grained horizons. The relative rates depend on the contrast in flow and diffusion characteristics between interbedded materials and the LNAPL saturations in each.

4. Vertical diminishment of LNAPL dissolved-phase concentrations is expected to be significant in the source zone under most conditions, barring a strong downward vertical gradient and flow rate. Thus, if one were to see significant dissolved-phase concentrations at the bottom of monitoring locations in the source zone, one might suspect the vertical extent of LNAPL impacts to be at or below the current screened interval.

LNAPL MOBILITY AND SATURATION RELATIONSHIPS

LNAPL mobility is an important factor in the analysis of LNAPL spills, their risk, and the relative benefits of active mitigation actions. A mobile LNAPL source could impact utilities and other underground structures and cause explosion and flammability dangers. Further, a spread in the LNAPL phase will cause a spread in the groundwater and vapor phase impacts in addition to the chemical transport already in progress in those phases. Mobility is also related to the recoverability of the LNAPL and to the saturation distribution in the pore space. The relationships are linked by interdependent definitions of phase conductivity, transmissivity, saturation, and relative permeability (see the saturation, conductivity, and relative permeability Equations in Appendix A).

Lab Measurements & Data Analysis

There are many laboratory measurements than can be made to assist in evaluations of LNAPL mobility and saturation. Because of the large number of individual methods suited for different materials, saturations, etc., the list given is by category rather than by specific test method. Any qualified petrophysical lab can provide details on specific analyses and their suitability to a particular set of samples. Only primary factors are given below, and other available analyses may assist further interpretation of site geologic conditions affecting LNAPL (e.g., grain-size sorting, bulk density, clay makeup, etc.):

- Capillarity
- Intrinsic permeability
- Native state pore saturation
- Residual phase saturation
- Interfacial tension (water/air, LNAPL/water, LNAPL/air)
- Fluid viscosity
- Phase mobility
- Relative permeability
- Fluid density
- Porosity (effective & total)

One may also use a variety of field data to estimate some of the parameters above. For instance, total petroleum hydrocarbon (TPH) concentrations given in mg/kg can be converted to saturation if one knows, or can estimate, the bulk density of the soil and LNAPL fluid density, as shown below. Note that the equation below assumes the chemical lab has not included soil pore water into their mass concentration results:

$$\theta_o = [TPH]_{mg/kg} \frac{\rho_b(g/cc)}{\rho_o(g/cc)} \cdot 10^{-6} \quad (1) \qquad \overline{S_o} = \frac{\theta_o - \theta_{sr}}{\theta_t - \theta_{sr}} \quad (2)$$

where TPH is the total petroleum hydrocarbon concentration (mg/kg), ρ_o & ρ_b are the LNAPL and soil bulk density, θ_o is the volumetric LNAPL content, θ_t is the total porosity, θ_{sr} is the residual volumetric water content, and $\mathbf{S}_o$ is the oil residual saturation.

One may also estimate a field value of effective LNAPL transmissivity by conducting a hydrocarbon baildown test (Huntley, 1997, 1999), which is similar to an aquifer slug test. Tests are conducted by quickly removing LNAPL from a well, and monitoring the logarithmic rate of recovery. Excerpts of the analysis method are provided below, the original reference provides field examples.

The hydrocarbon baildown test consists of (1) rapid removal of as much of the hydrocarbon in a well as is practical, followed by (2) monitoring of the elevations of the hydrocarbon/air and hydrocarbon/ water interfaces (which will hereafter be referred to as oil/air and oil/water interfaces for expediency) in the monitoring well. This test is applicable only to wells with light, nonaqueous phase liquids (LNAPL) filling a portion of the well casing. In a two-phase system, the flux of hydrocarbon is given by a modified form of Darcy's Law:

$$q_p = k_i k_{r\,n} \frac{\rho_n g}{\mu_n} i \quad (3)$$

where $\mathbf{k}_{rn}$ is the relative permeability of the non-wetting fluid (the hydrocarbon), $\mathbf{k}_i$ is the intrinsic permeability of the soil, ρ_n is the density of the hydrocarbon, $\mathbf{g}$ is the acceleration due to gravity, μ_n is the viscosity of the hydrocarbon, and $\mathbf{i}$ is the gradient.

The relative permeability of the non-wetting phase (k_{rn}) decreases markedly as hydrocarbon saturation decreases, as given by (Mualem, 1976):

$$k_{rn} = \left(1 - S_e\right)^{1/2} \left(1 - S_e^{1/m}\right)^{2m} \quad (4)$$

where $S_e = (S_w - S_{rw})/(S_m - S_{rw})$, $\mathbf{S}_w$ is the water saturation, $\mathbf{S}_{rw}$ is the residual water saturation, $\mathbf{S}_m$ is the

maximum water saturation (equal to 1 for the initial displacement of water by LNAPL and equal to $\mathbf{1-S_{r\,nw}}$ *for displacement of LNAPL by water),* $\mathbf{S_{r\,nw}}$ *is the residual NAPL saturation, and* $\mathbf{m}$ *is a capillary parameter used to fit the measured saturation data to the closed-form van Genuchten expression (van Genuchten, 1980).*

It is clear from this expression that as hydrocarbon saturation decreases (increasing S_w and S_e) the relative permeability of the hydrocarbon phase decreases exponentially. This, together with decreased density and increased viscosity, markedly decreases the mobility of hydrocarbon in the subsurface, both under natural conditions and under conditions of recovery.

As for pure groundwater conditions, the flow of LNAPL into a well is proportional to the effective LNAPL transmissivity. The hydrocarbon baildown test, though not providing any information about "true" or exaggerated thicknesses (as suggested in some literature), does provide very useful information about the mobility of hydrocarbon in the formation. It is apparent that increased hydrocarbon mobility will result in increased rates of recovery following removal of hydrocarbon from a monitoring well. Quantitatively, the rate of recovery of hydrocarbon in the monitoring well will be a function of the hydrocarbon transmissivity (T_o), defined as:

$$T_o = \int_{z_w}^{z_o} k_{ro} k_i \frac{\rho_o g}{\mu_o} dz \quad (5)$$

where $\mathbf{z_o}$ *is the elevation of the oil/air interface and* $\mathbf{z_w}$ *is the elevation of the oil/water interface.*

This hydrocarbon transmissivity can be used to assess recovery rates and lateral rates of mass flux of hydrocarbon.

The hydrocarbon baildown test affects both the hydrocarbon and the ground water in the vicinity of the well. If done carefully, extraction of hydrocarbon from the monitoring well removes little ground water, so ground water pressures in the formation are minimally affected by the test. As hydrocarbon is removed from the well, however, the ground water level in the well rises to correct for the decrease in fluid pressure in the well relative to that of the ground water in the aquifer. Because the mobility of water is typically greater than that of hydrocarbon in the formation near the well, in most cases the potentiometric surface in the well (often called the corrected water table) recovers very rapidly, and thereafter remains constant in the well. This potentiometric surface can be calculated as:

$$z_p = z_w + \rho_r\left(z_o - z_w\right) \qquad (6)$$

where $\mathbf{z_p}$ is the elevation of the potentiometric surface and ρ_r is the relative density of the hydrocarbon.

Therefore, as hydrocarbon enters the well during recovery, the oil/water interface declines to maintain that constant potentiometric surface, then:

$$\Delta z_p = 0 = \Delta z_w + \rho_r\left(\Delta z_o - \Delta z_w\right) \quad (7)$$

or,

$$\Delta z_w = \frac{-\rho_r}{1-\rho_r}\Delta z_o \quad (8)$$

For example, if the hydrocarbon has a relative density of 0.75, then , $\Delta z_w = -3\Delta z_o$, meaning that a 1 meter rise in the oil/air interface elevation will produce a 3 meter drop in the oil/water interface elevation.

Modification of Bouwer-Rice Slug Test Analysis

A hydrocarbon baildown test cannot be analyzed like a simple aquifer slug test, because the volume of hydrocarbon entering the borehole is not simply $\pi r_c^2 \partial h$, it is $\pi r_c^2(\partial z_o - \partial z_w)$, where $\mathbf{r_c}$ is the radius of the casing and $\boldsymbol{h}$ is the change in head. In the case where groundwater mobility is sufficiently high that the potentiometric surface recovers very rapidly, such as that seen in figure 3, equation (6) can be used to relate the change in the oil/water interface elevation to that of the oil/air interface elevation.

Following the approach that Bouwer and Rice used to derive analytic expressions for the analysis of slug tests, the relation between drawdown (s) and discharge (Q) at any point in time can be approximated by the Thiem equation:

$$s = \frac{Q}{2\pi T} ln\left(\frac{r_0}{r_w}\right) \quad (9)$$

where $\mathbf{T}$ is the aquifer transmissivity, $\mathbf{r_o}$ is the radius of influence, and $\mathbf{r_w}$ is the radius of the well.

In a simple water system, $Q = \pi r_c^2 \frac{\partial s}{\partial t}$. In an oil/water system though, we have stated that:

$$Q = \pi r_c^2 \left(\frac{\partial z_o}{\partial t} - \frac{\partial z_w}{\partial t} \right) \quad (10)$$

To solve this, we need a simplifying assumption. If ground water mobility is high relative to water, the potentiometric surface remains relatively constant during the test. Therefore, we can substitute equation (6) into equation (8), resulting in:

$$Q = \pi r_c^2 \left(\frac{1}{1-\rho_r} \right) \left(\frac{\partial z_o}{\partial t} \right) \quad (11)$$

recognizing that $\partial z_0 = -\partial s$, equation (9) can be substituted into equation (7) to produce:

$$s = - \frac{r_c^2 \left(\frac{1}{1-\rho_r} \right) \left(\frac{\partial s}{\partial t} \right)}{2T} ln \left(\frac{r_0}{r_w} \right) \quad (12)$$

rearranging:

$$T \int_0^t \partial t = - \frac{r_c^2 \left(\frac{1}{1-\rho_r} \right)}{2} ln \left(\frac{r_0}{r_w} \right) \int_{s_0}^{s} \left(\frac{\partial s}{s} \right) \quad (13)$$

after integrating from $t = 0$ to $t = t$ and from $s = s_0$ to $s = s$, we have:

$$T = \frac{2.3 r_c^2 \left(\frac{1}{1-\rho_r} \right)}{2t} ln \left(\frac{r_0}{r_w} \right) log \left(\frac{s_0}{s} \right) \quad (14)$$

This, of course, is the same equation as that derived by Bouwer and Rice (1976) for slug test analysis, except for the additional term $(1/(1-\rho_r))$. This implies that a plot of Log (s) versus t will yield a straight line (Figure 4). As in the traditional Bouwer and Rice analysis of slug test data, s_0, the drawdown at $t = 0$, is taken from the graph as the intercept of the straight line fit through the data, and t and s are the coordinates of a second point on the straight line. Transmissivity is calculated using those selected values and equation (12). In other words, the approach is the same as the analysis of Bouwer and Rice, except the transmissivity calculated using the Bouwer and Rice equations is multiplied by $1/(1-\rho_r)$ to arrive at the transmissivity of the hydrocarbon system. This implies that existing aquifer test analysis approaches and software can be used to analyze the data from hydrocarbon baildown tests, with the simple correction of multiplying the resulting transmissivity by $1/(1-\rho_r)$.

It is important to point out that the above approach assumes that the potentiometric surface equilibrate nearly instantly, such that changes in z_w in the monitoring well are related to changes in z_o by eq. (6). If this assumption is not met, substantial error will result.

Approaches Based on Cooper-Jacob Equation

In some cases, either because of limited permeability or a limited length of the well screen below the oil/water interface, the potentiometric surface may not equilibrate rapidly. In this case, the potentiometric surface is rising (recovering) throughout the entire test, such that equation (6) cannot be applied. As a result, the modification of the slug test analysis derived above cannot be used to analyze the LNAPL recovery data. An alternate approach is based on Jacob and Lohman's (1952) modification of the Cooper-Jacob method for constant-drawdown, variable discharge conditions. Jacob and Lohman (1952) noted that, except for very early times, the relationship between decreasing discharge and time, under constant drawdown conditions, is given by:

$$\frac{1}{Q} = \frac{2.3}{4\pi Ts} LOG \frac{2.25Tt}{r^2 S} \qquad (15)$$

*where **Q** is the discharge from the well, **s** is the drawdown (assumed constant), **t** is time, **r** is the distance to the monitoring well (or well radius for a single-well test), and **S** is the aquifer storage coefficient.*

Equation (13) implies that a plot of $1/Q$ versus Log t should be linear, and the slope can be used to calculate the transmissivity by:

$$T = \frac{2.3}{4\pi s\, \Delta(1/Q)} \qquad (16)$$

*where **Δ(1/Q)** is the change in **1/Q** per log cycle.*

Because, during the recovery from a baildown test, the well is not really being pumped, but is recovering from a rapid removal of hydrocarbon from the well, the discharge (Q) must be calculated from the change in volume of hydrocarbon in the well. That is:

$$Q = \frac{\pi r_c^2 \left(\Delta z_o - \Delta z_w\right)}{\Delta t} \qquad (17)$$

The method assumes that drawdown (*s*) is constant during the recovery period and is known. The drawdown for the hydrocarbon baildown test is simply the difference between the original hydrocarbon elevation and the hydrocarbon elevation during the recovery period. For this analysis, we often see three data segments: 1) Early time response of the filter pack material; 2) Early and intermediate time response of the formation under the quasi-constant "drawdown"; 3) Late-time response where the constant drawdown approximation is not met.

Two independent approaches have been derived that allow us to determine hydrocarbon transmissivity from the response of monitoring wells to a hydrocarbon baildown test. In many wells, in our experience, groundwater mobility is sufficiently greater than hydrocarbon mobility that the groundwater potentiometric surface recovers to its original value very rapidly compared to the recovery of the hydrocarbon elevation in the well. In this case, a modification of the Bouwer and Rice (1976) slug test analysis procedure can be applied to the data. However, in those cases where the potentiometric surface does not recover rapidly, this approach will lead to erroneous values of hydrocarbon transmissivity. Under these circumstances, a modification of the Jacob and Lohman (1952) analysis of transient aquifer test data is recommended.

HYDRAULIC SUMMARY

The outlined measurements and tests above are related through various principles (and equations given here and in Appendix A), and can therefore be used as cross-checks on the assumptions of the LNAPL conceptual models used to evaluate a site. Some example problems are provided at the end of this section that isolate simple aspects of various relationships that are important to understanding the LNAPL conceptual model. Significant divergence between values would suggest that the conceptual model is not representative. As with many geologic situations, it is sometimes as important to prove something wrong as it is to prove it right. For instance, as stated earlier, if a site has observable free product and low measured concentrations (e.g., < 5,000 mg/kg), you can bet sampling density was insufficient to characterize the LNAPL plume. This stepwise common sense approach and testing of conceptual assumptions through measurements and observations is critical to generating useful results.

Most of the field versus lab or assumption hydraulic cross-checks rely on interrelationships between saturation, and mobility. For instance, if one assumes a vertically equilibrated system with a corresponding saturation profile, one should see a similar range of measured saturations from the lab.

Based on measured or assumed capillary and permeability properties, one may calculate the LNAPL conductivity and transmissivity, which can in turn be compared to field estimates by baildown testing. If one estimates or calculates an LNAPL profile with an effective transmissivity of less than about 10^{-5} cm^2/sec, one would not expect to see significant accumulations in an observation well. The variety of cause and effect relationships is lengthy, but depend on the simple fundamentals between the primary variables discussed above.

LNAPL CHEMISTRY

As mentioned in the body of the report, for most sites the main indicator of consistency between the LNAPL conceptual model and actual site conditions is the dissolved-phase chemistry through time. That chemistry is directly linked to the LNAPL source and transport conditions, and is essentially a test of the assumptions regarding the distribution, mass and chemistry of the LNAPL in the formation. It is also usually the only time series data available for most sites. So while other indicators may be used, such as vapor phase measurements above the source zone, these are often not available through time with sufficient density. It is also important to recognize that one is looking for statistically relevant trends, and caution should be used when comparing sparse data sets in hydrologically variable settings to the conceptual model. Similarly, trends as opposed to absolute chemistry values are the better indicators of a good conceptual model. For a myriad of reasons, as documented in the report, it would be unusual for a screening model to agree in high detail with site specific concentrations, although general ranges may be consistent. Clearly, the depletion of the source is linked to rates of transport away from that material, and this is the litmus test of importance.

Definition of Mole Fractions of Concern

The most direct method of identifying the mole fractions of various chemicals in the LNAPL source is to collect representative samples for fingerprinting. Most labs can fingerprint using gas chromatography and mass spectrometry. In the absence of free product samples, one may use the dissolved-phase groundwater impacts in the source area to estimate a starting condition for the initial mole fractions of various COCs using Raoult's law (Appendix A). Using benzene as an example, we know the pure phase solubility is about 1,780 mg/l. Since the expected effective concentration is the product of the pure phase solubility and the mole fraction, all that is needed is to divide the site specific effective concentration in the source area by the pure phase solubility to derive the estimated mole fraction. If the effective solubility was 20 mg/l, the corresponding mole fraction would be about 0.01.

For this mole fraction estimate to work, you must use a well or wells in the source area screened in the LNAPL impacted interval. One back check is that the estimated solubility limit for gasoline is typically 60 to 150 mg/l TPH, though this can vary further depending on composition. If site concentrations are smaller than this range, the well may be outside the source zone or the well screen may intersect some "clean" water intervals.

CROSS-RELATIONSHIPS

Now we have in hand several potential cross-relationships that can be used to lend confidence or suspicion to the LNAPL conceptual model built for a particular site. Each is given in bullet format below, as the supporting equations and principles have been provided previously:

1. One may compare the estimated LNAPL transmissivity calculated using lab-derived or assumed parameters to that measured in the field. If the two are in general agreement, perhaps the conceptual model is well suited to the site. If not, one would suspect that the underlying soil and saturation properties assumed for calculations are inaccurate, or that an undefined set of non-ideal conditions is present.

2 One may compare TPH samples in and near the smear zone to the saturation values put into the conceptual model. They should obviously be consistent.

3. One may use inferential measurements, such as laser-fluorescence, to suggest the vertical distribution of hydrocarbons in the subsurface and compare to the vertical discretization in the LNAPL conceptual model. Shape and position are often as useful as hard measurements of saturation or concentration.

4. Vertical profiling of the dissolved-phase groundwater concentrations may suggest whether or not the conceptualization of the vertical distribution of LNAPL is correct. Concentrations should diminish exponentially with depth below the lowest LNAPL/water contact in the formation.

5. Contrasts between the predicted and observed dissolved-phase concentrations in source zone wells are another clear indication of potential conflict between the conceptual model and field conditions, particularly with respect to the shapes of the dissolution curves. Concentration values may be skewed in the field by fine-scale heterogeneity not accounted in calculations, but the general mass depletion trends should be in the ball park. If for instance, the calculations suggest a multi-decade residence time for a particular COC, but periodic groundwater sampling shows statistically relevant decreases of that compound in source zone mass, there is clearly less mass in place than conceptualized.

6. If one recovers liquid-phase hydrocarbons until no further recovery is feasible or demonstrated, one could expect to sample the adjacent formation in the LNAPL interval with the resultant saturation indicative of field residuals.

7. If a cleanup technique is used that targets specific amenable compounds, one should see a molar decrease in those compounds through the time of remediation. A drop in total concentration without a corresponding drop in mole fractions implies that some of the smear zone is not targeted by the particular remediation system.

Appendix E

LNAST SAMPLE INPUT AND OUTPUT FILES

User Input Parameters
(echo of input file structure)

Fine Sand (K= 1 m/day)

1	0.4	0.34	7.5	1.9	0.15	
0.14	3	0.15	0.01	0.003	1	
0.25	0.6944444	0.25				
True		True	True	False	True	False
True		True	True	False	True	
False		True	False	True	False	
0.01	1	10	10	5		

Gasoline

52	24	0.73	0.62			
5						
MTBE	48000	1204	0.11	1	9000	40
Benzene	780	324	0.018	2	90	5
Ethyl Benzene	135	57	0.018	3	65	700
Toluene	515	111	0.079	2.06	60	1000
Xylene	175	38	0.075	2.6	150	10000

Time (yrs)	MTBE	Benzene	Ethyl Benzene	Toluene	Xylene
0.e+0	5.28e+3	3.2e+1	2.43e+0	4.07e+1	1.31e+1
2.74e-7	5.28e+3	3.2e+1	2.43e+0	4.07e+1	1.31e+1
6.02e-7	5.28e+3	3.2e+1	2.43e+0	4.07e+1	1.31e+1
9.97e-7	5.28e+3	3.2e+1	2.43e+0	4.07e+1	1.31e+1
1.47e-6	5.28e+3	3.2e+1	2.43e+0	4.07e+1	1.31e+1
2.04e-6	5.28e+3	3.2e+1	2.43e+0	4.07e+1	1.31e+1
2.72e-6	5.28e+3	3.2e+1	2.43e+0	4.07e+1	1.31e+1
3.54e-6	5.28e+3	3.2e+1	2.43e+0	4.07e+1	1.31e+1
4.52e-6	5.28e+3	3.2e+1	2.43e+0	4.07e+1	1.31e+1

Representative of beginning and ending of a Source Area Dissolved Phase Concentration output file. Files can be several pages long.

3.11e+1	2.8e-45	9.6e-2	1.49e+0	7.95e+0	9.03e+0
3.13e+1	2.8e-45	9.06e-2	1.49e+0	7.81e+0	8.98e+0
3.17e+1	2.8e-45	8.44e-2	1.47e+0	7.64e+0	8.92e+0
3.21e+1	2.8e-45	7.75e-2	1.46e+0	7.45e+0	8.85e+0
3.26e+1	2.8e-45	6.98e-2	1.44e+0	7.23e+0	8.76e+0
3.31e+1	2.8e-45	6.16e-2	1.42e+0	6.96e+0	8.66e+0
3.38e+1	2.8e-45	5.28e-2	1.4e+0	6.66e+0	8.54e+0
3.47e+1	2.8e-45	4.38e-2	1.37e+0	6.3e+0	8.4e+0
3.57e+1	2.8e-45	3.48e-2	1.34e+0	5.9e+0	8.23e+0
3.69e+1	2.8e-45	2.61e-2	1.3e+0	5.45e+0	8.02e+0
3.83e+1	2.8e-45	1.83e-2	1.25e+0	4.95e+0	7.79e+0
4.e+1	2.8e-45	1.18e-2	1.2e+0	4.4e+0	7.51e+0
4.21e+1	2.8e-45	6.66e-3	1.14e+0	3.8e+0	7.18e+0
4.34e+1	2.8e-45	4.93e-3	1.1e+0	3.5e+0	6.99e+0
4.49e+1	2.8e-45	3.38e-3	1.06e+0	3.16e+0	6.77e+0
4.66e+1	2.8e-45	2.11e-3	1.01e+0	2.78e+0	6.51e+0
4.88e+1	2.8e-45	1.15e-3	9.58e-1	2.39e+0	6.21e+0
5.01e+1	2.8e-45	8.35e-4	9.26e-1	2.19e+0	6.04e+0
5.16e+1	2.8e-45	5.61e-4	8.89e-1	1.96e+0	5.83e+0
5.35e+1	2.8e-45	3.39e-4	8.46e-1	1.72e+0	5.6e+0
5.57e+1	2.8e-45	1.78e-4	7.97e-1	1.46e+0	5.32e+0
5.71e+1	2.8e-45	1.27e-4	7.69e-1	1.33e+0	5.16e+0
5.87e+1	2.8e-45	8.33e-5	7.37e-1	1.19e+0	4.98e+0
6.06e+1	2.8e-45	4.88e-5	7.e-1	1.04e+0	4.77e+0
6.29e+1	2.8e-45	2.46e-5	6.57e-1	8.74e-1	4.52e+0

Down-Gradient Extent of Dissolved Phase

Time (yrs)	MTBE	Benzene	Ethyl Benzene	Toluene	Xylene
1.e-2	1.55e+1	8.21e+0			
3.e-2	2.95e+1	1.41e+1			
5.e-2	4.05e+1	2.04e+1			
7.e-2	5.04e+1	2.5e+1		4.08e+0	
9.e-2	5.83e+1	3.01e+1		5.29e+0	
1.1e-1	6.71e+1	3.39e+1		6.16e+0	
1.3e-1	7.64e+1	3.8e+1		6.89e+0	
1.5e-1	8.36e+1	4.18e+1		7.47e+0	
1.7e-1	9.14e+1	4.53e+1		7.89e+0	
1.9e-1	1.e+2	4.9e+1		8.23e+0	
2.1e-1	1.04e+2	5.19e+1		8.49e+0	
2.3e-1	1.09e+2	5.45e+1		8.69e+0	
2.5e-1	1.13e+2	5.72e+1		8.84e+0	
2.7e-1	1.18e+2	6.01e+1		8.96e+0	
2.9e-1	1.24e+2	6.3e+1		9.06e+0	
3.1e-1	1.29e+2	6.61e+1		9.14e+0	
3.3e-1	1.35e+2	6.93e+1		9.2e+0	
3.5e-1	1.41e+2	7.26e+1		9.26e+0	
3.7e-1	1.48e+2	7.56e+1		9.31e+0	

Representative sample of the beginning and end of a Down-Gradient Extent of Dissolved Phase output file.

5.92e+0	1.06e+3	1.21e+2
6.24e+0	1.e+3	1.2e+2
6.56e+0	3.88e+1	1.18e+2
6.88e+0	3.74e+1	1.16e+2
7.2e+0	3.59e+1	1.15e+2
7.52e+0	3.42e+1	1.13e+2
7.84e+0	3.28e+1	1.11e+2
8.32e+0		1.03e+2
8.96e+0		1.e+2
9.6e+0		9.65e+1
1.02e+1		9.28e+1
1.09e+1		8.93e+1
1.15e+1		8.56e+1
1.22e+1		8.2e+1
1.28e+1		7.84e+1
1.34e+1		7.49e+1
1.41e+1		7.31e+1
1.47e+1		7.14e+1
1.54e+1		6.97e+1
1.6e+1		6.79e+1

Fluid Saturation Distribution

z(m)	Sw	So	kw
	1.e+0	0.e+0	1.e+0
.01	1.e+0	4.52e-4	9.21e-1
.02	9.98e-1	1.68e-3	8.55e-1
.03	9.96e-1	3.62e-3	7.95e-1
.04	9.94e-1	6.23e-3	7.39e-1
.05	9.91e-1	9.46e-3	6.87e-1
.06	9.87e-1	1.33e-2	6.38e-1
.07	9.82e-1	1.77e-2	5.93e-1
.08	9.77e-1	2.26e-2	5.5e-1
.09	9.72e-1	2.79e-2	5.1e-1
.1	9.66e-1	3.37e-2	4.72e-1
.11	9.6e-1	4.e-2	4.37e-1
.12	9.53e-1	4.65e-2	4.05e-1
.13	9.47e-1	5.35e-2	3.75e-1
.14	9.39e-1	6.07e-2	3.47e-1
.15	9.32e-1	6.81e-2	3.21e-1
.16	9.24e-1	7.58e-2	2.96e-1
.17	9.16e-1	8.37e-2	2.74e-1
.18	9.08e-1	9.18e-2	2.53e-1
.19	9.e-1	1.e-1	2.34e-1
.2	8.92e-1	1.08e-1	2.17e-1
.21	8.83e-1	1.17e-1	2.e-1
.22	8.75e-1	1.25e-1	1.85e-1
.23	8.66e-1	1.34e-1	1.71e-1

Representative sample of beginning and end of a
Fluid Saturation Distribution output file.
Files can be several pages long depending on input parameters.

1.12	4.38e-1	1.23e-1	0.e+0
1.13	4.36e-1	1.02e-1	0.e+0
1.14	4.34e-1	8.34e-2	0.e+0
1.15	4.32e-1	6.68e-2	0.e+0
1.16	4.3e-1	5.18e-2	0.e+0
1.17	4.28e-1	3.84e-2	0.e+0
1.18	4.26e-1	2.63e-2	0.e+0
1.19	4.25e-1	1.53e-2	0.e+0
1.2	4.23e-1	5.39e-3	0.e+0
1.21	4.21e-1	0.e+0	0.e+0
	0.e+0	0.e+0	0.e+0
	0.e+0	0.e+0	0.e+0
	0.e+0	0.e+0	0.e+0
	0.e+0	0.e+0	0.e+0
	0.e+0	0.e+0	0.e+0

Source Area Dissolved Phase Concentrations

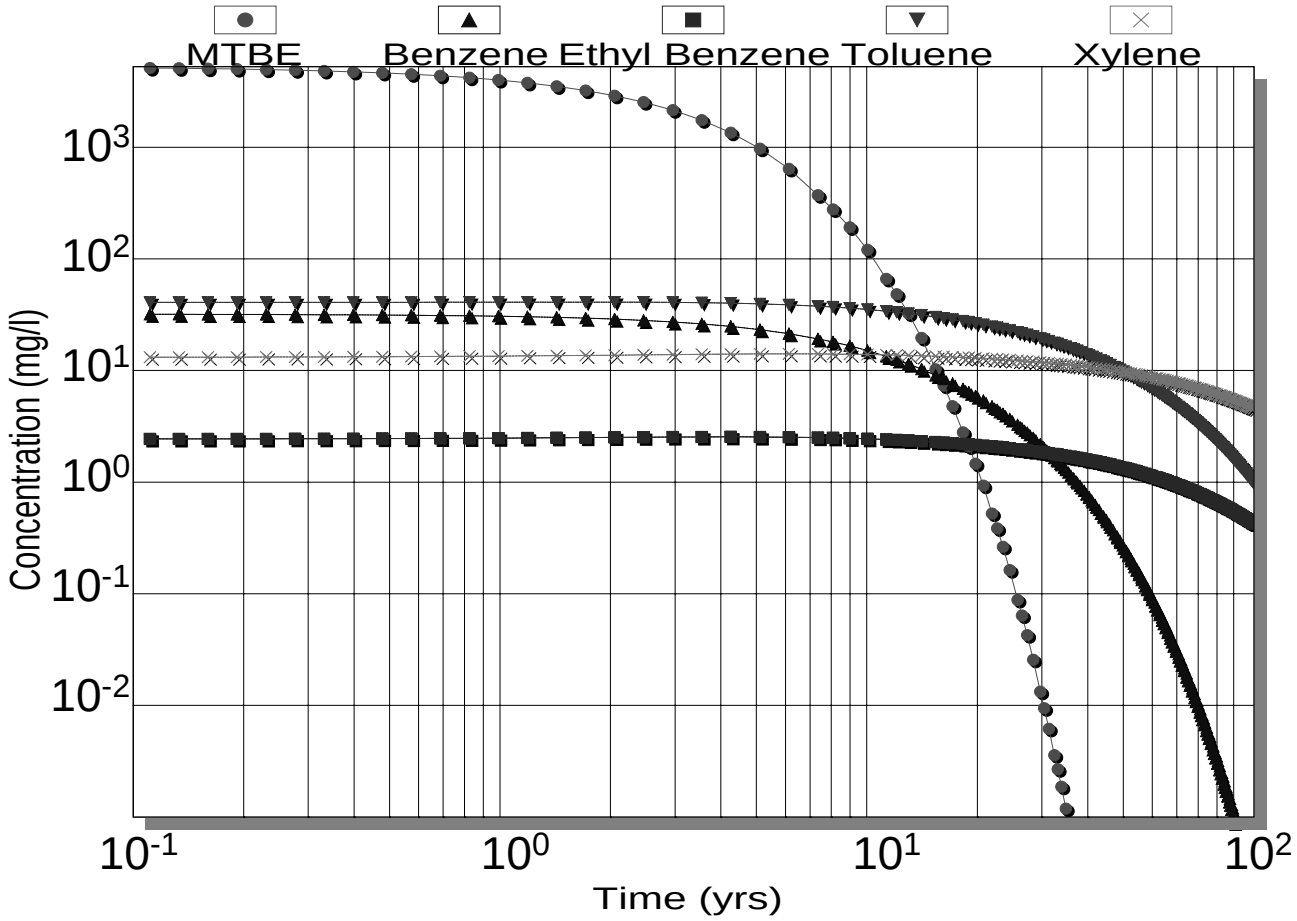

Maximum Downgradient Distance

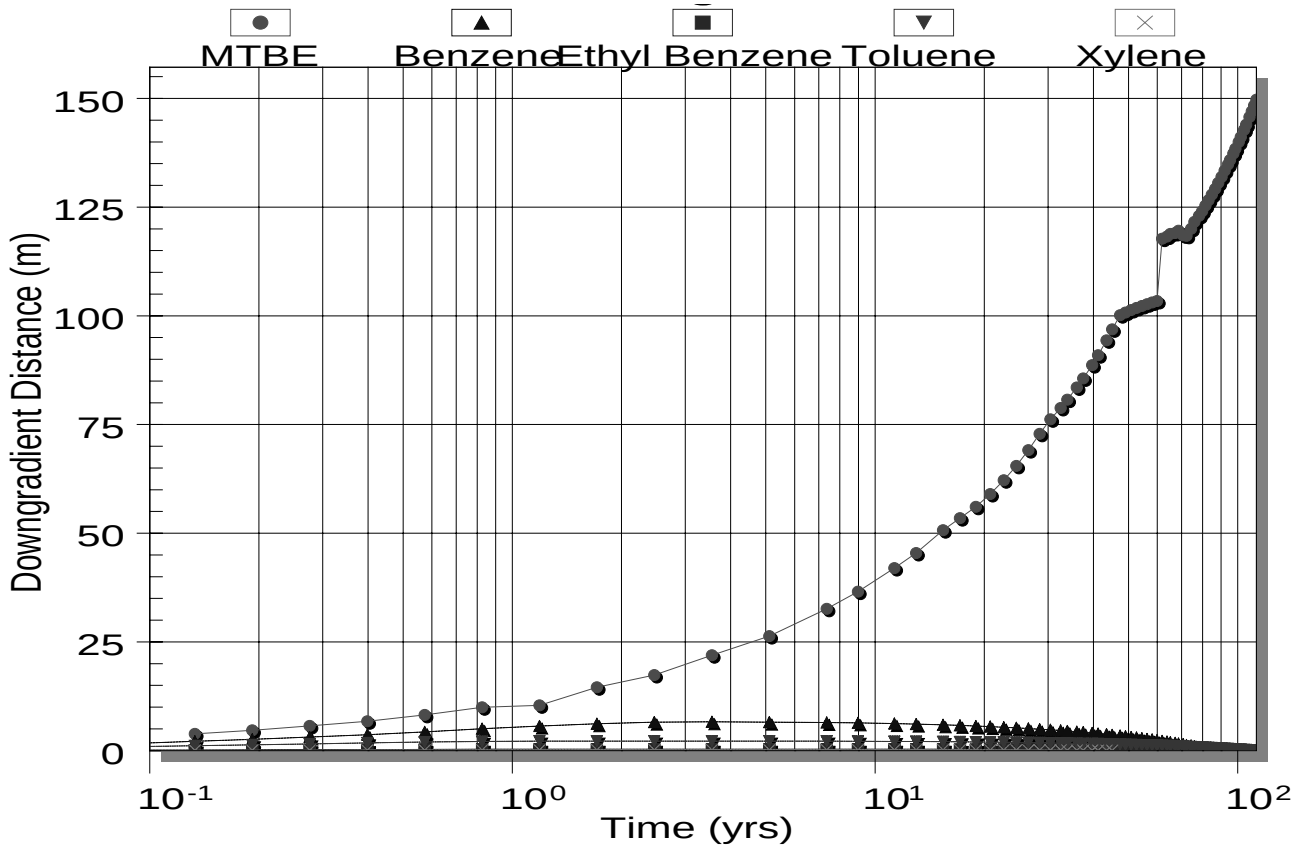

Additional copies are available through Global Engineering Documents at (800) 854-7179 or (303) 397-7956

Information about API Publications, Programs and Services is available on the World Wide Web at: http://www.api.org

American Petroleum Institute

1220 L Street, Northwest
Washington, D.C. 20005-4070
202-682-8000

Product No. I47150